UNIVERSITY OF DEFENCE IN BRNO

FACULTY OF MILITARY HEALTH SCIENCES

Doctoral degree program:

Military Radiobiology

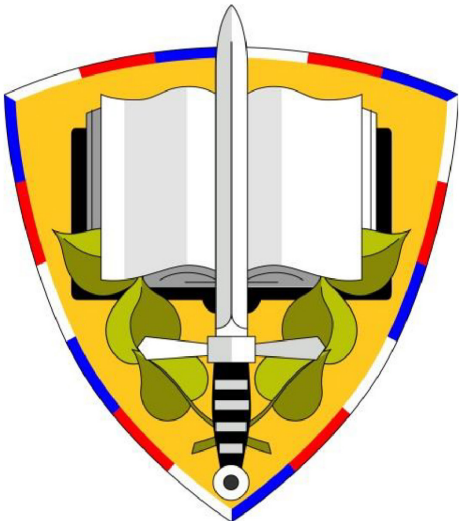

DISSERTATION THESIS

Radiosensitization of cancer cells by modulation of autophagy: Phosphoproteomic analysis

Author: Mgr. Martin Ondrej

Supervisor: Assoc. Prof. Aleš Tichý, PharmD., Ph.D.

Hradec Králové, 2020

Stanovení tématu disertační práce

Student: **Mgr. Martin ONDREJ**

Stanovené téma disertační práce: Radiosensibilizace nádorových buněk: fosfoproteomická analýza

Klíčová slova v ČJ (5-10):

Fosfopeptidy; hmotnostní spektrometrie; ionizující záření; inhibice; autofagie; nemalobuněčný karcinom plic;

Klíčová slova v AJ (5-10):

Phosphopeptides; mass spectrometry; ionizing radiation; inhibition; autophagy; non-small cell lung cancer

Stručná anotace disertační práce v ČJ (v rozsahu 5 řádků):

Hlavním předmětem této práce je studium změn fosforylace na úrovni buněčné signalizace a ovlivnění molekulárních mechanismů v kontextu radiosensibilizace nádorových buněk. Význam radiosensibilizace stoupá, neboť dvě třetiny onkologických pacientů jsou v současné době léčeny pomocí radioterapie. Studie bude prováděna na modelových buněčných liniích ovlivněných kombinací specifických inhibitorů a ionizujícího záření. Bude využito hmotnostní spektrometrie a vhodných bioinformatických nástrojů s důrazem na význam autofagie.

Stručná anotace disertační práce v AJ (v rozsahu 5 řádků):

The aim of this study is to characterize the changes of phosphorylation status within cell signalling and to address the importance of modulation of molecular mechanisms in the context of radio-sensitization of cancer cells. The impact of radio-sensitization increases, since nearly two thirds of oncological patients receive radiotherapy. The study will be conducted on model cell lines treated with combination of specific inhibitors and ionizing radiation. We will apply mass spectrometry approach combined with suitable bio-informatic tools with emphasis to autophagy.

Stanovisko oborové rady:

Souhlasím – ~~nesouhlasím~~*/ se stanoveným tématem disertační práce.

28. 11. 2014 ..... datum

Y. Bátorová ..... předseda oborové rady

Schvaluji.

27. XI. 2014 ..... datum

..... děkan

Acknowledgments

My greatest gratitude belongs to my supervisor, Assoc. Prof. Aleš Tichý, PharmD., Ph.D., for his valuable advice and guidance throughout my Ph.D. study and for his help with writing my publications and also this thesis. I am very grateful to my colleagues Lucie Čecháková M.S. for her excellent co-operation on all the experiments and during the writing of the articles, Barbora Šalovská Ph.D. for providing me with valued information at the beginning of my studies, and Aneta Douděrová M.S. who helped me with the biological part of the thesis. My big thanks also go to all my colleagues from the Department of Radiobiology and Department of Molecular Biology and Pathology, namely Pavel Rehulka, Ph.D., and Helena Rehulkova, Ph.D. I would also like to thank the laboratory assistants, especially Ms. Lenka Mervartová, for their exceptional technical assistance. Finally, I am very grateful to my family, especially to my wife, Veronika Ondrejová, who has supported me since the beginning of my studies.

This work was supported by the Ministry of Defense (A long-term organization development plan no. 1011) and by the Ministry of Education, Youth and Sport (Specific research project no: SV/FVZ201501), Czech Republic.

Declaration

I declare hereby that this dissertation thesis is my original work and that I indicated by references all used information sources. I also agree with depositing my dissertation in the Library of the University of Defence, Faculty of Military Health Sciences in Hradec Králové and with making use of it for study and educational purpose provided that anyone who will use it for his/her publication or lectures is obliged to refer to or cite my work properly.

I give my consent to the availability of my dissertation's electronic version in the information system of the University of Defence.

Hradec Králové

Signature of the author

Abstract (ENG)

Lung cancer, and in particular, non-small cell lung cancer (NSCLC), belongs to the most lethal oncological diseases worldwide. Choosing the proper therapeutic approach is, therefore, inevitable for the successful treatment of lung tumors. In this regard, radiotherapy is an essential therapeutic approach. However, like any other treatment option, radiotherapy has its limitations in the form of radioresistance. Autophagy has been generally accepted to be one of the most crucial factors in the radioresistance of tumor cells. It is, therefore, necessary to search for suitable approaches that would lead to the suppression of cytoprotective autophagy and, thus, to the radiosensitization of tumor cells.

In this respect, in our study, we employed methods of quantitative phosphoproteomics along with several techniques of molecular biology to examine the underlying molecular mechanisms and signaling pathways involved in the regulation and inhibition of the autophagic process. To inhibit the cytoprotective autophagy, we used a relatively new autophagy inhibitor—Lys05, the analog of a well-described autophagy inhibitor chloroquine. As a model, we chose the radioresistant NSCLC cells (H1299; p53-negative), because they represent the most problematic group of cells within non-small cell lung tumors.

The most important finding we present here is the successful radiosensitization of H1299 cells to ionizing radiation after pre-treatment with Lys05. Interestingly, we observed that inhibition of autophagy occurred in a late-stage after the treatment, most probably as a result of the down-regulation of AMPK–ULK1–ATG13 pathway. This annotated set of publications summarizes the most important findings obtained during the doctorate study. All results are described in detail in the individual articles in the appendix.

Keywords: autophagy; ionizing radiation; phosphoproteomic analysis; Lys05; non-small cell lung cancer

Abstrakt (CZE)

Rakovina plic, a zejména nemalobuněčný karcinom plic (NSCLC – z anglického non-small cell lung cancer), patří k nejsmrtelnějším onkologickým onemocněním na světě. Výběr správného terapeutického přístupu je proto pro úspěšnou léčbu nádorů plic zásadní. V tomto ohledu je proto radioterapie důležitým terapeutickým přístupem. Podobně jako u jakéhokoliv jiného terapeutického přístupu má však radioterapie svá omezení ve formě radiorezistence. Autofagie je obecně přijímána jako jeden z nejdůležitějších faktorů v radiorezistenci nádorových buněk. Je proto nutné hledat vhodné mechanismy, které by vedly k potlačení cytoprotektivní autofagie a tím k radiosenzibilizaci nádorových buněk.

V tomto ohledu jsme v naší studii použili metody kvantitativní fosfoproteomiky spolu s několika technikami molekulární biologie pro prozkoumání hlavních molekulárních mechanismů a signálních drah zapojených do regulace a inhibice autofagického procesu. K inhibici cytoprotektivní autofagie jsme použili relativně nový inhibitor autofagie – Lys05, analog dobře popsaného inhibitoru autofagie chlorochinu. Jako model jsme zvolili radiorezistentní buňky NSCLC (H1299, p53-negativní), protože představují nejproblematičtější skupinu buněk v nemalobuněčných plicních nádorech.

Nejdůležitější poznatek, který zde představujeme, je úspěšná radiosenzibilizace buněk H1299 vůči ionizujícímu záření, které jsme dosáhli po podání Lys05 před ozářením. Zajímavostí je, že k inhibici autofagie došlo až v pozdním stádiu, nejpravděpodobněji v důsledku regulace dráhy AMPK-ULK1-ATG13.

Klíčová slova: autofagie; ionizující záření; fosfoproteomická analýza; Lys05; nemalobuněčný karcinom plic

Table of contents

List of abbreviations 10

List of figures and tables 11

1 Preface 12

2 Aims of the study 14

3 The overview of autophagy 15

3.1 Forms of autophagy 15

3.2 Process of autophagy 16

3.3 Functions of autophagy 17

3.4 Autophagy in cancer 18

4 Cellular mechanisms and signaling pathways behind the autophagy modulation 20

4.1 Combined treatment of H1299 cells with Lys05 and IR leads to a concentration- and dose-dependent decrease in cell proliferation 20

4.2 Analysis of Lys05-treated cells suggests inhibition of autophagy via the AMPK–ULK1–ATG13 pathway 21

4.3 Lys05 blocks the autophagosome–lysosome fusion 28

5 Summary of the key results I 30

6 Optimization of the phosphoproteomic workflow 31

6.1 Optimization of the initial steps 31

6.2 Optimization of the phosphopeptide enrichment—the critical step of the phosphoproteomic study 32

6.3 Optimization of the phosphopeptide sample fractionation 33

7 Summary of the key results II 38

8 Conclusion 39

9 References 41

10 List of publications 46

11 Appendices 47

Publication no. 1 49

Publication no. 2 63

Publication no. 3 81

Publication no. 4 97

Publication no. 5 139

Publication no. 6 155

Publication no. 7 157

List of abbreviations

ACN	Acetonitrile
BMT	Bone marrow transplantation
CQ	Chloroquine
EGF	Epidermal growth factor
GO	Gene ontology
H1299	Non-small cell lung carcinoma cell line
HCQ	Hydroxychloroquine
IMAC	Immobilized metal affinity chromatography
IR	Ionizing radiation
LC	Liquid chromatography
Lys05	Coding name for an autophagy inhibitor
MOAC	Metal oxide affinity chromatography
MS	Mass spectrometry
NSCLC	Non-small cell lung cancer
PCD	Programmed cell death
qRT-PCR	Real-time quantitative reverse transcription polymerase chain reaction
ROS	Reactive oxygen species
RP	Reversed-phase
RT	Radiation therapy
SCLC	Small-cell lung cancer
SILAC	Stable isotope labeling by amino acids in cell culture
SIMAC	Sequential elution from IMAC
TEM	Transmission electron microscopy
TiO_2	Titanium dioxide
UV	Ultraviolet
WB	Western blot
ZrO_2	Zirconium dioxide

NOTE: For the sake of simplicity, abbreviations of all protein and gene names are not listed here but are declared directly in the text of the dissertation thesis when mentioned for the first time. Besides, these names are frequently used and known in the form of abbreviation.

List of figures and tables

List of figures

Figure 1. The process of autophagy and its regulation pathways 19

Figure 2. Real-time monitoring of cell proliferation and clonogenic assay 21

Figure 3. Gene ontology over-representation analysis 22

Figure 4. STRING pathway interaction network one hour after irradiation 24

Figure 5. STRING pathway interaction network 48 hours after irradiation 25

Figure 6. Western blot analysis and qRT-PCR analysis 27

Figure 7. Fluorescence microscopy and flow cytometry analysis 29

Figure 8. Incorporation rate of labeled lysine and arginine 32

Figure 9. LC–UV chromatograms of the conventionally fractionated sample 35

Figure 10. Analysis of the optimized fractionation scheme 37

List of tables

Table 1. Composition of the conventional and optimized elution mobile phases 36

1 Preface

Cancer represents one of the most severe illnesses in the world. In 2017, a total of 577 373 patients with malignant neoplasms were diagnosed in the Czech Republic. Of these, 27 320 became fatal [1].

Lung cancer belongs to a group of tumors that are widespread and generally considered to be the most serious. In fact, lung tumors are the most lethal among oncological diseases, with the mortality reaching 80% [1,2]. There are two types of lung cancer. Non-small cell lung carcinoma (NSCLC) represents the majority of lung cancers. The others are small cell lung carcinoma (SCLC).

A wide range of treatment methods can be applied to treat lung cancer. The choice of an appropriate one is conditioned by the stage of the disease [3]. In this regard, radiation therapy (RT) plays an important role. However, as a class, NSCLCs are relatively resistant to RT [4] and thus hamper the beneficial effects of RT, resulting in the use of excessively high doses of ionizing radiation (IR). Identification of the mechanisms of NSCLC radioresistance seems essential for the enhancement of RT efficacy.

It has been generally accepted that, among others, autophagy might play a key role in the NSCLC radioresistance. Autophagy, as a natural cell protection process, is able to protect cells from stressful conditions leading to their survival [5]. Therefore, the study of the mechanisms of autophagy and its contribution to radioresistance seems to be a reasonable approach leading to the sensitization of NSCLC cells to RT.

During our studies, we worked with a model radioresistant NSCLC cell line—H1299, that possess partial deletion of the TP53 gene and, as a result, does not express the tumor suppressor p53 protein. This cell line is, therefore, particularly suitable for the study of radiation-activated molecular mechanisms associated with autophagy inhibition. For the inhibition of autophagy, we used a relatively new autophagy inhibitor—Lys05, which we obtained in co-operation with Dr. McAfee as a kind gift from the University of Pennsylvania [6].

This dissertation thesis is an annotated set of publications dealing with the molecular mechanisms of autophagy, its signaling pathways that are activated after exposure of cancer cells to IR, and the possibilities of chemical modulation of these mechanisms in order to radiosensitize cancer cells towards IR.

The thesis is divided into three conceptual sections. In the first section, which is purely theoretical, we present autophagy as a mechanism of cell survival, its role in

tumor cells, and specific ways of autophagy modulation that lead to radiosensitization of tumor cells. The second part is the core section, where we discuss cellular mechanisms and molecular signaling pathways that contribute to the radiosensitization of H1299 cells by autophagy inhibition using methods of molecular biology and quantitative phosphoproteomics. In the third section, we describe the optimization steps that either must be performed before the quantitative phosphoproteomic study or could be added to improve the procedure. Although this arrangement may seem unconventional, we deliberately chose it to emphasize the findings of phosphoproteomic and biological analyzes in the first place as they form the basis of the thesis. Therefore, we have placed them before the optimization section that provides technical insights, which, in this case, completes the whole study.

This dissertation is developed in the form of free commenting on the results that have already been published in peer-reviewed journals with impact factor. The author of the thesis selected five publications, where he is the main author or co-author, and compiled them into a commented set. All publications follow each other logically and form a comprehensive work that describes the use of specific inhibitors of autophagy together with IR leading to radiosensitization of cancer cells. The mentioned publications are listed *in extenso* as an annex in chapter 11.

2 Aims of the study

The primary goal of our study was to investigate the molecular mechanisms and signaling pathways that are responsible for the resistance of non-small cell lung cancer cells (H1299; p53-negative) to IR and their potential modulation by the autophagy inhibitor—Lys05, leading to radiosensitization of these cells.

To achieve the primary goal of our study, we implemented specific aims, which included:

- to assess the response of H1299 cells to different doses of IR and concentrations of inhibitor at the cellular level;
- to screen for the changes in proteins that are responsible for the processes of autophagy and its inhibition;
- to identify of phosphoproteins involved in the inhibition of autophagy using the methods of quantitative phosphoproteomics;
- to verify the involvement of these proteins in the process of autophagy inhibition using immunodetection, gene expression, and microscopic techniques;
- to optimize the phosphoproteomic workflow in order to enhance the phosphoprotein identification and quantification.

3 The overview of autophagy

Autophagy is a natural evolutionarily conserved cellular process that enables degrading and recycling of the damaged organelles along with proteins that have lost their function in the cell to maintain homeostasis, especially during stress conditions. The term autophagy is derived from Greek auto-, "oneself" and phagein, "to eat" [7]. This intracellular degrading system is not only a simple degradation mechanism allowing the removal of unnecessary substances from the cell body, but it is essential for maintaining physiological properties in healthy cells. Therefore, the deregulation of autophagy may lead to many different diseases, such as cancer, neurodegeneration, cardiovascular diseases, and infections [8,9]. Autophagy may be activated as a response of various stimuli, involving nutrient, oxygen and growth factor shortage, DNA damage, chemotherapeutic drugs, and IR [10,11].

In the first section of this dissertation thesis, we deal briefly with the theoretical description of autophagy, its forms, molecular mechanisms, and methods of its modulation that lead to radiosensitization of tumor cells. All these findings are summarized in-depth and described clearly in the review **Publication no. 1**.

3.1 Forms of autophagy

Based on the mechanism of action, three forms of autophagy are commonly described: i) macroautophagy, ii) microautophagy, and iii) chaperone-mediated autophagy. There are also a few alternatives, such as mitophagy, lipophagy, and others less significant that are briefly introduced here [12]. A standard indicator of all forms of autophagy is that they are uniformly terminated by proteolytic degradation of cytosolic components in lysosomes [13].

Macroautophagy is the best known and most widely studied form of autophagy. It is characterized by the formation of a double-membrane vesicle recognized as an autophagosome, which eventually fuses with the lysosome to degrade and recycle the contents of the vesicle (further called an autolysosome) [13,14]. The process of macroautophagy can be characterized by five key stages [13]:

1. phagophore formation or nucleation regulated by Unc-51 like autophagy activating kinase 1 (ULK1) protein complex;

2. autophagy-related proteins 5 and 12 (Atg5–Atg12) conjugation and interaction with Atg16L resulting in phagophore elongation and multimerization;
3. microtubule-associated protein 1A/1B-light chain 3 (LC3) controlled phagophore elongation;
4. autophagosome maturation and capture of selective targets for degradation;
5. autophagosome–lysosome fusion, followed by proteolytic degradation by lysosomal proteases of engulfed molecules.

In our work, we focused exclusively on macroautophagy (further referred to as autophagy), so we will not address other forms of autophagy.

3.2 Process of autophagy

Autophagy is a dynamic process, and its progression can be divided into five consecutive phases—induction, nucleation, elongation, maturation, and degradation.

Briefly, during the induction phase, an isolated membrane called phagophore is formed. In the elongation phase, the phagophore elongates further, surrounding the intracellular material that is to be degraded, then closing and forming an autophagosome. In the maturation phase, the autophagosome fuses with the lysosome and degrades the autophagosomal content using lysosomal acidic proteases. Finally, lysosomal permeases and transporters export amino acids and other degradation by-products back to the cytoplasm, where they can be reused for macromolecule production and cell metabolism [13].

The induction of autophagy, the first stage of the autophagic process, is triggered in response to a various range of stress conditions. In mammals, complete depletion of amino acids seems to be the most potent activator of autophagy. Subsequent regulation of autophagy represents quite a sophisticated machinery [15]. Overall, autophagosome initiation and formation are centrally controlled by ULK1 (ULK1–mAtg13–FIP200–Atg101) protein complex [16].

The nucleation phase is characterized by the autophagosome formation. Various organelles, including mitochondria, endoplasmic reticulum, and Golgi complex, can provide the basis for autophagosome formation [13,17]. In mammalian cells, class III PI3K complex plays a critical role in the initial step of autophagosome formation. In this

complex, the class III PI3K (Vps34) protein associates with proteins Beclin-1 and p150 to form the core of the PI3K complex [18].

Elongation is a step in which the autophagosomal membrane is prolonged, and at the end of this step, it is successfully closed. During elongation, two essential regulatory complexes play a vital role—Atg12 and LC3.

The maturation of autophagy involves the last step—a fusion of the autophagosome with the lysosome to form the autolysosome [19]. Four key regulators regulate this step: N-ethylmaleimide-sensitive factor attachment protein receptor (SNARE) proteins, Rab family proteins, PI3K complex, and Rubicon.

The final stage of autophagic machinery is the degradation of autophagosomal cargo. This degradation is ensured by the lysosomal hydrolases, which degrade the inner membrane of the autophagosome and cleave substances destined for degradation [20]. At the end of this step, metabolites produced by lysosomal degradation are released into the cytosol [21].

Figure 1 provides a comprehensive overview of the mechanisms of autophagy. A more in-depth description of the autophagic process is given in the **Publication no. 1** and also reviewed here [13,15,16,20,21].

3.3 Functions of autophagy

The essential role of autophagy in the human body is to maintain cell and tissue homeostasis [22].

The physiological functions of autophagy focus mainly on maintaining cellular homeostasis. The key functions of this process include: i) reactions to nutrient stress caused by starvation, hypoxia, and shortage of growth factors, ii) repair mechanisms, iii) removal of misfolded proteins and damaged organelles iv) removal of invading intracellular pathogens and immunity, v) programmed cell death, and vi) aging and longevity [23,24].

Autophagy is generally considered a beneficial process in cells due to its contribution to the maintaining of cellular homeostasis. Therefore, it is not surprising that dysregulation of this process contributes to several pathologies, including cancer, neurodegeneration, cardiac diseases, liver diseases, lysosomal storage disease, muscle disorders, and more [24,25].

Autophagic programmed cell death (PCD) is an extreme function of autophagy that is triggered in conditions of an excessive amount of stress. The term autophagic PCD

has established for biological processes connected with the removal of the whole cells [26]. It provides the removal of abnormal cells that were exposed to genotoxic damage or infected by pathogens [27]. The frequent presence of elevated autophagic markers and morphological signs of autophagy in dying cells led to the presumption of autophagic PCD. On the other hand, autophagy is typically activated in conditions of cellular stress, so it is no wonder that dying cells show signs of autophagy [28]. Therefore, the important question remains whether autophagy in dying cells is the mechanism of death or whether it is, in fact, an attempt to prevent it [29,30].

3.4 Autophagy in cancer

The role of autophagy in tumorigenesis is rather complicated. It is probably highly dependent on the tissue that has been affected, and the type of cancer that has triggered tumorigenesis. So far, six biological capabilities have been identified as hallmarks of cancer. They involve: i) sustaining proliferative signaling, ii) evading growth suppressors, iii) resisting cell death, iv) enabling replicative immortality, v) activating invasion and metastasis, and vi) inducing angiogenesis [31].

It has been generally accepted that autophagy can act as a tumor suppressor in the early stages of tumorigenesis and as a tumor promoter in developed tumors [32,33]. There is, however, one another fact that should be born in mind when speaking about autophagy in cancer, especially in association with anti-cancer therapy. In fact, autophagy in anti-cancer therapy often serves as a protective mechanism that leads to cell survival and contributes to cellular resistance against therapy [34,35].

In advanced tumors, cancer cells located in the central part of solid tumors are often exposed to extremely stressful conditions. These include hypoxia and nutrient starvation that are caused by insufficient vascularization. In response, autophagy is activated in developed cancer cells to promote proliferation and, thus, the survival of these cells [36,37].

IR used in anti-cancer therapy directly causes DNA damage and leads to the formation of reactive oxygen species (ROS) [38]. Hence, developed tumors treated with RT are exposed to an enormous amount of stress due to the formation of ROS. In these tumors, cytoprotective autophagy triggers as a response to adverse conditions resulting in radioresistance. Several studies describe clinically relevant doses of radiation that promote cytoprotective autophagy in tumor cells [39–42]. It is, therefore, very likely that the crucial role of autophagy within irradiated cancer cells is not in the degradation of

cellular components and providing nutrients and metabolic precursors, but in the elimination of toxic species [43].

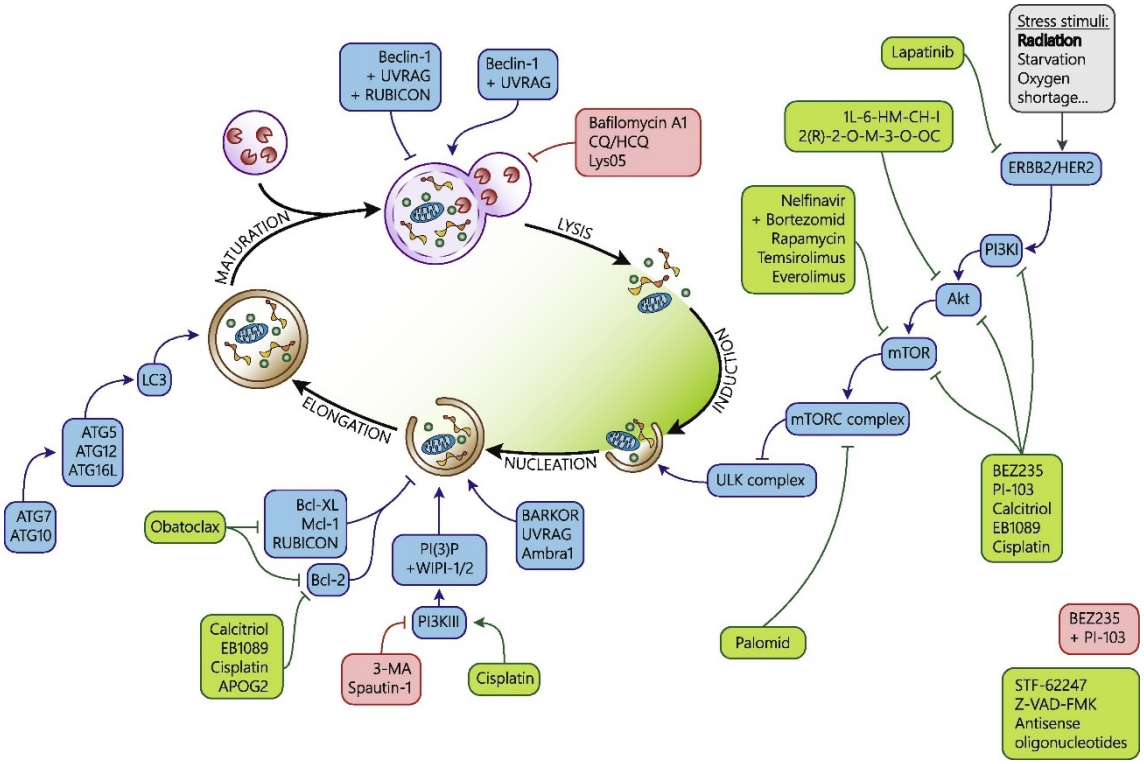

Figure 1. The process of autophagy and its regulation pathways (framed in blue) in the context of radiosensitizers (framed in green and red). The whole machinery of autophagy is divided into four main steps: (1) induction, (2) nucleation, (3) elongation, and (4) maturation, followed by lysis of autophagosomal content. There are plenty of stimuli, which can trigger autophagy, e.g., starvation, IR, oxygen shortage, and DNA damage. These stress stimuli lead to an activation of the mTORC complex through PI3K/Akt/mTOR pathway and subsequent activation of the ULK complex, which induces the autophagic process. The main regulator of nucleation is class III PI3K, which interacts with Beclin-1 and leads to the production of second messenger PI(3)P and formation of the autophagosome. Other positive regulators are BARKOR, UVRAG, and Ambra-1. Proteins Bcl-2, Bcl-XL, Mcl-1, and RUBICON belong to the negative regulators, which contribute to the stopping of nucleation. Proteins ATG7 and ATG10 regulate the formation of ATG12, ATG5, and ATG16L complex, which subsequently activates LC3 complex, an essential complex for the final step of autophagosome formation, leading to the enclosure of autophagosome membrane. In the end, autophagosome fuses with lysosome to form autolysosome and releases the acidic lysosomal hydrolases degrading the cytosolic content. Radiosensitization of cancer cells can be achieved by the application of both inducers and inhibitors of autophagy. The application of these substances, together with IR, leads to decreased clonogenic survival of cancer cells. The majority of inducers (framed in green) activate autophagy in its initial steps, mainly through inhibition of the mTOR signaling pathway. On the other hand, inhibitors of autophagy (framed in red) act in the late phase of the autophagic process. Bottom right, inhibitors, and inducers with a more complex mechanism of autophagy modulation are listed.

4 Cellular mechanisms and signaling pathways behind the autophagy modulation

Autophagy has been identified to play two opposite roles in irradiated cancer cells. On the one hand, it is involved in the elimination of ROS and other damaging substances, thus protecting cells from cell death. On the other hand, it may contribute to autophagic PCD declaring its cytotoxic function. Modulation of either of these autophagic roles might be used to radiosensitize cancer cells. Naturally, the original sensitization approach was to inhibit the cytoprotective autophagy. Nowadays, more and more researchers appear to be in favor of inducing autophagic PCD than inhibition of cytoprotective autophagy [5]. There are plenty of autophagic modulators that have been described so far. A brief overview of those associated with radiosensitization, together with their connection in signaling pathways is shown in Figure 1.

In our studies, we have focused exclusively on the inhibition of autophagy. In this regard, we used a relatively new inhibitor of autophagy—Lys05. It was introduced by McAfee et al. several years ago [44]. Structurally, Lys05 is a dimeric form of a well-established autophagy inhibitor chloroquine (CQ). Mechanistically, it blocks autophagy by accumulating within the lysosomes, similar to CQ and hydroxychloroquine (HCQ). Its advantage is that it exhibits stronger antitumor activity as a single agent than CQ or HCQ, both *in vitro* and *in vivo* [44].

In this section of the dissertation, we briefly present the results concerning the cellular mechanisms and signaling pathways that underlie the radiosensitization of tumor cells by inhibiting autophagy. They are addressed in more detail in **Publications no. 2** and **3**.

4.1 Combined treatment of H1299 cells with Lys05 and IR leads to a concentration- and dose-dependent decrease in cell proliferation

Initially, we applied real-time monitoring of H1299 cell proliferation along with a clonogenic assay to study the overall radiosensitizing effect of Lys05. Using these methods, we detected a concentration- and dose-dependent decrease in cell proliferation, as shown in Figure 2 and described in more detail in **Publication no. 2**. Based on the measured data, we concluded that the use of 2 μM Lys05 as a pre-treatment for IR with a dose of 2 Gy contributes to the radiosensitization of H1299 cells by

suppressing autophagy, similarly as observed by Koukourakis et al. [45]. Therefore, in the following studies, we always used the inhibitor concentration of 2 μM and a radiation dose of 2 Gy.

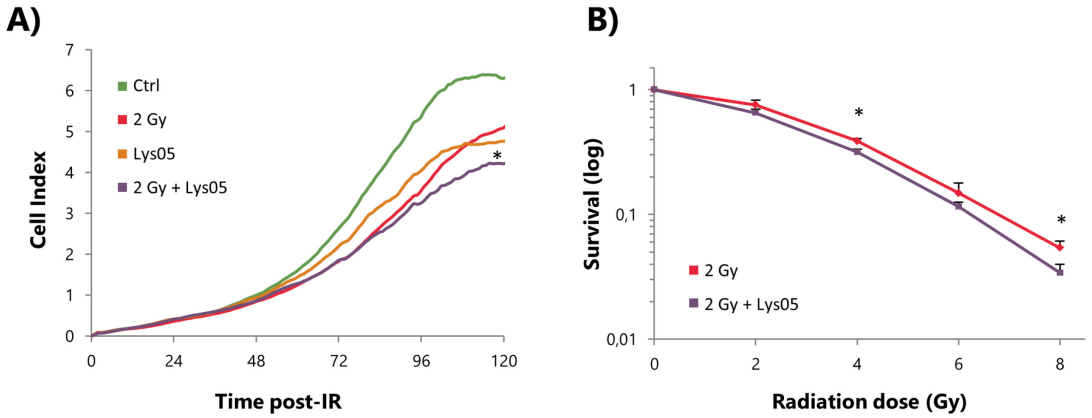

Figure 2. Autophagy inhibitor—Lys05 caused a decrease in H1299 cell proliferation. The H1299 cells were treated either with ionizing radiation (IR) or inhibitor alone or with their combination. Lys05 in 2 μM concentration was added to the cells one hour before irradiation (2 Gy). Real-time monitoring of cell proliferation was analyzed by the xCELLigence system and recorded every 30 minutes for six days **(A)**. * Significant difference compared to control (p-value ≤ 0.05) as a result of one experiment performed in triplicate. Clonogenic assay displays average values ± SD from three independent experiments in triplicates counted by eye after the 10-day incubation period **(B)**. * Significant difference compared to solely irradiated group (p-value ≤ 0.05).

4.2 *Analysis of Lys05-treated cells suggests inhibition of autophagy via the AMPK–ULK1–ATG13 pathway*

Further on, we examined the molecular mechanisms leading to autophagy inhibition. In this regard, we employed phosphoproteomic analysis to screen for relevant proteins with respect to their phosphorylation, which should contribute to autophagy inhibition.

In this case, we pre-treated the H1299 cells with Lys05 and irradiated them. Surprisingly, when performing an in-depth phosphoproteomic analysis, we expected to find autophagy somewhat inhibited early after irradiation. Instead, we found numerous deregulations of phosphorylated proteins leading rather to an increased rate of autophagy. Later after irradiation, the effect of Lys05 prevailed as we detected phosphorylation leading to reduced autophagic activity.

This observation was supported by the gene ontology (GO) analysis, which, one hour after irradiation, revealed an up-regulation of biosynthetic and metabolic processes and down-regulation of the main signaling regulator of autophagy—the target of

rapamycin (TOR) signaling. On the other hand, 48 hours after irradiation, we found these biosynthetic and metabolic processes along with the cellular response to stress to be down-regulated, suggesting the autophagy inhibition, as depicted in Figure 3. These findings are altogether reported in **Publication no. 3**.

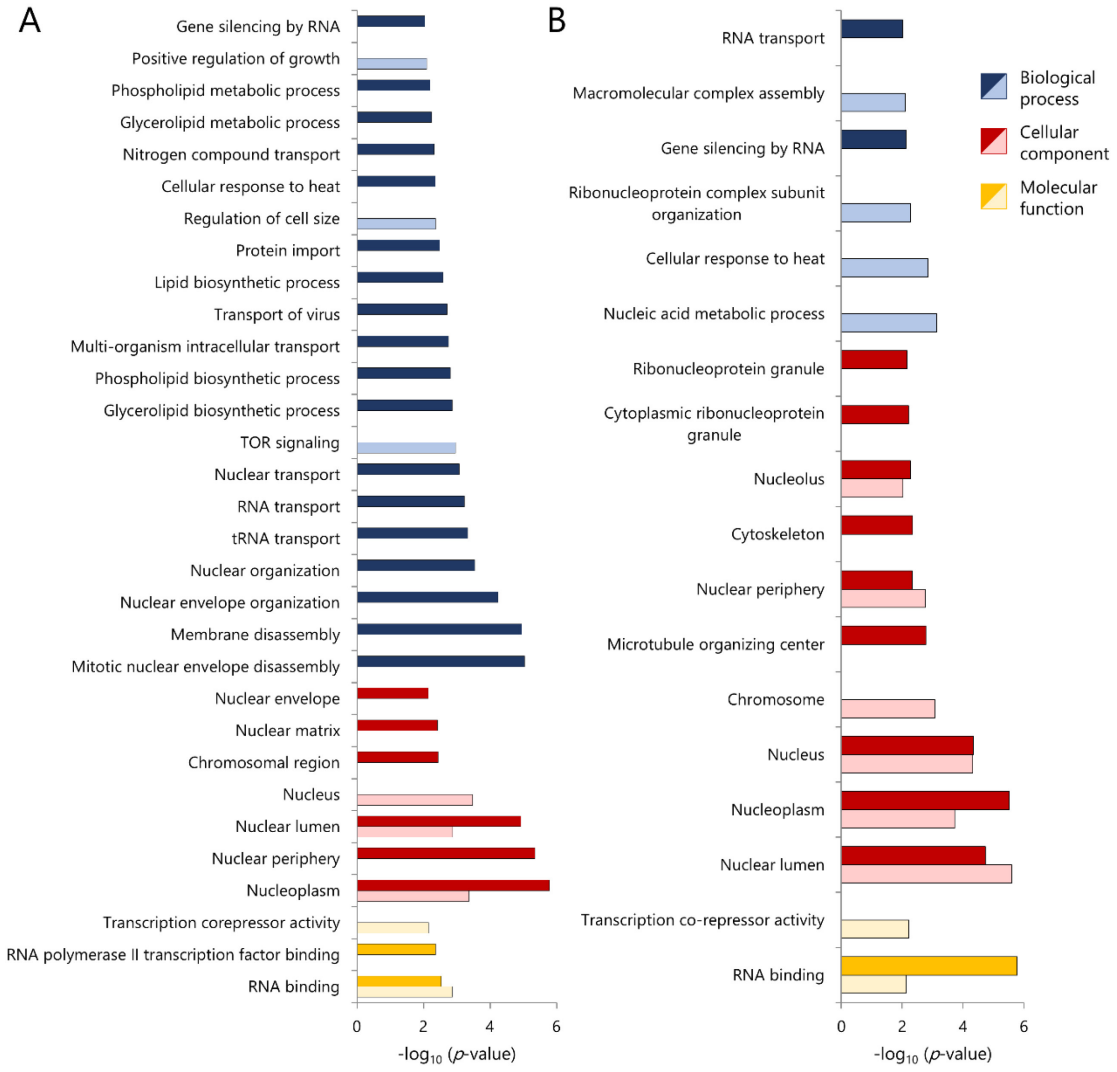

Figure 3. Gene ontology (GO) over-representation representation analysis of proteins with differentially regulated phosphosites identified one hour after irradiation **(A)** and 48 hours after irradiation **(B)** using the ConsensusPathDB level 4 terms. GO terms with darker colors correspond to proteins with up-regulated phosphosites. GO terms with brighter colors correspond to those with down-regulated phosphosites.

Subsequent more detailed analysis of phosphoproteomic data using the STRING web tool identified several phospho/proteins that might be involved in the activation of the autophagic process early after irradiation and its late inhibition.

One hour after irradiation, we recognized two significant groups: one associated with biosynthetic and metabolic processes, and another one associated with the

regulation of the cell cycle. The key regulators of the autophagy progression detected one hour after irradiation appeared to be the proline-rich AKT1 substrate 1 (known as AKT1S1 or PRAS40)—an initial autophagy inducer [46,47], and sequestosome 1 (known as SQSTM1 or p62)—a regulator of autophagosome formation [48]. Other critical regulatory proteins such as La ribonucleoprotein domain family member 1 (LARP1) [49], 60S ribosomal export protein NMD (NMD3) [50], or glycerol-3-phosphate acyltransferase 3 (known as GPAT3 or AGPAT9) [51] also participated in this process, as shown in Figure 4 and described in more detail in **Publication no. 3**.

Later, 48 hours after irradiation, we identified several smaller protein groups. Most of them were associated with the regulation of gene expression or transport mechanisms. The most relevant in terms of the late-stage autophagy inhibition seems to be the ULK1–ATG13 pathway [52,53]. Moreover, ULK1 itself, along with its phosphorylated forms, appeared to be the crucial regulator of autophagy inhibition 48 hours after irradiation [54], as shown in Figure 5 and described in more detail in **Publication no. 3**.

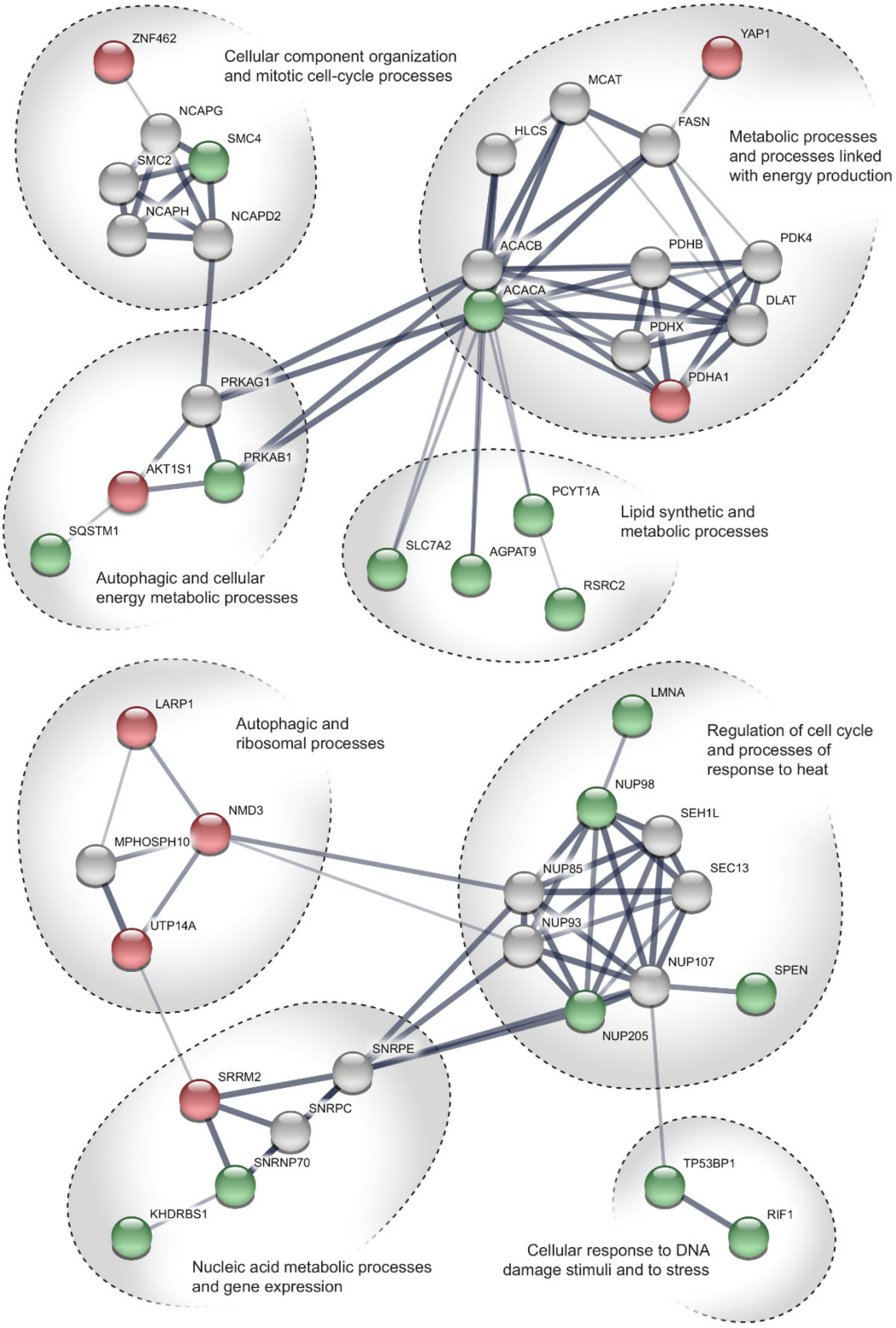

Figure 4. STRING pathway interaction network of proteins with differentially regulated phosphosites. The figure shows the proteins identified one hour after irradiation. Points colored green represent proteins with up-regulated phosphosites. Points colored red represent proteins with down-regulated phosphosites. Points colored grey were added automatically by the software. Line thickness indicates the strength of data support.

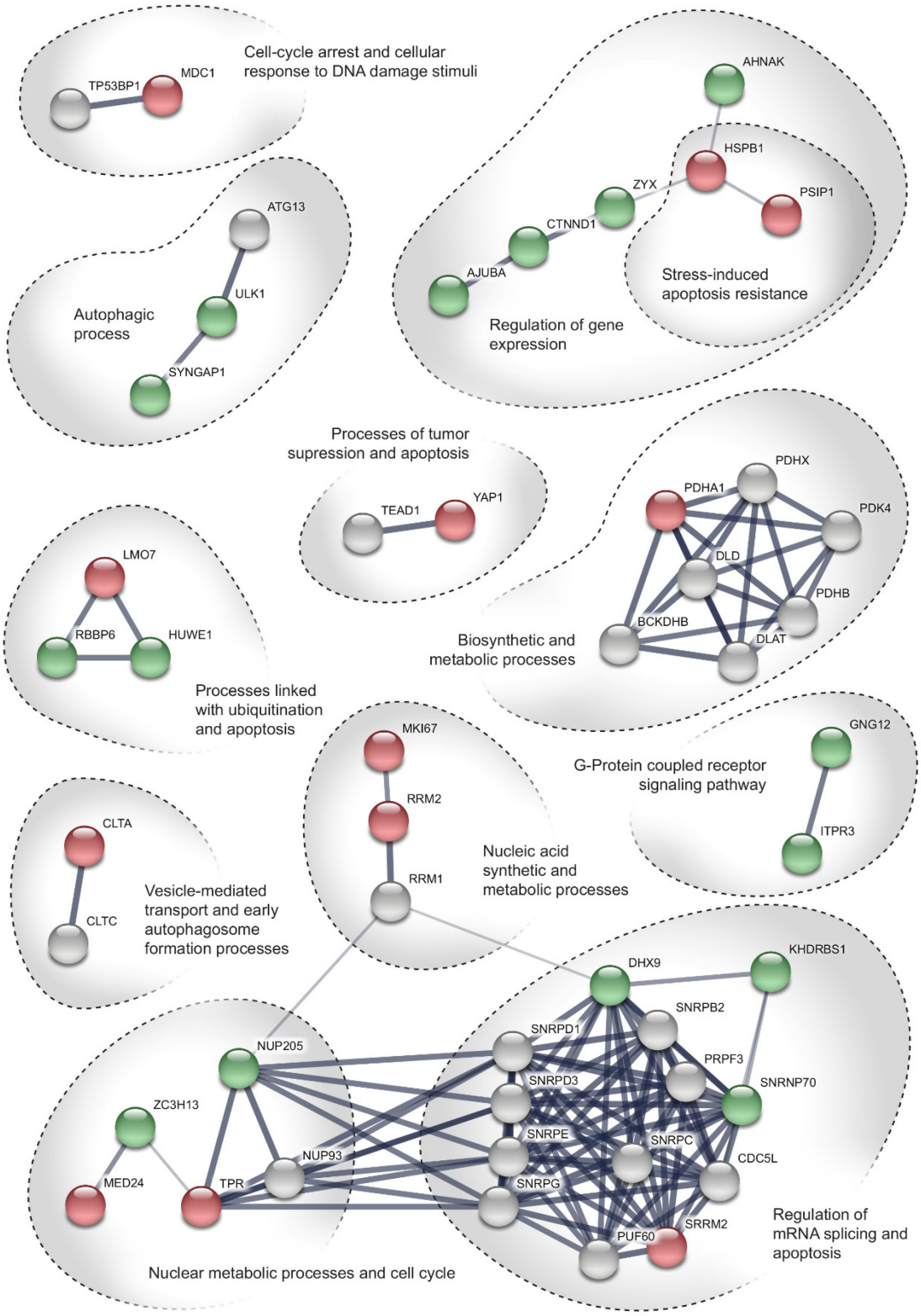

Figure 5. STRING pathway interaction network of proteins with differentially regulated phosphosites. The figure shows the proteins identified 48 hours after irradiation. Points colored green represent proteins with up-regulated phosphosites. Points colored red represent proteins with down-regulated phosphosites. Points colored grey were added automatically by the software. Line thickness indicates the strength of data support.

To validate the findings provided by phosphoproteomic analysis, we employed a western blot (WB) analysis to examine the protein level of the main autophagy regulatory proteins. We also examined the gene expression of the related genes—*SQSTM1* and *BNIP3* using the real-time quantitative reverse transcription PCR (qRT-PCR). All findings concerning these methods are in detail described in **Publication no. 2**.

According to WB analysis, we observed a slightly decreased protein level of phospho-ULK1 (Ser555) and increased levels of LC3 and p62 in Lys05 pre-treated cells 48 hours after irradiation, as depicted in Figure 6A. Similarly, using the qRT-PCR, we observed significantly increased gene expression of *SQSTM1* and significantly decreased gene expression of *BNIP3* 48 hours after irradiation, as depicted in Figure 6B.

These results confirmed the successful inhibition of autophagy 48 hours after irradiation for several reasons. First, the increased protein level of ULK1 phosphorylated on Ser555 has been proved to contribute to the progression of autophagy. On the other side, its depletion led to autophagy inhibition [55,56].

Moreover, since proteins p62 and LC3 are both affected by the ongoing autophagy, they have been established as markers of autophagy [57–59]. Generally, p62 tends to accumulate inside the cells when autophagy is suppressed, and it is degraded during the autophagic process [57]. During this process, LC3 cleaves to LC3-I (cytosolic form) and LC3-II (membrane-associated form), demonstrating the ongoing autophagy flux. Therefore, as reported by Mizushima and Yoshimori, a simultaneous increase in the protein level of p62 together with elevated LC3-II/I ratio indicate the real inhibition of autophagy [58,59].

On this basis, we came to an assumption of the late-stage autophagy inhibition because of the blockade of autophagosome–lysosome fusion, which is controlled by the AMPK–ULK1–ATG13 pathway.

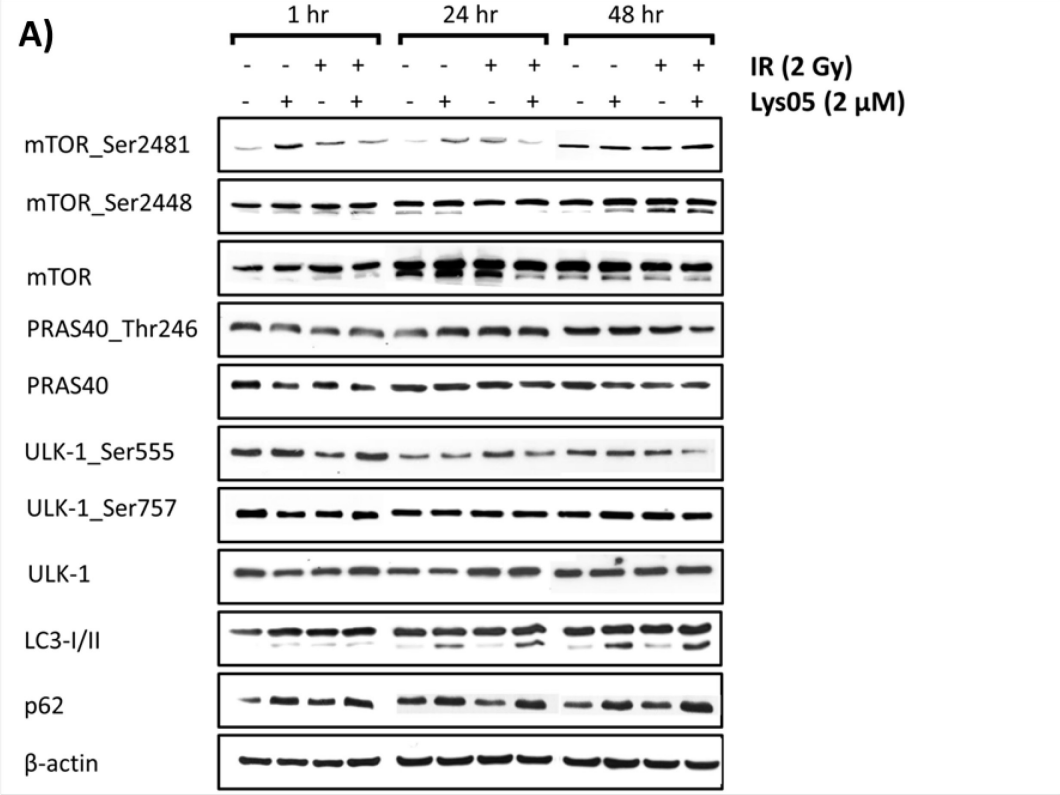

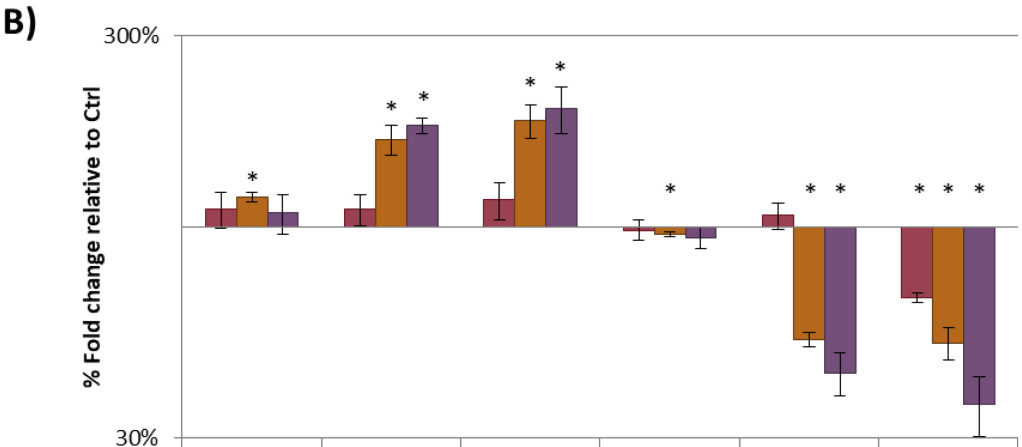

	1 H	24 H	48 H	1 H	24 H	48 H
	SQSTM1			BNIP3		
2Gy	111%	111%	117%	98%	107%	67%
Lys05	119%	165%	184%	96%	53%	52%
2Gy + Lys05	108%	179%	197%	94%	43%	36%

Figure 6. Administration of Lys05 blocks autophagosome–lysosome fusion. The H1299 cells were treated either with IR or the inhibitor alone or with their combination. Lys05 in 2 µM concentration was added to the cells one hour before irradiation (2 Gy). Data were analyzed one, 24, and 48 hours after irradiation. First, Western blot analysis of phosphorylated and non-phosphorylated proteins following treatment with IR and Lys05 were performed **(A)**. Second, qRT-PCR analysis of the expression of genes *SQSTM1* and *BNIP3* were performed **(B)**. Data represent the mean of the percentage fold change ±SD relative to control based on three independent experiments performed in duplicate. * Significant difference compared to control (p-value ≤ 0.05).

4.3 Lys05 blocks the autophagosome–lysosome fusion

Two traceable hallmarks accompany the late-stage autophagy inhibition induced by the blockade of autophagosome–lysosome fusion: i) accumulation of autophagosomes and ii) associated accumulation of lysosomes. We applied transmission electron microscopy (TEM) and fluorescence microscopy to study these hallmarks.

According to our TEM data, we observed increased accumulation of autophagic vacuoles after the treatment with Lys05. Moreover, substantial accumulation of autophagic vacuoles was present after the treatment with a combination of Lys05 with IR. These findings correlate with the study by Makowska et al., who observed elevated levels of autophagosomes after co-treatment of nasopharyngeal carcinoma by CQ and IR [60]. These data are not shown as a figure, but they are described in **Publication no. 2**.

Using fluorescence microscopy, we detected a significant increase in the fluorescence intensity of LysoSensor™ Green DND-189 staining after treatment with Lys05 or IR alone or with their combination. We also quantified it by using flow cytometry. We hypothesize that such an increase might be the result of lysosome accumulation caused by the blockade of autophagosome–lysosome fusion. This correlates with studies by Lu et al. [61] and Chikte et al. [62], who observed the time- and dose-dependent increase in fluorescence intensity using CQ as an autophagy inhibitor most probably due to the accumulation of lysosomes. These findings are depicted in Figure 7 and described in more detail in **Publication no. 2**.

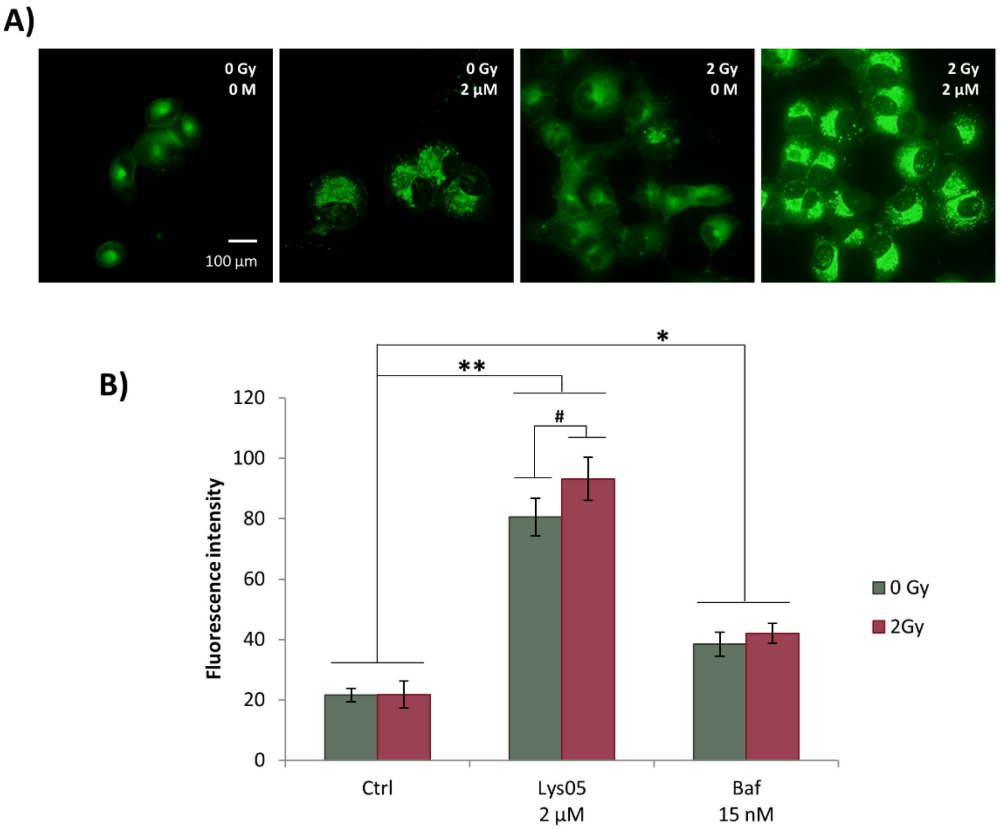

Figure 7. Administration of Lys05 leads to the accumulation of lysosomes. The H1299 cells were treated either with IR alone or the inhibitor alone or with their combination. Lys05 in 2 µM concentration was added to the cells one hour before irradiation (2 Gy). For the sake of visualization, the cells were stained with the green dye—LysoSensor Green DND-189. H1299 cells were imaged by fluorescence microscopy at an interval of 48 hours after the treatment **(A)**. The intensity of fluorescence was measured by flow cytometry 48 hours after the treatment **(B)**. The intensity plot displays average values ±SD from one experiment performed in triplicate. * Significant difference compared to control (p-value < 0.05). ** Significant difference compared to control (p-value < 0.01). # Significant difference compared to the non-irradiated group (p-value < 0.05).

5 Summary of the key results I

In this section, we discussed the mechanisms associated with the inhibition of autophagy using the autophagy inhibitor—Lys05. Based on all the analyzes we have performed in this regard, we can report the following key results:

- the dose- and concentration-dependent decrease in cell proliferation suggested a successful radiosensitization of H1299 cells;
- the phosphoproteomic analysis revealed AKT1S1 and p62 as the main regulatory proteins in autophagy activation and ULK1 phosphorylated on Ser638 as the main regulatory protein in autophagy inhibition;
- WB and qRT-PCR analyses confirmed the successful inhibition of autophagy by detecting the protein markers of autophagic flux—p62 and LC3 along with the gene expression of their related genes—*SQSTM1* and *BNIP3*;
- visible accumulation of autophagosomes and lysosomes inside the cells indicated the inhibition of autophagy by the blockade of autophagosome–lysosome fusion.

Taken together, we found out that one hour after irradiation, autophagy was preferably activated as a cell defensive response against IR. The inhibitory effect of Lys05 manifested itself 48 hours after irradiation. Our findings suggest that the critical regulatory pathway in the autophagy inhibition is the AMPK–ULK1–ATG13 signaling. Consistently, the inhibition of autophagy is presumably the result of a blockade of autophagosome–lysosome fusion.

6 Optimization of the phosphoproteomic workflow

In order to study molecular mechanisms of autophagy inhibition and to quantify the relative proteomic change using differential treatments, we employed a popular technique of quantitative proteomics—stable isotope labeling by amino acids in cell culture (SILAC). SILAC uses the incorporation of isotopically labeled amino acids, which differ in a mass recognized by a mass spectrometer. From the ratio of these masses, the relative quantity of a particular peptide is then determined [63,64]. However, the SILAC approach requires precise execution of all steps. Therefore, appropriate optimization of this technique is necessary before the analysis.

6.1 Optimization of the initial steps

In the beginning, we needed to optimize the first step of SILAC procedure—incorporation of amino acids into the cells. Since isotopically-labeled ("heavy") amino acids are biologically identical to natural unlabeled ("light") amino acids, cells do not distinguish them and incorporate them with the same affinity. However, a specified number of doublings needs to be performed to incorporate labeled amino acids entirely [65]. In this regard, we relied on the workflow by Ong and Mann, who reported at least five doublings for the complete incorporation of labeled amino acids [66]. We first applied this procedure to MOLT-4 cells, as described in **Publication no. 4**. Later, we successfully used the same strategy in our study on H1299 cells. Minimal incorporation of 95% should be achieved for proper phosphoproteomic analysis [67]. Histograms in Figure 8 depict the incorporation rates of the labeled lysine and arginine into the H1299 cells that we achieved in our study.

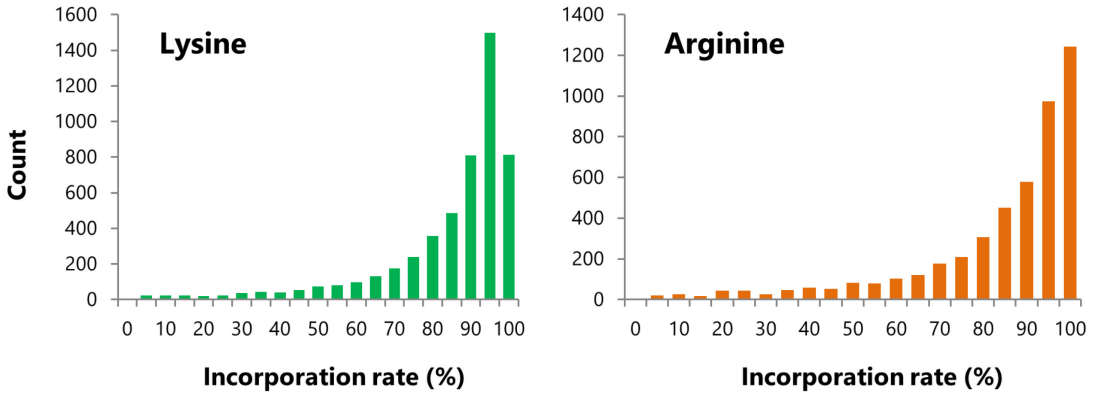

Figure 8. Incorporation rate of labeled lysine and arginine, respectively.

Another important issue we had to deal with was an arginine-to-proline conversion. When performing the SILAC technique, labeled arginine tends to convert to proline [68,69], which is undesired as it leads to the loss of the quantitative information provided by the labeled arginine. This issue could be overcome by adding a certain amount of proline into the cultivation medium, as proposed by Bendall et al. [70] and reported in **Publication no. 4**. Using this approach, we identified up to 33% more peptides containing labeled arginine in H1299 cells than without its addition.

6.2 *Optimization of the phosphopeptide enrichment—the critical step of the phosphoproteomic study*

Probably the most crucial step throughout the phosphoproteomic studies is the enrichment for phosphopeptides. Generally, phosphopeptide enrichment is essential for state-of-the-art phosphoproteomic analysis. Many different phosphopeptide enrichment techniques have been reviewed so far [71–73]. These techniques involve immunoprecipitation, immobilized metal affinity chromatography (IMAC), metal oxide affinity chromatography (MOAC) using titanium dioxide (TiO_2), or zirconium dioxide (ZrO_2), sequential elution from IMAC (SIMAC), and more [72].

Although a number of enrichment techniques were successfully introduced for phosphoproteomic research [74], TiO_2-based MOAC can be considered the most common. This is mainly due to the robustness of the workflow, selectivity of TiO_2 for phosphopeptides, and also due to the commercial availability of various TiO_2 materials such as TiO_2 microparticles (Titansphere, GL Sciences, and Sachtopore-NP, Sachtleben Chemie GmbH), pre-packed TiO_2 tips (Pierce— Spin Tips, Thermo Scientific and Glygen NuTips, Glygen Corp.), TiO_2 columns for on-line applications (TiO_2 Nano-Trap

Columns, Thermo Scientific), and more. Its popularity is also documented by the outstanding enrichment performance and the simple manipulation of the TiO_2 resins [75].

Pinkse et al. first introduced the TiO_2-based MAOC in 2004, which used TiO_2 microparticles (Titansphere®) for the selective phosphopeptide enrichment [76]. They loaded an acidified peptide sample onto a column filled with TiO_2 microspheres, and after several sequential washing steps, they eluted the enriched phosphopeptides using an alkaline buffer (pH 9) [76]. However, a significant improvement in the selectivity of phosphopeptide isolation was achieved by adding certain carboxylic compounds into the sample to prevent non-specific binding of non-phosphorylated peptides [77,78].

In our study, we employed a similar approach when using Titansphere® microparticles for phosphopeptide enrichment, as reported in **Publications 3**, **4**, and **5**. To prevent non-specific binding of non-phosphorylated peptides, we added a glutamic acid into samples, similarly as optimized in **Publication 4**. Besides, unlike Salovska et al. who performed enrichment for phosphopeptides in a test tube executing several rinsing and aspiration steps, we introduced Mobicol spin columns for easy and efficient enrichment, while avoiding the repeated aspiration.

6.3 Optimization of the phosphopeptide sample fractionation

Nowadays, in-depth phosphoproteomic methods do not rely solely on the simple identification of phosphoproteins/phosphopeptides. On the contrary, suitable improvements to these methods leading to the relative quantification of the identified phosphoproteins/phosphopeptides, come to the forefront. Several papers review possible approaches to the relative quantification of phosphopeptides in phosphoproteomic studies [79–81].

Currently, fractionation before LC–MS/MS analysis seems to become a common good practice in quantitative proteomics, due to the higher number of peptides identified and quantified by LC–MS/MS [82,83]. However, in the case of phosphoproteomics, there is a dilemma of whether it is better to fractionate first and consequently enrich each fraction for phosphopeptides or *vice versa*. In general, both approaches are applicable. In the first case, a more selective enrichment may be achieved, while the latter one may be less elaborate, yet still adequately efficient. For the time being, fractionation before enrichment for phosphopeptides remains the gold standard in phosphoproteomic analyses [84–86].

In this regard, we have attempted to change the usual standards and developed a workflow for a simple microgradient separation of enriched phosphopeptides based on C18 microcolumns. This technique enables enrichment for phosphopeptides before their fractionation, which substantially simplifies the entire workflow and extends the degree of phosphoproteome analysis straightforwardly. The most important findings concerning the development of our microgradient technique are summarized in this thesis. In depth, our technique is described *in extenso* in **Publication no. 5**.

When optimizing our microgradient fractionation technique, we have built our starting setup based on the commonly used proteomic workflow for high-pH-reversed-phase (high-pH-RP) fractionation of complex peptide mixtures [87] and phosphoproteomic analyses [86,88]. High-pH-RP fractionation is currently a leading peptide fractionation technique in quantitative proteomics, mainly due to its robustness and high resolution of quantified peptides [87]. However, we found out that in its conventional setting (mobile phases buffered around pH 10), phosphopeptides do not bind effectively to the RP; instead, they remain in the flow-through, and care has to be taken not to lose them during the analysis. This finding is shown in Figure 9, where the first fraction represents the flow-through. Moreover, although we detected some phosphopeptides in fractions 2 to 10, most of them eluted in fraction 1. In fact, the first fraction (flow-through) contained up to 25% of all identified phosphopeptides. Therefore, these phosphopeptides had to be carefully processed to avoid further undesired losses.

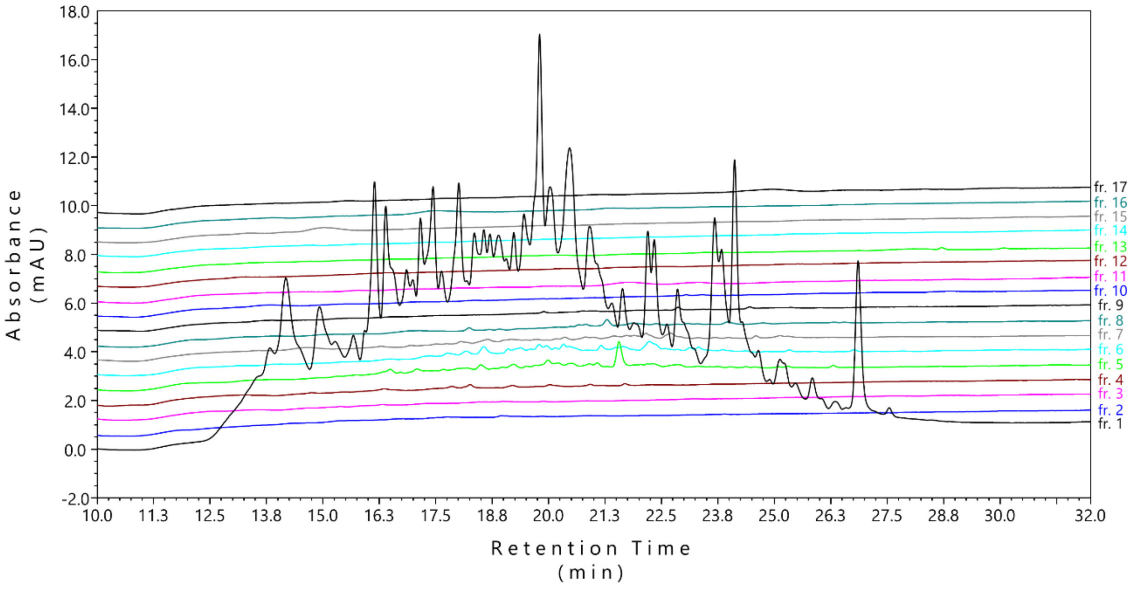

Figure 9. LC–UV chromatograms of the fractionated TiO_2-enriched phosphopeptide sample obtained from trypsin-digested H1299 cell lysate. The fractionation was performed using the conventional reversed-phase microgradient separation with the acetonitrile (ACN) gradient under basic pH conditions. The first fraction was the flow-through of the TiO_2-enriched phosphopeptides dissolved in loading buffer of 2% ACN/20 mM ammonium formate (pH 10), and fractions 2–17 were eluted from the microcolumn using the manually formed ACN gradient containing 20 mM ammonium formate buffered at pH 10 (see Table 1 for a detailed composition of the mobile phase used for phosphopeptide fractionation in conventional elution scheme).

Previous findings led us to a series of optimization steps of the conventional fractionation setup involving: i) changes in the composition of loading buffer, ii) introduction of pH gradient in the elution of phosphopeptide fractions, iii) narrowing the range of acetonitrile (ACN) concentration in the elution gradient, and iv) setting up the suitable elution volumes for particular fractions. Applying these optimizations, we introduced a pH/ACN-gradient-RP microcolumn fractionation. Table 1 describes the differences in mobile phase composition between the conventional and optimized approaches.

Table 1. Comparison of the composition of the conventional high-pH-RP and our optimized pH/acetonitrile (ACN)-gradient-RP elution mobile phases.

		1	2	3	4	5	6
Conventional elution mobile phase	ACN	400	320	240	160	80	20
	200 mM $HCOONH_4$	100	100	100	100	100	100
	H_2O	500	580	660	740	820	880
	ACN concentration	*40%*	*32%*	*24%*	*16%*	*8%*	*2%*
	Measured pH	*10.0*	*10.0*	*10.0*	*10.0*	*10.0*	*10.0*
Optimized elution mobile phase	1% acetic acid	100	100	100	100	100	100
	80% ACN/200 mM NH_4OH	300	250	200	150	100	50
	H_2O	600	650	700	750	800	850
	ACN concentration	*24%*	*20%*	*16%*	*12%*	*8%*	*4%*
	Measured pH	*6.57*	*5.64*	*5.19*	*4.80*	*4.42*	*3.92*

Conventional high-pH-RP elution mobile phase involved gradient of ACN (2%–40%). Optimized pH/ACN-gradient-RP elution mobile phase involved a gradient of both pH (3.92–6.57) and ACN (4%–24%). The volume of each component of mobile phases is given in microliters.

Using the optimized elution mobile phase, we successfully fractionated a phosphopeptide sample into 17 fractions, as shown in Figure 10A. In this case, we loaded the phosphopeptide sample onto microcolumn in a loading buffer acidified to pH 2, which contrasts with the conventional approach, where we used a loading buffer of pH 10. This modification is also advantageous because it minimizes the hydrolysis of phosphopeptides under alkaline conditions [89,90].

To optimize the elution of phosphopeptides, we adjusted the composition of the elution mobile phase by introducing the pH and ACN gradient to the mobile phase, ranging from pH 3.9 to pH 6.6 and 4% to 24% of ACN, respectively. Such optimization led to more evenly distributed phosphopeptide fractions.

We also optimized the elution volumes for each fraction. Previously, we collected flow-through as the first fraction and 2nd–17th fractions eluted in 1.5 μL. Now, we omitted the flow-through, and then the first fraction eluted in 3 μL, 2nd–16th fractions eluted in 1 μL and 17th fraction eluted in 6 μL. Although the last fraction collected a more significant part of the elution volume (6 uL of 24 uL) and the LC–UV analysis showed a significant portion of peptides, the number of identified phosphopeptides was similar to the previous fractions. This is depicted in Figure 10B. When analyzing the optimized setup in three biological replicates, we identified a significantly higher number of phosphopeptides (more than a 3-fold increase) in the fractionated sample compared to the purified one, as shown in Figure 10C.

Naturally, our optimized workflow has some limitations, such as the manual handling of the separation, the limited upper pressure applied during chromatography

separation, and the prolonged LC–MS/MS analysis time. On the other side, its most beneficial aspect is in a fast and easy setup. Moreover, it is fully reproducible and truly inexpensive.

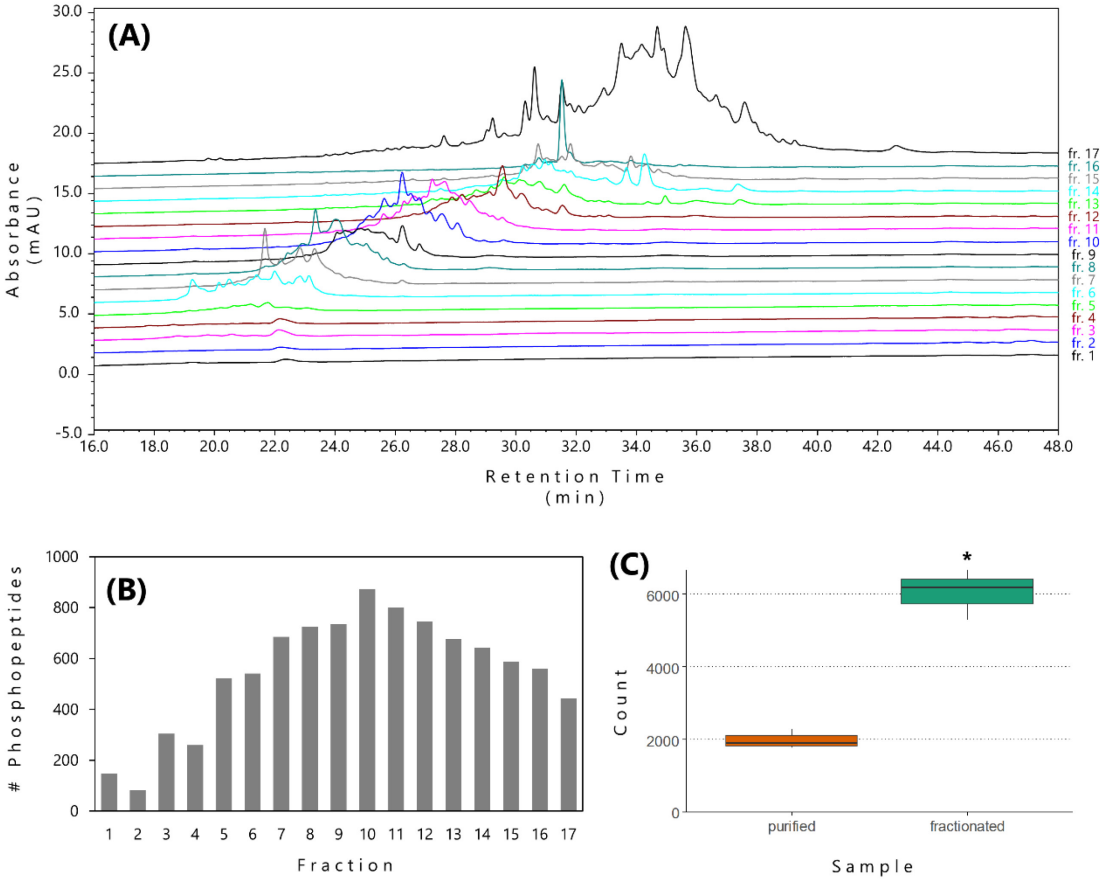

Figure 10. LC–UV chromatogram of fractionated TiO_2-enriched phosphopeptide sample obtained from trypsin-digested H1299 cell lysate **(A)**. The fractionation scheme of the microgradient elution was optimized for a more uniform distribution of peptides throughout the elution fractions (see Table 1 for the detailed composition of the mobile phases used for phosphopeptide fractionation in the optimized elution scheme). Phosphopeptides identified using LC–MS/MS in each fraction visualized as a histogram **(B)**. Statistical comparison between phosphopeptides identified in the purified sample and the fractionated sample visualized as a boxplot of all three replicates **(C)**. * Significant difference compared to purified sample (p-value < 0.005).

7 Summary of the key results II

In this section, we discussed all the optimization steps that either must be performed before the analysis for proper phosphoproteomic study or could be added to simplify and improve the quantitative phosphoproteomic study. In this regard, we can report the following key results:

- at least five doublings of H1299 cells are needed for proper incorporation of labeled amino acids to achieve a minimal incorporation rate of 95%;
- addition of the proper amount of proline successfully prevents the conversion of labeled arginine to proline that may hamper the optimal quantification;
- employing the Mobicol spin columns in the enrichment for phosphopeptides using the TiO_2 microparticles significantly simplifies the enrichment step;
- the introduction of pH/ACN-gradient-RP technique in the fractionation of phosphopeptides significantly increases the number of identified phosphopeptides and also simplifies the fractionation step itself.

8 Conclusion

Cytoprotective autophagy has been proved to play a crucial role in radioresistance of cancer cells. Suitable enhancement of the current treatment scheme leading to their sensitization towards IR is therefore necessary for a proper and effective anti-cancer therapy.

In this regard, in our study, we focused on mechanisms of cytoprotective autophagy in terms of molecular biology and quantitative phosphoproteomics to elucidate its connection with signaling pathways that underlie radioresistance. In more detail, we studied the impact of autophagy inhibitor—Lys05, which abrogated the cytoprotective autophagy and examined the influence of autophagy inhibition on radioresistance and associated radiosensitization.

In general, we confirmed the successful radiosensitization of non-small cell lung cancer cells (H1299, p53-negative) after combined treatment with Lys05 and IR, since we observed a decreased survival rate. Although we expected autophagy to be inhibited early after irradiation, we detected autophagy rather to be activated one hour after irradiation, and the real inhibitory effect of Lys05 prevailed 48 hours after irradiation.

Phosphoproteomic analysis with subsequent biological evaluation identified the AMPK–ULK1–ATG13 pathway as the fundamental regulatory signaling pathway in Lys05-activated inhibition of autophagy. This pathway contributes to the regulation of the autophagosome–lysosome fusion and its blockade. Importantly, it has been established as the Lys05 mechanism of action as we observed significant accumulation of autophagosomes and lysosomes within the H1299 cells.

In addition, the use of state-of-the-art detection devices has enabled us to obtain all these technically sounded results. However, even the best practices require optimization. Regarding quantitative phosphoproteomics, we attempted to change current procedures to improve the identification and quantification of phosphoproteins. We have introduced a microcolumn technique based on a C18 reversed-phase, which allows the fractionation of phosphopeptides after their enrichment. This is a significant step forward that simplifies current fractionation approaches while its operating costs are lower in many respects because it does not require expensive instrumentation.

Taken together, in our study, we focused on revealing the mechanisms associated with the radioresistance of non-small cell lung cancer, which is the most critical issue in the treatment of this type of cancer with IR. While there are only a limited number of

studies dealing with the effects of Lys05 in combination with IR on cancer cells, our work significantly contributes to the identification of the mechanisms by which Lys05 participates in the radiosensitization of tumor cells at both cellular and molecular level.

9 References

1. Linkos - Česká republika a rakovina v číslech. Available online: https://www.linkos.cz/narodni-onkologicky-program/co-musite-vedet/ceska-republika-a-rakovina-v-cislech/ (accessed on Jul 2, 2020).
2. Dušek, L.; Mužík, J.; Kubásek, M.; Koptíková, J.; Žaloudík, J.; Vyzula, R. Epidemiologie zhoubných nádorů v České republice Available online: www.svod.cz (accessed on Jul 2, 2020).
3. Zappa, C.; Mousa, S.A. Non-small cell lung cancer: current treatment and future advances. *Transl Lung Cancer Res* **2016**, *5*, 288–300, doi:10.21037/tlcr.2016.06.07.
4. PDQ Adult Treatment Editorial Board Non-Small Cell Lung Cancer Treatment (PDQ®): Health Professional Version. In *PDQ Cancer Information Summaries*; National Cancer Institute (US): Bethesda (MD), 2002.
5. Ondrej, M.; Cechakova, L.; Durisova, K.; Pejchal, J.; Tichy, A. To live or let die: Unclear task of autophagy in the radiosensitization battle. *Radiother Oncol* **2016**, *119*, 265–275, doi:10.1016/j.radonc.2016.02.028.
6. Amaravadi, R.K.; Winkler, J.D. Lys05: a new lysosomal autophagy inhibitor. *Autophagy* **2012**, *8*, 1383–1384, doi:10.4161/auto.20958.
7. Levine, B.; Klionsky, D.J. Development by self-digestion: molecular mechanisms and biological functions of autophagy. *Dev. Cell* **2004**, *6*, 463–477, doi:10.1016/s1534-5807(04)00099-1.
8. Mizushima, N.; Komatsu, M. Autophagy: renovation of cells and tissues. *Cell* **2011**, *147*, 728–741, doi:10.1016/j.cell.2011.10.026.
9. Hale, A.N.; Ledbetter, D.J.; Gawriluk, T.R.; Rucker, E.B. Autophagy: regulation and role in development. *Autophagy* **2013**, *9*, 951–972, doi:10.4161/auto.24273.
10. Liang, N.; Jia, L.; Liu, Y.; Liang, B.; Kong, D.; Yan, M.; Ma, S.; Liu, X. ATM pathway is essential for ionizing radiation-induced autophagy. *Cell. Signal.* **2013**, *25*, 2530–2539, doi:10.1016/j.cellsig.2013.08.010.
11. Chen, L.-H.; Chu, P.-M.; Lee, Y.-J.; Tu, P.-H.; Chi, C.-W.; Lee, H.-C.; Chiou, S.-H. Targeting protective autophagy exacerbates UV-triggered apoptotic cell death. *Int J Mol Sci* **2012**, *13*, 1209–1224, doi:10.3390/ijms13011209.
12. Reggiori, F.; Komatsu, M.; Finley, K.; Simonsen, A. Selective Types of Autophagy. *Int J Cell Biol* **2012**, *2012*, doi:10.1155/2012/156272.
13. Glick, D.; Barth, S.; Macleod, K.F. Autophagy: cellular and molecular mechanisms. *J. Pathol.* **2010**, *221*, 3–12, doi:10.1002/path.2697.
14. Xie, Z.; Klionsky, D.J. Autophagosome formation: core machinery and adaptations. *Nat. Cell Biol.* **2007**, *9*, 1102–1109, doi:10.1038/ncb1007-1102.
15. Yin, Z.; Pascual, C.; Klionsky, D.J. Autophagy: machinery and regulation. *Microb Cell* **2016**, *3*, 588–596, doi:10.15698/mic2016.12.546.
16. Pyo, J.O.; Nah, J.; Jung, Y.K. Molecules and their functions in autophagy. *Exp. Mol. Med.* **2012**, *44*, 73–80, doi:10.3858/emm.2012.44.2.029.
17. Yu, L.; Chen, Y.; Tooze, S.A. Autophagy pathway: Cellular and molecular mechanisms. *Autophagy* **2018**, *14*, 207–215, doi:10.1080/15548627.2017.1378838.
18. Heras-Sandoval, D.; Pérez-Rojas, J.M.; Hernández-Damián, J.; Pedraza-Chaverri, J. The role of PI3K/AKT/mTOR pathway in the modulation of autophagy and the clearance of protein aggregates in neurodegeneration. *Cell. Signal.* **2014**, *26*, 2694–2701, doi:10.1016/j.cellsig.2014.08.019.
19. Yang, Z.; Klionsky, D.J. An overview of the molecular mechanism of autophagy. *Curr. Top. Microbiol. Immunol.* **2009**, *335*, 1–32, doi:10.1007/978-3-642-00302-8_1.

20. Mizushima, N. Autophagy: process and function. *Genes Dev.* **2007**, *21*, 2861–2873, doi:10.1101/gad.1599207.
21. Mehrpour, M.; Esclatine, A.; Beau, I.; Codogno, P. Overview of macroautophagy regulation in mammalian cells. *Cell Res.* **2010**, *20*, 748–762, doi:10.1038/cr.2010.82.
22. Kroemer, G.; Mariño, G.; Levine, B. Autophagy and the integrated stress response. *Mol. Cell* **2010**, *40*, 280–293, doi:10.1016/j.molcel.2010.09.023.
23. Klionsky, D.J.; Codogno, P. The mechanism and physiological function of macroautophagy. *J Innate Immun* **2013**, *5*, 427–433, doi:10.1159/000351979.
24. Eskelinen, E.-L.; Saftig, P. Autophagy: a lysosomal degradation pathway with a central role in health and disease. *Biochim. Biophys. Acta* **2009**, *1793*, 664–673, doi:10.1016/j.bbamcr.2008.07.014.
25. Levine, B.; Kroemer, G. Autophagy in the pathogenesis of disease. *Cell* **2008**, *132*, 27–42, doi:10.1016/j.cell.2007.12.018.
26. Kroemer, G.; Levine, B. Autophagic cell death: the story of a misnomer. *Nat. Rev. Mol. Cell Biol.* **2008**, *9*, 1004–1010, doi:10.1038/nrm2529.
27. Fuchs, Y.; Steller, H. Programmed cell death in animal development and disease. *Cell* **2011**, *147*, 742–758, doi:10.1016/j.cell.2011.10.033.
28. Denton, D.; Nicolson, S.; Kumar, S. Cell death by autophagy: facts and apparent artefacts. *Cell Death Differ.* **2012**, *19*, 87–95, doi:10.1038/cdd.2011.146.
29. Denton, D.; Kumar, S. Autophagy-dependent cell death. *Cell Death Differ.* **2019**, *26*, 605–616, doi:10.1038/s41418-018-0252-y.
30. Tsujimoto, Y.; Shimizu, S. Another way to die: autophagic programmed cell death. *Cell Death Differ.* **2005**, *12 Suppl 2*, 1528–1534, doi:10.1038/sj.cdd.4401777.
31. Hanahan, D.; Weinberg, R.A. Hallmarks of cancer: the next generation. *Cell* **2011**, *144*, 646–674, doi:10.1016/j.cell.2011.02.013.
32. Rao, S.; Tortola, L.; Perlot, T.; Wirnsberger, G.; Novatchkova, M.; Nitsch, R.; Sykacek, P.; Frank, L.; Schramek, D.; Komnenovic, V.; et al. A dual role for autophagy in a murine model of lung cancer. *Nat Commun* **2014**, *5*, 3056, doi:10.1038/ncomms4056.
33. Strohecker, A.M.; Guo, J.Y.; Karsli-Uzunbas, G.; Price, S.M.; Chen, G.J.; Mathew, R.; McMahon, M.; White, E. Autophagy sustains mitochondrial glutamine metabolism and growth of BrafV600E-driven lung tumors. *Cancer Discov* **2013**, *3*, 1272–1285, doi:10.1158/2159-8290.CD-13-0397.
34. Thorburn, A.; Thamm, D.H.; Gustafson, D.L. Autophagy and cancer therapy. *Mol. Pharmacol.* **2014**, *85*, 830–838, doi:10.1124/mol.114.091850.
35. Fulda, S. Autophagy in Cancer Therapy. *Front Oncol* **2017**, *7*, 128, doi:10.3389/fonc.2017.00128.
36. Luo, T.; Fu, J.; Xu, A.; Su, B.; Ren, Y.; Li, N.; Zhu, J.; Zhao, X.; Dai, R.; Cao, J.; et al. PSMD10/gankyrin induces autophagy to promote tumor progression through cytoplasmic interaction with ATG7 and nuclear transactivation of ATG7 expression. *Autophagy* **2016**, *12*, 1355–1371, doi:10.1080/15548627.2015.1034405.
37. Liu, M.; Jiang, L.; Fu, X.; Wang, W.; Ma, J.; Tian, T.; Nan, K.; Liang, X. Cytoplasmic liver kinase B1 promotes the growth of human lung adenocarcinoma by enhancing autophagy. *Cancer Sci.* **2018**, *109*, 3055–3067, doi:10.1111/cas.13746.
38. Wang, J.-S.; Wang, H.-J.; Qian, H.-L. Biological effects of radiation on cancer cells. *Mil Med Res* **2018**, *5*, 20, doi:10.1186/s40779-018-0167-4.
39. Apel, A.; Herr, I.; Schwarz, H.; Rodemann, H.P.; Mayer, A. Blocked autophagy sensitizes resistant carcinoma cells to radiation therapy. *Cancer Res.* **2008**, *68*, 1485–1494, doi:10.1158/0008-5472.CAN-07-0562.
40. Ko, A.; Kanehisa, A.; Martins, I.; Senovilla, L.; Chargari, C.; Dugue, D.; Mariño, G.; Kepp, O.; Michaud, M.; Perfettini, J.-L.; et al. Autophagy inhibition radiosensitizes in vitro, yet reduces radioresponses in vivo due to deficient immunogenic signalling. *Cell Death Differ.* **2014**, *21*, 92–99, doi:10.1038/cdd.2013.124.

41. Lomonaco, S.L.; Finniss, S.; Xiang, C.; Decarvalho, A.; Umansky, F.; Kalkanis, S.N.; Mikkelsen, T.; Brodie, C. The induction of autophagy by gamma-radiation contributes to the radioresistance of glioma stem cells. *Int. J. Cancer* **2009**, *125*, 717–722, doi:10.1002/ijc.24402.
42. Paglin, S.; Hollister, T.; Delohery, T.; Hackett, N.; McMahill, M.; Sphicas, E.; Domingo, D.; Yahalom, J. A novel response of cancer cells to radiation involves autophagy and formation of acidic vesicles. *Cancer Res.* **2001**, *61*, 439–444.
43. Gewirtz, D.A. When cytoprotective autophagy isn't… and even when it is. *Autophagy* **2014**, *10*, 391–392, doi:10.4161/auto.27719.
44. McAfee, Q.; Zhang, Z.; Samanta, A.; Levi, S.M.; Ma, X.-H.; Piao, S.; Lynch, J.P.; Uehara, T.; Sepulveda, A.R.; Davis, L.E.; et al. Autophagy inhibitor Lys05 has single-agent antitumor activity and reproduces the phenotype of a genetic autophagy deficiency. *Proc. Natl. Acad. Sci. U.S.A.* **2012**, *109*, 8253–8258, doi:10.1073/pnas.1118193109.
45. Koukourakis, M.I.; Kalamida, D.; Mitrakas, A.; Pouliliou, S.; Kalamida, S.; Sivridis, E.; Giatromanolaki, A. Intensified autophagy compromises the efficacy of radiotherapy against prostate cancer. *Biochem. Biophys. Res. Commun.* **2015**, *461*, 268–274, doi:10.1016/j.bbrc.2015.04.014.
46. AKT1S1 - Proline-rich AKT1 substrate 1 - Homo sapiens (Human) - AKT1S1 gene & protein Available online: https://www.uniprot.org/uniprot/Q96B36 (accessed on Jan 6, 2020).
47. Nascimento, E.B.M.; Snel, M.; Guigas, B.; van der Zon, G.C.M.; Kriek, J.; Maassen, J.A.; Jazet, I.M.; Diamant, M.; Ouwens, D.M. Phosphorylation of PRAS40 on Thr246 by PKB/AKT facilitates efficient phosphorylation of Ser183 by mTORC1. *Cell. Signal.* **2010**, *22*, 961–967, doi:10.1016/j.cellsig.2010.02.002.
48. Matsumoto, G.; Wada, K.; Okuno, M.; Kurosawa, M.; Nukina, N. Serine 403 phosphorylation of p62/SQSTM1 regulates selective autophagic clearance of ubiquitinated proteins. *Mol. Cell* **2011**, *44*, 279–289, doi:10.1016/j.molcel.2011.07.039.
49. Hong, S.; Freeberg, M.A.; Han, T.; Kamath, A.; Yao, Y.; Fukuda, T.; Suzuki, T.; Kim, J.K.; Inoki, K. LARP1 functions as a molecular switch for mTORC1-mediated translation of an essential class of mRNAs. *Elife* **2017**, *6*, doi:10.7554/eLife.25237.
50. NMD3 - 60S ribosomal export protein NMD3 - Homo sapiens (Human) - NMD3 gene & protein Available online: https://www.uniprot.org/uniprot/Q96D46 (accessed on Jan 6, 2020).
51. GPAT3 - Glycerol-3-phosphate acyltransferase 3 - Homo sapiens (Human) - GPAT3 gene & protein Available online: https://www.uniprot.org/uniprot/Q53EU6 (accessed on Jan 6, 2020).
52. Alers, S.; Löffler, A.S.; Wesselborg, S.; Stork, B. The incredible ULKs. *Cell Commun. Signal* **2012**, *10*, 7, doi:10.1186/1478-811X-10-7.
53. Lin, M.G.; Hurley, J.H. Structure and function of the ULK1 complex in autophagy. *Curr. Opin. Cell Biol.* **2016**, *39*, 61–68, doi:10.1016/j.ceb.2016.02.010.
54. Puente, C.; Hendrickson, R.C.; Jiang, X. Nutrient-regulated phosphorylation of ATG13 inhibits starvation-induced autophagy. *J. Biol. Chem.* **2016**, *291*, 6026–6035, doi:10.1074/jbc.M115.689646.
55. Holczer, M.; Hajdú, B.; Lőrincz, T.; Szarka, A.; Bánhegyi, G.; Kapuy, O. A double negative feedback loop between mTORC1 and AMPK kinases guarantees precise autophagy induction upon cellular stress. *Int J Mol Sci* **2019**, *20*, doi:10.3390/ijms20225543.
56. Fan, X.-Y.; Tian, C.; Wang, H.; Xu, Y.; Ren, K.; Zhang, B.-Y.; Gao, C.; Shi, Q.; Meng, G.; Zhang, L.-B.; et al. Activation of the AMPK-ULK1 pathway plays an important role in autophagy during prion infection. *Sci Rep* **2015**, *5*, 14728, doi:10.1038/srep14728.
57. Bjørkøy, G.; Lamark, T.; Brech, A.; Outzen, H.; Perander, M.; Overvatn, A.; Stenmark, H.; Johansen, T. p62/SQSTM1 forms protein aggregates degraded by autophagy and has a protective effect on huntingtin-induced cell death. *J. Cell Biol.* **2005**, *171*, 603–614, doi:10.1083/jcb.200507002.

58. Mizushima, N.; Yoshimori, T. How to interpret LC3 immunoblotting. *Autophagy* **2007**, *3*, 542–545, doi:10.4161/auto.4600.
59. Tanida, I. Autophagy basics. *Microbiol. Immunol.* **2011**, *55*, 1–11, doi:10.1111/j.1348-0421.2010.00271.x.
60. Makowska, A.; Eble, M.; Prescher, K.; Hoß, M.; Kontny, U. Chloroquine sensitizes nasopharyngeal carcinoma cells but not nasoepithelial cells to irradiation by blocking autophagy. *PLoS ONE* **2016**, *11*, e0166766, doi:10.1371/journal.pone.0166766.
61. Lu, S.; Sung, T.; Lin, N.; Abraham, R.T.; Jessen, B.A. Lysosomal adaptation: how cells respond to lysosomotropic compounds. *PLoS ONE* **2017**, *12*, e0173771, doi:10.1371/journal.pone.0173771.
62. Chikte, S.; Panchal, N.; Warnes, G. Use of LysoTracker dyes: a flow cytometric study of autophagy. *Cytometry A* **2014**, *85*, 169–178, doi:10.1002/cyto.a.22312.
63. Ong, S.-E.; Blagoev, B.; Kratchmarova, I.; Kristensen, D.B.; Steen, H.; Pandey, A.; Mann, M. Stable isotope labeling by amino acids in cell culture, SILAC, as a simple and accurate approach to expression proteomics. *Mol. Cell Proteomics* **2002**, *1*, 376–386, doi:10.1074/mcp.m200025-mcp200.
64. Zhu, H.; Pan, S.; Gu, S.; Bradbury, E.M.; Chen, X. Amino acid residue specific stable isotope labeling for quantitative proteomics. *Rapid Commun. Mass Spectrom.* **2002**, *16*, 2115–2123, doi:10.1002/rcm.831.
65. Ong, S.-E.; Mann, M. A practical recipe for stable isotope labeling by amino acids in cell culture (SILAC). *Nat Protoc* **2006**, *1*, 2650–2660, doi:10.1038/nprot.2006.427.
66. Ong, S.-E.; Mann, M. Identifying and quantifying sites of protein methylation by heavy methyl SILAC. *Curr Protoc Protein Sci* **2006**, *Chapter 14*, Unit 14.9, doi:10.1002/0471140864.ps1409s46.
67. Stöhr, G.; Tebbe, A. Chapter 8:Quantitative LC-MS of Proteins. In *Protein and Peptide Analysis by LC-MS*; 2011; pp. 104–122.
68. Lössner, C.; Warnken, U.; Pscherer, A.; Schnölzer, M. Preventing arginine-to-proline conversion in a cell-line-independent manner during cell cultivation under stable isotope labeling by amino acids in cell culture (SILAC) conditions. *Anal. Biochem.* **2011**, *412*, 123–125, doi:10.1016/j.ab.2011.01.011.
69. Van Hoof, D.; Pinkse, M.W.H.; Oostwaard, D.W.-V.; Mummery, C.L.; Heck, A.J.R.; Krijgsveld, J. An experimental correction for arginine-to-proline conversion artifacts in SILAC-based quantitative proteomics. *Nat. Methods* **2007**, *4*, 677–678, doi:10.1038/nmeth0907-677.
70. Bendall, S.C.; Hughes, C.; Stewart, M.H.; Doble, B.; Bhatia, M.; Lajoie, G.A. Prevention of amino acid conversion in SILAC experiments with embryonic stem cells. *Mol. Cell Proteomics* **2008**, *7*, 1587–1597, doi:10.1074/mcp.M800113-MCP200.
71. Tichy, A.; Salovska, B.; Rehulka, P.; Klimentova, J.; Vavrova, J.; Stulik, J.; Hernychova, L. Phosphoproteomics: searching for a needle in a haystack. *J Proteomics* **2011**, *74*, 2786–2797, doi:10.1016/j.jprot.2011.07.018.
72. Fíla, J.; Honys, D. Enrichment techniques employed in phosphoproteomics. *Amino Acids* **2012**, *43*, 1025–1047, doi:10.1007/s00726-011-1111-z.
73. Dunn, J.D.; Reid, G.E.; Bruening, M.L. Techniques for phosphopeptide enrichment prior to analysis by mass spectrometry. *Mass Spectrom Rev* **2010**, *29*, 29–54, doi:10.1002/mas.20219.
74. Ruprecht, B.; Koch, H.; Medard, G.; Mundt, M.; Kuster, B.; Lemeer, S. Comprehensive and reproducible phosphopeptide enrichment using iron immobilized metal ion affinity chromatography (Fe-IMAC) columns. *Mol. Cell Proteomics* **2015**, *14*, 205–215, doi:10.1074/mcp.M114.043109.
75. Thingholm, T.E.; Larsen, M.R. The use of titanium dioxide for selective enrichment of phosphorylated peptides. *Methods Mol. Biol.* **2016**, *1355*, 135–146, doi:10.1007/978-1-4939-3049-4_9.

76. Pinkse, M.W.H.; Uitto, P.M.; Hilhorst, M.J.; Ooms, B.; Heck, A.J.R. Selective isolation at the femtomole level of phosphopeptides from proteolytic digests using 2D-NanoLC-ESI-MS/MS and titanium oxide precolumns. *Anal. Chem.* **2004**, *76*, 3935–3943, doi:10.1021/ac0498617.
77. Larsen, M.R.; Thingholm, T.E.; Jensen, O.N.; Roepstorff, P.; Jørgensen, T.J.D. Highly selective enrichment of phosphorylated peptides from peptide mixtures using titanium dioxide microcolumns. *Mol. Cell Proteomics* **2005**, *4*, 873–886, doi:10.1074/mcp.T500007-MCP200.
78. Thingholm, T.E.; Jørgensen, T.J.D.; Jensen, O.N.; Larsen, M.R. Highly selective enrichment of phosphorylated peptides using titanium dioxide. *Nat Protoc* **2006**, *1*, 1929–1935, doi:10.1038/nprot.2006.185.
79. Fenselau, C. A review of quantitative methods for proteomic studies. *J. Chromatogr. B Analyt. Technol. Biomed. Life Sci.* **2007**, *855*, 14–20, doi:10.1016/j.jchromb.2006.10.071.
80. Nita-Lazar, A.; Saito-Benz, H.; White, F.M. Quantitative phosphoproteomics by mass spectrometry: past, present, and future. *Proteomics* **2008**, *8*, 4433–4443, doi:10.1002/pmic.200800231.
81. Deracinois, B.; Flahaut, C.; Duban-Deweer, S.; Karamanos, Y. Comparative and quantitative global proteomics approaches: an overview. *Proteomes* **2013**, *1*, 180–218, doi:10.3390/proteomes1030180.
82. Manadas, B.; Mendes, V.M.; English, J.; Dunn, M.J. Peptide fractionation in proteomics approaches. *Expert Rev Proteomics* **2010**, *7*, 655–663, doi:10.1586/epr.10.46.
83. Wang, H.; Chang-Wong, T.; Tang, H.-Y.; Speicher, D.W. Comparison of extensive protein fractionation and repetitive LC-MS/MS analyses on depth of analysis for complex proteomes. *J. Proteome Res.* **2010**, *9*, 1032–1040, doi:10.1021/pr900927y.
84. Mertins, P.; Yang, F.; Liu, T.; Mani, D.R.; Petyuk, V.A.; Gillette, M.A.; Clauser, K.R.; Qiao, J.W.; Gritsenko, M.A.; Moore, R.J.; et al. Ischemia in tumors induces early and sustained phosphorylation changes in stress kinase pathways but does not affect global protein levels. *Mol. Cell Proteomics* **2014**, *13*, 1690–1704, doi:10.1074/mcp.M113.036392.
85. Mertins, P.; Qiao, J.W.; Patel, J.; Udeshi, N.D.; Clauser, K.R.; Mani, D.R.; Burgess, M.W.; Gillette, M.A.; Jaffe, J.D.; Carr, S.A. Integrated proteomic analysis of post-translational modifications by serial enrichment. *Nat. Methods* **2013**, *10*, 634–637, doi:10.1038/nmeth.2518.
86. Batth, T.S.; Francavilla, C.; Olsen, J.V. Off-line high-pH reversed-phase fractionation for in-depth phosphoproteomics. *J. Proteome Res.* **2014**, *13*, 6176–6186, doi:10.1021/pr500893m.
87. Gilar, M.; Olivova, P.; Daly, A.E.; Gebler, J.C. Two-dimensional separation of peptides using RP-RP-HPLC system with different pH in first and second separation dimensions. *J Sep Sci* **2005**, *28*, 1694–1703, doi:10.1002/jssc.200500116.
88. Batth, T.S.; Olsen, J.V. Offline high pH reversed-phase peptide fractionation for deep phosphoproteome coverage. *Methods Mol. Biol.* **2016**, *1355*, 179–192, doi:10.1007/978-1-4939-3049-4_12.
89. Kemp, B.E. Relative alkali stability of some peptide o-phosphoserine and o-phosphothreonine esters. *FEBS Lett.* **1980**, *110*, 308–312, doi:10.1016/0014-5793(80)80099-8.
90. Sickmann, A.; Meyer, H.E. Phosphoamino acid analysis. *Proteomics* **2001**, *1*, 200–206, doi:10.1002/1615-9861(200102)1:2<200::AID-PROT200>3.0.CO;2-V.

10 List of publications

Publications associated with the topic of dissertation thesis

1. **Ondrej M***, Cechakova L*, Durisova K, Pejchal J, Tichy A. To live or let die: Unclear task of autophagy in the radiosensitization battle. *Radiotherapy and Oncology*. 2016;119:265-75. **IF(2016) = 4.328; Q1**

2. Cechakova L, **Ondrej M**, Pavlik V, Jost P, Cizkova D, Bezrouk A, Pejchal J, Amaravadi RK, Winkler JD, Tichy A. A potent autophagy inhibitor (Lys05) enhances the impact of ionizing radiation on human lung cancer cells H1299. *International Journal of Molecular Sciences*. 2019;20(23):5881. **IF(2019) = 4.183; Q2**

3. **Ondrej M**, Cechakova L, Fabrik I, Klimentova J, Tichy A. Lys05 – A promising autophagy inhibitor in the radiosensitization battle: Phosphoproteomic perspective. *Cancer Genomics and Proteomics*. 2020;17(4):369-382. **IF(2019) = 3.147; Q2**

4. Šalovská B, Janečková H, Fabrik I, Karlíková R, Čecháková L, **Ondrej M**, Link M, Friedecký D, Tichý A. Radio-sensitizing effects of VE-821 and beyond: Distinct phosphoproteomic and metabolomic changes after ATR inhibition in irradiated MOLT-4 cells. *PLoS One*. 2018;13:e0199349. **IF(2018) = 2.776; Q1**

5. **Ondrej M**, Rehulka P, Rehulkova H, Kupcik R, Tichy A. Fractionation of enriched phosphopeptides using pH/acetonitrile-gradient-reversed-phase microcolumn separation in combination with LC–MS/MS analysis. *International Journal of Molecular Sciences*. 2020;21(11):3971. **IF(2019) = 4.183; Q2**

Other publications

6. Klionsky D, …, **Ondrej M**, et al. Guidelines for the use and interpretation of assays for monitoring autophagy (4th edition). *Autophagy.* 2020 (in press). **IF = 11.059; Q1**

7. Durisova K, Cechakova L, Jost P, Sinkorova Z, Kmochova A, Pejchal J, **Ondrej M**, Vavrova J, Tichy A. DNA repair inhibitors as radiosensitizers in human lung cells. *Journal of Applied Biomedicine*. 2018;16:66-74. **IF(2018) = 1.573; Q3**

8. Pejchal J, Sinkorova Z, Tichy A, Pruchova S, Kmochova A, Durisova K, Cechakova L, Lierova A, **Ondrej M**, et al. Epidermal growth factor attenuates delayed ionizing radiation-induced tissue damage in bone marrow transplanted mice. *Radiation Research*. 2016;186(3):264-74. **IF(2016) = 2.539; Q1**

11 Appendices

Further are enclosed author's publications *in extenso* and a brief overview of other co-authored publications.

Publication no. 1

To live or let die: Unclear task of autophagy in radiosensitization battle.

Ondrej M*, Cechakova L*, Durisova K, Pejchal J, Tichy A

Radiotherapy and oncology. 2016;119(2):265-75

IF(2016) = 4.328; Q1

Author contribution (50%)—main author; the author performed the literature search, took the lead in writing the article, and editing the article

In this review, the authors described autophagy as an elementary mechanism in cells, its forms, processes, and functions. They pointed out the role of autophagy in cancer cells and its relation to radiotherapy. Besides, the authors compared two opposing roles of autophagy in tumor cells and the possibilities of its modulation in the context of radiosensitization of cancer cells.

* These authors contributed to the work equally

Radiotherapy and Oncology 119 (2016) 265–275

Contents lists available at ScienceDirect

Radiotherapy and Oncology

journal homepage: www.thegreenjournal.com

Review

To live or let die: Unclear task of autophagy in the radiosensitization battle

Martin Ondrej [a,1], Lucie Cechakova [a,1], Kamila Durisova [a], Jaroslav Pejchal [a], Ales Tichy [a,b,*]

[a] Department of Radiobiology, Faculty of Military Health Sciences in Hradec Kralove, University of Defense in Brno; and [b] Centre of Biomedical Research, University Hospital, Hradec Kralove, Czech Republic

ARTICLE INFO

Article history:
Received 20 November 2015
Received in revised form 26 January 2016
Accepted 18 February 2016
Available online 15 March 2016

Keywords:
Autophagy
Ionizing radiation
Radiotherapy
Radiosensitization
Inhibition
Induction

ABSTRACT

Radiation-induced autophagy is believed to represent a radioprotective mechanism of cancer cells. Thus, its inhibition should support radiation treatment and increase its efficacy. On the other hand, there is evidence that radiation alone or in combination with various chemical agents can induce autophagy that results into increased cell death, especially within transformed apoptosis-resistant cells.

In this paper, besides description of autophagic process and its relation to cancer and radiotherapy, we compared two contradictory radiosensitization approaches that employ inhibition and induction of autophagy. In spite of the classical concept based on cytoprotective model, there is a plethora of recently developed inducers of autophagy, which indicates the future trend in radiosensitization via modulation of autophagy.

Because contemporary literature is conflicting and inconsistent in this respect, we reviewed the recent studies focused on enhancement of sensitivity of cancer cells toward radiation in regard to autophagy, revealing some striking discrepancies. The deeper the knowledge, the more complex this situation is. To interpret results of various studies correctly one has to take into account the methodology of autophagy assessment and also the fact that radiosensitization might be mediated by other than intrinsic mechanisms related to autophagy. Notwithstanding, targeting autophagy remains an attractive anti-tumor strategy.

© 2016 The Authors. Published by Elsevier Ireland Ltd. Radiotherapy and Oncology 119 (2016) 265–275
This is an open access article under the CC BY-NC-ND license (http://creativecommons.org/licenses/by-nc-nd/4.0/).

Autophagy is an evolutionarily conserved process enabling the degradation and recycling of long-lived proteins or whole organelles during cellular stress conditions or at homeostasis basis. The word autophagy comes from Greek *auto-*, "oneself" and *phagein*, "to eat". This intracellular degrading system is important for maintaining physiological properties in healthy cells and its deregulation may lead to many different diseases, including cancer [1].

Autophagy can be activated as a response of various stimuli, involving ionizing radiation (IR), DNA damage, chemotherapeutic drugs, nutrient, oxygen and growth factor shortage [2,3] or deprivation of amino acids [4]. In some cases, autophagy plays role in cell death, and thus it remains unclear whether autophagy is cytoprotective mechanism or if it contributes to the cell death. Because of the ability of autophagy to remove damaged proteins or organelles, it may paradoxically serve as a mechanism for maintaining irradiated (or otherwise damaged) cells alive [5].

There are many papers that cover the mechanism of autophagy in detail [6–10]. Our aim is to provide a comprehensive review of recent literature regarding modulation of autophagy as a promising tool in radiosensitization of cancer cells. Some authors hypothesized that inhibition of autophagy is for radiosensitization of tumor cells more beneficial than induction, because when autophagy is inhibited, cancer cells cannot utilize autophagy as a pro-survival process to overcome the stresses caused by anticancer therapy, including IR. From a different point of view, it is advantageous to induce autophagy, because it can restrict proliferation of tumor cells and contribute, via various mechanisms, to radiosensitization. Above that, the situation is intricate due to studies claiming that radiosensitization by inducers/inhibitors of autophagy is processed via other than intrinsic mechanisms related to autophagy.

Obviously, literature is in this respect very conflicting. Therefore we reviewed recent studies that focused on radiosensitization and we compared two different approaches that employ inhibition and induction of autophagy.

* Corresponding author at: Faculty of Military Health Sciences, University of Defense, Trebesska 1575, 500 01 Hradec Kralove, Czech Republic.
E-mail address: ales.tichy@unob.cz (A. Tichy).
[1] These authors contributed to the work equally.

http://dx.doi.org/10.1016/j.radonc.2016.02.028
0167-8140/© 2016 The Authors. Published by Elsevier Ireland Ltd.
This is an open access article under the CC BY-NC-ND license (http://creativecommons.org/licenses/by-nc-nd/4.0/).

The process of autophagy

There are three known types of autophagy yet: (1) macroautophagy, (2) microautophagy and (3) chaperone-mediated autophagy (CMA) [11,12].

All of them use lysosome as a tool for degradation of substrates. They differ from each other in mechanism by which cargo is delivered to the lysosome and each of them is also activated under different conditions [1,11,12]. Processes of microautophagy and macroautophagy include participation of membrane. During macroautophagy, a new double-membrane vesicle (autophagosome) is created and surrounds the targeted cytosolic area [13]. Microautophagy is then mediated by lysosomal membrane itself and cytosolic content is engulfed by lysosomal membrane directly [14]. Opposed to the micro- and macroautophagy, CMA is based on direct translocation of substrate across the lysosome membrane via special proteins called chaperones. CMA is a highly selective process which targets only cytosolic proteins. There are two major steps in CMA; firstly, proteins determined to degradation are recognized and secondly, they are delivered through the membrane of lysosome. Chaperone Hsc70 with co-chaperones recognizes a specific peptide sequence of protein. Then protein/chaperone complex interacts with lysosome-associated membrane protein type 2A (LAMP-2A) which is located on the cytosolic side of lysosomal membrane. The full unfolding of the protein is required in order to cross through the lysosomal membrane [15,16].

Macroautophagy (further referred to as autophagy) is a process in which the double-membrane autophagosome (phagophore) is formed to absorb molecules to be degraded. The whole machinery of autophagy is regulated by autophagy related proteins (ATG) coded by autophagy related genes (*ATG*) [17]. "Core" autophagic complexes in mammals are: (1) ULK kinase complex (ATG1/unc-51-like kinase), (2) class III PI3 kinase/vacuolar protein sorting 34 (Vps34) complex, (3) transmembrane protein ATG9-WIPI-1 and (4) two ubiquitin-like conjugation systems ATG12 and LC3 (mammalian homolog for yeast ATG8) [7,18,19].

From the perspective of molecular biology, activation of the ULK1/2 complex is necessary for proper induction of autophagy. Under normal conditions mammalian target of rapamycin complex 1 – mTORC1 (complex of mTOR and regulatory-associated protein of mTOR – RAPTOR) is activated and interacts with ULK complex [19]. This interaction makes mTORC1 phosphorylate ATG13 and ULK1/2 and then blocks kinase activity of ULK complex. Otherwise inhibition of mTOR, caused by nutrient shortage or rapamycin treatment, results in the disconnection of mTOR with the ULK complex [20] and subsequent activation of ULK [18–21].

Nucleation is a step when the isolation membrane is being formed. The main protein complex, which is required for this process, is class III phosphatidylinositol-3-kinase (PI3K). The core of this complex is built-up from proteins Vps34 (class III PI3K), p150 (mammalian homolog for yeast Vps15) and Beclin-1 (mammalian homolog of yeast ATG6). Interaction of Vps34 and Beclin-1 leads to the production of second messenger, phosphatidylinositol 3-phosphate (PI(3)P), which is important for further development of autophagosome [22]. Beclin-1, the crucial protein in modulation of autophagy, has an ability to either induce or inhibit the process of nucleation in dependence on its binding partners [2,21].

Once the isolation membrane is formed, it elongates and closes on itself to form an autophagosome. This process is dependent on two ubiquitin-like conjugation systems, ATG12 and LC3. ATG12 complex takes part in elongation, while LC3 complex is required for the enclosing of double-membrane autophagosome [21]. ATG12 conjugation system involves proteins ATG12, ATG5 and ATG16L which create a multimeric complex and mediate closure of the isolation membrane by LC3 conjugation system [7,19,22,23]. Complex LC3 (mammalian homolog of yeast ATG8) is a key complex for the final step of autophagosome formation [24,25].

Maturation is the last step in autophagolysosome formation. This step is divided into two sub-steps. At first, autophagosome fuses with endosome to form a structure called amphisome. In the second sub-step, amphisome merges with lysosome and produce autophagolysosome [12,13,21]. Degradation of autophagolysosome content is performed by acidic lysosomal hydrolases, which degrade also the inner membrane of autophagolysosome. Products of degradation are released to the cytosol and can be reutilized once again [24]. The process of maturation is controlled by Beclin-1 and its binding partners [21].

Autophagy meets cancer

Development of cancer is related to six biological capabilities, which are characteristic as hallmarks of cancer. They include sustaining proliferative signaling, evading growth suppressors, resisting cell death, enabling replicative immortality, activating invasion and metastasis, and inducing angiogenesis [26]. Angiogenesis is the most significant one, in context of autophagy, because new blood vessels provide nutrition for cancer cells. Defects in angiogenesis and also increased need for ATP and anabolic substrates for biosynthetic processes lead to nutritional misbalance of cancers [27]. This nutritional misbalance developed in cancer cells might be suppressed by activation of autophagy.

Autophagy is in tumor cells activated as a response to various stresses, including starvation, growth factor deprivation, hypoxia, damaging stimuli and proteasome inhibition. The different roles of autophagy in cancer cells seem to depend on tumor type, stage, and genetic context. It is now well established that autophagy can act as a tumor suppressor in early stages of tumorigenesis and as a tumor promoter in developed tumors [28,29]. At the beginning of cancer formation, autophagy suppresses the initiation and further tumor progression. The first reference of autophagy as a tumor suppressor appeared in 1999. It was declared through genetic studies of Beclin-1 [30]. Further examinations on mice with allelic loss of the essential autophagy gene *BECLIN1* (*BECN1*; also known as *ATG6*) revealed development of hepatocellular carcinomas, which clearly demonstrated the necessity of this gene [31,32]. The liver tumors burdened by loss of *BECN1*, suffered from obligate haploinsufficiency and could not tolerate the complete loss of *BECN1* and autophagy. A higher amount of spontaneous tumors appeared in mice lacking one copy of *BECN1* [31,32]. Also autophagy-deficient $BECN1^{+/-}$ and $ATG5^{-/-}$ immortalized baby mouse kidney epithelial cells which were reported to be more susceptible to DNA damage, gene amplification, chromosome instability, and aneuploidy, all of which are clinically associated with tumor progression and poor prognosis [33]. In the initial phase of tumor formation, autophagy plays several roles; it (1) inhibits necrosis and inflammation, (2) prevents oxidative stress and genomic instability, (3) contributes to tumor cell death, (4) modulates the anti-tumor immune response, and (5) inhibits metastasis [34].

Rapidly growing and developed solid tumors are highly exposed to nutrient, growth factor, and oxygen deprivation due to inadequate vascularization. Tumor growth is conditioned via neovascularization in order to pass the metabolic barrier and expand in size. When this requirement is not fulfilled under physiological conditions, the starving cells die by apoptosis [35]. In tumors with defective apoptosis, sustained autophagy possibly contributes to cell survival. Autophagy is localized in metabolically stressed, hypoxic regions of solid tumors and can maintain survival for several weeks [29,33,36].

Starvation is one of the most potent inducers of autophagy. But how do cells recognize nutrient starvation? It seems that tumor cells can recognize the amount of AMP. AMP-activated protein kinase (AMPK) is well described in mediating various stress signals including hypoxia, nutrient starvation, and physical stresses [37]. Only a few minutes are required to recognize nutrient starvation, followed by induction of autophagy. Under conditions of nutrient deprivation, autophagy can also suppress latent apoptotic program, prevent cell death, and thus preserve cellular homeostasis [38]. Indeed, $Braf^{V600E}$ autophagy-deficient tumor cells without alleles of the essential autophagy gene *ATG7* were unable to survive the starvation. Thus, due to the absence of internally supplied glutamine, provided by autophagy-mediated recycling of proteins, *ATG7*-lacking cells were reliant on exogenously supplied glutamine. It seems that autophagy may be a mechanism to provide the tumor cells with glutamine and sustain $Braf^{V600E}$ tumor growth and metabolism [29].

Hypoxia (oxygen concentration <3%) and anoxia (oxygen concentration <0.1%) are both strong inducers of autophagy. Oxygen deprivation can induce autophagy also in the absence of additional stress such as glucose deprivation or serum withdrawal. Induction of autophagy is in human tumor cells performed through various mechanisms [20]. Hypoxia-induced autophagy depends on hypoxia-inducible factor (HIF), while anoxia-induced autophagy is HIF-independent. Upon moderate hypoxia (1–3% oxygen), HIF activates the transcription of *BNIP3* and *BNIP3L*, two proteins which activate further autophagic processes [39]. The role of the *BNIP3* in hypoxia-induced autophagy has been examined by Tracy et al., who proposed that levels of *BNIP3* are modulated by RB tumor suppressor and the amount of *BNIP3* is crucial for the type of cell death [40]. Moreover, Shaaf et al. reported that protective autophagy occurred during hypoxia as a result of ULK1 upregulation which is associated with hypoxia tolerance. Increased level of ULK1 was unfolded protein response- (UPR-) and HIF-1α-pathways-dependent [41]. Additional pathways have also been implicated in hypoxia-induced autophagy. Papandreou et al. showed that hypoxia-induced autophagy is independent of nutrient deprivation, HIF-1α activity, and expression of BCL-2/adenovirus E1B 19 kDa interacting protein 3 (BNIP3). Especially AMP-activated protein kinase (AMPK) signaling pathway was linked with the induction of autophagy under oxygen shortage [42]. Other HIF-independent signaling pathways have been studied by Rouschop et al., who described the importance of UPR protein in activation of autophagy in hypoxic cells. UPR maintains levels of MAP1LC3B and ATG5 through PKR-like ER kinase (PERK) and thus promotes hypoxia tolerance [43].

The withdrawal of growth factors is another potent inducer of autophagy. Growth factors determine the formation of tumors and promote cell survival by maintaining the ability of cells to take up sufficient nutrients to continue ATP production. Thus, low level of growth factors may lead to an impaired development of cancer. Autophagy reflects these conditions and supports survival of growth factors-deprived cells [44]. Autophagic process is then regulated through the mTORC1-unc-51 like autophagy activating kinase 1 (ULK1) complex interactions. When mTORC1 activity is suppressed due to growth factor withdrawal, ULK1 complex becomes derepressed and autophagy is induced [45].

Tumor cells are assumed to prefer glycolysis, which means that they mainly generate energy by non-oxidative breakdown of glucose, even when oxygen is present to respire properly. They display high level of glucose uptake and lactate production as an end product of glucose fermentation in contrast to "healthy" cells, which use oxidative breakdown with pyruvate as an end product of respiration. This form of aerobic glycolysis is termed the "Warburg Effect" [46]. High demands on energy supply in cancerous cells may lead to a severe shortage of energy. Tumor cells that are not able to obtain energy can die by necrosis. Products of necrosis lead then to formation and accumulation of reactive oxygen species (ROS), which induce oxidative stress in the tumor microenvironment. Bystander tumor cells react to this harmful situation by inducing autophagy to remove ROS together with damaged cellular organelles and use this housekeeping program to support their own growth [47].

Anoikis is a form of programed cell death (PCD) that occurs when anchorage-dependent cancer cells detach from the surrounding extracellular matrix (ECM) with the ability to become invasive and to spread into the distant tissues. Under physiological conditions, cells stay close to the tissue to which they belong and share essential signals for growth or survival. When cells are detached from the ECM, cell signalization is interrupted, and they may undergo anoikis. Autophagy is largely used by cancer cells in order to avoid anoikis and induce the later stages of cancer progression, such as dissemination and metastasis [48,49]. Subpopulation of cells within tumors, termed cancer stem cells, is responsible for tumor recurrence and metastasis. They may generate tumors through processes of self-renewal and differentiation into multiple cell types and some of them may persist in tumors as a distinct population and cause relapse and metastasis. It seems that autophagy plays an important role also in the survival, differentiation and self-renewal of cancer stem cells [49,50].

Taken together, autophagy provides cells a resilient capacity for regeneration, which is proved by increasing cell size and resumption of cell proliferation after the removal of stressors. Autophagy-deficient cells are not only capable of tolerating metabolic stress but they also fail in the process of recovery. This suggests that autophagy is crucial process in progression and resistance of tumor cells [51].

The role of autophagy in irradiated cancer cells

Radiation treatment triggers an enormous amount of stress. If applied on cancer cells, it leads to conditions which are not suitable for proper development of these cells and thus induces autophagy. There are several studies which describe that clinically relevant doses of radiation promote autophagy in tumor cells [52–55]. These studies assume that autophagy, induced as a reaction on stressful conditions, has a protective role in cancer cells. It presumably prevents tumor cells from cell death through apoptosis which cooperates with autophagy via convoluted crosstalk between autophagic and apoptotic signaling pathways [56,57]. It is very likely that the key role of autophagy within radiation therapy is not in degradation of cellular components and providing nutrients and metabolic precursors, but in elimination of toxic species. Tumor cells are not actually experiencing deficiency of metabolic materials, but they are endangered by toxic species, such as free radicals and possibly damaged and misfolded proteins or organelles, which should be eliminated [58]. IR induces autophagy via hypophosphorylation of mTOR [59]. It leads to decreased phosphorylation of mTOR at its autophosphorylation site (Ser2481) and subsequent activation of autophagy. Complete mechanism of mTOR hypophosphorylation has to be clarified, but it is possible that activation of the ataxia telangiectasia mutated (ATM) protein kinase following the IR exposure leads to activation of Liver Kinase B1 (LKB-1) and to inhibition of mTOR through an ATM/LKB-1/AMPK/Tuberous Sclerosis Complex 2 (TSC2) pathway [60]. Soto-Pantoja et al. described on $CD47^{-}$ Jurkat T cells and $CD47^{-/-}$ murine lung endothelial cells that transmembrane protein receptor CD47 has a substantial role in activation/inhibition of autophagic response to IR. Inhibition or complete shortage of this protein resulted into increased autophagosome formation and cell protection to radiation stress [61].

Cytoprotective function of autophagy to nutrient deprivation and other external stress factors has been known for years. However, it was described in some studies that autophagy plays also a role in cell death as a response to a variety of chemotherapeutic agents as well as to IR [62]. It seems that some authors support the idea of autophagy as a mode of radiosensitization more than protection from radiation injury and cell death [63].

There has been a tendency to consider radiation-induced autophagy as a cytoprotective mechanism, which has (from its origin) a presumable role in radioresistance of cancer cells. However, this conclusion seems to be unconvincing when we take into account a wide spectrum of tumor cell lines where autophagy is induced. Above that, there is no clear evidence that autophagy induction is directly linked with radiosensitization and that fact is limited only to tumor cells that might be considered as radioresistant. Hence it is reasonable to explore other roles that autophagy might have; i.e. besides the cytoprotective one, the cytostatic or even cytotoxic [64].

Inhibition of autophagy: does the original idea really work?

The first observation linked with autophagy led to a presumption that autophagy is a cytoprotective mechanism in tumor cells. Hence, the first apparent approach to sensitize cancer cells to IR was by using the autophagy inhibitors. The following section is dedicated to inhibition of autophagy in the context of radiosensitization.

Chloroquine (CQ) together with 3-methyladenine (3-MA) is among the most widely used autophagy inhibitors. By blocking the fusion of autophagosome and lysosome, CQ inhibits later stages of autophagy, while 3-MA interferes with PI3K pathway. RT, as well as chemotherapy with 5-fluorouracil (5-FU), induces autophagy in colorectal cancer cells. Schonewolf et al. found out that inhibition of RT-induced autophagy (8 Gy) by CQ radiosensitized p53-deficient HT-29 cells, but not p53-wild type (p53-wt) HCT-116 cells. Treatment of HT-29 cells with CQ also improved the effect of combined chemo-RT [65].

ATM kinase affects many pathways, including autophagy, and therefore is among the suitable targets for radiosensitization. Toulany et al. reported that ATM can stimulate autophagy after IR. They examined effect of cisplatin, which causes DNA damage, in lung cancer cell lines A549 and H460. H460 cells were sensitized to IR by cisplatin, but on the contrary A549 cells were not. In A549 cells, cisplatin activated ATM and autophagy, which led to radioresistance. Further experiments with combining the inhibitors of ATM pathway (KU-55933) and autophagy (CQ) resulted in radiosensitization of both A549 and H460 cells to IR. Importantly, treatment of H460 and A549 cells with cisplatin and CQ did not influence their radiosensitization, underlining the role of ATM [66].

Jin et al. published that application of autophagy inhibitors CQ or 3-MA may sensitize human cervical cancer cells (HeLa) and human breast cancer cell lines (MDA-MB-231, MCF-7) to high linear energy transfer (high-LET) radiation. Irradiated tumor cells also displayed a dose-dependent increase in the level of autophagy. Furthermore, pre-treatment of cells by 3-MA accelerated apoptotic cell death and enhanced radiosensitization of tumor cells [67].

To assess the role of autophagy in radiosensitization, Chaachouay et al. used two different breast cancer cell lines: radioresistant MDA-MB-231 and radiosensitive HBL-100 cells. Induction of autophagy by radiation was observed in MDA-MB-231 but not in HBL-100, suggesting protective role of autophagy contributing to the mechanism of radioresistance in MDA-MB-231 cells. Radioresistant MDA-MB-231 cells treated by either CQ or 3-MA and IR showed increased radiosensitization represented by a significant decrease in clonogenic survival [68].

In addition, hypopharyngeal carcinoma cells (FaDu cells) irradiated by 2 or 4 Gy and treated with 3-MA showed reduced clonogenic survival and more severe DNA damage than untreated cells. Combined treatment with 3-MA and IR led to increased radiosensitization of FaDu cells, due to dose-dependent G2/M cell cycle arrest enhancement, as well as escalation in p62 production. Level of cyclin B1, on the other hand, demonstrated dose-dependent decrease [69].

Cheng et al. examined the role of p53, which could potentially regulate radiosensitivity in H1299 non-small cell lung cancer cells (NSCLCC). 3-MA and Z-VAD-FMK were used as autophagy and apoptosis inhibitors. Decreased cell viability was observed in irradiated (8 Gy) H1299-p53 cells (p53-wt). On the contrary, inhibition of apoptosis by Z-VAD-FMK led in the identical cells to increase in cell viability. Furthermore, Z-VAD-FMK-mediated inhibition of apoptosis caused enhancement of autophagic activity in H1299-p53, but not in H1299 (p53-deficient) cells. These outcomes suggest that pre-treatment of cells by 3-MA may lead to increased radiosensitivity [70].

Another approach used in radiosensitization of cancer cells is the targeting of signal transducer and activator of transcription 3 (STAT3) signaling pathway by WP1066 inhibitor or short hairpin RNA plasmid (shRNA). Cell permeable WP1066 is an analog of tyrosine kinase inhibitor Tyrphostin AG 490, which selectively inhibits the epidermal growth factor receptor (EGFR). Both WP1066 and STAT3 shRNA radiosensitized human malignant glioma cells (U251) probably due to induction of intrinsic apoptosis, which can contribute to sensitization toward IR. Moreover, inhibition of STAT3 led to increased autophagic activity. Additionally, clonogenic survival of glioma cells was reduced by using autophagy inhibitor 3-MA or knockdown of one of major autophagic protein ATG5 by siRNA [71].

PI3K/Akt pathway is one of the most common signaling pathways activated as a response to IR in cancer cells. It is an upstream regulator of mTOR and controls cell growth and proliferation [72,73]. PI3K/Akt pathway may also contribute to the radioresistance of tumor cells during cancer therapy [72,74]. PI3K/Akt/mTOR pathway is a crucial regulator of autophagy. Many researchers use this pathway to modulate autophagic process in order to understand radioresistance and radiosensitization of cancer cells [75,76].

NVP-BEZ-235 (BEZ235) is a dual inhibitor of PI3K/mTOR pathway, which induced autophagy and caused radiosensitization of SQ20B head and neck cancer cells, U251 glioblastoma cells and also increased *in vivo* radiation response of SQ20B xenografts. Cerniglia et al. proved that BEZ235 alone may lead to the attenuation of radiosensitization, but pre-treatment of SQ20B cells with CQ or 3-MA followed by BEZ235 treatment resulted into decreased clonogenic survival compared to mere BEZ235 treatment [77].

In contrast to the previous studies, Schaaf et al. published that radioresistance of cancer cells is independent of canonical autophagy that involves lysosomal degradation. Experiments with CQ on colorectal adenocarcinoma (HT29, HCT116), mammary adenocarcinoma (MCF7, MDA-MB-231) and lung carcinoma (A549) cells showed that CQ truly inhibits autophagy but does not increase the radiosensitization. The anti-tumor effect of CQ is mediated via reduction of the hypoxic radioresistant cell population within the tumor, rather than affecting intrinsic radiosensitivity of cancer cells. Even more surprising were other experiments with 3-MA which displayed potential radiosensitizing effect with no signs of autophagy inhibition leading to a conclusion that 3-MA does impact mechanisms which induce radiosensitization but are unrelated to autophagy itself [78]. These were unexpected and important observations revealing additional effects, which enable misinterpretation. Such reports open space for an extensive disputation about conclusions of many studies regardless of publishing in prestigious journals.

Similarly, Rouschop et al. reported radiosensitizing effect of CQ on the small fraction of hypoxic HCT116 colorectal adenocarcinoma xenografts but apparently not via inhibition of autophagy or intrinsic change in cellular radiosensitivity. Instead, they proclaimed enhancement of tumor radiosensitivity via reduction in the fraction of viable radiation-resistant hypoxic cells in the CQ-treated tumors. However, this effect is limited to hypoxic conditions and was not observed in normoxic cells [43].

Commonly, inhibition of PI3K/Akt/mTOR pathway is linked with radiosensitization with inducing autophagy. However, Chang et al. found out that a combination of dual inhibitors of PI3K and mTOR (BEZ235 and PI-103) and IR (6 Gy) can efficiently suppress tumor colony growth, induce more apoptosis, abrogate cell-protective autophagy and improve radiosensitivity of three prostate cancer cell lines (PC-3RR, DU145RR and LNCaPRR). They also found that a combination of dual inhibitors (BEZ235 and PI-103) with IR greatly changed cell cycle distribution, caused higher cell cycle arrest in G2/M phase (the most sensitive phase to radiation) and reduction of cells in G0/G1 and S phases (the most resistant phases to radiation) compared with combination of single inhibitors (BKM120 and rapamycin) with IR [72].

Bafilomycin A1 is a widely used inhibitor of autophagy. It prevents maturation of autophagic vacuoles by inhibiting fusion between autophagosome and lysosome. He et al. studied trichostatin A (histone deacetylases inhibitor – TSA) as a potential radiosensitizing agent on human colon cancer cells (HCT-116). They found out that TSA radiosensitized HCT-116 cells, but also increased autophagy which hampered the radiosensitizing effect. Further pre-treatment with Bafilomycin A1 inhibited cytoprotective autophagy and increased level of apoptotic proteins Bax and Bak together with caspase-3 ergo triggered apoptosis. Thus, inhibition of cytoprotective autophagy was proved to enhance the radiosensitization of HCT-116 cells [79].

IR induces autophagy in various cancer cell lines. Apel et al. observed accumulation of autophagic vesicles in MDA-MB-231 breast cancer cells with mutant p53 proteins; HTB43 pharyngeal cancer cells with mutant p53, HTB35 cervical squamous cell carcinoma cells with mutant p53 and A549 lung cancer cells transfected with an Ectysone-inducible mutant p53 construct. Accumulation of autophagic vesicles was apparent 1–12 h after IR exposure; furthermore, there was a dose-dependent (2, 4 and 10 Gy) increase in expression of *ATG* genes. Importantly, formation of autophagosome after IR was not dependent on p53 status or level of radioresistance. Knocking down of autophagy-related genes (*BECN1*, *ATG3*, *ATG4B*, *ATG4C*, *ATG5* and *ATG12*) prevented formation of autophagosomes in all tested cell lines, but the same dose of IR had different impacts on clonogenic survival of radioresistant and radiosensitive cells. Apel et al. suggest that autophagy can serve as a cytoprotective mechanism and its inhibition leads to radiosensitization. Nevertheless, clonogenic survival can be increased by autophagy inhibition in untreated radioresistant cells [52].

Recently two new autophagic inhibitors, Spautin-1 and Lys05, have been described. Spautin-1 targets the activity of two ubiquitin-specific peptidases, USP10 and USP13 and causes PI3K complex degradation. Park et al. examined the role of Beclin-1 and UVRAG in managing DNA damage and repair response to cancer therapy in colorectal cancer cells (HT-29, DLD1). They reported that inhibition of autophagy by Spautin-1 increased cell death due to accumulation of DNA damage [80]. In addition, a new inhibitor Lys05 was discovered by McAffee et al. Lys05 is a dimeric form of CQ which has a potential to accumulate in the lysosome and block autophagy more effectively compared to hydroxychloroquine (HCQ). Recently, it exhibited more potent anti-tumor activity as a single agent both *in vitro* and *in vivo*. Despite this fact, further experiments with this substance with regards to radiosensitization are still needed [81,82].

Inhibition of cytoprotective autophagy was the original idea leading to radiosensitization of cancer cells. Many studies have been performed in order to sensitize tumor cells toward IR resulting in various outcomes. It has been proved that radiosensitization of cancer cells toward IR using autophagy inhibitors is possible, but definitely not in all types of cancer. The situation is obviously intricate due to the unexpected conclusions of the studies such as Schaaf et al. [78], which opens space for disputation.

We must bear in mind that it depends greatly on the inhibitors and particular properties of cancer cell lines used in order to conclude, whether targeting autophagy via inhibition would be the right approach to radiosensitize tumor cells.

Activation of autophagy: new opportunities for radiosensitization

Many experiments with inhibitors of autophagy have been performed, but so far, not all of them presented the expected outcomes. Another group of studies focused on radiosensitization of cancer cells describes activation of autophagy (mostly in combination with other compounds) as a process leading to their radiosensitization. However, there is a question which still remains unanswered. Do the cancer cells die *with* autophagy or *by* autophagy?

PI3K/Akt/mTOR inhibition conceivably appears among the primary targets for autophagy induction. For instance, it has a significant effect on cisplatin-resistant NSCLCC, CDDP-R. Combination of BEZ235 with IR led to enhanced formation of autophagosomes which was monitored in real time via fluorescence microscopy. Pre-treatment by BEZ235 radiosensitized both parental (NCI-H460-Luc2) and radioresistant (CDDP-R H460-Luc2) cell lines. In addition to *in vitro* results, this combination induced a dramatic tumor growth delay in a mouse xenograft model [83].

Choi et al. radiosensitized lung cancer cell lines (A549, H460 and H1299) using siRNA (specific for either EGFR or K-RAS) and variety of kinase inhibitors: PD98059 (c-RAF), UO126 (mitogen-activated protein/ERK kinase kinase), LY294002 (PI3K), and PI-103. Inhibition of PI3K and mTOR signaling by PI-103 effectively increased the radiosensitivity of A549 and H460 cells. It is likely that combination of PI-103 and IR led to mixed modes of cell death [84]. Similar endpoints were observed in another study by No et al. using PI-103 dual inhibitor in combination with IR in order to radiosensitize SKBR3 breast cancer cells resistant to HER-2 inhibitors [85].

mTOR was also targeted indirectly by nelfinavir and bortezomib, which primarily cause endoplasmic reticulum (ER) stress in cancer cells and thus induce sestrin-2 (SESN2), a known mTOR inhibitor. Generally, inhibition of mTOR leads to activation of autophagy. Brüning et al. applied this autophagy activating strategy and they successfully radiosensitized breast cancer (HTB-131), ovarian cancer (HTB-161), and cervical adenocarcinoma (HeLa) cell lines [86].

Furthermore, mTOR inhibition by rapamycin allowed overcoming of radioresistance in glioma-initiating cells (GIC). This combination effectively blocked the tumor growth and associated mortality in mice after intracerebral grafting of human GIC [87] and proliferation of lung cancer cells (A549) [88]. Palomid 529 (also known as P529, an mTORC1/mTORC2 inhibitor) was combined with IR and tested on a wide panel of prostate cancer models and xenografts. Its radiosensitizing effect is based on GSK-3β, cyclin-D1, and c-myc modulation. In addition, delayed DNA repair, autophagy and tumor senescence were involved [89].

Anbalagan et al. used IR to overcome resistance to standard cytotoxic chemotherapy on a panel of different renal carcinoma cell lines and found it effective in combination with two autophagy inducers: STF-62247 (interferes with Golgi-ER transport via

Table 1
An overview of discussed radiosensitizers. Substances are divided into two groups based on assumption of their impact on autophagy. For each substance the mechanisms of action and relation to radiation are described together with cell type used in the particular study and relevant reference.

INHIBITORS of autophagy	Mechanism of action	Relation to the radiation	Type of cells	
3-Methyladenine	Inhibits PI3K signaling pathway	Pre-treatment by 3-MA led in combination with IR to radiosensitization of breast and cervical cancer cells	MDA-MB-231, HBL-100, HeLa	[77,78]
		Pre-treatment by 3-MA led in combination with IR to radiosensitization of hypopharyngeal carcinoma cells	FaDu	[69]
		Combined treatment with Z-VAD-FMK radiosensitized NSCLCC	H1299	[70]
		Combined treatment with WP1066 and STAT3 shRNA radiosensitized malignant glioma cells	U251	[71]
		Combined treatment with BEZ235 radiosensitized head and neck cancer cells	SQ20B	[77]
		Pre-treatment by 3-MA led in combination with IR to radiosensitization of colorectal adenocarcinoma, mammary adenocarcinoma and lung carcinoma cells	HT29, HCT116, MCF7, MDA-MB-231, A549	[78]
Bafilomycin A1	Prevents fusion of autophagosomes and lysosomes	Combined treatment with TSA radiosensitized colon cancer cells via increased level of apoptosis	HCT-116	[79]
Chloroquine	Impairs fusion of autophagosomes and lysosomes, and inhibits lysosomal protein degradation	Combined treatment with 5-FU radiosensitized colorectal cancer cells	HCT-116, HT-29	[65]
		Combined treatment with KU-55933 radiosensitized lung cancer cells	A549, H460	[66]
		Pre-treatment by CQ led in combination with IR to radiosensitization of breast cancer cells	MDA-MB-231	[68]
		Combined treatment with BEZ235 radiosensitized head and neck cancer cells	SQ20B	[77]
		Pre-treatment by CQ led to inhibition of autophagy but not to radiosensitization of colorectal adenocarcinoma, mammary adenocarcinoma and lung carcinoma cells	HT29, HCT116, MCF7, MDA-MB-231, A549	[78]
		Pre-treatment by CQ led in combination with IR to radiosensitization of colorectal adenocarcinoma xenografts	HCT116	[43]
Lys05	Accumulates within and deacidifies the lysosomes	No experiments have been performed yet		[81]
siRNA	Downregulates the major autophagic proteins	Combined treatment with WP1066 and STAT3 shRNA radiosensitized malignant glioma cells	U251	[71]
		Pre-treatment by siRNA led in combination with IR to radiosensitization of various cancer cell lines	MDA-MB-231, HTB43, HTB35, A549	[52]
Spautin-1	Promotes degradation of Beclin-1 subunit of PI3K complex by inhibiting the activity of USP10 and USP13	Pre-treatment by Spautin-1 led in combination with IR to radiosensitization of colorectal cancer cells due to accumulation of DNA damage	HT-29, DLD1	[80]
INDUCERS of autophagy	**Mechanism of action**	**Relation to the radiation**	**Type of cells**	
1L-6-hydroxymethyl-chiro-inositol 2(R)-2-O-methyl-3-O-octadecylcarbonate	Downregulates Akt signaling pathway	Combined therapy with IR radiosensitized malignant glioma cells	U87-MG, U87-MGΔEGRF	[73]
Antisense oligonucleotides	Abrogates the activity of DNA-PKcs	Pre-treatment by antisense oligonucleotides led in combination with IR to radiosensitization of malignant glioma and fibroblast cells	M059K, U373-MG, T98G, MRC5	[97]
Apogossypolone	Inhibits the binding of Bcl-2 to Beclin-1	Pre-treatment by ApoG2 led in combination with IR to radiosensitization of nasopharyngeal carcinoma cells and mice xenografts	CNE1, CNE2	[93]
Bortezomib Nelfinavir	Cause ER stress and thus induce SESN2, an mTOR inhibitor	Combination of these two activators with IR led to radiosensitization of ovarian, breast and cervical cancer cells	HTB-131, HTB-161, HeLa	[86]
Calcitriol	Inhibits PI3K/Akt/mTOR signaling pathway	Pre-treatment by calcitriol led in combination with IR to radiosensitization of breast tumor cells	ZR-75-1 MCF-7	[98] [99]
Cisplatin	Induces PI3K activation signaling pathway and decreases the level of Bcl-2 proteins	Combined therapy with IR radiosensitized lung cancer cells and mouse xenografts	A549	[96]
EB1089	Inhibits PI3K/Akt/mTOR signaling pathway	Pre-treatment by EB1089 led in combination with IR to radiosensitization of breast tumor xenografts	MCF-7	[100]
Everolimus	Inhibits mTOR signaling pathway	Pre-treatment by everolimus led in combination with IR to radiosensitization of Ras-transformed cells	RK3E/tv-a	[91]
		Combined treatment with Z-DEVD radiosensitized lung tumor xenografts	H460	[92]
Lapatinib Obatoclax	Inhibits ErbB1/ErbB2 signaling pathway Inhibits activity of Bcl-2/Bcl-XL/Mcl-1 proteins	Combination of lapatinib and obatoclax led to radiosensitization of breast cancer cells	BT474, MCF-7, HCC38, BT549, HCC1187, MDA-MB-453, MDA-MB-175	[94]

Table 1 (*continued*)

INHIBITORS of autophagy	Mechanism of action	Relation to the radiation	Type of cells	
NVP-BEZ-235	Inhibits PI3K/Akt/mTOR signaling pathway	Pre-treatment by BEZ235 led in combination with IR to radiosensitization of lung cancer cells	NCI-H460-Luc2, CDDP-R H460-Luc2	[83]
Palomid 529	Inhibits mTORC1/mTORC2 complex	Pre-treatment by P529 led in combination with IR to radiosensitization of prostate cancer cells and xenografts	LnCaP, 22rv1, DU145, PC3, LAPC-4, C4-2B	[89]
PI-103	Inhibits both PI3K	Pre-treatment by PI-103 led in combination with IR to radiosensitization of lung cancer cells	A549, H460	[84]
		Pre-treatment by PI-103 led in combination with IR to radiosensitization of breast cancer cells	SKBR3	[85]
Rapamycin	Inhibits mTOR signaling pathway	Pre-treatment by rapamycin led in combination with IR to radiosensitization of glioma-initiating cells	GICs	[87]
		Pre-treatment by rapamycin led in combination with IR to radiosensitization of lung cancer cells	A549	[88]
		Combined treatment with ABT-737 radiosensitized lung cancer cells and lung xenografts	H460	[101]
STF-62247	Interferes with Golgi-endoplasmic reticulum transport	Pre-treatment by STF-62247 led in combination with IR to radiosensitization of renal carcinoma cells	RCC4, 786-O	[90]
Temsirolimus	Inhibits mTOR signaling pathway	Pre-treatment by temsirolimus led in combination with IR to radiosensitization of renal carcinoma cells	RCC4, 786-O	[90]
Z-VAD-FMK	Inhibits the action of caspase proteases	Pre-treatment by Z-VAD-FMK led in combination with IR to radiosensitization of breast and lung cancer cells via total inhibition of apoptosis and subsequent activation of autophagy	MDA-MB-231, H460	[95]

targeting von Hippel-Lindau tumor suppressor gene) or temsirolimus (inhibits mTOR) [90]. A related compound, everolimus, was reported to sensitize Ras-transformed cells to radiation *in vitro* [91] and combined administration of Z-DEVD (caspase-3 inhibitor) together with everolimus into xenografted H460 lung tumors resulted in superior radiation cytotoxicity compared with either agent alone [92].

He et al. tested apogossypolone (ApoG2), a small-molecule inhibitor of Bcl-2, to induce radiosensitization both *in vitro* in nasopharyngeal carcinoma cells and *in vivo* using mice xenografts. They proclaimed that ApoG2 inhibited the binding of Bcl-2 to Beclin-1 and induced autophagy [93]. Cruickshanks et al. used lapatinib (an inhibitor of ErbB1/2/4) and obatoclax (an inhibitor of the anti-apoptotic Bcl-2/Bcl-XL/Mcl-1 proteins). Such a combination eradicated multiple breast cancer cells through a mechanism that involved ER stress signaling and caused DNA damage, which occurred downstream of ROS generation and autophagy. The authors point out an essential role of mitochondrial function and "mitophagy" in radiosensitization by this drug combination, since over-expression of Mcl-1 protected the cells [94]. The importance of apoptotic signaling is indisputable. It has been demonstrated by a study of Moretti et al., who radiosensitized breast tumor MDA-MB-231 and lung H460 cancer cells by Z-VAD (a pan-caspase inhibitor), where inhibition of all caspase pathways led to inhibition of apoptosis. At the same time, a transient burst of autophagic protein expression was noticed suggesting that autophagy and apoptosis are mutually regulated [95].

On the other hand, Liu et al. used combination of cisplatin and IR to radiosensitize NSCLCC (A549) and mouse xenografts. Besides inducing pro-autophagic mechanism, they observed also a decrease in Bcl-2 expression and a marked upregulation of p21 expression, indicating that activation of pro-apoptotic cell death mechanism is also involved [96].

Fujiwara et al. presented a different strategy for the tumors that are resistant to apoptosis induction. Downregulating Akt signalization (by specific inhibitor 1L-6-hydroxymethyl-chiro-inositol 2(R)-2-O-methyl-3-O-octadecylcarbonate), they demonstrated anti-cancer and radiosensitizing effects on malignant glioma U87-MG and radioresistant U87-MGΔEGFR cells [73]. Another non-apoptotic approach used antisense oligonucleotides against DNA-PKcs to radiosensitize human malignant glioma cells (M059K, U373-MG, and T98G) and human fibroblast cells (MRC5) [97].

Several studies accented potential of vitamin D (vit. D) as well as its analogs [63]. Calcitriol, or 1,25-dihydroxyvitamin D3 (the hormonally active form of vit. D – 1,25D3), has been shown to enhance radiosensitivity of ZR-75-1 breast tumor cells [98]. Bristol et al. observed minimal apoptosis, but the effects of 1,25D3 on cell proliferation were proved to be mediated through Akt/mTOR signaling [99]. Besides that, Dr. Gerwitz's lab provided a proof of principle for another vit. D analog (EB 1089). Its pre-incubation before irradiation converted the senescence response observed with radiation alone to one of the cell death mechanisms [100]. Above that, they presented an attractive theory on so-called "autophagic switch", which described autophagy as a cytoprotective process in irradiated breast tumor cells, however, promotion of increased autophagy can also confer them radiosensitivity. Moreover, both cytoprotective and cytotoxic autophagy can occur together in one experimental system as a part of radiation response [98,99].

So far, many modulators of autophagy have been described. Table 1 summarizes those applied with intention to increase radiosensitivity of variety of cancer cells in the past few years. Fig. 1 shows how do they interfere with the process of autophagy.

Autophagy seems to have multiple functions. Besides its cytoprotective role, autophagy is recognized as cytostatic, non-protective and cytotoxic process [64]. There are a few compounds which have a potential to activate autophagy and simultaneously sensitize cancer cells to IR. For quite a long time it has been thought that mere induction of cytotoxic autophagy ("autophagic PCD") is the reason underlying cancer cells radiosensitization. For instance, Kim et al. reported that a combined effect of ABT-737 (a Bcl-2 inhibitor) and rapamycin resulted in the effective radiosensitization of lung cancer cells (H460) and xenografts probably through death by self-digestion [101]. Such studies underline the concept of collaborative role of autophagy and apoptosis. Targeting both pathways simultaneously is advantageous due to synergism.

On the other hand, recently accumulating evidence indicates that this issue is far more complicated than it seems. A promising potential of inhibition of both mTOR and apoptotic signaling to

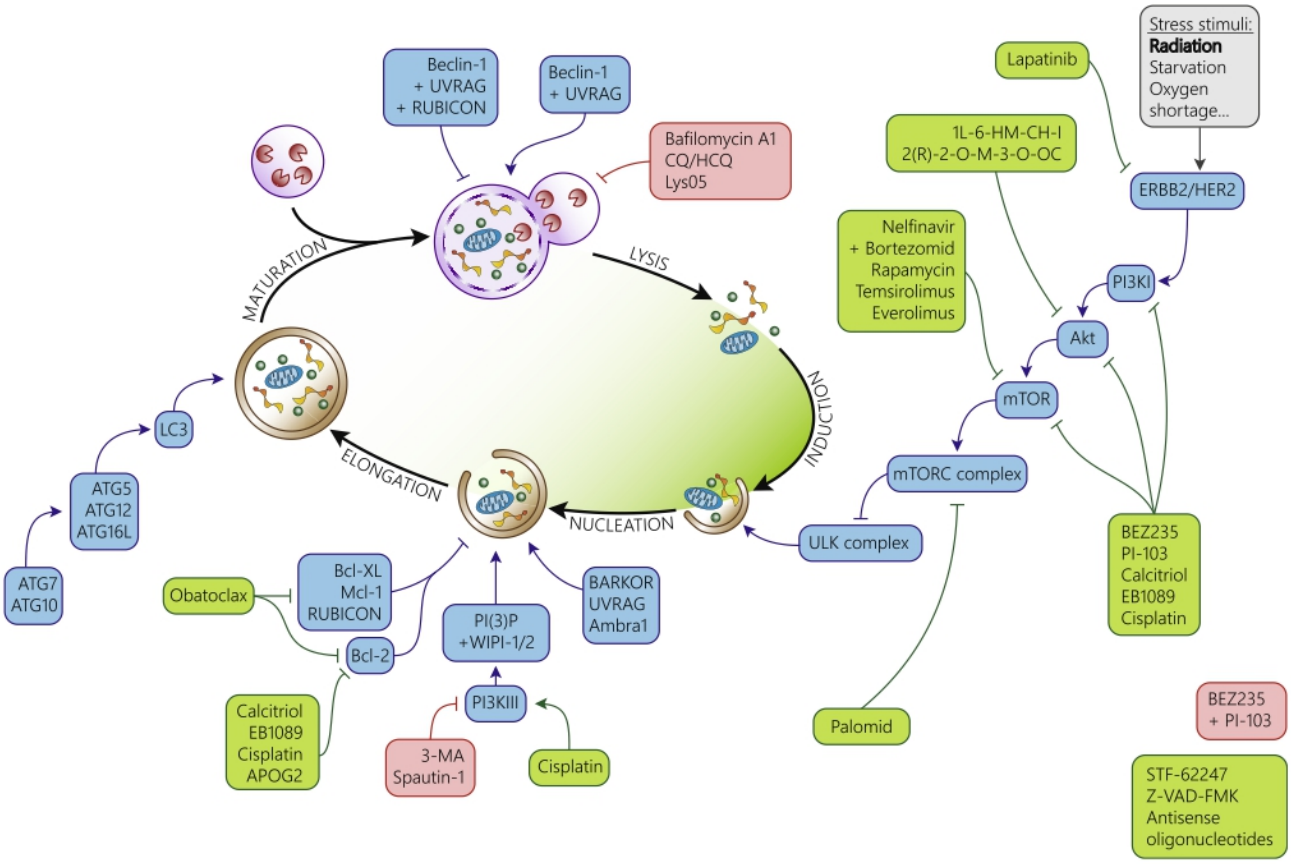

Fig. 1. The process of autophagy and its regulation pathways (framed in blue) in context of radiosensitizers (framed in green and red). The whole machinery of autophagy is divided into 4 main steps: (1) induction, (2) nucleation, (3) elongation, and (4) maturation; followed by lysis of autophagosomal content. There are plenty of stimuli, which can trigger autophagy, e.g. starvation, IR, oxygen shortage and DNA damage. These stress stimuli lead to an activation of mTORC complex through PI3K/Akt/mTOR pathway and subsequent activation of ULK complex, which induces autophagic process. The main regulator of nucleation is class III PI3K, which interacts with Beclin-1 and leads to the production of second messenger PI(3)P and formation of autophagosome. Other positive regulators are BARKOR, UVRAG and Ambra-1. Proteins Bcl-2, Bcl-XL, Mcl-1 and RUBICON belong to the negative regulators, which contribute to stopping of nucleation. Proteins ATG7 and ATG10 regulate formation of ATG12, ATG5 and ATG16L complex, which subsequently activates LC3 complex, a key complex for the final step of autophagosome formation, leading to enclosure of autophagosome membrane. At the end, lysosome fuses with autophagosome to form autophagolysosome and releases the acidic lysosomal hydrolases degrading the cytosolic content. Radiosensitization of cancer cells can be achieved by application of both inducers and inhibitors of autophagy. Application of these substances together with IR leads to decreased clonogenic survival of cancer cells. Majority of inducers (framed in green) activates autophagy in its initial steps, mainly through inhibition of mTOR signaling pathway. On the other hand, inhibitors of autophagy (framed in red) act in the late phase of autophagic process. Bottom right, inhibitors and inducers with more complex mechanism of autophagy modulation are listed. (For interpretation of the references to color in this figure legend, the reader is referred to the web version of this article.)

improve the efficacy of radiation therapy was proved by another study of Kim et al., who reported evidence that the pro-apoptotic proteins of Bcl-2 family (Bax and Bak) play a critical role in mediating the post-radiation mechanism of cell death. Their findings led to the hypothesis that IR upregulates non-apoptotic PCD (autophagy) in cells which are unable to undergo Bax/Bak-mediated apoptosis and that radiosensitivity can be increased by attenuating the given proteins in several cancer cells [102].

Strikingly, other authors such as Kroemer and Levine raised speculations about the process of "autophagic PCD". They admitted that there were some cancer cells which could be eradicated by autophagy, especially *in vitro*. However, this statement cannot be generalized to all cancer cells and the question of whether mammalian cancer cells die by autophagy cannot be answered definitively. In this sense, the term "autophagic PCD" could be considered to be a misnomer [103]. Moreover, according to Shen et al. there are no such studies which could formally establish that autophagy itself is responsible for cell killing [104]. In addition, also the method of autophagy assessment should be seriously taken into account as proposed in guidelines compiled by Klionsky et al. [105,106]. Increased fluorescent LC3B puncta or changed ratio in LC3B-I/II is simply not sufficient to claim that autophagy is induced/reduced. Flux analysis seems to be more convenient test because it enables dynamic monitoring. Taken together, there is no definite answer to the question whether the cancer cells die *by* or *with* autophagy and certainly further studies are required before the end of a term "autophagic PCD" will be proclaimed.

Concluding remarks

Radiation-induced autophagy is believed to represent a radioprotective mechanism, thus its inhibition can support radiosensitization treatment and increase its efficacy. On the other hand, there is accumulating and clear evidence that IR alone or in combination with various chemicals induces autophagy, which can result into increased cell death, e.g. within transformed apoptosis-resistant cells. Besides that, it will be very important to exploit radiation-induced autophagy as a therapeutic agent against those tumors, which are not exactly classified as radiation "sensitive" or "resistant" [107].

Obviously, a single universal conclusion can be hardly achieved. Many reports suggesting radiosensitization of certain cancer cell types via inhibition of autophagy are opposed by conflicting similar studies with contradictory results. There is a common presump-

tion that using inducers of autophagy leads to the cell death with autophagy. Furthermore, the amount of recently developed inducers of autophagy indicates that the future trend in radiosensitization using modulation of autophagy will tend to application of inducers rather than inhibitors. But, one has to bear in mind that using inducers of autophagy does not have to lead to radiosensitization solely via modulation of autophagy and also other than intrinsic cellular mechanisms might be involved. Such discrepancy could be reduced with application of coherent methodological approaches for autophagy assessment. Our field is evolving dramatically and what was believed as a good methodology a decade ago might be considered misleading today. Additionally, the correct interpretation of data is crucial too. Although a deeper understanding of the different roles of autophagy is needed, it is apparent that its modulation offers a promising and attractive strategy for tumor treatment along with infectious diseases and neurodegenerative disorders. Therefore, the future work should be carried out under isogenic conditions within cells differing only in a particular gene and with appropriate methods.

In spite of the fact that the fundamental understanding of autophagy is escalating rapidly, its translation into clinical trials is draggy. For instance, HCQ has recently shown some promising results in phase I/II clinical trials [108]. However, it lacks tolerability and efficiency for other types of cancers. Such findings drive a concept of a personalized anti-cancer strategy that should be tailored for an individual patient rather than development of versatile and all-embracing approach for modulation of autophagy.

Disclosure of potential conflicts of interest

No potential conflicts of interest were disclosed.

Acknowledgments

This work was supported by the Ministry of Defense (A long-term organization development plan no. 1011) and by Ministry of Education, Youth and Sport (Specific research project no: SV/FVZ201501), Czech Republic.

References

[1] Levine B, Klionsky DJ. Development by self-digestion: molecular mechanisms and biological functions of autophagy. Dev Cell 2004;6:463–77. http://dx.doi.org/10.1016/S1534-5807(04)00099-1.
[2] Liang N, Jia L, Liu Y, Liang B, Kong D, Yan M, et al. ATM pathway is essential for ionizing radiation-induced autophagy. Cell Signal 2013;25:2530–9. http://dx.doi.org/10.1016/j.cellsig.2013.08.010.
[3] Chen L-H, Chu P-M, Lee Y-J, Tu P-H, Chi C-W, Lee H-C, et al. Targeting protective autophagy exacerbates UV-triggered apoptotic cell death. Int J Mol Sci 2012;13:1209–24. http://dx.doi.org/10.3390/ijms13011209.
[4] Ogier-Denis E, Codogno P. Autophagy: a barrier or an adaptive response to cancer. Biochim Biophys Acta BBA – Rev Cancer 2003;1603:113–28. http://dx.doi.org/10.1016/S0304-419X(03)00004-0.
[5] Panganiban R-AM, Snow AL, Day RM. Mechanisms of radiation toxicity in transformed and non-transformed cells. Int J Mol Sci 2013;14:15931–58. http://dx.doi.org/10.3390/ijms140815931.
[6] Hale AN, Ledbetter DJ, Gawriluk TR, Rucker III EB. Autophagy. Autophagy 2013;9:951–72. http://dx.doi.org/10.4161/auto.24273.
[7] Tanida I. Autophagy basics. Microbiol Immunol 2011;55:1–11. http://dx.doi.org/10.1111/j.1348-0421.2010.00271.x.
[8] Mizushima N, Komatsu M. Autophagy: renovation of cells and tissues. Cell 2011;147:728–41. http://dx.doi.org/10.1016/j.cell.2011.10.026.
[9] Van Limbergen J, Stevens C, Nimmo ER, Wilson DC, Satsangi J. Autophagy: from basic science to clinical application. Mucosal Immunol 2009;2:315–30. http://dx.doi.org/10.1038/mi.2009.20.
[10] Lorenzo Galluzzi JMV. To die or not to die: that is the autophagic question. Curr Mol Med 2008;8:78–91. http://dx.doi.org/10.2174/156652408783769616.
[11] Glick D, Barth S, Macleod KF. Autophagy: cellular and molecular mechanisms. J Pathol 2010;221:3–12. http://dx.doi.org/10.1002/path.2697.
[12] Platini F, Perez-Tomas R, Ambrosio S, Tessitore L. Understanding autophagy in cell death control. Curr Pharm Des 2010;16:101–13. http://dx.doi.org/10.2174/138161210789941810.
[13] Mizushima N, Ohsumi Y, Yoshimori T. Autophagosome formation in mammalian cells. Cell Struct Funct 2002;27:421–9.
[14] Li W, Li J, Bao J. Microautophagy: lesser-known self-eating. Cell Mol Life Sci 2012;69:1125–36. http://dx.doi.org/10.1007/s00018-011-0865-5.
[15] Kon M, Cuervo AM. Chaperone-mediated autophagy in health and disease. FEBS Lett 2010;584:1399–404. http://dx.doi.org/10.1016/j.febslet.2009.12.025.
[16] Dice JF. Chaperone-mediated autophagy. Autophagy 2007;3:295–9. http://dx.doi.org/10.4161/auto.4144.
[17] Klionsky DJ. Look people, "Atg" is an abbreviation for "autophagy-related." That's it. Autophagy 2012;8:1281–2. http://dx.doi.org/10.4161/auto.21812.
[18] Yang Z, Klionsky DJ. Mammalian autophagy: core molecular machinery and signaling regulation. Curr Opin Cell Biol 2010;22:124–31. http://dx.doi.org/10.1016/j.ceb.2009.11.014.
[19] Rosenfeldt MT, Ryan KM. The multiple roles of autophagy in cancer. Carcinogenesis 2011;32:955–63. http://dx.doi.org/10.1093/carcin/bgr031.
[20] Kroemer G, Mariño G, Levine B. Autophagy and the integrated stress response. Mol Cell 2010;40:280–93. http://dx.doi.org/10.1016/j.molcel.2010.09.023.
[21] Mehrpour M, Esclatine A, Beau I, Codogno P. Overview of macroautophagy regulation in mammalian cells. Cell Res 2010;20:748–62. http://dx.doi.org/10.1038/cr.2010.82.
[22] Pyo JO, Nah J, Jung YK. Molecules and their functions in autophagy. Exp Mol Med 2012;44:73–80. http://dx.doi.org/10.3858/emm.2012.44.2.029.
[23] Sou Y, Waguri S, Iwata J, Ueno T, Fujimura T, Hara T, et al. The Atg8 conjugation system is indispensable for proper development of autophagic isolation membranes in mice. Mol Biol Cell 2008;19:4762–75. http://dx.doi.org/10.1091/mbc.E08-03-0309.
[24] Geng J, Klionsky DJ. The Atg8 and Atg12 ubiquitin-like conjugation systems in macroautophagy. EMBO Rep 2008;9:859–64. http://dx.doi.org/10.1038/embor.2008.163.
[25] Kabeya Y, Mizushima N, Yamamoto A, Oshitani-Okamoto S, Ohsumi Y, Yoshimori T. LC3, GABARAP and GATE16 localize to autophagosomal membrane depending on form-II formation. J Cell Sci 2004;117:2805–12. http://dx.doi.org/10.1242/jcs.01131.
[26] Hanahan D, Weinberg RA. Hallmarks of cancer: the next generation. Cell 2011;144:646–74. http://dx.doi.org/10.1016/j.cell.2011.02.013.
[27] Mathew R, White E. Autophagy, stress, and cancer metabolism: what doesn't kill you makes you stronger. Cold Spring Harb Symp Quant Biol 2011;76:389–96. http://dx.doi.org/10.1101/sqb.2012.76.011015.
[28] Rao S, Tortola L, Perlot T, Wirnsberger G, Novatchkova M, Nitsch R, et al. A dual role for autophagy in a murine model of lung cancer. Nat Commun 2014;5:3056. http://dx.doi.org/10.1038/ncomms4056.
[29] Strohecker AM, Guo JY, Karsli-Uzunbas G, Price SM, Chen GJ, Mathew R, et al. Autophagy sustains mitochondrial glutamine metabolism and growth of BrafV600E-driven lung tumors. Cancer Discov 2013;3:1272–85. http://dx.doi.org/10.1158/2159-8290.CD-13-0397.
[30] Liang XH, Jackson S, Seaman M, Brown K, Kempkes B, Hibshoosh H, et al. Induction of autophagy and inhibition of tumorigenesis by beclin 1. Nature 1999;402:672–6. http://dx.doi.org/10.1038/45257.
[31] Qu X, Yu J, Bhagat G, Furuya N, Hibshoosh H, Troxel A, et al. Promotion of tumorigenesis by heterozygous disruption of the beclin 1 autophagy gene. J Clin Invest 2003;112:1809–20. http://dx.doi.org/10.1172/JCI200320039.
[32] Yue Z, Jin S, Yang C, Levine AJ, Heintz N. Beclin 1, an autophagy gene essential for early embryonic development, is a haploinsufficient tumor suppressor. Proc Natl Acad Sci 2003;100:15077–82. http://dx.doi.org/10.1073/pnas.2436255100.
[33] Mathew R, Kongara S, Beaudoin B, Karp CM, Bray K, Degenhardt K, et al. Autophagy suppresses tumor progression by limiting chromosomal instability. Genes Dev 2007;21:1367–81. http://dx.doi.org/10.1101/gad.1545107.
[34] Janji B, Viry E, Baginska J, Van K, Berchem G. Role of Autophagy in Cancer and Tumor Progression. In: Bailly Y, editor. Autophagy – Double-Edged Sword – Cell Surviv. Death, InTech; 2013.
[35] Folkman J. Angiogenesis and apoptosis. Semin Cancer Biol 2003;13:159–67. http://dx.doi.org/10.1016/S1044-579X(02)00133-5.
[36] Degenhardt K, Mathew R, Beaudoin B, Bray K, Anderson D, Chen G, et al. Autophagy promotes tumor cell survival and restricts necrosis, inflammation, and tumorigenesis. Cancer Cell 2006;10:51–64. http://dx.doi.org/10.1016/j.ccr.2006.06.001.
[37] Izuishi K, Kato K, Ogura T, Kinoshita T, Esumi H. Remarkable tolerance of tumor cells to nutrient deprivation: possible new biochemical target for cancer therapy. Cancer Res 2000;60:6201–7.
[38] Boya P, González-Polo R-A, Casares N, Perfettini J-L, Dessen P, Larochette N, et al. Inhibition of macroautophagy triggers apoptosis. Mol Cell Biol 2005;25:1025–40. http://dx.doi.org/10.1128/MCB.25.3.1025-1040.2005.
[39] Bellot G, Garcia-Medina R, Gounon P, Chiche J, Roux D, Pouysségur J, et al. Hypoxia-induced autophagy is mediated through hypoxia-inducible factor induction of BNIP3 and BNIP3L via their BH3 domains. Mol Cell Biol 2009;29:2570–81. http://dx.doi.org/10.1128/MCB.00166-09.
[40] Tracy K, Dibling BC, Spike BT, Knabb JR, Schumacker P, Macleod KF. BNIP3 is an RB/E2F target gene required for hypoxia-induced autophagy. Mol Cell Biol 2007;27:6229–42. http://dx.doi.org/10.1128/MCB.02246-06.
[41] Schaaf MBE, Cojocari D, Keulers TG, Jutten B, Starmans MH, de Jong MC, et al. The autophagy associated gene, ULK1, promotes tolerance to chronic and

acute hypoxia. Radiother Oncol J Eur Soc Ther Radiol Oncol 2013;108:529–34. http://dx.doi.org/10.1016/j.radonc.2013.06.015.
[42] Papandreou I, Lim AL, Laderoute K, Denko NC. Hypoxia signals autophagy in tumor cells via AMPK activity, independent of HIF-1, BNIP3, and BNIP3L. Cell Death Differ 2008;15:1572–81. http://dx.doi.org/10.1038/cdd.2008.84.
[43] Rouschop KMA, van den Beucken T, Dubois L, Niessen H, Bussink J, Savelkouls K, et al. The unfolded protein response protects human tumor cells during hypoxia through regulation of the autophagy genes MAP1LC3B and ATG5. J Clin Invest 2010;120:127–41. http://dx.doi.org/10.1172/JCI40027.
[44] Lum JJ, Bauer DE, Kong M, Harris MH, Li C, Lindsten T, et al. Growth factor regulation of autophagy and cell survival in the absence of apoptosis. Cell 2005;120:237–48. http://dx.doi.org/10.1016/j.cell.2004.11.046.
[45] Rangwala R, Chang YC, Hu J, Algazy KM, Evans TL, Fecher LA, et al. Combined MTOR and autophagy inhibition. Autophagy 2014;10:1391–402. http://dx.doi.org/10.4161/auto.29119.
[46] Warburg O. On the origin of cancer cells. Science 1956;123:309–14.
[47] Mah LY, Ryan KM. Autophagy and Cancer. Cold Spring Harb Perspect Biol 2012;4:a008821. http://dx.doi.org/10.1101/cshperspect.a008821.
[48] Fung C, Lock R, Gao S, Salas E, Debnath J. Induction of autophagy during extracellular matrix detachment promotes cell survival. Mol Biol Cell 2008;19:797–806. http://dx.doi.org/10.1091/mbc.E07-10-1092.
[49] Lorin S, Hamaï A, Mehrpour M, Codogno P. Autophagy regulation and its role in cancer. Semin Cancer Biol 2013;23:361–79. http://dx.doi.org/10.1016/j.semcancer.2013.06.007.
[50] Salemi S, Yousefi S, Constantinescu MA, Fey MF, Simon H-U. Autophagy is required for self-renewal and differentiation of adult human stem cells. Cell Res 2012;22:432–5. http://dx.doi.org/10.1038/cr.2011.200.
[51] Mathew R, Karantza-Wadsworth V, White E. Role of autophagy in cancer. Nat Rev Cancer 2007;7:961–7. http://dx.doi.org/10.1038/nrc2254.
[52] Apel A, Herr I, Schwarz H, Rodemann HP, Mayer A. Blocked autophagy sensitizes resistant carcinoma cells to radiation therapy. Cancer Res 2008;68:1485–94. http://dx.doi.org/10.1158/0008-5472.CAN-07-0562.
[53] Ko A, Kanehisa A, Martins I, Senovilla L, Chargari C, Dugue D, et al. Autophagy inhibition radiosensitizes in vitro, yet reduces radioresponses in vivo due to deficient immunogenic signalling. Cell Death Differ 2014;21:92–9. http://dx.doi.org/10.1038/cdd.2013.124.
[54] Lomonaco SL, Finniss S, Xiang C, DeCarvalho A, Umansky F, Kalkanis SN, et al. The induction of autophagy by γ-radiation contributes to the radioresistance of glioma stem cells. Int J Cancer 2009;125:717–22. http://dx.doi.org/10.1002/ijc.24402.
[55] Paglin S, Hollister T, Delohery T, Hackett N, McMahill M, Sphicas E, et al. A novel response of cancer cells to radiation involves autophagy and formation of acidic vesicles. Cancer Res 2001;61:439–44.
[56] Rikiishi H. Novel insights into the interplay between apoptosis and autophagy. Int J Cell Biol 2012;2012:e317645. http://dx.doi.org/10.1155/2012/317645.
[57] Su M, Mei Y, Sinha S. Role of the crosstalk between autophagy and apoptosis in cancer. J Oncol 2013;2013:e102735. http://dx.doi.org/10.1155/2013/102735.
[58] Gewirtz DA. When cytoprotective autophagy isn't… and even when it is. Autophagy 2014;10:391–2. http://dx.doi.org/10.4161/auto.27719.
[59] Paglin S, Lee N-Y, Nakar C, Fitzgerald M, Plotkin J, Deuel B, et al. Rapamycin-sensitive pathway regulates mitochondrial membrane potential, autophagy, and survival in irradiated MCF-7 cells. Cancer Res 2005;65:11061–70. http://dx.doi.org/10.1158/0008-5472.CAN-05-1083.
[60] Paglin S, Yahalom J. Pathways that regulate autophagy and their role in mediating tumor response to treatment. Autophagy 2006;2:291–3. http://dx.doi.org/10.4161/auto.2835.
[61] Soto-Pantoja DR, Miller TW, Pendrak ML, DeGraff WG, Sullivan C, Ridnour LA, et al. CD47 deficiency confers cell and tissue radioprotection by activation of autophagy. Autophagy 2012;8:1628–42. http://dx.doi.org/10.4161/auto.21562.
[62] Jo GH, Bögler O, Chwae Y-J, Yoo H, Lee SH, Park JB, et al. Radiation-induced autophagy contributes to cell death and induces apoptosis partly in malignant glioma cells. Cancer Res Treat 2014;47:221–41. http://dx.doi.org/10.4143/crt.2013.159.
[63] Gewirtz DA, Hilliker ML, Wilson EN. Promotion of autophagy as a mechanism for radiation sensitization of breast tumor cells. Radiother Oncol 2009;92:323–8. http://dx.doi.org/10.1016/j.radonc.2009.05.022.
[64] Gewirtz DA. The four faces of autophagy: implications for cancer therapy. Cancer Res 2014;74:647–51. http://dx.doi.org/10.1158/0008-5472.CAN-13-2966.
[65] Schonewolf CA, Mehta M, Schiff D, Wu H, Haffty BG, Karantza V, et al. Autophagy inhibition by chloroquine sensitizes HT-29 colorectal cancer cells to concurrent chemoradiation. World J Gastrointest Oncol 2014;6:74–82. http://dx.doi.org/10.4251/wjgo.v6.i3.74.
[66] Toulany M, Mihatsch J, Holler M, Chaachouay H, Rodemann HP. Cisplatin-mediated radiosensitization of non-small cell lung cancer cells is stimulated by ATM inhibition. Radiother Oncol 2014;111:228–36. http://dx.doi.org/10.1016/j.radonc.2014.04.001.
[67] Jin X, Liu Y, Ye F, Liu X, Furusawa Y, Wu Q, et al. Role of autophagy in high linear energy transfer radiation-induced cytotoxicity to tumor cells. Cancer Sci 2014;105:770–8. http://dx.doi.org/10.1111/cas.12422.
[68] Chaachouay H, Ohneseit P, Toulany M, Kehlbach R, Multhoff G, Rodemann HP. Autophagy contributes to resistance of tumor cells to ionizing radiation. Radiother Oncol J Eur Soc Ther Radiol Oncol 2011;99:287–92. http://dx.doi.org/10.1016/j.radonc.2011.06.002.
[69] Tang Z, Xu Y, Peng J, Ou Y, Guan Z. Mechanism of radiosensitization of 3-methyladenine in human hypopharynx cancer cells. Zhonghua Er Bi Yan Hou Tou Jing Wai Ke Za Zhi 2012;47:937–41.
[70] Cheng G, Kong D, Hou X, Liang B, He M, Liang N, et al. The tumor suppressor, p53, contributes to radiosensitivity of lung cancer cells by regulating autophagy and apoptosis. Cancer Biother Radiopharm 2013;28:153–9. http://dx.doi.org/10.1089/cbr.2012.1297.
[71] Yuan X, Du J, Hua S, Zhang H, Gu C, Wang J, et al. Suppression of autophagy augments the radiosensitizing effects of STAT3 inhibition on human glioma cells. Exp Cell Res 2015;330:267–76. http://dx.doi.org/10.1016/j.yexcr.2014.09.006.
[72] Chang L, Graham PH, Hao J, Ni J, Bucci J, Cozzi PJ, et al. PI3K/Akt/mTOR pathway inhibitors enhance radiosensitivity in radioresistant prostate cancer cells through inducing apoptosis, reducing autophagy, suppressing NHEJ and HR repair pathways. Cell Death Dis 2014;5:e1437. http://dx.doi.org/10.1038/cddis.2014.415.
[73] Fujiwara K, Iwado E, Mills GB, Sawaya R, Kondo S, Kondo Y. Akt inhibitor shows anticancer and radiosensitizing effects in malignant glioma cells by inducing autophagy. Int J Oncol 2007;31:753–60.
[74] Zhan M, Han ZC. Phosphatidylinositide 3-kinase/AKT in radiation responses. Histol Histopathol 2004;19:915–23.
[75] Chang L, Graham PH, Hao J, Ni J, Bucci J, Cozzi PJ, et al. Acquisition of epithelial-mesenchymal transition and cancer stem cell phenotypes is associated with activation of the PI3K/Akt/mTOR pathway in prostate cancer radioresistance. Cell Death Dis 2013;4:e875. http://dx.doi.org/10.1038/cddis.2013.407.
[76] Nakamura JL, Karlsson A, Arvold ND, Gottschalk AR, Pieper RO, Stokoe D, et al. PKB/Akt mediates radiosensitization by the signaling inhibitor LY294002 in human malignant gliomas. J Neurooncol 2005;71:215–22. http://dx.doi.org/10.1007/s11060-004-1718-y.
[77] Cerniglia GJ, Karar J, Tyagi S, Christofidou-Solomidou M, Rengan R, Koumenis C, et al. Inhibition of autophagy as a strategy to augment radiosensitization by the dual phosphatidylinositol 3-kinase/mammalian target of rapamycin inhibitor NVP-BEZ235. Mol Pharmacol 2012;82:1230–40. http://dx.doi.org/10.1124/mol.112.080408.
[78] Schaaf MBE, Jutten B, Keulers TG, Savelkouls KGM, Peeters HJM, van den Beucken T, et al. Canonical autophagy does not contribute to cellular radioresistance. Radiother Oncol 2015;114:406–12. http://dx.doi.org/10.1016/j.radonc.2015.02.019.
[79] He G, Wang Y, Pang X, Zhang B. Inhibition of autophagy induced by TSA sensitizes colon cancer cell to radiation. Tumor Biol 2013;35:1003–11. http://dx.doi.org/10.1007/s13277-013-1134-z.
[80] Park JM, Tougeron D, Huang S, Okamoto K, Sinicrope FA. Beclin 1 and UVRAG confer protection from radiation-induced DNA damage and maintain centrosome stability in colorectal cancer cells. PLoS ONE 2014;9:e100819. http://dx.doi.org/10.1371/journal.pone.0100819.
[81] McAfee Q, Zhang Z, Samanta A, Levi SM, Ma X-H, Piao S, et al. Autophagy inhibitor Lys05 has single-agent antitumor activity and reproduces the phenotype of a genetic autophagy deficiency. Proc Natl Acad Sci 2012;109:8253–8. http://dx.doi.org/10.1073/pnas.1118193109.
[82] Amaravadi RK, Winkler JD. Lys05: a new lysosomal autophagy inhibitor. Autophagy 2012;8:1383–4. http://dx.doi.org/10.4161/auto.20958.
[83] Kim KW, Myers CJ, Jung DK, Lu B. NVP-BEZ-235 enhances radiosensitization via blockade of the PI3K/mTOR pathway in cisplatin-resistant non-small cell lung carcinoma. Genes Cancer 2014;5:293–302.
[84] Choi EJ, Ryu YK, Kim SY, Wu HG, Kim JS, Kim IH, et al. Targeting epidermal growth factor receptor-associated signaling pathways in non-small cell lung cancer cells: implication in radiation response. Mol Cancer Res 2010;8:1027–36. http://dx.doi.org/10.1158/1541-7786.MCR-09-0507.
[85] No M, Choi EJ, Kim IA. Targeting HER2 signaling pathway for radiosensitization: alternative strategy for therapeutic resistance. Cancer Biol Ther 2009;8:2351–61.
[86] Brüning A, Rahmeh M, Friese K. Nelfinavir and bortezomib inhibit mTOR activity via ATF4-mediated sestrin-2 regulation. Mol Oncol 2013;7:1012–8. http://dx.doi.org/10.1016/j.molonc.2013.07.010.
[87] Zhuang W, Li B, Long L, Chen L, Huang Q, Liang Z. Induction of autophagy promotes differentiation of glioma-initiating cells and their radiosensitivity. Int J Cancer J Int Cancer 2011;129:2720–31. http://dx.doi.org/10.1002/ijc.25975.
[88] Chang S-H, Minai-Tehrani A, Shin J-Y, Park S, Kim J-E, Yu K-N, et al. Beclin1-induced autophagy abrogates radioresistance of lung cancer cells by suppressing osteopontin. J Radiat Res (Tokyo) 2012;53:422–32.
[89] Gravina GL, Marampon F, Sherris D, Vittorini F, Di Cesare E, Tombolini V, et al. Torc1/Torc2 inhibitor, Palomid 529, enhances radiation response modulating CRM1-mediated survivin function and delaying DNA repair in prostate cancer models. Prostate 2014;74:852–68. http://dx.doi.org/10.1002/pros.22804.
[90] Anbalagan S, Pires IM, Blick C, Hill MA, Ferguson DJP, Chan DA, et al. Radiosensitization of renal cell carcinoma in vitro through the induction of autophagy. Radiother Oncol J Eur Soc Ther Radiol Oncol 2012;103:388–93. http://dx.doi.org/10.1016/j.radonc.2012.04.001.
[91] Su Y-C, Yu C-C, Hsu F-T, Fu S-L, Hwang J-J, Hung L-C, et al. Everolimus sensitizes Ras-transformed cells to radiation in vitro through the autophagy pathway. Int J Mol Med 2014;34:1417–22. http://dx.doi.org/10.3892/ijmm.2014.1927.
[92] Kim KW, Hwang M, Moretti L, Jaboin JJ, Cha YI, Lu B. Autophagy upregulation by inhibitors of caspase-3 and mTOR enhances radiotherapy in a mouse model of lung cancer. Autophagy 2008;4:659–68.

[93] He J-H, Liao X-L, Wang W, Li D-D, Chen W-D, Deng R, et al. Apogossypolone, a small-molecule inhibitor of Bcl-2, induces radiosensitization of nasopharyngeal carcinoma cells by stimulating autophagy. Int J Oncol 2014;45:1099–108. http://dx.doi.org/10.3892/ijo.2014.2497.
[94] Cruickshanks N, Tang Y, Booth L, Hamed H, Grant S, Dent P. Lapatinib and obatoclax kill breast cancer cells through reactive oxygen species-dependent endoplasmic reticulum stress. Mol Pharmacol 2012;82:1217–29. http://dx.doi.org/10.1124/mol.112.081539.
[95] Moretti L, Kim KW, Jung DK, Willey CD, Lu B. Radiosensitization of solid tumors by Z-VAD, a pan-caspase inhibitor. Mol Cancer Ther 2009;8:1270–9. http://dx.doi.org/10.1158/1535-7163.MCT-08-0893.
[96] Liu M, Ma S, Liu M, Hou Y, Liang B, Su X, et al. Synergistic killing of lung cancer cells by cisplatin and radiation via autophagy and apoptosis. Oncol Lett 2014;7:1903–10. http://dx.doi.org/10.3892/ol.2014.2049.
[97] Daido S, Yamamoto A, Fujiwara K, Sawaya R, Kondo S, Kondo Y. Inhibition of the DNA-dependent protein kinase catalytic subunit radiosensitizes malignant glioma cells by inducing autophagy. Cancer Res 2005;65:4368–75. http://dx.doi.org/10.1158/0008-5472.CAN-04-4202.
[98] Wilson EN, Bristol ML, Di X, Maltese WA, Koterba K, Beckman MJ, et al. A switch between cytoprotective and cytotoxic autophagy in the radiosensitization of breast tumor cells by chloroquine and vitamin D. Horm Cancer 2011;2:272–85. http://dx.doi.org/10.1007/s12672-011-0081-7.
[99] Bristol ML, Di X, Beckman MJ, Wilson EN, Henderson SC, Maiti A, et al. Dual functions of autophagy in the response of breast tumor cells to radiation: cytoprotective autophagy with radiation alone and cytotoxic autophagy in radiosensitization by vitamin D 3. Autophagy 2012;8:739–53. http://dx.doi.org/10.4161/auto.19313.
[100] Sundaram S, Sea A, Feldman S, Strawbridge R, Hoopes PJ, Demidenko E, et al. The combination of a potent vitamin D3 analog, EB 1089, with ionizing radiation reduces tumor growth and induces apoptosis of MCF-7 breast tumor xenografts in nude mice. Clin Cancer Res Off J Am Assoc Cancer Res 2003;9:2350–6.
[101] Kim KW, Moretti L, Mitchell LR, Jung DK, Lu B. Combined Bcl-2/mTOR inhibition leads to enhanced radiosensitization via induction of apoptosis and autophagy in non-small-cell lung tumor xenograft model. Clin Cancer Res Off J Am Assoc Cancer Res 2009;15:6096–105. http://dx.doi.org/10.1158/1078-0432.CCR-09-0589.
[102] Kim KW, Mutter RW, Cao C, Albert JM, Freeman M, Hallahan DE, et al. Autophagy for cancer therapy through inhibition of pro-apoptotic proteins and mammalian target of rapamycin signaling. J Biol Chem 2006;281:36883–90. http://dx.doi.org/10.1074/jbc.M607094200.
[103] Kroemer G, Levine B. Autophagic cell death: the story of a misnomer. Nat Rev Mol Cell Biol 2008;9:1004–10. http://dx.doi.org/10.1038/nrm2527.
[104] Shen S, Kepp O, Kroemer G. The end of autophagic cell death? Autophagy 2012;8:1–3. http://dx.doi.org/10.4161/auto.8.1.16618.
[105] Klionsky DJ, Abeliovich H, Agostinis P, Agrawal DK, Aliev G, Askew DS, et al. Guidelines for the use and interpretation of assays for monitoring autophagy in higher eukaryotes. Autophagy 2008;4:151–75.
[106] Klionsky DJ, Abdalla FC, Abeliovich H, Abraham RT, Acevedo-Arozena A, Adeli K, et al. Guidelines for the use and interpretation of assays for monitoring autophagy. Autophagy 2012;8:445–544. http://dx.doi.org/10.4161/auto.19496.
[107] Gewirtz DA. The autophagic response to radiation: relevance for radiation sensitization in cancer therapy. Radiat Res 2014;182:363–7. http://dx.doi.org/10.1667/RR13774.1.
[108] Rosenfeld MR, Ye X, Supko JG, Desideri S, Grossman SA, Brem S, et al. A phase I/II trial of hydroxychloroquine in conjunction with radiation therapy and concurrent and adjuvant temozolomide in patients with newly diagnosed glioblastoma multiforme. Autophagy 2014;10:1359–68. http://dx.doi.org/10.4161/auto.28984.

Publication no. 2

A potent autophagy inhibitor (Lys05) enhances the impact of ionizing radiation on human lung cancer cells H1299.

Cechakova L, **Ondrej M**, Pavlik V, Jost P, Cizkova D, Bezrouk A, Pejchal J, Amaravadi RK, Winkler JD, Tichy A

International Journal of Molecular Sciences. 2019;20(23):5881

IF(2019) = 4.183; Q2

Author contribution (30%)—co-author, the author participated in the drafting of the manuscript as well as its revision and editing. The author also participated in several experiments, such as PCR, fluorescence microscopy, and flow cytometry analysis, as well as in the evaluation of the results.

This experimental study analyzed the impact of pre-treatment of non-small cell lung cancer cells (H1299, p53-negative) with various autophagy inhibitors before exposure to ionizing radiation. Concomitant treatment with autophagy inhibitors led to the successful radiosensitization of H1299 cells. Besides, treatment with the most studied autophagy inhibitor—Lys05 caused a reduction in cell proliferation and reduced ability of H1299 cells in clonogenicity. Inhibition of the autophagy itself is likely due to the blockade of autophagosome–lysosome fusion. The results, therefore, suggested that Lys05 could be used as a useful tool for the radiosensitization of H1299 cells and could provide a promising approach as a therapeutic strategy for lung cancer.

International Journal of
Molecular Sciences

MDPI

Article

A Potent Autophagy Inhibitor (Lys05) Enhances the Impact of Ionizing Radiation on Human Lung Cancer Cells H1299

Lucie Cechakova [1], Martin Ondrej [1], Vojtech Pavlik [2,3], Petr Jost [4], Dana Cizkova [5], Ales Bezrouk [6], Jaroslav Pejchal [4], Ravi K. Amaravadi [7], Jeffrey D. Winkler [7] and Ales Tichy [1,*]

1 Department of Radiobiology, Faculty of Military Health Sciences, University of Defense in Brno, 500 01 Hradec Kralove, Czech Republic; lucie.cechakova@unob.cz (L.C.); martin.ondrej@unob.cz (M.O.)
2 Cell Physiology Research Group, Contipro, 561 02 Dolni Dobrouc, Czech Republic; vojtech.pavlik@contipro.com
3 Institute of Dermatology, Third Faculty of Medicine, Charles University in Prague, 100 00 Prague 10-Vinohrady, Czech Republic
4 Department of Toxicology and Military Pharmacy, Faculty of Military Health Sciences, University of Defense in Brno, 500 01 Hradec Kralove, Czech Republic; petr.jost@unob.cz (P.J.); jaroslav.pejchal@unob.cz (J.P.)
5 Department of Histology and Embryology, Faculty of Medicine in Hradec Kralove, Charles University in Prague, 500 01 Hradec Kralove, Czech Republic; CizkovaD@lfhk.cuni.cz
6 Department of Medical Biophysics, Faculty of Medicine in Hradec Kralove, Charles University in Prague, 500 01 Hradec Kralove, Czech Republic; BezroukA@lfhk.cuni.cz
7 Abramson Cancer Center and Perelman School of Medicine, University of Pennsylvania, Philadelphia, PA 19104, USA; Ravi.Amaravadi@uphs.upenn.edu (R.K.A.); winkler@sas.upenn.edu (J.D.W.)
* Correspondence: ales.tichy@unob.cz; Tel.: +420-973-253-216

Received: 4 October 2019; Accepted: 20 November 2019; Published: 23 November 2019

Abstract: Autophagy inhibition through small-molecule inhibitors is one of the approaches to increase the efficiency of radiotherapy in oncological patients. A new inhibitor—Lys05—with the potential to accumulate within lysosomes and to block autophagy was discovered a few years ago. Several studies have addressed its chemosensitizing effects but nothing is known about its impact in the context of ionizing radiation (IR). To describe its role in radiosensitization, we employed radioresistant human non-small cell lung carcinoma cells (H1299, p53-negative). Combined treatment of H1299 cells by Lys05 together with IR decreased cell survival in the clonogenic assay and real-time monitoring of cell growth more than either Lys05 or IR alone. Immunodetection of LC3 and p62/SQSTM1 indicated that autophagy was inhibited, which correlated with increased *SQSTM1* and decreased *BNIP3* gene expression determined by qRT-PCR. Fluorescence microscopy and flow cytometry uncovered an accumulation of lysosomes. Similarly, transmission electron microscopy demonstrated the accumulation of autophagosomes confirming the ability of Lys05 to potentiate autophagy inhibition in H1299 cells. We report here for the first time that Lys05 could be utilized in combination with IR as a promising future strategy in the eradication of lung cancer cells.

Keywords: autophagy; ionizing radiation; Lys05; cancer; non-small cell lung carcinoma

1. Introduction

Lung cancer and non-small cell lung carcinoma (NSCLC) in particular represents the leading cause of cancer-related mortality worldwide [1,2]. Because of conditions making progressed tumor inoperable, the majority of patients are treated by radiation therapy (RT). However, the radioresistance of NSCLC contributes to unsatisfactory recurrence, driving an escalating interest in the improvement of the treatment [1,2].

One of the options, which could increase the efficacy of RT, is the modulation of autophagy. Autophagy is an intracellular mechanism enabling the eradication of damaged organelles and proteins in order to protect cells from stress triggered by various stimuli, including IR. It utilizes lysosomes as the tools for the degradation of substrates [3]. Typically, the double-membrane autophagosome (phagophore) is formed in order to absorb molecules to be degraded. This process consists of induction, nucleation, elongation, and maturation. While the main regulator of nucleation is phosphoinositide 3-kinase (PI3K), autophagosome formation relies on ubiquitin-like conjugation systems (ATG12 and LC3). Finally, lysosome fuses with autophagosome to form autophagolysosome and triggers the release of the acidic lysosomal hydrolases, which degrade the cytosolic substrates [4]. Notwithstanding, autophagy is a somewhat controversial process. Current literature describes autophagy as a mechanism with two opposing roles in tumor cells. In the early stages of cancer development, autophagy contributes to the suppression of tumor growth. On the other hand, in the advanced stages of cancer development, it acts as a promoter of carcinogenesis [4]. Since autophagy has been believed to be a protective mechanism in developed cancers, inhibition of this process seems to be a promising strategy to enhance the efficacy of RT.

Lys05—a new autophagy inhibitor—was reported for the first time by McAfee et al. several years ago. It is a dimeric form of a well-established autophagy inhibitor chloroquine (CQ). Mechanistically, Lys05 similarly as CQ and hydroxychloroquine (HCQ) has the potential to accumulate within lysosomes and to block autophagy even more effectively than CQ or HCQ. Moreover, it exhibits the most potent anti-tumor activity as a single agent among the three above-mentioned inhibitors both in vitro and in vivo [5]. Although Lys05 is a promising agent, no study examined its sensitizing effect in combination with IR so far.

The aim of our study was to sensitize the radioresistant H1299 cells toward IR using the specific autophagy inhibitor Lys05 and to describe the underlying molecular mechanisms involved in this process. For comparison of the Lys05-induced anti-proliferative effect, we used two established autophagy inhibitors: Bafilomycin A1 (Baf) and Spautin-1. Baf is an inhibitor with a similar mechanism of action as Lys05. It inhibits the final step of the autophagic process—a fusion between autophagosomes and lysosomes [6]. Spautin-1 works differently. It specifically targets the Beclin-1 subunit of the PI3K complex and causes its degradation [7,8]. It has been shown to enhance IR-induced cell death [9] and to reduce tumor growth in mice xenografts without side effects [8]. CQ or HCQ has not been used as controls in our study since head-to-head comparison with Lys05 had previously been described by McAfee et al. [5].

The combination of IR and Lys05 led to more efficient eradication of radioresistant cells compared to either agent alone. These results suggest that Lys05 might provide an efficient tool for the radiosensitization of cancer cells and could be utilized as a promising future strategy in radiotherapy of lung cancer.

2. Results

2.1. Treatment of H1299 Cells by Autophagy Inhibitors and IR Causes a Decrease in Proliferation in a Concentration- and Dose-Dependent Manner

The xCELLigence system enables non-invasive real-time monitoring of cell characteristics such as viability, proliferation, and adhesion. This assay is performed in microtiter plates with gold electrodes on the bottom of each well and changes in electrical impedance are measured. Cell culture was monitored every 30 min for five days. Obtained data were expressed as cell index. The higher the cell index value, the more cells are attached to the electrodes [10,11].

Initially, we performed experiments with different concentrations of inhibitors and doses of IR. Spautin-1 was selected as a control in proliferation evaluating the methods. In order to compare the overall inhibition effect of the studied autophagy inhibitor—Lys05, we used the inhibitor possessing a different mechanism of action (unlike for further experiments with autophagosome accumulation). For the sake of simplicity, we compared our results with only one inhibitor in each method. We observed

a concentration-dependent decrease in cell proliferation in the groups treated by both Spautin-1 and Lys05 alone. Similarly, the higher the dose of IR, the more pronounced decrease in proliferation was achieved (data are shown in Figure S1). Based on these results, we selected 2 μM Lys05 or 2 μM Spautin-1 as the lowest concentration and the lowest dose of 2 Gy (actually a D0 that causes cell death in 63% of the cell population) for the further experiments. The higher concentration and doses would probably lead to more intensive effects, but our effort was driven by the radiosensitization hypothesis—the combined effect of the lowest doses of agents possibly leading to a mutual potentiation of the anti-proliferative effect.

The combination of 2 Gy and 2 μM Lys05 or Spautin-1 resulted in a more pronounced decrease in proliferation than single treatment (Figure 1A).

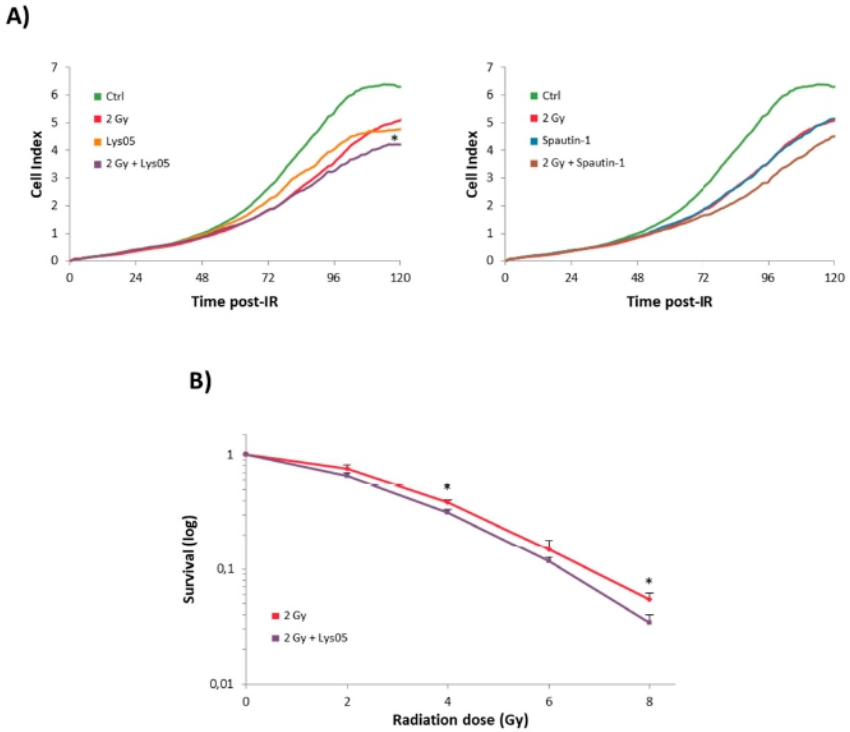

Figure 1. Autophagy inhibitors caused a decline in H1299 cell proliferation. The H1299 cells were treated either by ionizing radiation (IR) or inhibitor alone or by their combination. Lys05 or Spautin-1 in 2 μM concentration was added to the cells one hour prior to irradiation (2, 4, 6, and 8 Gy). (**A**) Cell proliferation was measured by the xCELLigence system and recorded every 30 min for six days. * Significant difference compared to control (p-value ≤ 0.05) as a result of one experiment performed in triplicate. (**B**) Clonogenic assay displays average values ± SD from three independent experiments in triplicates counted by eye after the 10-day incubation period. * Significant difference compared to solely irradiated group (p-value ≤ 0.05).

2.2. Lys05 Renders H1299 Cells More Sensitive to IR

The real-time monitoring provided valuable insight into cell-culture dynamics after the treatment. However, taking into account its limitations, we assessed the influence of Lys05 on H1299 cells in terms of radiosensitization by a more traditional radiobiological approach. Hence, the clonogenic assay was used.

H1299 cells were treated by Lys05 (2 μM) one hour prior to irradiation (2, 4, and 8 Gy). The survival fraction decreased in a dose-dependent manner. Administration of Lys05 resulted in statistically significant suppression of clonogenic ability compared to the cells exposed to IR only (Figure 1B). These results support our conclusion that the inhibition of autophagy by Lys05 enhanced the cytotoxicity of IR. Complete data are shown in Supplementary Figure S1.

2.3. The Combination of Inhibitors with Irradiation Shows an Additive Effect

Although the combined treatment of H1299 cells resulted in the most pronounced decrease in proliferation, we analyzed the combination index (CI) in order to determine the estimation of the extent of synergy or antagonism between each inhibitor and IR. CI was calculated based on the Chou–Talalay method (briefly reviewed in [12]) using the CompuSyn software. According to the CI value description published by Hernández et al. CI values under the 0.9 indicate synergism, CI values between 0.9 and 1.2 indicate additive effect, and CI values higher than 1.2 indicate antagonism [13].

We calculated the CI based on the anti-proliferative effects of the inhibitors and IR observed at a time point when the changes in proliferation were most prominent—100 hours after irradiation. Our data indicate the additive effects of both inhibitors and IR (Table 1 and Figure 2A).

Table 1. Combination index values for the combination of autophagy inhibitors Lys05 and Spautin-1 with IR. Data are of values from Figure 2. Fa = Fraction affected/cytotoxicity and CI = combination index.

IR Dose [Gy]	Dose of Lys05 [μM]	Fa	CI	IR Dose [Gy]	Dose of Spautin-1 [μM]	Fa	CI
2	2	0.39	1.02	2	2	0.43	1.04
2	5	0.47	0.94	2	5	0.39	1.91
2	10	0.52	0.97	2	10	0.65	0.83
4	2	0.52	1.23	4	2	0.65	0.92
4	5	0.65	0.93	4	5	0.63	1.14
4	10	0.58	1.27	4	10	0.74	0.89
8	2	0.77	1.23	8	2	0.85	0.93
8	5	0.82	1.02	8	5	0.82	1.07
8	10	0.78	1.20	8	10	0.85	0.96

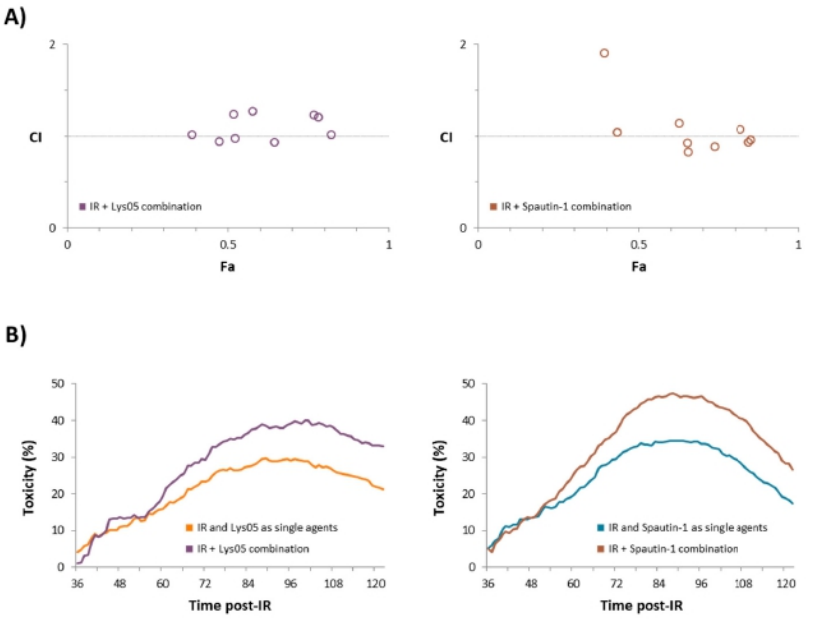

Figure 2. The combination of inhibitors with irradiation shows an additive effect. Data for these computations were derived from real-time monitoring of cell characteristics measured by the xCELLigence system. (**A**) Combination index was calculated based on the Chou–Talalay method using the CompuSyn software. The relevant Fa-CI plots are shown according to the data available in Table 1. Fa = fraction affected/toxicity and CI = combination index. (**B**) The time-dependent combined toxicity level was calculated based on the real-time monitoring data with a selected concentration of 2 μM for each inhibitor and a radiation dose of 2 Gy. The time-dependent combined toxicity level shows the ratio of the sum of anti-proliferative effects of each inhibitor and IR as single agents relative to the control compared with the ratio of the combination of inhibitor and IR relative to the control. The combined toxicity values were plotted versus time in hours.

Considering that CI evaluates the extent of synergism/antagonism only at one point in time, we compared the ratio of the sum of anti-proliferative effects of each inhibitor and IR as single agents relative to the control with the ratio of the combination of inhibitor and IR relative to the control. The concentration of each inhibitor and the dose of irradiation selected for this measurement were 2 μM and 2 Gy, respectively.

Based on this calculation, we observed stronger anti-proliferative effects provided by the combination of each inhibitor with IR depending on the time than their sum when acting as single agents (Figure 2B).

2.4. Lys05 Does Not Affect the Apical Parts of mTOR Signaling but Results in Increased LC3-II and p62/SQSTM1

To evaluate how Lys05 interferes with autophagy signaling pathways, we used two methods: (i) Western blotting (WB) and (ii) real-time quantitative reverse transcription PCR (qRT-PCR).

Using WB, we examined the level of mammalian target of rapamycin (mTOR) and its phosphorylated forms (serine 2448 and 2481), Unc-51 like autophagy activating kinase 1 (ULK-1) and its phosphorylated forms (serine 555 and 757), and proline-rich Akt substrate of 40 kDa (PRAS40) and its phosphorylated form (threonine 246) one, 24, and 48 h after irradiation. We did not notice any significant changes in any of the groups or time-points indicating that Lys05 does not affect the initial stage of autophagy signaling (Figure 3A).

Further on, we examined the microtubule-associated protein 1A/1B-light chain 3 (LC3) and ubiquitin-binding protein p62 (p62/SQSTM1). Administration of Lys05 and/or irradiation (2 Gy) led to an increase in LC3-II protein form and also to a non-significant increase in protein p62/SQSTM1 in the groups of cells treated either by Lys05 alone or by its combination with IR, especially after 48 h (Figure 3A). Increased LC3II/I ratio together with elevated levels of p62/SQSTM1 demonstrated the inhibition of autophagy via blockade of autophagosome-lysosome fusion [14].

As Western blotting is considered only a semi-quantitative approach, we utilized the microarray assay to perform a complex screening of the effects of Lys05 on the level of mRNA (data are available in Supplementary Tables S1 and S2, and GEO repository: GSE138650), which led us to further examination of two particular genes using qRT-PCR: *SQSTM1* and Bcl2 interacting protein 3 (*BNIP3*). These genes are well-known to be associated with autophagy [15,16]. Administration of Lys05 and/or irradiation (2 Gy) led to a significant increase in *SQSTM1* expression and decrease in *BNIP3* expression in the groups of cells treated either by Lys05 alone or by its combination with IR both after 24 and 48 h (Figure 3B).

2.5. Lys05 Induces the Early-Stage Autophagy but Subsequently Leads to Its Inhibition Resulting in Lysosome Accumulation

To further study the impact of autophagy inhibitors and IR on lysosomes, we used fluorescence microscopy focused on lysosome visualization and flow cytometry for quantification of changes in their fluorescence intensity. In both cases, we used a fluorescence dye Lysosensor Green DND-189 (LSG). LSG is a weak base that accumulates in acidic organelles. It can be used to measure the pH of acidic organelles—such as lysosomes—as it becomes more fluorescent in acidic environments.

We studied H1299 cells both one and 48 h after irradiation (2 Gy) pre-treated by Lys05 (2 μM) and Baf (15 nM) one hour prior to IR. Baf was selected as a control in this method because of its mechanism of action similar to Lys05—blockade of autophagosome-lysosome fusion. We presumed that using Baf as a control would enable comparison of the characteristics and intensity of the inhibition (rate of the autophagosome or lysosome accumulation). One hour after irradiation, we did not observe any changes in fluorescence intensity, cell shape, or lysosome number. However, 48 h after irradiation, we observed the increased granularity of cells followed by the increased fluorescence intensity and changes in cell size—cell enlargement, which could be caused by the accumulation of lysosomes. Similar results were obtained by experiments with Baf (Figure 4A,B).

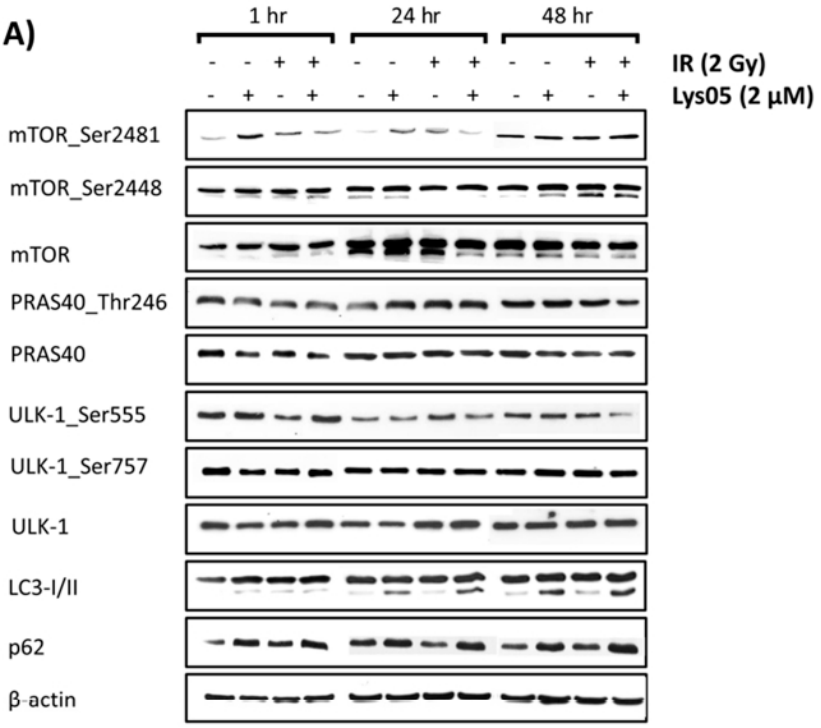

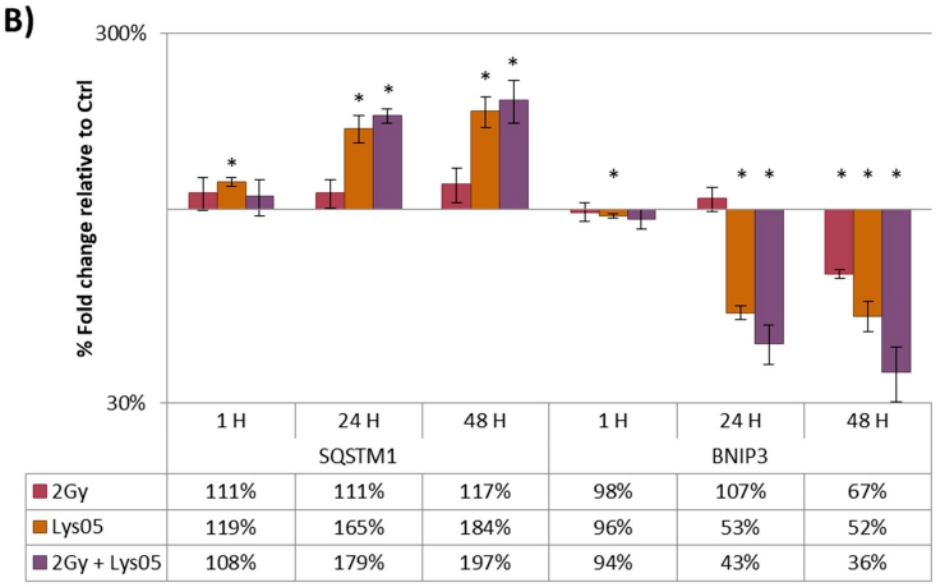

	1 H	24 H	48 H	1 H	24 H	48 H
	SQSTM1			BNIP3		
2Gy	111%	111%	117%	98%	107%	67%
Lys05	119%	165%	184%	96%	53%	52%
2Gy + Lys05	108%	179%	197%	94%	43%	36%

Figure 3. Administration of Lys05 blocks autophagosome-lysosome fusion. The H1299 cells were treated either by IR or the inhibitor alone or by their combination. Lys05 in 2 µM concentration was added to the cells one hour prior to irradiation (2 Gy). Data were analyzed one, 24, and 48 h after irradiation. (**A**) Western blot analysis of phosphorylated and non-phosphorylated proteins following treatment by IR and Lys05. Full-length blots are presented in Supplementary Figure S2. (**B**) qRT-PCR analysis of the expression of genes *SQSTM1* and *BNIP3*. Data represent the mean of the percentage fold change (±SD) relative to control based on three independent experiments performed in duplicate. * Significant difference compared to control (p-value ≤ 0.05).

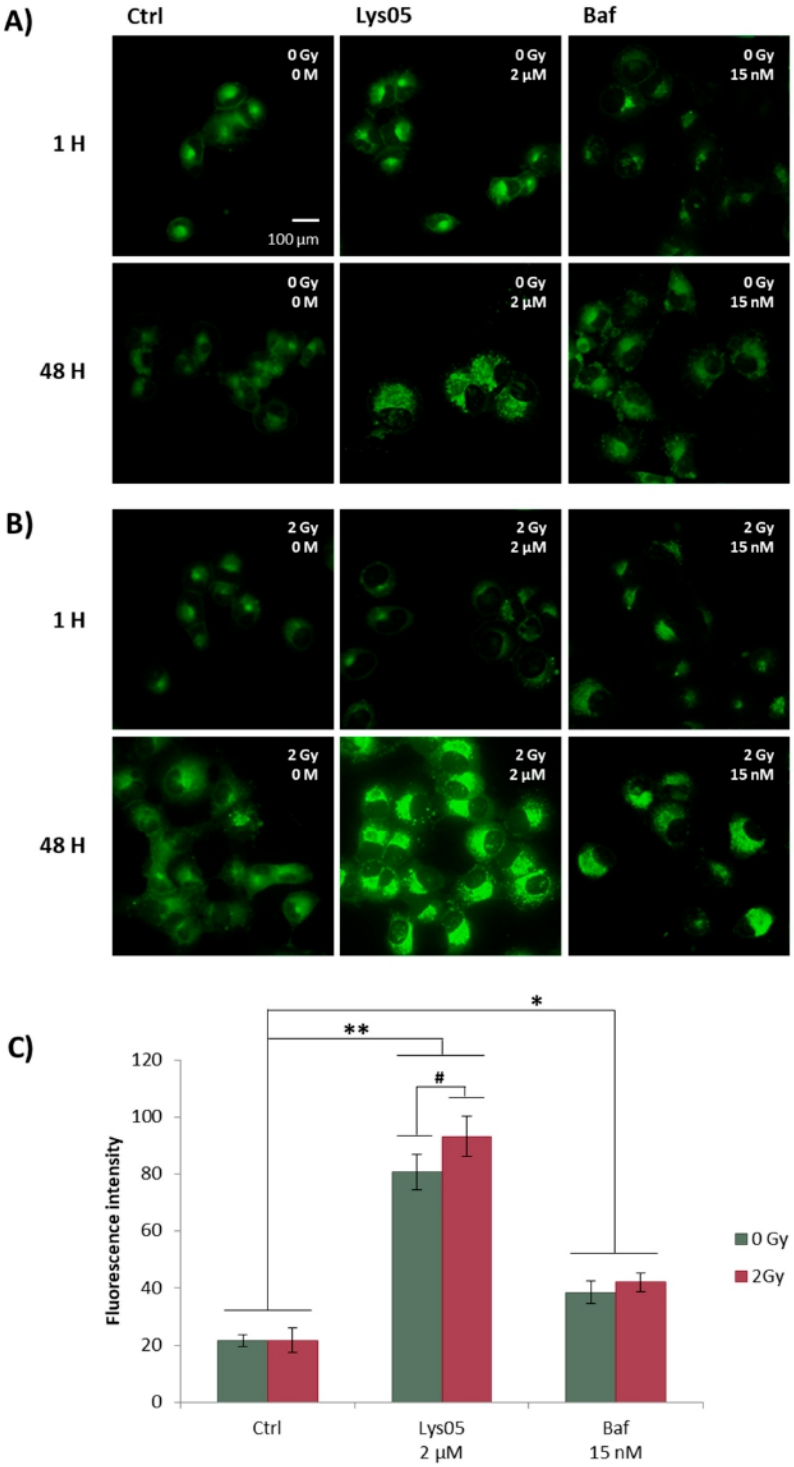

Figure 4. Administration of Lys05 leads to the accumulation of lysosomes. The H1299 cells were treated either by IR or the inhibitor alone or by their combination. Lys05 in 2 µM and Baf in 15 nM concentrations were added to the cells one hour prior to irradiation (2 Gy). For the sake of visualization, the cells were stained with the green dye—LysoSensor Green DND-189. (**A**) Non-irradiated H1299 cells were imaged by fluorescence microscopy at intervals of one and 48 h after the treatment. (**B**) Irradiated H1299 cells were imaged by fluorescence microscopy at intervals of one and 48 h after irradiation. (**C**) The intensity of fluorescence was measured by flow cytometry 48 h after irradiation only. The intensity plot displays average values ±SD from one experiment performed in triplicate * Significant difference compared to control (p-value ≤ 0.05). ** Significant difference compared to control (p-value ≤ 0.01). # Significant difference compared to non-irradiated group (p-value ≤ 0.05).

In order to quantify changes in fluorescence intensity, we performed flow cytometry determination with the same treatment scheme as used for fluorescence microscopy. Since no changes in fluorescence intensity were observed in the group visualized one hour after irradiation, we quantified the fluorescence intensity 48 h after irradiation only. The results from flow cytometry correlate with those from fluorescence microscopy, demonstrating a significant increase in fluorescence intensity in the cells treated both with Lys05 and Baf (Figure 4C). We speculate that such a substantial increase in fluorescence intensity might be the result of two subsequent events: (i) Activation of autophagy by the inhibitor in the early stage, and (ii) actual inhibition of autophagy due to blockade of autophagosome-lysosome fusion in the late stage of the autophagic process.

2.6. Lys05 Potentiates Autophagy Inhibition in H1299 Cells via Accumulation of Autophagosomes

Consistently with fluorescence microscopy and flow cytometry, transmission electron microscopy (TEM) was used for ultrastructural visualization. Autophagy suppression induced by the inhibitor in the late stage of the autophagic process resulted in autophagy vacuole accumulation. Autophagy was inhibited in cells treated by Lys05 alone, which is evidenced by the increased number of autophagic vesicles. The cells irradiated by a dose of 2 Gy also showed a higher number of vesicles in comparison to the control group. Importantly, the combination of Lys05 and IR resulted in a substantial increase in the number of autophagic vacuoles in H1299 cells, indicating the efficient inhibition of autophagy (Figure 5).

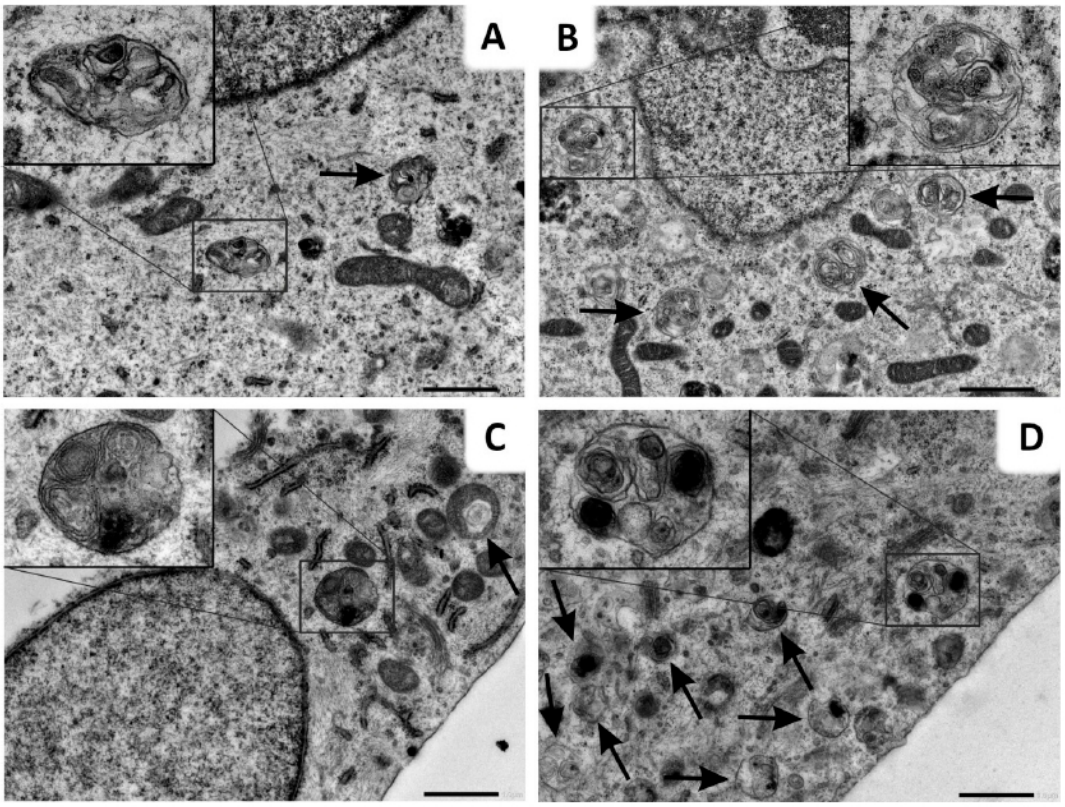

Figure 5. Administration of Lys05 leads to the accumulation of autophagosomes. (**A**) Some of the control group cells contained autophagosomes in their cytoplasm. In comparison with cells of other experimental groups, autophagosomes of the control cells were apparently smaller and less numerous. (**B**) Lys05-treated cells (2 μM) contained medium-sized and frequent autophagosomes. (**C**) In irradiated cells (2 Gy), large autophagosomes were often observed in their cytoplasm. (**D**) All irradiated and Lys05-treated cells (2 Gy + 2 μM) contained numerous autophagosomes of various sizes in their cytoplasm. Black arrows indicate autophagosomes. Scale bar (**A**–**D**) 1 μm (mag. 8000×); insert mag. (**A**) 19700×, (**B**) 17000×, (**C**,**D**) 17600×.

In order to validate our data, we compared the effect of Lys05 with Baf treatment. Similarly to fluorescence microscopy, we aimed to compare the nature of autophagosome–lysosome blockade, therefore we selected an inhibitor with a similar mechanism of action as Lys05. Initially, we found out that several control group cells contained structures resembling autophagosomes. They lacked some characteristic features—they were not double-membraned. On the other hand, Baf-treated cells contained medium-sized autophagosomes in their cytoplasm as well as irradiated-only cells. Similarly to Lys05, the combination of the inhibitor and IR led to the intensive formation of autophagosomes, as the majority of the cells contained more autophagosomes than after IR- or Baf-treatment only (Figure 6).

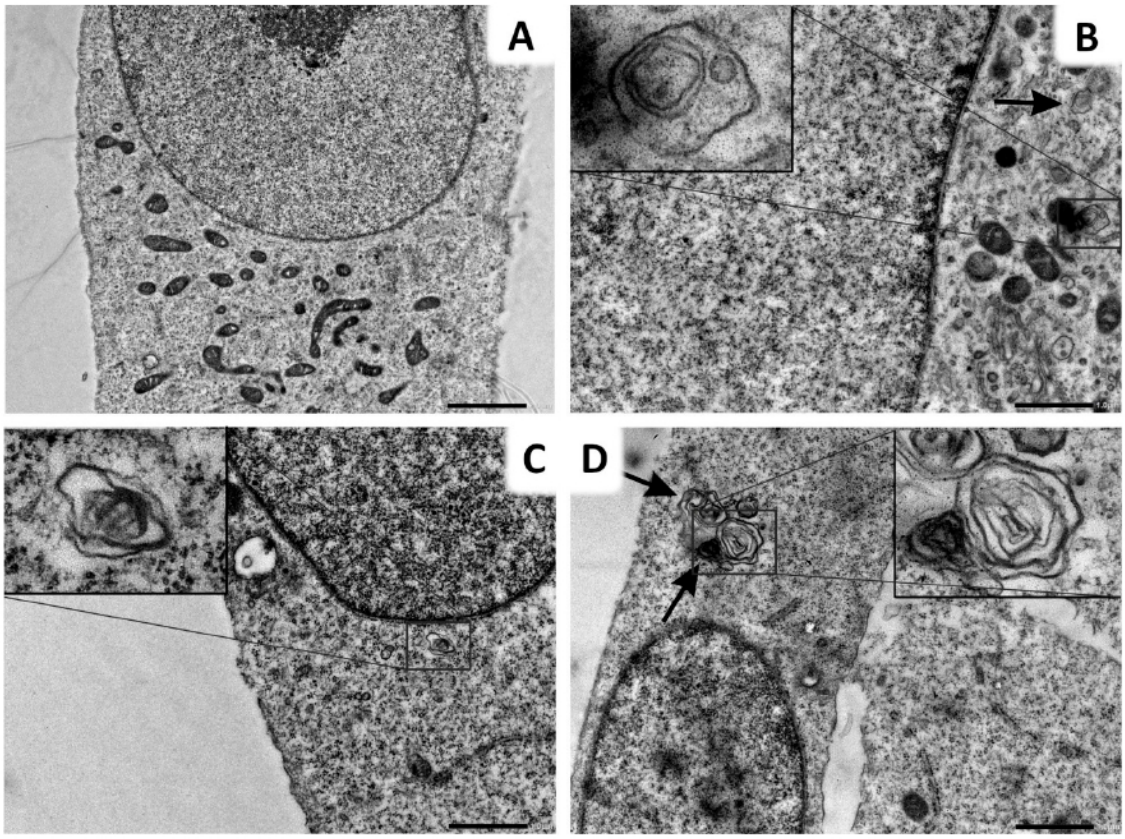

Figure 6. Administration of Baf leads to the accumulation of autophagosomes. (**A**) Several control group cells contained structures resembling autophagosomes, but they lacked some characteristic features—they were not double-membraned. (**B**) Baf-treated cells (15 nM) contained medium-sized autophagosomes (arrow). (**C**) In solely irradiated cells (2 Gy) autophagosomes were formed as well. (**D**) Almost all irradiated and Baf treated cells (2 Gy + 15 nM) contained numerous autophagosomes (arrows) in their cytoplasm. Scale bar (**A**) 2 μm (mag. 4 000×); (**B**–**D**) 1 μm (mag. 8000×); insert mag. (**B**) 32000×, (**C**) 31600× and (**D**) 21000×.

3. Discussion

The majority of patients with NSCLC are treated by RT. Autophagy is believed to be a radioprotective mechanism in cancer cells. Thus, its inhibition may render cells more vulnerable, thereby increasing the efficiency of RT. We employed radioresistant human non-small cell lung carcinoma cells (H1299, p53-negative) in order to examine their response to IR and combined treatment with the specific autophagy inhibitor Lys05.

Autophagy inhibitors have been addressed in a plethora of studies with the aim of the radiosensitization of cancer cells. For example, CQ derivatives are commonly-used inhibitors of autophagy which are already approved for clinical trials focusing on cancer therapy [17]. Regarding these studies, Toulany et al. [18], as well as Karagounis et al. [19], reported the radiosensitizing effect

of CQ on lung cancer cells as a result of autophagy blockade. Even though both CQ and HCQ can effectively inhibit autophagy, the doses necessary for the appropriate effect in vitro are not consistently achievable in patients, and there is an identified need for new inhibitors with better physicochemical and pharmacokinetic properties. The autophagy inhibitor Lys05, a derivative of CQ, was described by Amaravadi et al. in 2012 [20]. Lys05 can accumulate inside the lysosomes more potently than HCQ and is, therefore, a promising newly-developed autophagy inhibitor.

To study the radiosensitizing effect of Lys05, we applied real-time monitoring of H1299 cell proliferation by which we detected a concentration-dependent decrease in cell proliferation. According to our data, we argue that such treatment might contribute to suppressed autophagy that serves as a promoter of carcinogenesis in advanced tumors, providing nutrients for higher metabolic requirements [4,21]. Moreover, a drop in cell proliferation after combined treatment by IR suggests that pre-incubation with Lys05 leads to the radiosensitization of H1299 cells.

In regards to molecular mechanisms of Lys05 action, we examined the level of the key regulatory proteins of the autophagic process as well as gene expression of related genes: *SQSTM1* and *BNIP3*. Since protein p62/SQSTM1 accumulates inside the cells when autophagy is suppressed, and it is degraded during the autophagic process, it was established as a marker of autophagy [15]. It has been generally accepted that IR induces autophagy in radioresistant H1299 cells [22] and in several other cell lines [23]. In this respect, we observed the rather unchanged levels of protein p62/SQSTM1 and its coding gene *SQSTM1* in solely-irradiated H1299 cells after 48 h. On the other side, we found an elevated level of p62/SQSTM1 together with increased gene expression of *SQSTM1* 48 h after IR combined with pre-treatment by Lys05. These findings are consistent with the study of Koukourakis et al., who similarly described an unchanged level of p62/SQSTM1 in the solely-irradiated and elevated level of p62/SQSTM1 in Baf-pre-treated radioresistant PC3 prostate cancer cells [21].

Furthermore, in ongoing autophagy, BNIP3 interacts with LC3 to recycle endoplasmic reticulum and mitochondria. When inactive BNIP3 is activated, LC3 binds to the LC3-interacting region motif on BNIP3 and facilitates the formation of an autophagosome [24]. Since activation of BNIP3 is a pro-autophagic mechanism [16], downregulation of the expression of its coding gene *BNIP3* may indicate the inhibition of autophagy [25]. Besides, LC3 is cleaved to LC3-I (cytosolic form) and LC3-II (membrane-associated form) during autophagy. Thus, detectable LC3 cleavage is generally considered as a marker of ongoing autophagic flux. Physiologically, LC3-II is in later stages of autophagy degraded by lysosomal hydrolases along with intra-autophagosomal content resulting in complete LC3 disappearance [14,26]. However, using of specific autophagy inhibitors, e.g., Baf [6,27], might lead to a late-stage increase in LC3-II, consistent with our data, that suggests either the enhanced autophagosome synthesis or reduced autophagosome recycling [28,29].

Moreover, in terms of autophagy inhibition, interpreting p62/SQSTM1 level or LC3II/I ratio separately is discouraged in favor of the conclusions provided by their mutual interpretation. In this respect, Mizushima and Yoshimori demonstrated that increased levels of p62/SQSTM1 together with elevated LC3II/I ratio indicate rather the inhibition of autophagic process than its activation [14]. On this basis, we came to an assumption of the late-stage autophagy inhibition because of the blockade of autophagosome-lysosome fusion.

Apparently, there are two traceable hallmarks that accompany the late-stage autophagy inhibition: (i) accumulation of autophagosomes and (ii) associated accumulation of lysosomes. According to our TEM data, increased accumulation of autophagic vacuoles was observed both in the Baf- and Lys05-treated cells. Importantly, the cells treated by a combination of Lys05 with IR exhibited substantial accumulation of autophagic vacuoles. This is consistent with the study by Makowska et al. who observed elevated levels of autophagosomes after co-treatment of nasopharyngeal carcinoma by CQ and IR [30].

Using fluorescence microscopy, we detected a significant increase in LSG fluorescence intensity (in parallel quantified by flow cytometry) in cells treated by either IR alone or in combination with the inhibitors of autophagy. We assume that such an increase might be the result of lysosome accumulation

caused by the blockade of autophagosome–lysosome fusion. These results are in correlation with studies by Lu et al. [31] and Chikte et al. [32], who used CQ as an autophagy inhibitor. In both studies, the time- and dose-dependent increase in fluorescence intensity was observed. According to Lu et al. an increase in LSG staining intensity could be attributed to the elevated lysosome volume [31]. Similarly, Chikte et al. speculated that CQ induced the autophagic process in early stages but consequently, as the process progressed, it inhibited the autophagosome–lysosome fusion resulting in an incomplete autophagic flux [32].

Lys05 seems to be a promising autophagy inhibitor. Several studies engaging with its effects on tumor cells have been published lately. For example, Gade et al. used Lys05 for the treatment of rat hepatocellular carcinoma in association with transarterial embolization [33]. Ndoye et al. studied the link between the Wnt5A pathway and autophagy in melanoma cells [34]. DeVorkin et al. examined hypoxia-induced autophagy inhibition using Lys05 in combination with sunitinib in clear cell ovarian carcinoma demonstrating the remarkable chemosensitizing effect of the autophagy inhibitor—Lys05 [35].

4. Materials and Methods

4.1. Cell Cultures and Cultivation

Non-small cell lung carcinoma cells (H1299) were obtained from the American Type Culture Collections (Manassas, VA, USA). The cells were cultured at 37 °C in a humidified incubator under a controlled 5% CO_2 atmosphere and maintained in RPMI medium 1640 (Gibco, Paisley, UK) supplemented with 10% fetal bovine serum, 150 UI/mL penicillin, and 50 mg/mL streptomycin (all from Sigma-Aldrich, St. Louis, MO, USA). The culture was divided twice per week by dilution to a concentration of 2×10^5 cells/10 mL. The cell line in the maximal range of up to 15 passages was used for this study.

4.2. Cell Treatment

The cells were treated by autophagy inhibitors Lys05 (a kind gift from Dr. Amaravadi, Pennsylvania University, Philadelphia, PA, USA) and Spautin-1 (Calbiochem, San Diego, CA, USA) in various concentrations of 2, 5, and 10 μM and Baf in 15 nM concentration. Inhibitors were added to the cells 1 h prior to irradiation. The cells in either flask, tube, or 6-well plate, were irradiated using a ^{60}Co gamma-ray source with a dose rate of 0.44 Gy/min. After irradiation, the cells were transferred back into an incubator and cultivated further for the prescribed time according to the particular experiment.

4.3. Cell Growth Real-Time Monitoring

The xCELLigence system was used according to the manufacturer's instructions (ACEA Biosciences, Inc.; San Diego, CA, USA). First, 50 μL of a growth medium was added to each well, and the background impedance was measured. One hundred microliter of cell suspension (a total number of 3×10^3 per well) were then added, and the plate was left at room temperature for 30 min to allow the cells to attach homogeneously. The cells were treated by either IR or inhibitor alone, or by their combination. Various concentrations of both Spautin-1 and Lys05 (2, 5, and 10 μM) were added into the cell culture 1 h prior to irradiation (2, 4, and 8 Gy). The cell proliferation was measured and recorded continuously every 30 min for 5 days. Statistical analysis was performed by an independent two-sample t-test with unequal variances and a critical p-value equal to 0.05.

4.4. Clonogenic Assay

The cells were trypsinized, re-plated in 6-well plates, treated by Lys05 (2 μM) 1 h prior to irradiation (2, 4, 6, and 8 Gy) and then left to form colonies. After a 10-day incubation period (37 °C, 5% CO_2), colonies were stained using 1% crystal violet in methanol and counted by eye with a cut-off of 50 viable cells.

4.5. The Combination Index and a Time-Dependent Combined Toxicity Level Calculations

The real-time monitoring data were used to calculate both the CI and a time-dependent combined toxicity level. Median-effect computer software CompuSyn for Windows (ComboSyn, Inc., available here: http://www.combosyn.com) set up by Dr. Dorothy Chou was used to generate the combination index values. The extent of synergy/antagonism was evaluated according to the CI value description published by Hernandez et al. where CI values under the 0.9 indicate synergism, CI values between 0.9 and 1.2 indicate additive effect, and CI values higher than 1.2 indicate antagonism (full CI value description table available here: [13]).

A time-dependent combined toxicity levels were calculated based on these equations:

$$T_{L+IR} = \frac{(T_L + T_{IR})}{2 * T_{Ctrl}} \quad (1)$$

$$T_{LIR} = \frac{(T_{LIR_comb})}{T_{Ctrl}} \quad (2)$$

$$T_{S+IR} = \frac{(T_S + T_{IR})}{2 * T_{Ctrl}} \quad (3)$$

$$T_{SIR} = \frac{(T_{SIR_comb})}{T_{Ctrl}} \quad (4)$$

where T, in general, represents the antiproliferative/toxic effects of Lys05, Spautin-1, IR, or their combination. Following, T_{L+IR} represents the antiproliferative/toxic effect of the sum of Lys05 and IR when acting as single agents, T_{LIR} represents the antiproliferative/toxic effect of the combination of Lys05 and IR, T_{S+IR} represents the antiproliferative/toxic effect of the sum of Spautin-1 and IR when acting as single agents, and T_{SIR} represents the antiproliferative/toxic effect of the combination of Spautin-1 and IR.

4.6. Western Blot

The cells were harvested at different time intervals, and proteins were extracted using lysis buffer (137 mM NaCl; 10% glycerol; 1% n-octyl-β-glucopyranoside; 50 mM NaF; 20 mM Tris, pH 8; 1 mM Na_3VO_4) supplemented by cocktail protease inhibitor (Complete Mini, Roche, Basel, CHN). Equivalent amounts of samples (30 µg) were mixed with sample loading buffer and heated at 95 °C for 5 min. Proteins were separated on 10% gel by SDS-PAGE (200 V, 40 min) and subsequently transferred onto a PVDF membrane (100 V, 120 min). The membrane was blocked using 5% non-fat dry milk in TBST at room temperature (RT) for 1 h. After blocking, primary antibodies (p62/SQSTM1 Antibody 1:1000; LC3B Antibody 1:1000; p-PRAS40 (Thr246) Antibody 1:1000; Cell Signaling Technology, Danvers, MA, USA) were added and incubated overnight on a shaker at 4 °C. Afterward, the membrane was rinsed with TBST (3 × 10 min) and incubated with peroxidase-labeled secondary antibody (Dako, Glostrup, DEN) at RT for 1 h. The membrane was developed using ECL reagent (BM Chemiluminescence—POD, Roche, Manheim, GER). Representative blots from three independent experiments are shown.

4.7. Real-Time Quantitative Reverse Transcription PCR

The cells were lysed using the RLT buffer (QIAGEN, Hilden, Germany) with the addition of 1% β-mercaptoethanol 1, 24, and 48 h after irradiation. Then, RNA was isolated from the lysates using the RNeasy lipid tissue mini kit (QIAGEN) and QIAcube (QIAGEN) according to the manufacturer's instructions. The quality and concentration of eluted RNA was assessed spectrophotometrically on NanoDrop One Microvolume UV-Vis Spectrophotometer (Thermo Fisher Scientific, Waltham, MA, USA). Two-step qRT-PCR was used to analyze the changes in gene expression. In the first step, RNA (1 µg) in a concentration of 100 ng/µL was transcribed into cDNA using the high capacity cDNA reverse transcription kit (Thermo Fisher Scientific) according to the manufacturer's instructions. In the

second step, each qRT-PCR reaction was prepared according to the manufacturer's instructions in duplicate containing TaqMan fast advanced master mix (Life Technologies, Thermo Fisher Scientific), *TBP* (Hs00427620_m1), *SQSTM1* (Hs00177654_m1), *BNIP3* (Hs00969291_m1) probes and 10 ng (1 ng/μL) of cDNA template. The qRT-PCR analyses were performed using the fast-cycling profile of StepOnePlus real-time PCR system and StepOnePlus Software (Life Technologies, Thermo Fisher Scientific). Obtained data were analyzed by the Livak method [36] using *TBP* as a reference gene. Statistical analysis was performed by an independent two-sample t-test with unequal variances and a critical *p*-value equal to 0.05.

4.8. Transmission Electron Microscopy

The cells were harvested 45 h after irradiation. Then, 3% glutaraldehyde (in 0.1 M cacodylate buffer, pH 7.2; Sigma) was used for cell fixation and the cells were fixed for 5 min at 37 °C and then for 3 h at room temperature. Subsequently, the cells were washed in cacodylate buffer (0.1 M, pH 7.2) and post-fixed in 1% OsO_4 (in 0.1 M cacodylate buffer, pH 7.2; Sigma) for 1 h at room temperature. After the rinsing procedure, the cells were dehydrated in graded alcohols (50%, 75%, 96%, and 100%), clarified in propylene oxide and embedded in a mixture of Epon 812 and Durcupan (Sigma; polymerization for 3 days at 60 °C). Toluidine blue was used to stain the semithin sections. Ultrathin sections were cut on Ultrotome Nova (LKB, Sweden). These sections were then collected onto formvar carbon-coated copper grids, counterstained with uranyl acetate and lead citrate and examined under JEOL JEM-1400Plus transmission electron microscope (at 120 kV JEOL, Japan). The images were taken with the integrated 8Mpix CCD camera and processed further using software TEM Center (Ver. 1.7.3.1537, JEOL, Japan).

4.9. Fluorescence Microscopy

One and 48 h after irradiation, the cultivation medium was replaced by 1 μM LysoSensor Green DND-189 in a fresh medium, and the cells were then incubated for an additional 30 min. After incubation, the cells were washed twice with PBS and examined immediately under the Olympus BX51 microscope (Olympus, Tokyo, Japan) with a green excitation fluorescence filter. The images were captured by the integrated Olympus DP73 camera (Olympus, Tokyo, Japan) and processed using microscope imaging software cellSens (Entry, Olympus, Tokyo, Japan).

4.10. Flow Cytometry

One and 48 h after irradiation, the cultivation medium was replaced by 1 μM LysoSensor Green DND-189 in a fresh medium, and the cells were then incubated for an additional 30 min. After incubation, the cells were washed twice with PBS and scraped off with a scraper. The cells were analyzed immediately using CyAn ADP Flow Cytometer (Beckman Coulter, Inc., Brea, CA, USA) and the obtained data were then processed by the flow cytometry analysis software Summit 4.2 (Beckman Coulter, Inc., Brea, CA, USA). Statistical analysis was performed by an independent two-sample t-test with unequal variances and critical *p*-values equal to 0.05 and 0.01, respectively.

5. Conclusions

Taken together, co-treatment of H1299 cells by Lys05 and IR caused significant autophagy inhibition compared to the control and the solely-irradiated group. According to our data, autophagy is blocked by Lys05 in the later stage of the autophagic process, autophagosome–lysosome fusion.

Concerning autophagy, the current literature is conflicting. As Karagounis et al. concluded that the impact of IR on autophagy is complex and varies not only with cell type and radiation dose but is influenced by many other factors [19]. Although some groups reported IR-induced autophagy, others including us observed autophagy that was inhibited (possibly because of different experimental setup). Obviously, general conclusions and implications for therapy are limited. A crucial question is whether it is more beneficial to support autophagy inhibition or induction in order to diminish most of the cancer cells.

While several papers already covered the chemo-sensitizing effect of Lys05, more has to be learned about its application together with IR. Overall, this study contributes to the limited knowledge about novel autophagy inhibitor—Lys05—presenting the first study so far dedicated to combination with radiation. Our data indicate that the autophagy inhibitors can be used as an effective tool for the radiosensitization of H1299 cells, and it is tempting to conclude that it might provide a promising approach for lung cancer therapeutic strategy.

Supplementary Materials: Supplementary materials can be found at http://www.mdpi.com/1422-0067/20/23/5881/s1.

Author Contributions: Conceptualization, L.C., M.O., and A.T.; formal analysis, M.O., V.P., and P.J.; investigation, L.C., M.O., D.C., and A.B.; methodology, A.T.; project administration, A.T.; resources, R.K.A. and J.D.W.; supervision, A.T.; validation, V.P., P.J., and J.P.; visualization, L.C., M.O., D.C., and A.B.; writing—original draft, L.C., M.O., and A.T.; writing—review and editing, L.C., M.O., V.P., P.J., J.P., and A.T.

Funding: This work was supported by the Ministry of Defense of the Czech Republic through the long-term organization development plan Medical Aspects of Weapons of Mass Destruction of the Faculty of Military Health Sciences, University of Defense in Brno and by The Specific Research grant of Ministry of Education, Youth and Sports of the Czech Republic no. SV/FVZ201501. This study was supported by project PROGRES Q40/06 and Q40/09.

Acknowledgments: Lys05 was a kind gift of Ravi Amaravadi from Perelman School of Medicine (University of Pennsylvania, PA, USA). The authors are grateful to Ian McColl for assistance with the manuscript.

Conflicts of Interest: J.D.W. and R.K.A. are inventors on a patent reporting Lys05 derivatives, which has been licensed by the University of Pennsylvania to the company Pinpoint Therapeutics Inc. to enable drug development. The funders had no role in the design of the study; in the collection, analyses, or interpretation of data; in the writing of the manuscript, or in the decision to publish the results.

Abbreviations

Baf	Bafilomycin A1
BNIP3	Bcl2 interacting protein 3
CI	Combination Index
CQ	Chloroquine
H1299	Non-small cell lung carcinoma cell line
HCQ	Hydroxychloroquine
IR	Ionizing radiation
LC3	Microtubule-associated protein 1A/1B light chain 3
LSG	Lysosensor Green DND-189
Lys05	Coding name for an autophagy inhibitor
mTOR	Mammalian target of rapamycin
NSCLC	Non-small cell lung carcinoma
p53	Cellular tumor antigen 53
p62	Ubiquitin-binding protein p62
PRAS40	Proline-rich Akt substrate of 40 kDa
RT	Radiation therapy
SQSTM1	Sequestosome-1
TEM	Transmission electron microscopy
ULK-1	Unc-51 like autophagy activating kinase 1

References

1. Farhat, F.S.; Houhou, W. Targeted therapies in non-small cell lung carcinoma: What have we achieved so far? *Ther. Adv. Med. Oncol.* **2013**, *5*, 249–270. [CrossRef]
2. Yu, L.; Shang, Z.-F.; Hsu, F.-M.; Zhang, Z.; Tumati, V.; Lin, Y.-F.; Chen, B.P.C.; Saha, D. NSCLC cells demonstrate differential mode of cell death in response to the combined treatment of radiation and a DNA-PKcs inhibitor. *Oncotarget* **2015**, *6*, 3848–3860. [CrossRef]
3. Levine, B.; Klionsky, D.J. Development by self-digestion: Molecular mechanisms and biological functions of autophagy. *Dev. Cell* **2004**, *6*, 463–477. [CrossRef]

4. Ondrej, M.; Cechakova, L.; Durisova, K.; Pejchal, J.; Tichy, A. To live or let die: Unclear task of autophagy in the radiosensitization battle. *Radiother. Oncol. J. Eur. Soc. Ther. Radiol. Oncol.* **2016**, *119*, 265–275. [CrossRef]
5. McAfee, Q.; Zhang, Z.; Samanta, A.; Levi, S.M.; Ma, X.-H.; Piao, S.; Lynch, J.P.; Uehara, T.; Sepulveda, A.R.; Davis, L.E.; et al. Autophagy inhibitor Lys05 has single-agent antitumor activity and reproduces the phenotype of a genetic autophagy deficiency. *Proc. Natl. Acad. Sci. USA* **2012**, *109*, 8253–8258. [CrossRef]
6. Yamamoto, A.; Tagawa, Y.; Yoshimori, T.; Moriyama, Y.; Masaki, R.; Tashiro, Y. Bafilomycin A1 prevents maturation of autophagic vacuoles by inhibiting fusion between autophagosomes and lysosomes in rat hepatoma cell line, H-4-II-E cells. *Cell Struct. Funct.* **1998**, *23*, 33–42. [CrossRef]
7. Shao, S.; Li, S.; Qin, Y.; Wang, X.; Yang, Y.; Bai, H.; Zhou, L.; Zhao, C.; Wang, C. Spautin-1, a novel autophagy inhibitor, enhances imatinib-induced apoptosis in chronic myeloid leukemia. *Int. J. Oncol.* **2014**, *44*, 1661–1668. [CrossRef]
8. Horie, R.; Nakamura, O.; Yamagami, Y.; Mori, M.; Nishimura, H.; Fukuoka, N.; Yamamoto, T. Apoptosis and antitumor effects induced by the combination of an mTOR inhibitor and an autophagy inhibitor in human osteosarcoma MG63 cells. *Int. J. Oncol.* **2016**, *48*, 37–44. [CrossRef]
9. Park, J.M.; Tougeron, D.; Huang, S.; Okamoto, K.; Sinicrope, F.A. Beclin 1 and UVRAG confer protection from radiation-induced DNA damage and maintain centrosome stability in colorectal cancer cells. *PLoS ONE* **2014**, *9*, e100819.
10. Dowling, C.M.; Herranz Ors, C.; Kiely, P.A. Using real-time impedance-based assays to monitor the effects of fibroblast-derived media on the adhesion, proliferation, migration and invasion of colon cancer cells. *Biosci. Rep.* **2014**, *34*, e00126. [CrossRef]
11. Limame, R.; Wouters, A.; Pauwels, B.; Fransen, E.; Peeters, M.; Lardon, F.; De Wever, O.; Pauwels, P. Comparative analysis of dynamic cell viability, migration and invasion assessments by novel real-time technology and classic endpoint assays. *PLoS ONE* **2012**, *7*, e46536. [CrossRef]
12. Chou, T.-C. Drug combination studies and their synergy quantification using the Chou-Talalay method. *Cancer Res.* **2010**, *70*, 440–446. [CrossRef]
13. Hernández, J.L.; Padilla, L.; Dakhel, S.; Coll, T.; Hervas, R.; Adan, J.; Masa, M.; Mitjans, F.; Martinez, J.M.; Coma, S.; et al. Therapeutic targeting of tumor growth and angiogenesis with a novel anti-S100A4 monoclonal antibody. *PLoS ONE* **2013**, *8*, e72480. [CrossRef]
14. Mizushima, N.; Yoshimori, T. How to interpret LC3 immunoblotting. *Autophagy* **2007**, *3*, 542–545. [CrossRef]
15. Bjørkøy, G.; Lamark, T.; Brech, A.; Outzen, H.; Perander, M.; Overvatn, A.; Stenmark, H.; Johansen, T. p62/SQSTM1 forms protein aggregates degraded by autophagy and has a protective effect on huntingtin-induced cell death. *J. Cell Biol.* **2005**, *171*, 603–614. [CrossRef]
16. Zhang, J.; Zhang, C.; Jiang, X.; Li, L.; Zhang, D.; Tang, D.; Yan, T.; Zhang, Q.; Yuan, H.; Jia, J.; et al. Involvement of autophagy in hypoxia-BNIP3 signaling to promote epidermal keratinocyte migration. *Cell Death Dis.* **2019**, *10*, 234. [CrossRef]
17. Manic, G.; Obrist, F.; Kroemer, G.; Vitale, I.; Galluzzi, L. Chloroquine and hydroxychloroquine for cancer therapy. *Mol. Cell. Oncol.* **2014**, *1*, e29911. [CrossRef]
18. Toulany, M.; Mihatsch, J.; Holler, M.; Chaachouay, H.; Rodemann, H.P. Cisplatin-mediated radiosensitization of non-small cell lung cancer cells is stimulated by ATM inhibition. *Radiother. Oncol. J. Eur. Soc. Ther. Radiol. Oncol.* **2014**, *111*, 228–236. [CrossRef]
19. Karagounis, I.V.; Kalamida, D.; Mitrakas, A.; Pouliliou, S.; Liousia, M.V.; Giatromanolaki, A.; Koukourakis, M.I. Repression of the autophagic response sensitises lung cancer cells to radiation and chemotherapy. *Br. J. Cancer* **2016**, *115*, 312–321. [CrossRef]
20. Amaravadi, R.K.; Winkler, J.D. Lys05: A new lysosomal autophagy inhibitor. *Autophagy* **2012**, *8*, 1383–1384. [CrossRef]
21. Koukourakis, M.I.; Kalamida, D.; Mitrakas, A.; Pouliliou, S.; Kalamida, S.; Sivridis, E.; Giatromanolaki, A. Intensified autophagy compromises the efficacy of radiotherapy against prostate cancer. *Biochem. Biophys. Res. Commun.* **2015**, *461*, 268–274. [CrossRef]
22. Cheng, G.; Kong, D.; Hou, X.; Liang, B.; He, M.; Liang, N.; Ma, S.; Liu, X. The tumor suppressor, p53, contributes to radiosensitivity of lung cancer cells by regulating autophagy and apoptosis. *Cancer Biother. Radiopharm.* **2013**, *28*, 153–159. [CrossRef]
23. Apel, A.; Herr, I.; Schwarz, H.; Rodemann, H.P.; Mayer, A. Blocked autophagy sensitizes resistant carcinoma cells to radiation therapy. *Cancer Res.* **2008**, *68*, 1485–1494. [CrossRef]

24. Hanna, R.A.; Quinsay, M.N.; Orogo, A.M.; Giang, K.; Rikka, S.; Gustafsson, Å.B. Microtubule-associated protein 1 light chain 3 (LC3) interacts with Bnip3 protein to selectively remove endoplasmic reticulum and mitochondria via autophagy. *J. Biol. Chem.* **2012**, *287*, 19094–19104. [CrossRef]
25. Huang, Z.; Ye, B.; Dai, Z.; Wu, X.; Lu, Z.; Shan, P.; Huang, W. Curcumin inhibits autophagy and apoptosis in hypoxia/reoxygenation-induced myocytes. *Mol. Med. Rep.* **2015**, *11*, 4678–4684. [CrossRef]
26. Tanida, I. Autophagy basics. *Microbiol. Immunol.* **2011**, *55*, 1–11. [CrossRef]
27. Tanida, I.; Minematsu-Ikeguchi, N.; Ueno, T.; Kominami, E. Lysosomal turnover, but not a cellular level, of endogenous LC3 is a marker for autophagy. *Autophagy* **2005**, *1*, 84–91. [CrossRef]
28. Mizushima, N.; Yamamoto, A.; Hatano, M.; Kobayashi, Y.; Kabeya, Y.; Suzuki, K.; Tokuhisa, T.; Ohsumi, Y.; Yoshimori, T. Dissection of autophagosome formation using Apg5-deficient mouse embryonic stem cells. *J. Cell Biol.* **2001**, *152*, 657–668. [CrossRef]
29. Mizushima, N.; Ohsumi, Y.; Yoshimori, T. Autophagosome formation in mammalian cells. *Cell Struct. Funct.* **2002**, *27*, 421–429. [CrossRef]
30. Makowska, A.; Eble, M.; Prescher, K.; Hoß, M.; Kontny, U. Chloroquine Sensitizes Nasopharyngeal Carcinoma Cells but Not Nasoepithelial Cells to Irradiation by Blocking Autophagy. *PLoS ONE* **2016**, *11*, e0166766. [CrossRef]
31. Lu, S.; Sung, T.; Lin, N.; Abraham, R.T.; Jessen, B.A. Lysosomal adaptation: How cells respond to lysosomotropic compounds. *PLoS ONE* **2017**, *12*, e0173771. [CrossRef] [PubMed]
32. Chikte, S.; Panchal, N.; Warnes, G. Use of LysoTracker dyes: A flow cytometric study of autophagy. *Cytom. Part. J. Int. Soc. Anal. Cytol.* **2014**, *85*, 169–178. [CrossRef] [PubMed]
33. Gade, T.P.F.; Tucker, E.; Nakazawa, M.S.; Hunt, S.J.; Wong, W.; Krock, B.; Weber, C.N.; Nadolski, G.J.; Clark, T.W.I.; Soulen, M.C.; et al. Ischemia Induces Quiescence and Autophagy Dependence in Hepatocellular Carcinoma. *Radiology* **2017**, *283*, 702–710. [CrossRef] [PubMed]
34. Ndoye, A.; Budina-Kolomets, A.; Kugel, C.H.; Webster, M.R.; Kaur, A.; Behera, R.; Rebecca, V.W.; Li, L.; Brafford, P.A.; Liu, Q.; et al. ATG5 Mediates a Positive Feedback Loop between Wnt Signaling and Autophagy in Melanoma. *Cancer Res.* **2017**, *77*, 5873–5885. [CrossRef] [PubMed]
35. DeVorkin, L.; Hattersley, M.; Kim, P.; Ries, J.; Spowart, J.; Anglesio, M.S.; Levi, S.M.; Huntsman, D.G.; Amaravadi, R.K.; Winkler, J.D.; et al. Autophagy Inhibition Enhances Sunitinib Efficacy in Clear Cell Ovarian Carcinoma. *Mol. Cancer Res. MCR* **2017**, *15*, 250–258. [CrossRef] [PubMed]
36. Livak, K.J.; Schmittgen, T.D. Analysis of relative gene expression data using real-time quantitative PCR and the 2(-Delta Delta C(T)) Method. *Methods* **2001**, *25*, 402–408. [CrossRef]

© 2019 by the authors. Licensee MDPI, Basel, Switzerland. This article is an open access article distributed under the terms and conditions of the Creative Commons Attribution (CC BY) license (http://creativecommons.org/licenses/by/4.0/).

Publication no. 3

Lys05 – A promising autophagy inhibitor in the radiosensitization battle: Phosphoproteomic perspective.

Ondrej M, Cechakova L, Fabrik I, Klimentova J, Tichy A

Cancer Genomics and Proteomics. 2020;17(4):369-382

IF(2019) = 3.147; Q2

Author contribution (75%)—main author; the author took the lead in the experimental part (mainly MS analysis and bioinformatic analysis) and the drafting of the manuscript, its revision, and editing.

This study examined the impact of the autophagy inhibitor—Lys05 on irradiated non-small cell lung cancer cells (H1299, p53-negative). The main goal of this study was to describe mechanisms and signaling pathways that contribute to the radiosensitization of these cells after the treatment with Lys05. For this purpose, the authors employed the methods of quantitative phosphoproteomics. The authors revealed an early-stage autophagy induction and a late-stage autophagy inhibition. The early-stage induction of autophagy was characterized mainly by the activation of biosynthetic and metabolic processes through up- or down-regulation of the critical autophagic regulatory proteins Sequestosome-1 (SQSTM1) and proline-rich AKT1 substrate 1 (AKT1S1). The late-stage inhibition of autophagy was attributed mainly to the up-regulation of Unc-51 like autophagy-activating kinase 1 (ULK1) through phosphorylation at Ser638. According to these results, Lys05 has proven to be a promising therapeutic in the treatment of lung cancer.

CANCER GENOMICS & PROTEOMICS *17*: 369-382 (2020)
doi:10.21873/cgp.20196

Lys05 – A Promising Autophagy Inhibitor in the Radiosensitization Battle: Phosphoproteomic Perspective

MARTIN ONDREJ[1], LUCIE CECHAKOVA[1], IVO FABRIK[2], JANA KLIMENTOVA[2] and ALES TICHY[1]

[1]*Department of Radiobiology, Faculty of Military Health Sciences, University of Defense in Brno, Hradec Kralove, Czech Republic;*
[2]*Department of Molecular Biology and Pathology, Faculty of Military Health Sciences, University of Defense in Brno, Hradec Kralove, Czech Republic*

Abstract. *Background: Autophagy is a crucial factor contributing to radioresistance during radiotherapy. Although Lys05 has proven its ability to improve the results of radiotherapy through the inhibition of autophagy, molecular mechanisms of this inhibition remain elusive. We aimed to describe the molecular mechanisms involved in Lys05-induced inhibition of autophagy. Materials and Methods: Radioresistant human non-small cell lung carcinoma cells (H1299, p53-negative) and methods of quantitative phosphoproteomics were employed to define the molecular mechanisms involved in Lys05-induced inhibition of autophagy. Results: We confirmed that at an early stage after irradiation, autophagy was induced, whereas at a later stage after irradiation, it was inhibited. The early-stage induction of autophagy was characterized mainly by the activation of biosynthetic and metabolic processes through up- or down-regulation of the critical autophagic regulatory proteins Sequestosome-1 (SQSTM1) and proline-rich AKT1 substrate 1 (AKT1S1). The late-stage inhibition of autophagy was attributed mainly to down-regulation of Unc-51 like autophagy-activating kinase 1 (ULK1) through phosphorylation at Ser638. Conclusion: This work contributes to emerging phosphoproteomic insights into autophagy-mediated global signaling in lung cancer cells, which might consequently facilitate the development of precision medicine therapeutics.*

This article is freely accessible online.

Correspondence to: Associate Professor Ales Tichy, PharmD, Ph.D., Faculty of Military Health Sciences, University of Defense in Brno, Trebesska 1575, 500 01, Hradec Kralove, Czech Republic. E-mail: ales.tichy@unob.cz

Key Words: Phosphoproteomics, lung cancer, autophagy, inhibitor, Lys05.

Lung cancer is one of the most widespread tumor diseases worldwide. Approximately 80% of all lung cancer cases are non-small cell lung cancer (NSCLC) (1, 2). Treatment of NSCLC includes several approaches from which radiation therapy (RT) is one of the most common. According to radiation oncologists, radioresistance seems to be the most severe issue in treatment efficacy, and importantly, it involves autophagy as a crucial factor (3).

Autophagy is a natural degradation mechanism allowing the regulated destruction and recycling of cellular components in order to maintain homeostasis, especially during stress conditions (4). This degradation process takes place in both healthy and cancer cells. Figure 1 briefly depicts the critical steps of the autophagic process. The leading role of autophagy in emerging tumors is to provide nutrients and other metabolic precursors and thus maintain survival. On the other hand, developed tumors do not usually suffer from a nutrient shortage. However, they are often exposed to various kinds of anticancer therapy, which causes an extensive amount of cellular stress. Under these conditions, autophagy takes part in the elimination of toxic species (*e.g.* free radicals, damaged and misfolded proteins or organelles) and plays a cytoprotective role (5). Therefore, inhibition of autophagy seems to be a practical approach for improving cancer therapy.

Several studies have already described the sensitizing effects of autophagy inhibitors against ionizing radiation (IR) (5). For example, both Chen *et al.* (6) and Tao *et al.* (7) referred to the radiosensitization of esophageal squamous cell carcinoma using 3-methyladenine as an autophagy inhibitor. Similarly, Park *et al.* observed the radiosensitization of colorectal cancer cells due to the accumulation of DNA damage using spautin-1 as an autophagy inhibitor (8).

In our recent study, we described the effect of autophagy inhibitor Lys05 together with IR, which reduced the survival of H1299 NSCLC cells compared to the inhibitor or IR alone (9). Lys05 is a relatively new inhibitor that was firstly introduced by McAfee *et al.* (10). Chemically, it is a dimeric

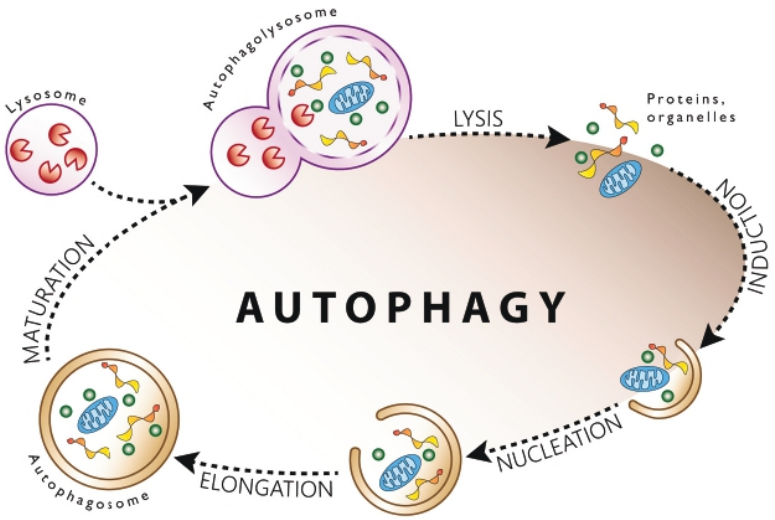

Figure 1. *Schematic overview of the autophagic process. Various stimuli such as starvation, oxygen shortage, and ionizing radiation induce autophagy. Initially, a phagophore is formed and begins to encapsulate molecules that will degrade. Subsequent nucleation and elongation lead to the formation of the characteristic double-membraned autophagosome. After the formation of the autophagosome, lysosome approaches to fuse. The formation of an autophagolysosome accompanies fusion. After fusion, the degradation of the sequestered cytoplasmic cargo involves several acid hydrolases. These hydrolases are then recycled.*

form of chloroquine which accumulates within lysosomes and thus inhibits autophagosome–lysosome fusion (10). We examined the effects of Lys05 on H1299 cells, mostly using classical biological methods. However, a deeper understanding of the molecular mechanisms underlying Lys05-mediated radiosensitization is still required.

The present study aimed to investigate the mechanisms of radiosensitization of H1299 NSCLC cells. As in our previous work, we applied Lys05 as the autophagy inhibitor, and using the methods of quantitative phosphoproteomics, we studied the mechanisms of autophagy inhibition and subsequent radiosensitization.

Materials and Methods

Cells and cultivation. H1299 Non-small cell lung carcinoma cells were obtained from the American Type Culture Collection (Manassas, VA, USA). Cells were cultured at 37˚C in a humidified incubator under 5% CO_2 and maintained in RPMI medium 1640 (Gibco, Paisley, UK) supplemented with a 10% fetal bovine serum, 150 Ul/ml penicillin and 50 mg/ml streptomycin (all from Sigma-Aldrich, St. Louis, MO, USA). The maintenance culture was divided twice per week by dilution to a density of 2×10^5 cells/10 ml. The cell line was used up to a maximum of 15 passages for this study.

Stable isotope labeling by amino acids in cell culture (SILAC). The phosphoproteomic analysis was performed using a SILAC-based approach, as described previously (11). For labeling, H1299 cells were divided into two groups and transferred into SILAC RPMI medium (Gibco) with the addition of either non-labeled L-lysine (32 mg/l), L-arginine (200 mg/l) and L-glutamine (300 mg/l) – a 'light' group or labeled L-lysine-4,4,5,5-d_4 hydrochloride,L-arginine-$^{13}C_6$ hydrochloride and L-glutamine (in equimolar amounts) – a 'heavy' group, both supplemented with 10% dialyzed fetal bovine serum, 150 Ul/ml penicillin and 50 mg/ml streptomycin (all from Sigma-Aldrich). L-Proline (300 mg/l) was added to the media to avoid the metabolic conversion of arginine to proline (12). At least six doublings were required for the full incorporation of labeled amino acids.

Cell treatment. The cells from the heavy group were treated by autophagy inhibitor Lys05 (a kind gift of Dr. Ravi Amaravadi, Pennsylvania University, Philadelphia, PA, USA) at a concentration of 2 μM. The inhibitor was added to the cells 1 h before irradiation. The cells from the light group were left untreated. Both groups were irradiated with a single dose of 2 Gy using a ^{60}Co gamma-ray source at a dose rate of 1.04 Gy/min. After irradiation, each group was divided into two subgroups, returned to an incubator and cultivated further for a 1 and 48 h, respectively.

Recovery of proteins. The cells were lysed using a lysis buffer with the composition of 50 mM ammonium bicarbonate, 1% sodium deoxycholate, and phosphatase inhibitor cocktails 2 and 3 (Sigma-Aldrich). The appropriate subgroups of 'heavy' and 'light' proteins were pooled together in a 1:1 ratio and digested with trypsin (Sequencing Grade Modified Trypsin; Promega Corporation, Madison, WI, USA) as mentioned elsewhere (11). Thus, two sets of cells were formed: Set 1 consisting of light and heavy cells processed 1 h after irradiation and Set 2 consisting of light and heavy cells processed 48 h after irradiation. Figure 2 schematically depicts the procedure of our experiment.

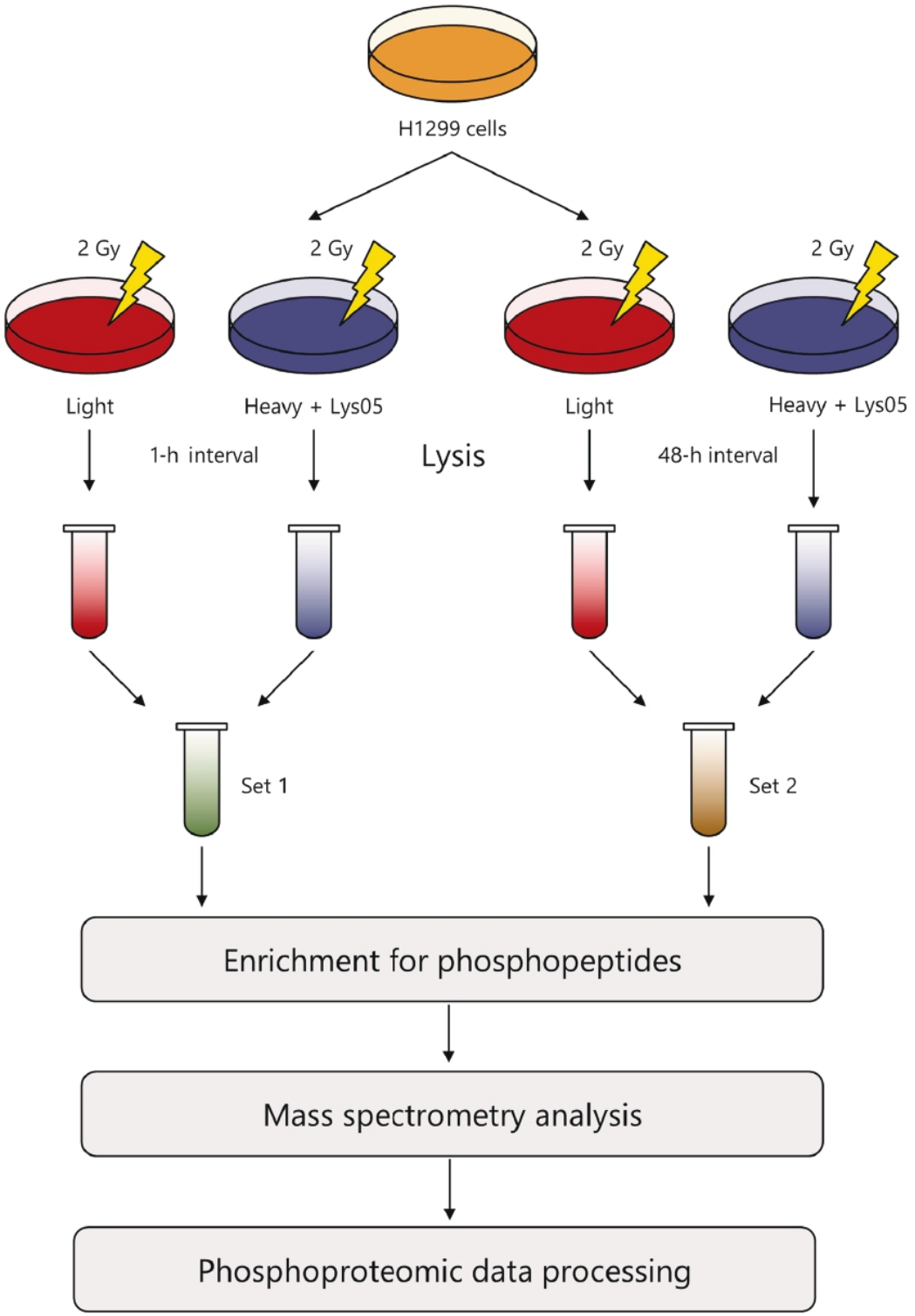

Figure 2. *The workflow of sample processing. H1299 cells were irradiated and cultivated in a 'heavy' or 'light' stable isotope labeling by amino acids in cell culture (SILAC) medium. One and 48 h after irradiation, the cells were lysed and samples from the heavy and light media were pooled together to form Set 1 and Set 2, respectively. Samples from both sets were enriched for phosphopeptides, analyzed using mass spectrometry and processed based on the principles of quantitative phosphoproteomics.*

Number of identified protein groups	1,193	
Number of identified peptides	1,958	
Number of identified phosphopeptides	1,559	
Number of identified phosphosites	6,297	
	Set 1	**Set 2**
Number of pS phosphorylations	1,865	1,209
Number of pT phosphorylations	237	202
Number of pY phosphorylations	3	4

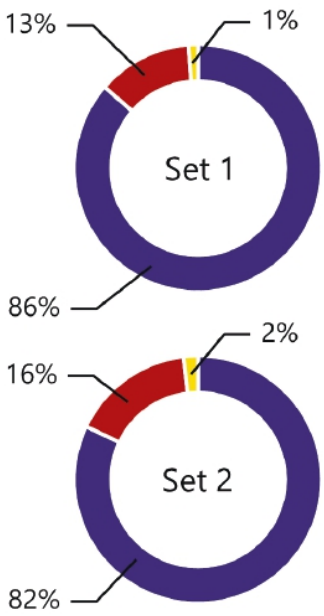

Figure 3. *A general overview of the phosphoproteomic analysis. The table indicates the number of identified proteins, peptides, phosphopeptides, and phosphosites. The number of phosphorylations refers to identified phosphorylations of a particular amino acid in each set: pS: serine, pT: threonine, pY: tyrosine. The percentage distribution of phosphorylation among serine (blue), threonine (red), and tyrosine (yellow) residues is visualized using the ring plots.*

Enrichment for phosphopeptides. After digestion, redundant sodium deoxycholate was extracted by ethyl acetate (13) and samples from both sets were desalted using C18 solid-phase extraction cartridges (3M™ Empore™ , St. Paul, MN, USA) with subsequent elution by 60% acetonitrile/0.1% trifluoroacetic acid. Afterward, the samples were enriched for phosphopeptides using titanium dioxide chromatography (14). Enrichment for phosphopeptides was performed using Mobicol spin columns (MoBiTec GmbH, Goettingen, Germany). Firstly, the samples were supplemented with loading buffer (65% acetonitrile, 2% TFA, 100 mM glutamic acid). Then titanium dioxide microparticles (Titansphere® 5 μm particles; GL Sciences, Torrance, CA, USA) suspended in loading buffer were added to the samples (peptide:TiO_2 ratio, 1:10) and left mixing for 30 minutes at room temperature. Afterward, the microparticles were washed with 200 μl of loading buffer, 200 μl of washing buffer 1 (65% acetonitrile with 0.5% TFA), then sequentially with 200 μl and 100 μl of washing buffer 2 (65% acetonitrile with 0.1% TFA). Phosphopeptides were then eluted by 150 μl of elution buffer (NH_4OH, pH 11.5). After elution, they were acidified with 10% TFA to pH 2 and desalted using C18 spin columns (Harvard Apparatus, Holliston, MA, USA). Desalted TiO_2-enriched peptides were dried out in an Eppendorf™ Concentrator Plus (Eppendorf, Hamburg, Germany).

Mass spectrometry. For the mass spectrometric analysis, we used a Dionex Ultimate™ 3000 RSLCnano system coupled through Nanospray Flex ion source with a Q-Exactive mass spectrometer (both Thermo Fisher Scientific, Bremen, Germany). The TiO_2-enriched peptide mixture (2% acetonitrile/0.05% TFA; 1 μl) was injected onto a capillary trap column (C18 PepMap100, 3 μm, 100 A, 0.075×20 mm; Dionex) and then eluted and separated on capillary column (C18 PepMap RSLC, 2 μm, 100 A, 0.075×150 mm; Dionex) with a step linear gradient of mobile phase B (80% acetonitrile/0.1% formic acid) over mobile phase A (0.1% formic acid) from 4% to 34% B in 68 minutes and from 34% to 55% B in 21 minutes, at flow rate of 300 nl/min. The column was maintained at 40°C and the eluent was monitored at 215 nm.

Phosphoproteomic data processing. Raw mass spectrometric files were processed with MaxQuant software v. 1.5.6.5 (available online: https://maxquant.org) (15). Peak lists were searched against the human UniProt database using the Andromeda search engine (16). The parameters applied for protein identification were: MS/MS tolerance=0.02 Da; peptide mass tolerance for MS=6 ppm and for MS2=20 ppm; missed cleavages=0; enzyme=trypsin; fixed modification: carbamidomethyl (C) and variable modification: oxidation (M), acetyl (protein N-term), phospho (STY). Additionally, appropriate SILAC labels were selected (Arg6, Lys4). Only proteins, peptides, and phosphorylation sites with a false-discovery rate (FDR) lower than 0.01 were accepted. Both razor and unique peptides were used for the calculation of heavy/light protein ratios.

Statistical analysis. Statistical analysis was performed using Perseus software v. 1.5.6.0 (available online: https://maxquant.net/perseus). Contaminants and reversed hits were removed first before further data processing. To identify significantly differentially regulated phosphosites, 'Significance B test' was used with Benjamini-Hochberg FDR correction (FDR<0.05). Proteins with differentially regulated phosphosites were subjected to Gene Ontology (GO) analysis. GO analysis was performed using the ConsensusPathDB

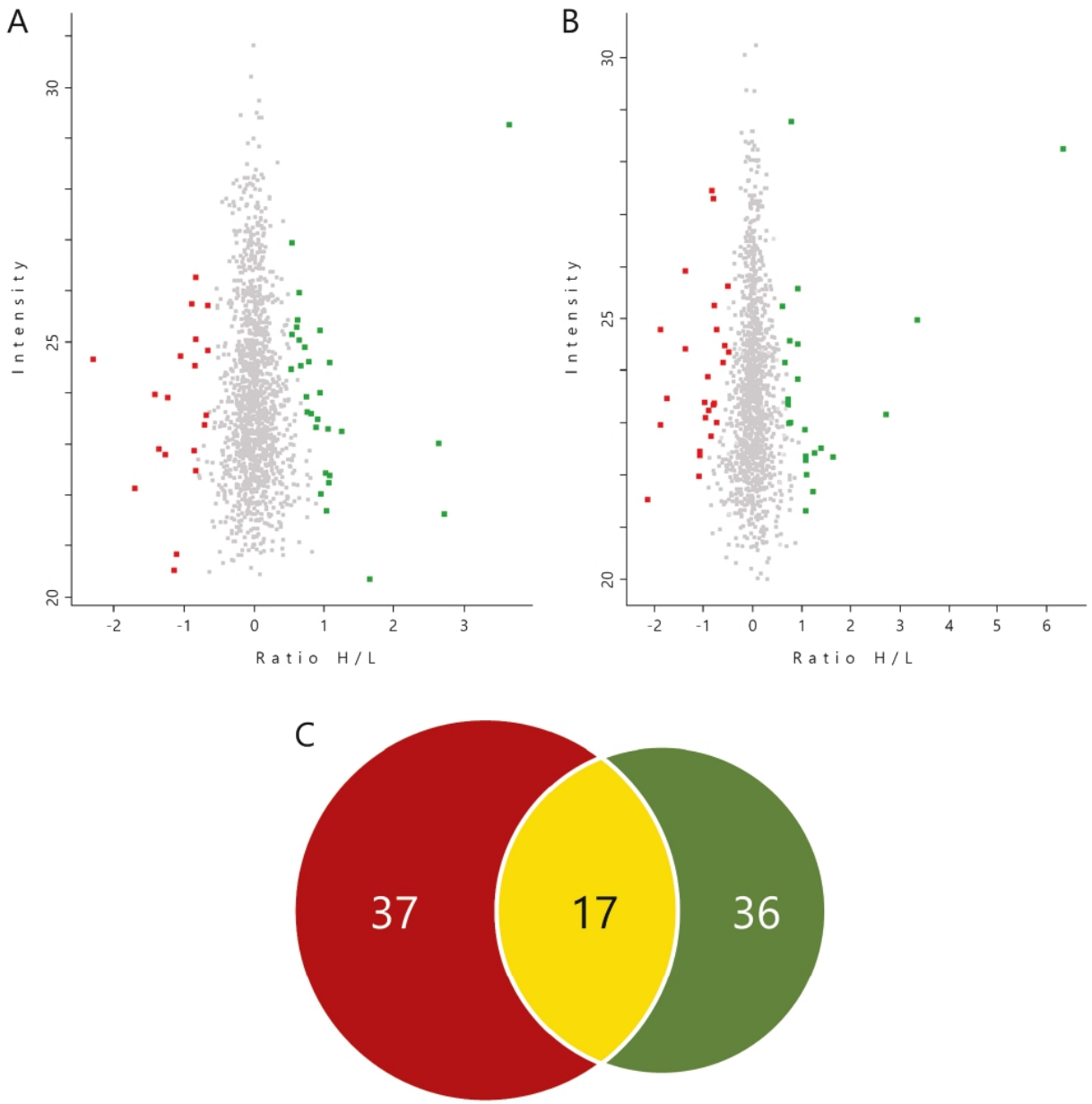

Figure 4. *Overview of proteins with differentially regulated phosphosites. A: Proteins with significantly differentially regulated phosphosites identified 1 h after irradiation (Set 1). B: Proteins with significantly differentially regulated phosphosites identified 48 h after irradiation (Set 2). C: Venn diagram of proteins with differentially regulated phosphosites identified 1 h (red) and 48 h (green) after irradiation. H: Heavy labeled; L: light labeled.*

over-representation analysis web tool v. 32 (p-value<0.01; available online: http://consensuspathdb.org). We deployed STRING software v. 10.5 (available online: http://string-db.org) to identify potential protein-protein interactions of phosphorylated proteins, applying a minimum confidence score of 0.4 and a maximum number of 20 additional interactors (added by the STRING software). The resulting inferred networks were visualized using the STRING network viewer.

Results

General phosphoproteomic description. We performed a phosphoproteomic (SILAC-based) analysis to investigate the mechanisms involved in the radiosensitization of H1299 cells mediated by the abrogation of autophagy. In general, we worked with two sets of H1299 cells: i) Those processed 1

h after irradiation (Set 1), and ii) those processed 48 h after irradiation (Set 2).

Overall, we identified 1,193 protein groups with 6,297 phosphorylation sites (Figure 3). Of these proteins, the most abundantly phosphorylated amino acid detected in both Set 1 and Set 2 was serine (86% and 82%, respectively), followed by threonine (13% and 16%, respectively) and tyrosine (1% and 2%, respectively) (Figure 3).

Overview of the differentially regulated phosphosites. Differential regulation of phosphosites correlated with an impact of the inhibitor on H1299 cells and with subsequent changes in the signaling pathways. We identified 54 proteins with differentially regulated phosphosites in Set 1. In this Set, we observed the up-regulation of 33 phosphosites and down-regulation of 21 phosphosites (Figure 4A). Additionally, we identified 53 proteins with differentially regulated phosphosites in Set 2. This Set included 26 up-regulated and 27 down-regulated phosphosites (Figure 4B). Finally, we detected 17 phosphosites differentially regulated in both sets (Figure 4C). Tables I and II summarize all proteins with differentially regulated phosphosites identified in sets 1 and 2, respectively.

GO analysis suggests delayed onset of autophagy inhibition in H1299 cells. In order to biologically evaluate proteins with differentially regulated phosphosites, we subjected both sets to GO analysis. According to the ConsensusPathDB GO analysis (level 4 terms), most of the proteins with differentially regulated phosphosites from Set 1 (displayed in Figure 5A) were localized in various parts of the nucleus. On the other hand, proteins with differentially regulated phosphosites from Set 2 (displayed in Figure 5B) were localized in both the nucleus and the cytosol. Proteins with differentially regulated phosphosites found in both sets performed molecular functions associated with transcription and RNA binding.

In terms of biological processes, proteins with differentially up-regulated phosphosites from Set 1 took part mostly in cellular transport, biosynthetic and metabolic processes, gene expression, and in response to heat. The up-regulation of biosynthetic, metabolic, and transporting processes might represent one of the specific signs indicating activation of autophagy. Moreover, up-regulated processes of response to heat might be associated with the cellular reaction to various kinds of stress. On the other hand, proteins with differentially down-regulated phosphosites from Set 1 took part in processes associated with the regulation of cell growth (size) or with the main signaling pathway of autophagy, target of rapamycin signaling (TOR). Typically, an activated TOR signaling pathway leads to the inhibition of autophagy. In our setting, down-regulation of TOR signaling might suggest activation of autophagy.

Proteins with differentially up-regulated phosphosites from Set 2 fulfilled tasks associated with the RNA processing. Processes of cellular response to heat, as well as biosynthetic and metabolic processes, were down-regulated in this set, suggesting eventual inhibition of autophagy.

String analysis suggests inhibition of autophagy through Unc-51 like autophagy activating kinase 1 (ULK1)-autophagy-related protein 13 (ATG13) pathway. STRING is a database of known and predicted protein-protein interactions. We used STRING to study the potential interactions among the proteins with differentially regulated phosphosites and to outline the functional groups of proteins identified in both sets.

In regards to Set 1 (Figure 6), we recognized two significant groups: one associated with biosynthetic and metabolic processes, and one associated with regulation of the cell cycle. In the first group, we detected proteins with up-regulated phosphosites that control lipid synthetic and metabolic processes. These proteins interact with proteins that control processes linked to energy production. The up-regulation of these proteins suggests activation of autophagy. Moreover, regulatory proteins sequestosome 1 (SQSTM1), proline-rich AKT1 substrate 1 (AKT1S1), and protein kinase AMP-activated non-catalytic subunit beta 1 (PRKAB1), which are linked with autophagy induction and formation of autophagosomes, were detected. In the second group, we detected proteins that regulate the cellular response to stress. Their up-regulation suggests activation of autophagy. Considering these findings, we assume that autophagy is activated 1 h after irradiation.

In Set 2 (Figure 7), we identified several smaller protein groups. Most of them were associated with the regulation of gene expression or transport mechanisms. The most relevant in terms of autophagy inhibition would seem to be the ULK1–ATG13 pathway. In this pathway, the mammalian target of rapamycin (mTOR) together with AMP-activated protein kinase (AMPK) play a critical role as they cooperate in phosphorylation of ULK1 at Ser638 (17). We identified ULK1 with up-regulation of a phosphosite on Ser638. There is evidence that such phosphorylation leads to reduced autophagic activity (18).

Discussion

Our previous study highlighted the benefits of combined treatment using the autophagy inhibitor, Lys05, together with IR on lung cancer cells. We demonstrated that autophagy is activated at an early stage (1 h after IR) and at a later stage (48 h after IR) is inhibited (9). However, the mechanisms regulating these processes remain unclear. In this respect, we performed a phosphoproteomic study to elucidate molecular mechanisms triggered by Lys05 treatment.

The GO analysis provided the first insight into the proteins involved in biological processes, molecular

Table I. *List of all proteins with differentially regulated phosphosites identified in Set 1.*

	Gene symbol	Protein name	Position	H/L ratio
Down-regulated	*NMD3*	60S ribosomal export protein NMD3	S468	–2.302
	NMD3	60S ribosomal export protein NMD3	T470	–2.302
	ERF	ETS domain-containing transcription factor ERF	T526	–1.700
	FAM193A	Protein FAM193A	S998	–1.415
	PDHA1	Pyruvate dehydrogenase E1 component subunit alpha 1	S232	–1.361
	SERBP1	Plasminogen activator inhibitor 1 RNA-binding protein	S330	–1.268
	ATP13A3	Probable cation-transporting ATPase 13A3	S540	–1.231
	ZNF462	Zinc finger protein 462	S688	–1.142
	MAP1B	Microtubule-associated protein 1B	S1852	–1.109
	MAP1B	Microtubule-associated protein 1B	S1389	–1.051
	PPIG	Peptidyl-prolyl cis-trans isomerase G	T351	–0.892
	UTP14A	U3 small nucleolar RNA-associated protein 14 homolog A	T448	–0.854
	PDHA1/2	Pyruvate dehydrogenase E1 component subunit alpha	S300	–0.850
	SRRM2	Serine/arginine repetitive matrix protein 2	S1101	–0.836
	SRRM2	Serine/arginine repetitive matrix protein 2	S1102	–0.836
	SRRM2	Serine/arginine repetitive matrix protein 2	S1103	–0.836
	PRKD2	Serine/threonine-protein kinase D2	T211	–0.835
	FARP1	FERM, RhoGEF and pleckstrin domain-containing protein 1	S427	–0.713
	AKT1S1	Proline-rich AKT1 substrate 1	T246	–0.683
	YAP1	Transcriptional coactivator YAP1	T110	–0.666
	LARP1	La ribonucleoprotein domain family member 1	S766	–0.663
Up-regulated	*SLC4A7*	Sodium bicarbonate cotransporter 3	S727	0.533
	SMC4	Structural maintenance of chromosomes protein 4	S41	0.535
	ARFGEF1	Brefeldin A-inhibited guanine nucleotide-exchange protein 1	S530	0.538
	ZYX	Zyxin	S312	0.605
	STMN1	Stathmin	S25	0.621
	TP53BP1	Tumor suppressor p53-binding protein 1	S530	0.640
	RSRC2	Arginine/serine-rich coiled-coil protein 2	S32	0.641
	FAM65A	Protein FAM65A	S310	0.663
	ZC3H13	Zinc finger CCCH domain-containing protein 13	S370	0.718
	ZC3H13	Zinc finger CCCH domain-containing protein 13	S372	0.718
	ZC3H13	Zinc finger CCCH domain-containing protein 13	S381	0.718
	SLC4A7	Anion exchange protein	S258	0.741
	ATN1	Atrophin-1	S77	0.755
	PRKAB1	Protein kinase AMP-activated non-catalytic subunit beta 1	S108	0.778
	RIF1	Telomere-associated protein RIF1	S2144	0.818
	SPEN	Msx2-interacting protein	S1278	0.879
	ACACA	Acetyl-CoA carboxylase alpha	S80	0.904
	SRRM2	Serine/arginine repetitive matrix protein 2	S1401	0.937
	SRRM2	Serine/arginine repetitive matrix protein 2	S1403	0.937
	SNRNP70	U1 small nuclear ribonucleoprotein 70 kDa	S410	0.945
	MPZL1	Myelin protein zero-like protein 1	Y263	0.952
	OSBPL11	Oxysterol-binding protein-related protein 11	S172	1.024
	LMNA	Prelamin-A/C;Lamin-A/C	S651	1.037
	LMNA	Prelamin-A/C;Lamin-A/C	S652	1.037
	MAP4K4	Mitogen-activated protein kinase kinase kinase kinase 4	S553	1.061
	PCYT1A	Choline-phosphate cytidylyltransferase A	S331	1.063
	PI4K2A	Phosphatidylinositol 4-kinase type 2-alpha	S462	1.076
	NUP205	Nuclear pore complex protein Nup205	S1165	1.077
	NUP98	Nuclear pore complex protein Nup98-Nup96	S1028	1.246
	SLC7A2	Cationic amino acid transporter 2	S646	1.656
	PHF12	PHD finger protein 12	S41	2.632
	AGPAT9	Glycerol-3-phosphate acyltransferase 3	S68	2.723
	KHDRBS1	KH domain-containing, RNA-binding, signal transduction-associated protein 1	S20	3.647

Table II. *List of all proteins with differentially regulated phosphosites identified in Set 2.*

	Gene symbol	Protein name	Position	H/L ratio
Down-regulated	*PDHA1*	Pyruvate dehydrogenase E1 component subunit alpha 1	S232	−2.138
	PDHA1/2	Pyruvate dehydrogenase E1 component subunit alpha	S293	−1.881
	PDHA1/2	Pyruvate dehydrogenase E1 component subunit alpha	S300	−1.881
	FAM193A	Protein FAM193A	S998	−1.745
	SRRM2	Serine/arginine repetitive matrix protein 2	S1101	−1.372
	SRRM2	Serine/arginine repetitive matrix protein 2	S1102	−1.372
	SRRM2	Serine/arginine repetitive matrix protein 2	S1103	−1.372
	HSPB1	Heat shock protein beta-1	S15	−1.093
	ERF	ETS domain-containing transcription factor ERF	T526	−1.083
	SLAIN2	SLAIN motif-containing protein 2	S220	−1.080
	MAP4	Microtubule-associated protein 4	S1970	−0.974
	MED24	Mediator of RNA polymerase II transcription subunit 24	S38	−0.964
	MED24	Mediator of RNA polymerase II transcription subunit 24	S39	−0.964
	RRM2	Ribonucleoside-diphosphate reductase subunit M2	S20	−0.912
	SRRM2	Serine/arginine repetitive matrix protein 2	S2121	−0.895
	MKI67	Antigen KI-67	S2708	−0.845
	CLTA	Clathrin light chain A	S105	−0.832
	ATP13A3	Probable cation-transporting ATPase 13A3	S540	−0.807
	HSPB1	Heat shock protein beta-1	S82	−0.792
	LMO7	LIM domain only protein 7	S591	−0.780
	YAP1	Transcriptional coactivator YAP1	T110	−0.777
	PDHA1/2	Pyruvate dehydrogenase E1 component subunit alpha	S293	−0.739
	TPR	Nucleoprotein TPR	S2155	−0.727
	MDN1	Midasin	S4538	−0.600
	MAP4	Microtubule-associated protein 4	T538	−0.575
	PSIP1	PC4 and SFRS1-interacting protein	S106	−0.509
	MDC1	Mediator of DNA damage checkpoint protein 1	S329	−0.493
Up-regulated	*ZYX*	Zyxin	S312	0.606
	FAM65A	Protein FAM65A	S310	0.652
	NUP205	Nuclear pore complex protein Nup205	S1165	0.714
	AJUBA	LIM domain-containing protein ajuba	S119	0.716
	AHNAK	Neuroblast differentiation-associated protein AHNAK	T4766	0.732
	ZC3H13	Zinc finger CCCH domain-containing protein 13	S370	0.744
	ZC3H13	Zinc finger CCCH domain-containing protein 13	S372	0.744
	CTNND1	Catenin delta-1	S230	0.768
	KHDRBS1	KH domain-containing, RNA-binding, signal transduction-associated protein 1	S20	0.785
	CHD3	Chromodomain-helicase-DNA-binding protein 3	S1601	0.916
	CHD3	Chromodomain-helicase-DNA-binding protein 3	S1605	0.916
	SNRNP70	U1 small nuclear ribonucleoprotein 70 kDa	S410	0.919
	ITPR3	Inositol 1,4,5-trisphosphate receptor type 3	S2670	1.058
	PKP4	Plakophilin-4	S406	1.081
	UBAP2L	Ubiquitin-associated protein 2-like	S478	1.085
	DHX9	ATP-dependent RNA helicase A	S321	1.086
	RBBP6	E3 ubiquitin-protein ligase RBBP6	S1625	1.098
	ATN1	Atrophin-1	S77	1.218
	ATN1	Atrophin-1	S79	1.218
	MAP4	Microtubule-associated protein 4	S2073	1.264
	HUWE1	E3 ubiquitin-protein ligase HUWE1	S2362	1.384
	HMGXB4	HMG domain-containing protein 4	S512	1.641
	SYNGAP1	Ras/Rap GTPase-activating protein SynGAP	S423	2.706
	SYNGAP1	Ras/Rap GTPase-activating protein SynGAP	T421	2.706
	IQCA1	IQ and AAA domain-containing protein 1	S797	3.343
	GNG12	Guanine nucleotide-binding protein G(I)/G(S)/G(O) subunit gamma-12	S26	6.334

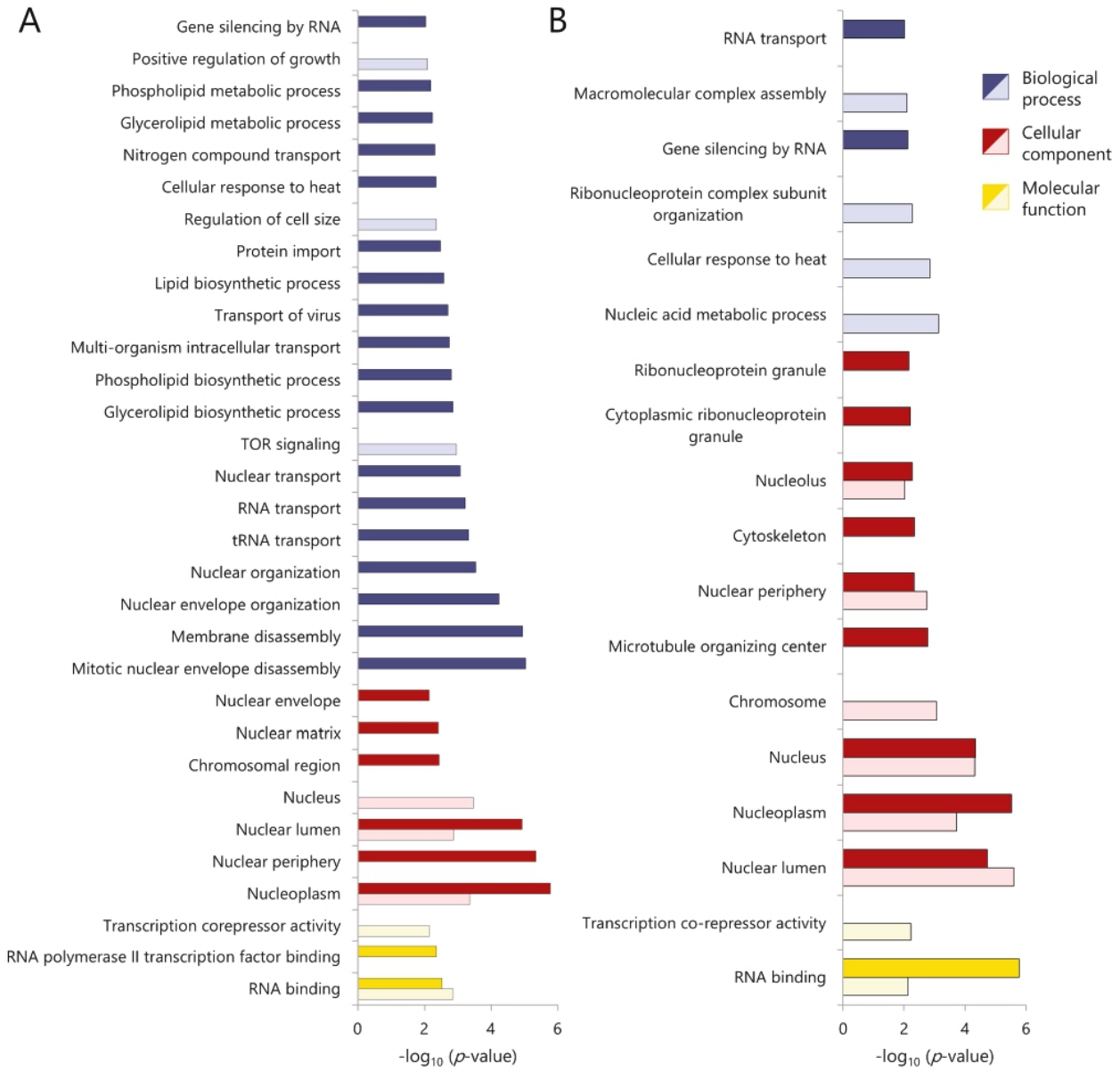

Figure 5. *Gene ontology (GO) over-representation analysis of proteins of Set 1 (A) and Set 48 2 (B) with differentially regulated phosphosites using the ConsensusPathDB level 4 terms. GO terms with darker colors correspond to proteins with up-regulated phosphosites. GO terms with brighter colors correspond to those with down-regulated phosphosites.*

functions, and cellular compartments. Analyzing data in more detail, we identified proteins with differentially regulated phosphosites that take part in autophagy.

One hour after irradiation, we identified several proteins with significantly up- or down-regulated phosphosites. Interactions between these proteins suggest the activation of autophagy early after the combined treatment by Lys05 together with IR.

We identified KH domain-containing, RNA-binding, signal transduction-associated protein 1 (KHDRBS1) as a protein with the most significantly up-regulated phosphosite 1 h after irradiation. Once phosphorylated, KHDRBS1 functions as an adapter protein in signal transduction cascades (19). It is predominantly a nuclear protein, and its primary function is to regulate alternative splicing. It influences alternative splicing of the mTOR kinase (20) and plays a role as an adapter

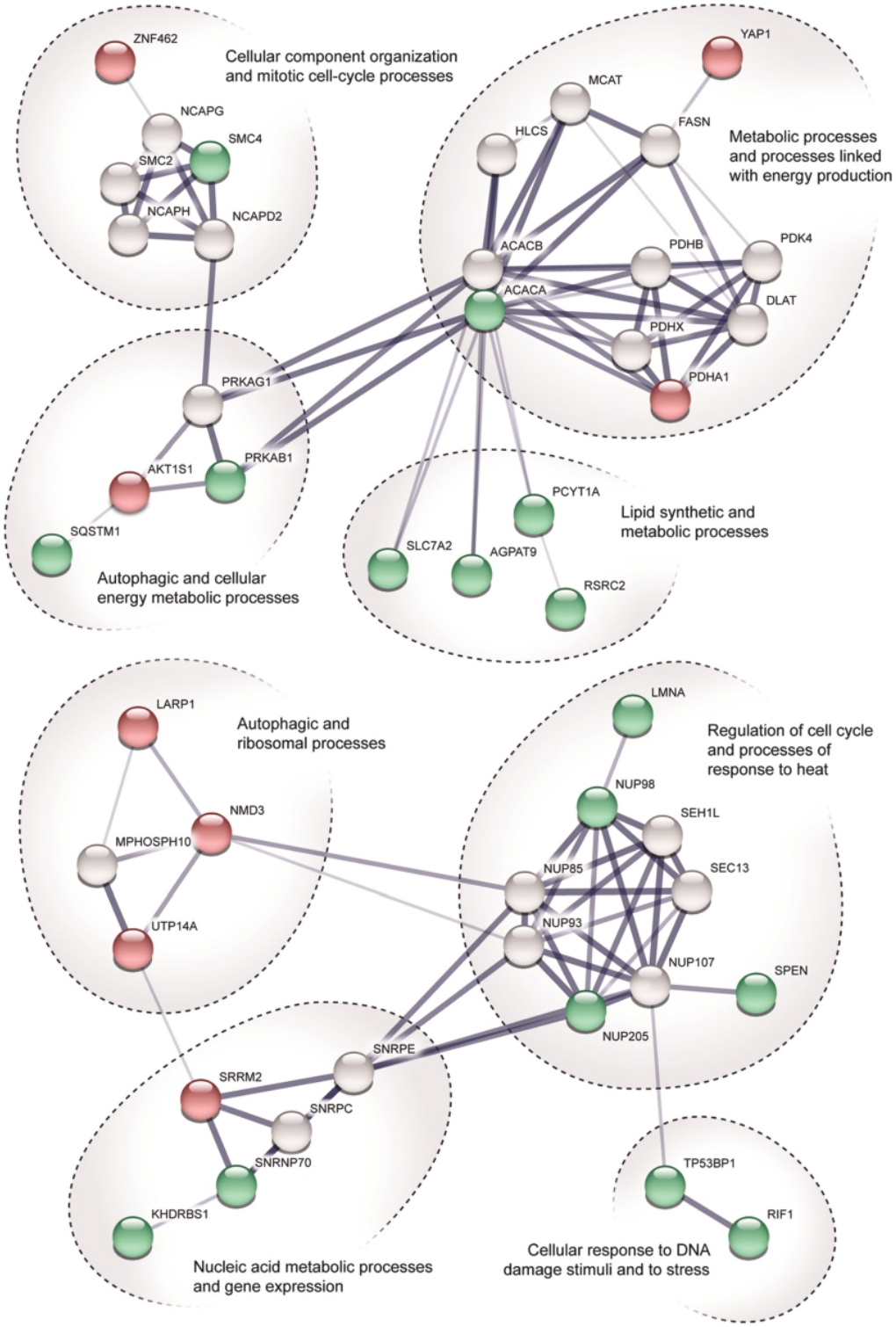

Figure 6. *STRING pathway interaction network of proteins with differentially regulated phosphosites. The figure shows the proteins identified 1 h after irradiation. Points colored green represent proteins with up-regulated phosphosites. Points colored red represent proteins with down-regulated phosphosites. Proteins colored grey were added automatically by the software. Line thickness indicates the strength of data support. See Tables I and II for protein names.*

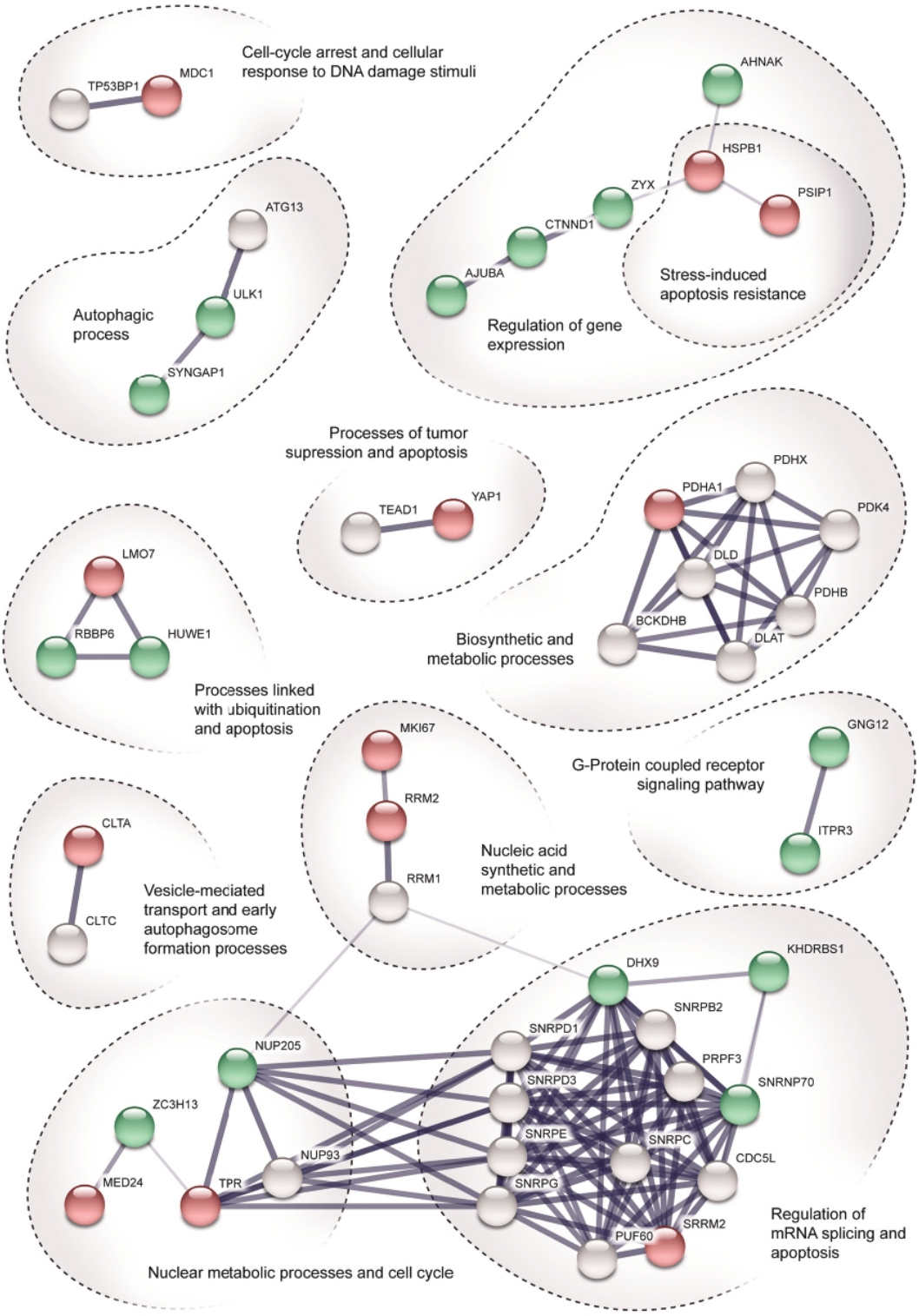

Figure 7. *STRING pathway interaction network of proteins with differentially regulated phosphosites. The figure shows the proteins identified 48 h after irradiation. Points colored green represent proteins with up-regulated phosphosites. Points colored red represent proteins with down-regulated phosphosites. Proteins colored grey were added automatically by the software. Line thickness indicates the strength of data support. See Tables I and II for protein names.*

between the autophagic machinery and misfolded proteins (21). KHDRBS1 may serve as a regulatory protein in autophagy activation since its loss in liver cells markedly attenuated liver injury caused by autophagy deficiency (22).

Furthermore, we identified glycerol-3-phosphate acyltransferase 3 (GPAT3, previously known as AGPAT9) as a protein with the second most significantly up-regulated phosphosite. GPAT3 catalyzes the initial step of de novo triacylglycerol synthesis. It transfers the acyl-group from acyl-CoA and plays a significant role in glycerolipid and phospholipid synthesis (23). It also contributes to autophagosome formation by its biosynthetic activity (24), and its function is controlled by insulin-mediated phosphorylation (25). We identified protein GPAT3 to be phosphorylated on Ser68, which is one of the 'known sites', according to PhosphoSitePlus (www.phosphositeplus.org).

SQSTM1 was another protein that was substantially up-regulated 1 h after irradiation. SQSTM1 is an autophagosome cargo protein. It targets other proteins that bind to it for selective autophagy (26). We observed this protein to be phosphorylated on Ser272. Phosphorylation of SQSTM1 on Ser272 contributes to the activation of autophagy (27).

Similarly, proteins with down-regulated phosphosites contribute to the apparent activation of autophagy early after treatment. For example, 60S ribosomal export protein NMD3 (NMD3), a protein with the most significantly down-regulated phosphosite 1 h after IR, acts as an adapter for exportin 1 (XPO1) also known as chromosomal maintenance 1 (CRM1)-mediated export of the 60S ribosomal subunit (28). According to Wengrod *et al*., inhibition of NMD3 may induce autophagy, and the hyperactivation of NMD3 may abate it (29).

AKT1S1, another protein with a down-regulated phosphosite 1 h after IR, is a subunit of mammalian target of rapamycin complex 1 (mTORC1). It possesses a regulatory function at the intersection of the AKT serine/threonine kinase 1 (AKT1) and mTORC1 signaling pathway and regulates cell growth and survival (30, 31). AKT1S1 is also an autophagy regulatory protein, which binds to regulatory associated protein of MTOR complex 1 (RAPTOR) in the mTORC1 complex. Phosphorylation of AKT1S1 by AKT causes its dissociation from RAPTOR, resulting in mTOR activation and suppression of autophagy (32). We identified AKT1S1 as having down-regulation of phosphorylation on Thr246, indicating enhanced autophagic activity. It is known that AKT can phosphorylate AKT1S1 near its C-terminus on Thr246. This phosphorylation appears to release its inhibitory effect on mTORC1 (33).

Furthermore, we identified La ribonucleoprotein domain family member 1 (LARP1), another protein tightly associated with mTOR machinery. LARP1 is a downstream substrate of mTORC1 and promotes the translation of specific classes of mRNAs. LARP1 regulates global protein synthesis, cell growth, and proliferation, as well as cell migration and invasion (34, 35). With its ability to reversibly phosphorylate and dephosphorylate, we consider LARP1 to be a phosphorylation-sensitive molecular switch in the translation of some mRNAs as well as an essential regulator of mTORC1 (36). We identified LARP1 with down-regulation of phosphosite on Ser766. This phosphosite is reportedly dephosphorylated during autophagy (37).

Taken together, all the deregulations of phosphorylated proteins mentioned above contribute to an increased rate of autophagy. The key regulators of this process appear to be the AKT1S1 pathway—initial autophagy inducer and SQSTM1 pathway—a regulator of autophagosome formation together with other regulatory proteins such as LARP1, NMD3, and GPAT3 (see Figure 6).

On the other hand, 48 h after IR, we identified proteins with significantly up- or down-regulated phosphosites that contribute to the inhibition of autophagy.

One of these proteins, Ras/Rap GTPase-activating protein SynGAP (SYNGAP1), is a Ras GTPase-activating protein that not only is critical for proper synapse function, but also takes part in other signaling processes (38). Importantly, it is a binding partner of the protein ULK1 (39), which was also detected 48 h after IR. ULK1 is a serine/threonine-protein kinase involved in autophagy regulation. It acts upstream of phosphatidylinositol 3-kinase to regulate the formation of autophagophores (the precursors of autophagosomes). ULK1 takes part in regulatory feedback loops in autophagy. It acts both as a downstream effector and a negative regulator of mTORC1 and is activated *via* phosphorylation by AMPK (40). When activated, mTORC1 inhibits autophagy by phosphorylating both ULK1 and ATG13 while reducing ULK1 kinase activity (41, 42). AMPK can also negatively regulate autophagy by phosphorylating ULK1 at Ser638, leading to reduced autophagy-related activity of ULK1 (18).

It seems that the ULK1–ATG13 pathway might be the key regulator of the late-stage inhibition of autophagy. ULK1 appears to be the crucial regulator of autophagy inhibition 48 h after irradiation (see Figure 7).

It is far beyond the extent of this article to describe in full detail all the observed alterations of phosphorylated proteins. Therefore, we outlined the most prominent ones and included an overview of all detected up- and down-regulated phosphosites in the supplementary material (Supplementary Tables I and II).

Conclusion

When performing the in-depth phosphoproteomic analysis, we expected to find autophagy somewhat inhibited early after irradiation. Instead, we found numerous deregulations of phosphorylated proteins leading to an increased rate of

autophagy. We assume that we can attribute such an effect to IR. Later after irradiation, the effect of Lys05 prevailed, as we detected phosphorylation leading to reduced autophagic activity. These findings add to the conclusions of our previous work, which confirmed inhibited autophagy by several different methodological approaches. Moreover, we presume that it is ULK1 and its binding partners which play a crucial role in such inhibition.

This work contributes to emerging phosphoproteomic insights into autophagy-mediated global signaling in lung cancer cells, which might consequently facilitate the development of precision medicine therapeutics.

Conflicts of Interest

The Authors declare that they have no conflicts of interest.

Authors' Contributions

M.O. and A.T. conceived the study and wrote the article; M.O. performed the phosphoproteomic analysis; L.C. contributed to the study design and reviewed the article; I.F. and J.K. performed mass spectrometric analysis and provided technical information; A.T. provided project administration and supervision. All Authors read and approved the article.

Acknowledgements

Lys05 was a kind gift of Dr. Ravi Amaravadi from the Perelman School of Medicine (University of Pennsylvania, PA, USA). The Authors are grateful to Ian McColl, MD, Ph.D. for assistance with the article.

Funding

This work was supported by the Ministry of Defense of the Czech Republic through the long-term organization development plan Medical Aspects of Weapons of Mass Destruction of the Faculty of Military Health Sciences, University of Defense in Brno.

All supplementary material is available at: http://dx.doi.org/10.17632/djmfr34hdn.1

References

1 The American Cancer Society: Lung Cancer Statistics | How Common is Lung Cancer, 2019. Available at: https://www.cancer.org/cancer/lung-cancer/about/key-statistics.html [Last accessed on January 6, 2020]

2 Ueki N, Matsuo Y, Togashi Y, Kubo T, Shibuya K, Iizuka Y, Mizowaki T, Togashi K, Mishima M and Hiraoka M: Impact of pretreatment interstitial lung disease on radiation pneumonitis and survival after stereotactic body radiation therapy for lung cancer. J Thorac Oncol *10*: 116-125, 2015. PMID: 25376512. DOI: 10.1097/JTO.0000000000000359

3 Chaachouay H, Fehrenbacher B, Toulany M, Schaller M, Multhoff G and Rodemann HP: AMPK-independent autophagy promotes radioresistance of human tumor cells under clinical relevant hypoxia *in vitro*. Radiother Oncol *116*: 409-416, 2015. PMID: 26318663. DOI: 10.1016/j.radonc.2015.08.012

4 Dikic I and Elazar Z: Mechanism and medical implications of mammalian autophagy. Nat Rev Mol Cell Biol *19*: 349-364, 2018. PMID: 29618831. DOI: 10.1038/s41580-018-0003-4

5 Ondrej M, Cechakova L, Durisova K, Pejchal J and Tichy A: To live or let die: Unclear task of autophagy in the radiosensitization battle. Radiother Oncol *119*: 265-275, 2016. PMID: 26993419. DOI: 10.1016/j.radonc.2016.02.028

6 Chen Y, Li X, Guo L, Wu X, He C, Zhang S, Xiao Y, Yang Y and Hao D: Combining radiation with autophagy inhibition enhances suppression of tumor growth and angiogenesis in esophageal cancer. Mol Med Rep *12*: 1645-1652, 2015. PMID: 25891159. DOI: 10.3892/mmr.2015.3623

7 Tao H, Qian P, Lu J, Guo Y, Zhu H and Wang F: Autophagy inhibition enhances radiosensitivity of ECA-109 cells *via* the mitochondrial apoptosis pathway. Int J Oncol *52*: 1853-1862, 2018. PMID: 29620258. DOI: 10.3892/ijo.2018.4349

8 Park JM, Tougeron D, Huang S, Okamoto K and Sinicrope FA: Beclin 1 and UVRAG confer protection from radiation-induced DNA damage and maintain centrosome stability in colorectal cancer cells. PloS One *9*: e100819, 2014. PMID: 24956373. DOI: 10.1371/journal.pone.0100819

9 Cechakova L, Ondrej M, Pavlik V, Jost P, Cizkova D, Bezrouk A, Pejchal J, Amaravadi RK, Winkler JD and Tichy A: A potent autophagy inhibitor (Lys05) enhances the impact of ionizing radiation on human lung cancer cells H1299. Int J Mol Sci *20*: pii: E5881, 2019. PMID: 31771188. DOI: 10.3390/ijms20235881

10 McAfee Q, Zhang Z, Samanta A, Levi SM, Ma X-H, Piao S, Lynch JP, Uehara T, Sepulveda AR, Davis LE, Winkler JD and Amaravadi RK: Autophagy inhibitor Lys05 has single-agent antitumor activity and reproduces the phenotype of a genetic autophagy deficiency. Proc Natl Acad Sci USA *109*: 8253-8258, 2012. PMID: 22566612. DOI: 10.1073/pnas.1118193109

11 Šalovská B, Fabrik I, Ďurišová K, Link M, Vávrová J, Řezáčová M and Tichý A: Radiosensitization of human leukemic HL-60 cells by ATR kinase inhibitor (VE-821): Phosphoproteomic analysis. Int J Mol Sci *15*: 12007-12026, 2014. PMID: 25003641. DOI: 10.3390/ijms150712007

12 Bendall SC, Hughes C, Stewart MH, Doble B, Bhatia M and Lajoie GA: Prevention of amino acid conversion in SILAC experiments with embryonic stem cells. Mol Cell Proteomics *7*: 1587-1597, 2008. PMID: 18487603. DOI: 10.1074/mcp.M800113-MCP200

13 Yeung Y-G and Stanley ER: Rapid detergent removal from peptide samples with ethyl acetate for mass spectrometry analysis. Curr Protoc Protein Sci *16*: Unit 16.12, 2010. PMID: 20155730. DOI: 10.1002/0471140864.ps1612s59

14 Larsen MR, Thingholm TE, Jensen ON, Roepstorff P and Jørgensen TJD: Highly selective enrichment of phosphorylated peptides from peptide mixtures using titanium dioxide microcolumns. Mol Cell Proteomics *4*: 873-886, 2005. PMID: 15858219. DOI: 10.1074/mcp.T500007-MCP200

15 Cox J and Mann M: MaxQuant enables high peptide identification rates, individualized p.p.b.-range mass accuracies and proteome-wide protein quantification. Nat Biotechnol *26*: 1367-1372, 2008. PMID: 19029910. DOI: 10.1038/nbt.1511

16 Cox J, Neuhauser N, Michalski A, Scheltema RA, Olsen JV and Mann M: Andromeda: a peptide search engine integrated into the MaxQuant environment. J Proteome Res *10*: 1794-1805, 2011. PMID: 21254760. DOI: 10.1021/pr101065j

17 Shang L and Wang X: AMPK and mTOR coordinate the regulation of ULK1 and mammalian autophagy initiation. Autophagy *7*: 924-926, 2011. PMID: 21521945. DOI: 10.4161/auto.7.8.15860

18 Puente C, Hendrickson RC and Jiang X: Nutrient-regulated phosphorylation of ATG13 inhibits starvation-induced autophagy. J Biol Chem *291*: 6026-6035, 2016. PMID: 26801615. DOI: 10.1074/jbc.M115.689646

19 KHDRBS1 - KH domain-containing, RNA-binding, signal transduction-associated protein 1 - *Homo sapiens* (Human) - *KHDRBS1* gene & protein. Available at: https://www.uniprot.org/uniprot/Q07666 [Last accessed on January 6, 2020]

20 Huot M-É, Vogel G, Zabarauskas A, Ngo CT-A, Coulombe-Huntington J, Majewski J and Richard S: The Sam68 STAR RNA-binding protein regulates mTOR alternative splicing during adipogenesis. Mol Cell *46*: 187-199, 2012. PMID: 22424772. DOI: 10.1016/j.molcel.2012.02.007

21 Chen Z, Fu Q, Shen B, Huang X, Wang K, He P, Li F, Zhang F and Shen H: Enhanced p62 expression triggers concomitant autophagy and apoptosis in a rat chronic spinal cord compression model. Mol Med Rep *9*: 2091-2096, 2014. PMID: 24715058. DOI: 10.3892/mmr.2014.2124

22 Komatsu M, Waguri S, Koike M, Sou Y-S, Ueno T, Hara T, Mizushima N, Iwata J-I, Ezaki J, Murata S, Hamazaki J, Nishito Y, Iemura S-I, Natsume T, Yanagawa T, Uwayama J, Warabi E, Yoshida H, Ishii T, Kobayashi A, Yamamoto M, Yue Z, Uchiyama Y, Kominami E and Tanaka K: Homeostatic levels of p62 control cytoplasmic inclusion body formation in autophagy-deficient mice. Cell *131*: 1149-1163, 2007. PMID: 18083104. DOI: 10.1016/j.cell.2007.10.035

23 GPAT3 - Glycerol-3-phosphate acyltransferase 3 - *Homo sapiens* (Human) - *GPAT3* gene & protein. Available at: https://www.uniprot.org/uniprot/Q53EU6 [Last accessed on January 6, 2020]

24 Dupont N, Chauhan S, Arko-Mensah J, Castillo EF, Masedunskas A, Weigert R, Robenek H, Proikas-Cezanne T and Deretic V: Neutral lipid stores and lipase PNPLA5 contribute to autophagosome biogenesis. Curr Biol CB *24*: 609-620, 2014. PMID: 24613307. DOI: 10.1016/j.cub.2014.02.008

25 Shan D, Li J, Wu L, Li D, Hurov J, Tobin JF, Gimeno RE and Cao J: GPAT3 and GPAT4 are regulated by insulin-stimulated phosphorylation and play distinct roles in adipogenesis. J Lipid Res *51*: 1971-1981, 2010. PMID: 20181984. DOI: 10.1194/jlr.M006304

26 Cassidy LD and Narita M: Cell biology. GATA get a hold on senescence. Science *349*: 1448-1449, 2015. PMID: 26404812. DOI: 10.1126/science.aad2501

27 Matsumoto G, Wada K, Okuno M, Kurosawa M and Nukina N: Serine 403 phosphorylation of p62/SQSTM1 regulates selective autophagic clearance of ubiquitinated proteins. Mol Cell *44*: 279-289, 2011. PMID: 22017874. DOI: 10.1016/j.molcel.2011.07.039

28 NMD3 - 60S ribosomal export protein NMD3 - *Homo sapiens* (Human) - *NMD3* gene & protein. Available at: https://www.uniprot.org/uniprot/Q96D46 [Last accessed on January 6, 2020]

29 Wengrod J, Martin L, Wang D, Frischmeyer-Guerrerio P, Dietz HC and Gardner LB: Inhibition of nonsense-mediated RNA decay activates autophagy. Mol Cell Biol *33*: 2128-2135, 2013. PMID: 23508110. DOI: 10.1128/MCB.00174-13

30 AKT1S1 - Proline-rich AKT1 substrate 1 - *Homo sapiens* (Human) - *AKT1S1* gene & protein. Available at: https://www.uniprot.org/uniprot/Q96B36 [Last accessed on January 6, 2020]

31 Nascimento EBM, Snel M, Guigas B, van der Zon GCM, Kriek J, Maassen JA, Jazet IM, Diamant M and Ouwens DM: Phosphorylation of PRAS40 on Thr246 by PKB/AKT facilitates efficient phosphorylation of Ser183 by mTORC1. Cell Signal *22*: 961-967, 2010. PMID: 20138985. DOI: 10.1016/j.cellsig.2010.02.002

32 Sancak Y, Thoreen CC, Peterson TR, Lindquist RA, Kang SA, Spooner E, Carr SA and Sabatini DM: PRAS40 is an insulin-regulated inhibitor of the mTORC1 protein kinase. Mol Cell *25*: 903-915, 2007. PMID: 17386266. DOI: 10.1016/j.molcel.2007.03.003

33 Yang Q and Guan K-L: Expanding mTOR signaling. Cell Res *17*: 666-681, 2007. PMID: 17680028. DOI: 10.1038/cr.2007.64

34 Tcherkezian J, Cargnello M, Romeo Y, Huttlin EL, Lavoie G, Gygi SP and Roux PP: Proteomic analysis of cap-dependent translation identifies LARP1 as a key regulator of *5'TOP* mRNA translation. Genes Dev *28*: 357-371, 2014. PMID: 24532714. DOI: 10.1101/gad.231407.113

35 Mura M, Hopkins TG, Michael T, Abd-Latip N, Weir J, Aboagye E, Mauri F, Jameson C, Sturge J, Gabra H, Bushell M, Willis AE, Curry E and Blagden SP: LARP1 post-transcriptionally regulates mTOR and contributes to cancer progression. Oncogene *34*: 5025-5036, 2015. PMID: 26921696. DOI: 10.1038/onc.2014.428. PMID: 25531318

36 Hong S, Freeberg MA, Han T, Kamath A, Yao Y, Fukuda T, Suzuki T, Kim JK and Inoki K: LARP1 functions as a molecular switch for mTORC1-mediated translation of an essential class of mRNAs. eLife *6*: e25237, 2017. PMID: 28650797. DOI: 10.7554/eLife.25237

37 Casado P, Bilanges B, Rajeeve V, Vanhaesebroeck B and Cutillas PR: Environmental stress affects the activity of metabolic and growth factor signaling networks and induces autophagy markers in MCF7 breast cancer cells. Mol Cell Proteomics *13*: 836-848, 2014. PMID: 24425749. DOI: 10.1074/mcp.M113.034751

38 SYNGAP1 - Ras/Rap GTPase-activating protein SynGAP - *Homo sapiens* (Human) - SYNGAP1 gene & protein. Available at: https://www.uniprot.org/uniprot/Q96PV0 [Last accessed on January 6, 2020]

39 Lee JW, Park S, Takahashi Y and Wang H-G: The association of AMPK with ULK1 regulates autophagy. PloS One *5*: e15394, 2010. PMID: 21072212. DOI: 10.1371/journal.pone.0015394

40 ULK1 - Serine/threonine-protein kinase ULK1 - *Homo sapiens* (Human) - *ULK1* gene & protein. Available at: https://www.uniprot.org/uniprot/O75385 [Last accessed on January 6, 2020]

41 Alers S, Löffler AS, Wesselborg S and Stork B: The incredible ULKs. Cell Commun Signal CCS *10*: 7, 2012. PMID: 22413737. DOI: 10.1186/1478-811X-10-7

42 Lin MG and Hurley JH: Structure and function of the ULK1 complex in autophagy. Curr Opin Cell Biol *39*: 61-68, 2016. DOI: 10.1016/j.ceb.2016.02.010

Received January 28, 2020
Revised March 13, 2020
Accepted March 17, 2020

Publication no. 4

Radio-sensitizing effects of VE-821 and beyond: Distinct phosphoproteomic and metabolomic changes after ATR inhibition in irradiated MOLT-4 cells.

Šalovská B, Janečková H, Fabrik I, Karlíková R, Čecháková L, **Ondrej M**, Link M, Friedecký D, Tichý A

PLoS One. 2018;13:e0199349

IF(2018) = 2.776; Q1

Author contribution (10%)—co-author, the author participated in the manuscript revisions. The author also participated in several preparatory steps of the experiment, such as the cell cultivation and treatment, sample preparation for proteomic analysis and its optimization, and HILIC fractionation of the sample.

This study investigated molecular mechanisms underlying the radiosensitization of MOLT-4 cells by a specific inhibitor of ATR (VE-821). Treatment with VE-821 resulted in IR-induced metabolic disruption and increased oxidative stress. The results suggest that VE-821 could influence the recovery of dNTPs in response to IR. The deficiency of dNTP might hamper DNA repair.

PLOS ONE

RESEARCH ARTICLE

Radio-sensitizing effects of VE-821 and beyond: Distinct phosphoproteomic and metabolomic changes after ATR inhibition in irradiated MOLT-4 cells

Barbora Šalovská[1,2], Hana Janečková[3,4], Ivo Fabrik[5,6], Radana Karlíková[4,7], Lucie Čecháková[1], Martin Ondrej[1], Marek Link[5], David Friedecký[3,4,7], Aleš Tichý[1,6]*

1 Department of Radiobiology, Faculty of Military Health Sciences in Hradec Králové, University of Defence in Brno, Hradec Králové, Czech Republic, **2** Department of Genome Integrity, Institute of Molecular Genetics of the Czech Academy of Sciences, Prague, Czech Republic, **3** Laboratory for Inherited Metabolic Disorders, Faculty of Medicine and Dentistry, Palacký University Olomouc, Olomouc, Czech Republic, **4** Department of Clinical Biochemistry, University Hospital Olomouc, Olomouc, Czech Republic, **5** Department of Molecular Pathology and Biology, Faculty of Military Health Sciences in Hradec Králové, University of Defence in Brno, Hradec Králové, Czech Republic, **6** Biomedical Research Center, University Hospital, Hradec Králové, Czech Republic, **7** Institute of Molecular and Translational Medicine, Faculty of Medicine and Dentistry, Palacký University Olomouc, Olomouc, Czech Republic

* ales.tichy@unob.cz

Check for updates

OPEN ACCESS

Citation: Šalovská B, Janečková H, Fabrik I, Karlíková R, Čecháková L, Ondrej M, et al. (2018) Radio-sensitizing effects of VE-821 and beyond: Distinct phosphoproteomic and metabolomic changes after ATR inhibition in irradiated MOLT-4 cells. PLoS ONE 13(7): e0199349. https://doi.org/10.1371/journal.pone.0199349

Editor: Roberto Amendola, ENEA Centro Ricerche Casaccia, ITALY

Received: February 12, 2018

Accepted: June 6, 2018

Published: July 12, 2018

Copyright: © 2018 Šalovská et al. This is an open access article distributed under the terms of the Creative Commons Attribution License, which permits unrestricted use, distribution, and reproduction in any medium, provided the original author and source are credited.

Data Availability Statement: The mass spectrometry proteomics data have been deposited to the ProteomeXchange Consortium via the PRIDE partner repository with the dataset identifier PXD008925. Other relevant data are within the paper and its Supporting information files.

Funding: This work was supported by Ministry of Defence, Czech Republic (project: Long-term organization development plan 1011), by the Czech Science Foundation Grant 18-12204S. The

Abstract

Current anti-cancer strategy takes advantage of tumour specific abnormalities in DNA damage response to radio- or chemo-therapy. Inhibition of the ATR/Chk1 pathway has been shown to be synthetically lethal in cells with high levels of oncogene-induced replication stress and in p53- or ATM- deficient cells. In the presented study, we aimed to elucidate molecular mechanisms underlying radiosensitization of T-lymphocyte leukemic MOLT-4 cells by VE-821, a higly potent and specific inhibitor of ATR. We combined multiple approaches: cell biology techniques to reveal the inhibitor-induced phenotypes, and quantitative proteomics, phosphoproteomics, and metabolomics to comprehensively describe drug-induced changes in irradiated cells. VE-821 radiosensitized MOLT-4 cells, and furthermore 10 μM VE-821 significantly affected proliferation of sham-irradiated MOLT-4 cells. We detected 623 differentially regulated phosphorylation sites. We revealed changes not only in DDR-related pathways and kinases, but also in pathways and kinases involved in maintaining cellular metabolism. Notably, we found downregulation of mTOR, the main regulator of cellular metabolism, which was most likely caused by an off-target effect of the inhibitor, and we propose that mTOR inhibition could be one of the factors contributing to the phenotype observed after treating MOLT-4 cells with 10 μM VE-821. In the metabolomic analysis, 206 intermediary metabolites were detected. The data indicated that VE-821 potentiated metabolic disruption induced by irradiation and affected the response to irradiation-induced oxidative stress. Upon irradiation, recovery of damaged deoxynucleotides might be affected by VE-821, hampering DNA repair by their deficiency. Taken together, this is the first study describing a complex scenario of cellular events that might be ATR-dependent or triggered

infrastructural part (Institute of Molecular and Translational Medicine) was supported by NPU I (LO1304). The funders had no role in study design, data collection and analysis, decision to publish, or preparation of the manuscript.

Competing interests: The authors have declared that no competing interests exist.

by ATR inhibition in irradiated MOLT-4 cells. Data are available via ProteomeXchange with identifier PXD008925.

Introduction

DNA damage induction by either radio- or chemo-therapy has been the most widely used approach in oncology. Since most of the cancer cells possess defects in one or more DNA damage response (DDR) pathways and suffer from elevated levels of replication stress [1], an effective approach is to target tumour-specific abnormalities in DDR based on the synthetic lethality principle. An appropriate example of such a strategy is targeting the S and G2/M DNA damage checkpoints in G1/S DNA damage checkpoint deficient cells [2]. In a recent study investigating mutational profiles in 3,281 tumours across 12 tumour types [3], genes from the ATM/Chk2/p53 pathway were affected by mutations in almost a half of the investigated cancer cells. As this pathway is essential for maintaining the G1/S DNA damage checkpoint after irradiation, the results of this study suggested that targeting the remaining DNA damage checkpoints might be a promising strategy in a considerable proportion of solid tumours conventionally treated using radiotherapy. Another promising strategy is targeting proteins and protein kinases involved in replication stress response. Cancer cells deficient in G1/S checkpoint or with mutations deregulating replication origin firing suffer from premature entry into S-phase, and thus DNA replication can start before the necessary resources have been generated [4,5].

Inhibition of the ATR/Chk1 pathway has been shown to be synthetically lethal in both above-mentioned scenarios. It has been shown selectively toxic in cells with high levels of oncogene-induced replication stress [4,6–11], and ATR inhibition might be also efficient in combination with genotoxic therapy in p53- or ATM-deficient cells [12–16]. Importantly, two highly potent and selective inhibitors are currently being evaluated in clinical trials: VE-822 (or VX-970; [12]) and AZD6738 [16]. Taken together, selective targeting of the ATR/Chk1 pathway offers a promising therapeutic approach for cancer treatment in a broad range of tumours in both monotherapy and for the purpose of selectively sensitizing cancer cells to current genotoxic treatment.

The effects of ionizing radiation (IR) and other DNA damage inducing agents in MOLT-4 (p53-wildtype, T-cell acute lymphoblastic leukemia; T-ALL) cells have been previously studied [17–28]. Our team addressed the response of these cells to ionizing radiation extensively and we described IR-induced cell death [18,29], cell signalling [17,21,24], and suggested possible defect in DNA repair pathways promoting their radiosensitivity [22]. The presented study was driven by the fact that MOLT-4 cells suffer from multiple heterozygous mutations in several DDR genes (such as *ATM*, *BRCA1*, *FANCA*, and *TP53*) [30,31], implying the cell line might be sensitive to ATR inhibitor treatment.

In this study, we aimed to elucidate molecular mechanisms underlying radiosensitization of the MOLT-4 cell line by specific inhibition of ATR using a highly potent and selective inhibitor–VE-821. To do so, we adopted a unique strategy combining multiple approaches: i) cell biology techniques to investigate the inhibitor-induced phenotypes, ii) shotgun proteomics and phosphoproteomics to study protein phosphorylation triggered by irradiation and its modulation by kinase inhibitors, and iii) targeted metabolomics to reveal drug-induced changes in the metabolome of irradiated cells.

Materials and methods

Cell culture and cell culture conditions

MOLT-4 cells (European Collection of Authenticated Cell Cultures, Porton Down, Salisbury, UK) were cultured in IMDM (Thermo Fisher Scientific, MA, USA) containing 20% foetal bovine serum (Thermo Fisher Scientific, Waltham, MA, USA), 2 mM glutamine, 100 UI/mL penicillin, and 0.1 mg/mL streptomycin (all Sigma-Aldrich, St. Louis, MO, USA) at 37˚C under a controlled 5% CO_2 and humidified atmosphere. The cultures were split every other day by dilution to a concentration of $2x10^5$ cells/mL. Cell counts were assessed by a haemocytometer, and cell membrane integrity was assessed by the Trypan Blue exclusion technique.

For the quantitative proteomic and phosphoproteomic experiments, MOLT-4 cells well cultured in IMDM for SILAC (Thermo Fisher Scientific, Waltham, MA, USA), containing 20% dialyzed foetal bovine serum (Sigma-Aldrich, St. Louis, MO, USA). Media were further supplemented with either unlabelled L-lysine (100 mg/L, K0) and L-arginine (84 mg/L, R0) or equimolar amounts of L-$^{13}C_6$-lysine (K6) and L-$^{13}C_6$-arginine (R6; all Sigma-Aldrich, St. Louis, MO, USA). L-proline (300 mg/L; Sigma-Aldrich, St. Louis, MO, USA) was added to cell culture media to avoid metabolic conversion of arginine to proline [32]. For complete incorporation of labelled amino acids, cells were cultured for more than six cell doublings, usually 10 [33].

Cell treatment (kinase inhibition and gamma-irradiation)

A selective inhibitor of ATR kinase, 3-amino-6-(4-(methylsulfonyl)phenyl)-*N*-phenylpyrazine-2-carboxamide (VE-821; APIs Chemical Co., Ltd., Shanghai, China) was dissolved in dimethyl sulfoxide (DMSO; Sigma-Aldrich, St. Louis, MO, USA) to a concentration of 10 mM, and the aliquots were stored at −20˚C. Additional dilutions (1 mM, 2 mM, 5 mM, and inhibitor combinations as indicated) were also prepared in DMSO to maintain the same concentration of DMSO in all inhibitor-treated samples. In all experiments presented in this study, the inhibitors were added to the cell culture 30 minutes prior to gamma irradiation. The inhibitors were washed out after one hour or 24 hours when indicated. Cells were irradiated using a ^{60}Co gamma-ray source (VF, Cerna Hora, Czech Republic) with a dose rate of 0.5–0.45 Gy/min. Since MOLT-4 cells are relatively sensitive to gamma irradiation, the doses of irradiation were carefully chosen based on our previous publications [34–36] to only induce either cytostatic or sub-lethal damage.

Electrophoresis and western blotting

Cells were pre-treated with different concentrations of inhibitors or DMSO (control) and irradiated by an indicated dose of IR. One or six hours after irradiation, cells were washed with cold phosphate buffer saline (PBS; Thermo Fisher Scientific, MA, USA), and whole cell extracts were prepared by lysis in 500 μL of lysis buffer per $1x10^7$ cells (137 mM NaCl; 10% glycerol; 50 mM NaF; 20 mM Tris-HCl, pH = 8; 1% n-octyl-β-glucopyranoside; 1:100 Phosphatase inhibitor cocktail 2 and 3 –all from Sigma-Aldrich, St. Louis, MO, USA; 1 tablet of protease inhibitors Complete™ Mini/ 10 mL–Roche, Mannheim, Germany). The lysate was clarified by centrifugation, and the protein concentration measured by bicinchoninic acid protein assay. The lysates containing equal amounts of protein (30 μg) were loaded on to a 12% SDS polyacrylamide gel. After electrophoresis, proteins were transferred to a polyvinylidene difluoride membrane and hybridized with an appropriate antibody: anti-Chk1 (1:500; no. 2360, Cell signalling Technology®), anti-phospho-Chk1 (Ser345, 1:500; no. 2348, Cell signalling Technology®), anti-Chk2 (1:250; no. 2662, Cell signalling Technology®), anti-phospho-Chk2 (Thr68, 1: 250; no. 2197, Cell signalling Technology®), anti-p70s6k (1:1000; no. 2708,

Cell signalling Technology®), anti-phospho p70s6k (Thr389; 1:1000; no. 9234, Cell signalling Technology®) and beta actin (1: 20,000; no. A5316, Sigma-Aldrich, St. Louis, MO, USA). After washing, the membranes were incubated with secondary peroxidase-conjugated antibody (no. P0447 and P039901, Dako, Glostrup, Denmark), and the signal was developed using a BM Chemiluminescence Western Blotting Kit (Roche, Mannheim, Germany).

Cell proliferation/viability WST-1 assay

Proliferation of MOLT-4 cells was evaluated by WST-1 (4-[3-(4-iodophenyl)-2-(4-nitrophenyl)-2H-5-tetrazolio]-1,3-benzene disulphonate) colorimetric assay (Roche Diagnostics, Mannheim, Germany). The assay is based on cleavage of WST-1 by mitochondrial dehydrogenases, and the absorbance of the cleavage product correlates with the number of viable cells. Prior to treatment, MOLT-4 cells were placed in 96-well microplates; the number of cells plated into each well were $3x10^4$, $1x10^4$, and $2.5x10^3$ for 24, 72, and 144 hour long experiments, respectively. After the addition of inhibitors and subsequent irradiation, the microplates were placed in an incubator and cultivated at 37˚C. Finally, WST-1 was added, and the plates were incubated for three hours at 37˚C. Absorbance of samples was then measured at 440 nm using a PARADIGM™ Detection Platform (Beckman Coulter, Brea, CA, USA). Controls were normalized to 100% for each assay, and all values were expressed as a percentage of the normalized controls.

Cell cycle analysis and apoptosis detection by flow cytometry

For cell cycle analysis, cells were collected 24 hours after irradiation by a dose of 3 Gy (± inhibitor pre-treatment), washed with ice-cold PBS, and fixed with ice-cold 70% ethanol. Prior to flow cytometry, the cells were washed with ice-cold PBS, and DNA was stained using Vindelov's solution (10 mM Tris-HCl pH = 7.6, 0.6 mg/mL NaCl, 0.01 mg/mL Ribonuclease A, 0.05 mg/mL PI; all Sigma-Aldrich, St. Louis, MO, USA).

For apoptosis detection, an Apoptest-FITC kit was used (DakoCytomation, Copenhagen, Denmark). The kit contains Annexin V, which binds to phosphatidylserine at the surface of apoptotic cells, and propidium iodide (PI) to detect cells with increased cell membrane permeability. Cells were pre-treated with the inhibitors and irradiated by a dose of 1 Gy. The proportion of apoptotic cells in each condition was measured 24 hours and 72 hours after IR according to the manufacturer's instructions.

Flow cytometric analysis was performed on a FACS analyser CyAn DakoCytomation (Beckman Coulter, Miami, FL, USA). At least 20,000 cells were analysed per sample. Listmode data were analysed using Summit v4.3 software (Beckman Coulter, Miami, FL, USA).

Sample preparation for quantitative proteomic and phosphoproteomic experiment

MOLT-4 cells well cultured in IMDM for SILAC containing 20% of dialyzed foetal calf serum for at least six cell doublings as described before [33,37]. Thirty minutes before irradiation, VE-821 was added to the "heavy" cells (K6/R6) at a concentration of 10 μM; the "light" cells (K0/R0) were mock treated with DMSO, whose final concentration in culture was lower than 0.1%. Both groups were irradiated using a ^{60}Co gamma-ray source by a dose of 1.5 Gy. After irradiation, the flasks were placed into an incubator. Three biological replicates were analysed.

One hour after irradiation, the cells were washed with ice-cold PBS and lysed as was published [38] with minor modifications. Briefly, the cells were thoroughly resuspended in 2 mL ice-cold lysis buffer/$1x10^7$ cells (50 mM ammonium bicarbonate, 1% sodium deoxycholate, 1:100 Phosphatase inhibitor cocktail 2 and 3, all Sigma-Aldrich, St. Louis, MO, USA). The lysate was immediately placed into a boiling water bath, and after 5 min incubation, the

samples were cooled down to room temperature on ice. To cleave nucleic acids and decrease the viscosity of the lysate, bensonase nuclease (2.5 U/μL) and $MgCl_2$ (1.5 mM) were added to the samples (both Sigma-Aldrich, St. Louis, MO, USA). The lysate was then clarified by centrifugation at 14,000 rpm, and protein concentration was measured by bicinchoninic acid assay. Sample volumes corresponding to 2 mg of "light" proteins and 2 mg of "heavy" proteins were pooled together to make a 1:1 protein sample.

The protein samples for phosphoproteomic analyses were diluted in lysis buffer and reduced with 10 mM DTT, alkylated with 20 mM IAA (both Sigma-Aldrich, St. Louis, MO, USA), and digested with trypsin (Sequencing grade modified, Promega Corporation, Madison, WI, USA) overnight at an enzyme-to-substrate ratio of 1:60 (sequence grade modified trypsin). Sodium deoxycholate was then extracted by ethyl acetate as described earlier [39]; tryptic peptides were desalted via 500 mg Supelco C18 SPE cartridges according to the manufacturer's instructions and dried using SpeedVac.

Sample preparation for the proteome analysis followed the protocol described above with minor modifications to adjust the volume and concentration of chemicals to a smaller sample amount (10+10 μg of the "heavy" and "light" samples).

Hydrophilic interaction liquid chromatography fractionation

Dried peptide samples were fractionated by HILIC according to a protocol that has been published previously [40] using a 4.6 × 25 cm TSKgel® Amide-80 HR 5 μm particle column with a TSKgel® Amide-80 HR 5 μm 4.6 × 1 cm guard column (Tosoh Biosciences, Stuttgart, Germany) operated with Waters Separations Module e2695 (Waters, Milford, MA, USA) at 0.5 mL/min. Briefly, 3.5 mg of evaporated samples were reconstituted in 80% B and loaded on to the HILIC column. Peptides were then separated by a gradient of A over B from 80% to 60% B in 40 min and from 60% to 0% B in 5 min. Across the gradient, 22 fractions were collected (2 × 2 and 20 × 1 mL) from each replicate. Mobile phase B consisted of 98% acetonitrile (Acn)/0.1% TFA; mobile phase A consisted of 2% Acn/0.1% TFA (all solvents purchased from Sigma-Aldrich, St. Louis, MO, USA).

Phosphopeptide enrichment

Each HILIC fraction was enriched for phosphopeptides using titanium dioxide chromatography [41] using a protocol optimized in previous experiments [42–44]. At first, each fraction was supplemented with TFA and glutamic acid to reach final concentrations of 2% TFA and 100 mM glutamic acid. Titanium dioxide particles (Titansphere® 5 μm particles, GL Sciences, Japan) were suspended in a loading solution (65% Acn, 2% TFA, 100 mM glutamic acid; all Sigma-Aldrich, St. Louis, MO, USA), and a volume of titanium dioxide suspension depending on the expected proportion of peptides and phosphopeptides in a particular fraction (based on previous experiments) was added to each sample. Microparticles with bound phosphopeptides were washed with 200 μL of loading solution, 200 μL of washing solution 1 (65% Acn/0.5% TFA), 200 μL of washing solution 2 (65% Acn/0.1% TFA) and 100 μL of washing solution 2. Phosphopetides were eluted by 150 μL of elution solution (20% Acn/NH_4OH, pH 11.5) in two sequential elutions. Late fractions were subjected to a second enrichment. Eluates from the first and second enrichment were pooled together, acidified with 100% formic acid, and placed in a SpeedVac until all crystals of ammonium formate were evaporated.

Mass spectrometric analysis

Liquid chromatography coupled with tandem mass spectrometry (LC-MS/MS) analyses were performed on a Thermo Scientific Dionex Ultimate™ 3000 RSLCnano system (Thermo

Scientific, Bremen, Germany) coupled through Nanospray Flex ion source with Q Exactive mass spectrometer (Thermo Scientific, Bremen, Germany). TiO_2-enriched HILIC fractions were dissolved in 18 μL of 2% Acn/0.05% TFA and 3–8 μL according to the estimated peptide sample concentration were injected into the RSLCnano system. Peptides were loaded on a capillary trap column (C18 PepMap100, 3 μm, 100 Å, 0.075 × 20 mm) by 2% Acn/0.05% TFA mobile phase at flow rate 5 μL/min for 5 min and then eluted and separated on capillary column C18 PepMap RSLC, 2 μm, 100 Å, 0.075 × 150 mm (Dionex, Thermo Scientific™, Bremen, Germany). Elution was performed by step linear gradient of mobile phase B (80% Acn/0.1% FA) over mobile phase A (0.1% FA) from 4% to 34% B in 48 min and from 34% to 55% B in 15 min at a flow rate of 300 nl/min. The temperature of the column was 40˚C and eluent was monitored at 215 nm during the separation. Spraying voltage was 1.7 kV and heated capillary temperature was 250˚C. The mass spectrometer was operated in the positive ion mode performing a survey MS (range 300 to 1800 m/z) and data-dependent MS/MS scans performed on the six most intense precursors with dynamic exclusion window of 40 s. MS scans were acquired with 70,000 resolution at 200 m/z from 1×10^6 accumulated charges (maximum fill time was 100 ms). Intensity threshold for triggering MS/MS was set at 5×10^4 for ions with $z \geq 2$ with a 1.6 Da isolation window. Precursor ions were accumulated with AGC of 1×10 (maximum fill time was 100 ms) and the normalized collisional energy for HCD fragmentation was 27 units. MS/MS spectra were acquired with 17,500 resolution (at 200 m/z). The mass spectrometry proteomics data have been deposited to the ProteomeXchange Consortium via the PRIDE [45] partner repository with the dataset identifier PXD008925.

Mass spectrometry data processing and bioinformatic analysis

Raw data processing. Raw data files acquired by LC-MS/MS were processed with MaxQuant *v1.5.2.8* [46]. Peak lists were searched against the human SwissProt database (November 2015) using Andromeda search engine [47]. Minimum peptide length was set to seven amino acids, and two missed cleavages were allowed. Carbamidomethylation of cysteine was set as a fixed modification while oxidation of methionine, protein N-terminal acetylation, and phosphorylation of serine, threonine, and tyrosine residues were used as variable modifications. Additionally, appropriate SILAC labels were selected (R6, K6), and the labelled amino acid filtering was disabled. Mass tolerances of 10 and 20 ppm were allowed for MS and MS^2 peaks, respectively. Only proteins, peptides, and phosphorylation sites with false discovery rate (FDR) lower than 0.01 were accepted. For modified peptides, a minimal score (40) and minimal delta score (6) were set as additional cut-offs. For protein quantification, only unmodified peptides, peptides oxidized at methionine residues, or acetylated at the *N*-terminus were accepted; both razor and unique peptides were used for calculation of protein H/L ratios. The Re-quantify function was disabled, whereas Match between runs was enabled during the search.

MaxQuant output data filtering and identification of significantly changed phosphorylation sites. Potential contaminants and hits from the reversed database were removed before further data processing, and data were further manually inspected to look for possible misquantifications caused by the labelling status (K6/R6) and disabled "Filter labelled amino acids" option in MaxQuant. Global rank test (GRT) was used to find differentially regulated phosphorylation sites. Only phosphorylation sites quantified in all three replicates were subjected to GRT, and FDR was estimated non-parametrically as described by Zhou et al. [48]. The significance cut-off for differentially regulated sites was set to FDR < 0.005.

Gene ontology and signalling pathways over-representation analyses. Gene ontology (GO) and signalling pathways over-representation analyses were performed using the

ConsensusPathDB over-representation analysis web tool [49,50]. For the GO terms over-representation, proteins containing differentially regulated phosphorylation sites (both up- and down-) were tested against a custom background reference set comprising all phosphoproteins with at least one quantified phosphorylation site that was subjected to GRT (*i.e.* all phosphoproteins with at least one phosphorylation site quantified in all three biological replicates). Statistical significance of the over-representation analysis was estimated using hypergeometric testing with Benjamini-Hochberg FDR correction of calculated p-values, and the cut-off was set to FDR < 0.05. For the signalling pathways over-representation analysis, phosphoproteins with at least one regulated phosphorylation site were mapped to signalling pathways from three different databases: KEGG [51,52], REACTOME [53], and PID [54]. Pathway-coverage was calculated for overrepresented pathways (FDR < 0.05, tested against a default background reference set comprising all Uniprot proteins included in at least one signalling pathway from a corresponding database).

Network analysis. Log_2 transformed SILAC H/L ratios of phosphorylation sites quantified in all three biological replicates were normalized (z-score calculation) and subjected to SubExtractor algorithm [55]. Human protein-protein interactions with STRING score above 900 were used as the second input for the algorithm, and regulated subnetworks were extracted (FDR = 0.005, $\alpha = 0.2$, $\sigma = 4$). Extracted networks were visualized using Cytoscape *v3.2.1* [56].

Sequence motif analyses. To analyse and visualize sequence motifs surrounding phosphorylation sites identified and quantified in our study, we employed the iceLogo tool [57] and motif-x algorithm [58]. In both motif analyses, amino acid sequences (± 7 residues) surrounding either significantly up- or down-regulated phosphorylation sites were tested against a background reference set composed of sequences surrounding non-regulated phosphorylation sites detected in our study (as evaluated using GRT) that reached a minimal localization probability of 0.75 (*i.e.*, "class I phosphosites" [59]). Motif-x was employed to extract significantly enriched linear motifs. Search parameters were set to at least 10 occurrences of a motif, and the significance level to $p < 0.00003$ (which approximately corresponds to a q-value of 0.01 after Bonferroni correction for multiple hypothesis testing).

Identification of protein kinases responsible for the observed protein phosphorylations and evaluation of global changes in their activities. Class I phosphorylation sites quantified in all three biological replicates were annotated with previously known kinase-substrate relationships downloaded from the PhosphoSitePlus database [60]. To increase the number of annotated phosphorylation sites, two kinase predictors were employed: NetworKIN 3 [61] and iGPS *v1.0* [62]. Both predictors combine motif scoring with contextual information (*i.e.* protein-protein interaction scoring downloaded from the STRING database [63]). The kinase predictions were further filtered to reach NetworKIN score > 3 or "medium" significance threshold in iGPS (*i.e.* FDR of 6% for S/T kinases and FDR of 9% for Y kinases). The significance of global changes in kinase activities was evaluated using the "1D annotation enrichment" tool available in Perseus software *v1.5.2.6* [64].

To further facilitate the interpretation of the results we also downloaded the "Regulatory sites" dataset from the PhosphoSitePlus database, which summarizes the current up-to-date knowledge about the known functions of specific phosphorylation sites. In the text, these sites are referred as "regulatory" sites.

Targeted metabolomic analysis

For the targeted metabolomic analysis, MOLT-4 cells were pre-treated either with VE-821 (10 μM) or DMSO (control groups) 30 minutes prior to IR (1.5 Gy). Six and twelve hours after irradiation, the cells were counted using a haemocytometer, and a cell suspension volume

containing $2x10^6$ cells was pipetted into five sample volumes of a pre-cooled (-40˚C) quenching solution (60% methanol, 0.85% ABC, pH 7.4) as described previously [65]. The samples were gently mixed, and the cells were pelleted by centrifugation (1,000 g for 3 min). The supernatant was removed and the cells were in one step resuspended, lysed and deproteinated in 150 μL of pre-cooled (-80˚C) methanol, and freeze dried. Three replicates were prepared for each condition. Prior the LC-MS/MS analysis the lyophilisates were dissolved in 100 μl of 80% methanol and centrifuged (14,000 g for 10 min).

A quality control sample (QC) was prepared by pooling equal volumes (10 μl) of cell extract samples. It was analysed randomly throughout the run to provide a measurement not only of the stability of the system and performance, but also of the reproducibility of the sample preparation.

The metabolite profiling of cell extracts and the QC samples were performed by the high-performance LC-MS/MS method modified from Asara [66]. The method enabled the analysis of 354 intermediary metabolites (acylcarnitines, amino acids, organic acids, saccharides, etc.; [67]). Data processing, treatment, and statistical analysis of data were described in detail previously [67].

Results and discussion

VE-821 treatment abrogated the radiation-induced phosphorylation of checkpoint kinase-1 and did not affect ATM-mediated signalling

To confirm the inhibitory effect of VE-821 on ATR in our experimental model, we assessed phosphorylation of its effector kinase: checkpoint kinase-1 (Chk1) Ser 345 by immunoblotting (Fig 1A). As expected, the monitored phosphorylation site was upregulated upon irradiation (3 Gy, one hour after irradiation), and it was proportionally inhibited by increasing concentration of VE-821. Additionally, we observed that VE-821 did not inhibit radiation-induced phosphorylation of checkpoint kinase-2 (Chk2) Thr 68, a marker of IR-triggered ATM activity. Therefore, we confirmed that in our cell line model pre-incubation with VE-821 inhibited ATR kinase activity upon irradiation while ATM activity was not affected.

VE-821 is a potent inhibitor of MOLT-4 cell growth both in single treatment and in combination with irradiation

To asses the effects of VE-821 on MOLT-4 cells viability, we first analysed whether the inhibitor affects proliferation of MOLT-4 cells after single treatment. We observed that VE-821 significantly inhibited proliferation of MOLT-4 cells at 1 μM concentration (Fig 1B). This effect was further accentuated in correlation with increasing inhibitor concentration. Thus, in MOLT-4 cells, inhibition of ATR by VE-821 has a strong effect on proliferation.

In combination with IR, VE-821 significantly abated the number of viable cells in both irradiated groups just 72 hours after irradiation (Fig 1C and 1D). As both concentrations used in our experiments directly affected the proliferation of sham-irradiated cells, we further calculated a ratio between the irradiated and sham-irradiated group for each inhibitor-treated condition to resolve if the combination of irradiation and the inhibitor has a more profound effect on proliferation than the inhibitor itself (Fig 1E). Whereas the irradiation caused nearly 50% decrease of control cell viability after 72 hours of treatment, the irradiation of pre-treated cells (2 μM VE-821) led to almost 75% loss of viability in comparison to inhibitor-treated cells, suggesting an additive effect of the VE-821 and IR combination. Additionally, we also observed that VE-821 in 2 μM and 10 μM concentrations modulated the proliferation of irradiated

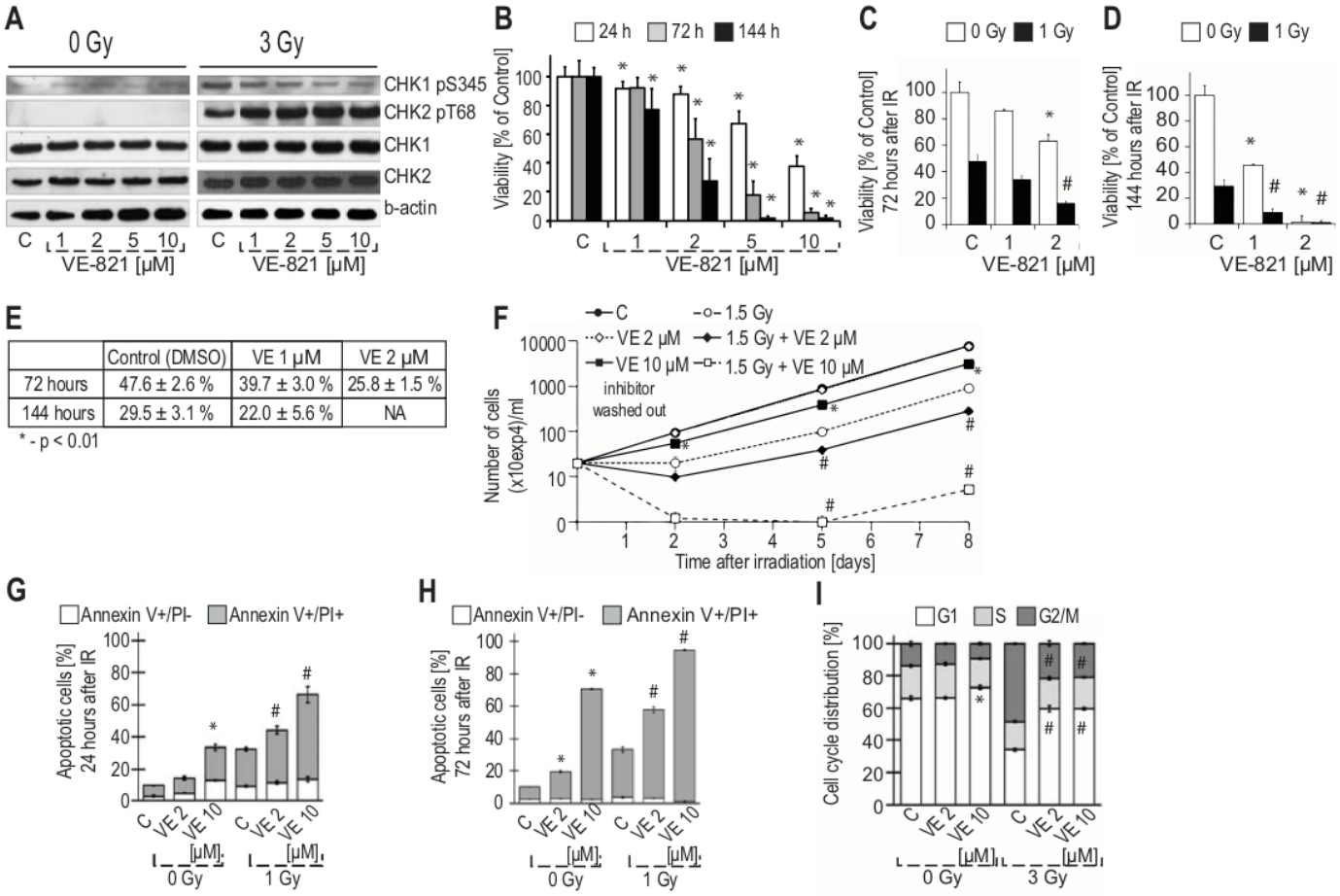

	Control (DMSO)	VE 1 μM	VE 2 μM
72 hours	47.6 ± 2.6 %	39.7 ± 3.0 %	25.8 ± 1.5 %
144 hours	29.5 ± 3.1 %	22.0 ± 5.6 %	NA

* - p < 0.01

Fig 1. Radiosensitization of MOLT-4 cells by ATR kinase inhibitor VE-821. (A) Effect of VE-821 on activation of ATM and ATR kinases by gamma-irradiation. Cells were collected 1 hour after IR (3 Gy). Activation of both kinases and its suppression in the presence of VE-821 was monitored via detection of their specific phosphorylations targets. (B) Characterization of VE-821 treatment effects on proliferation of MOLT-4 cells. Viability was examined by WST-1 assay after 24, 72, and 144 hours of continuous inhibitor treatment. Data are expressed as percentage of viability (metabolic activity) of controls for each time interval. Mean values ± SD from at least five measurements are presented. *$p \leq 0.01$ vs. corresponding controls. (C, D, E, F) Radio-sensitization of MOLT-4 cells using VE-821. Cells were irradiated by the indicated dose. Viability (metabolic activity) was examined by WST-1 assay after 72 hours (C) and 144 hours (D) of continuous inhibitor treatment. (E) Table shows an irradiated group/sham-irradiated group ratio for each treatment condition depicted in (C) and (D). (F) VE-821 was washed out 24 hours after irradiation and the number of viable cells was assessed by a haemocytometer 2, 5, and 8 days after irradiation with subsequent dilution to a concentration of $2x10^5$ cells/ml. Mean values ± SD from five measurements are presented. (G, H) Apoptosis induction in VE-821 treated irradiated MOLT-4 cells. Cell death was detected by Annexin V/PI staining 24 (G) and 72 hours (H) after IR (1 Gy). Mean values ± SD from three measurements are presented. (I) Cell cycle effects of ATR inhibition in irradiated MOLT-4 cells: Cell cycle perturbation was examined using propidium iodide staining of DNA detected by flow cytometry 24 hours after IR (3 Gy). Data are expressed as relative proportion of viable cells in different phases of the cell cycle. Mean values ± SD from three measurements are presented. In (A-I), * indicates statistical significance ($p < 0.01$) of comparison to non-irradiated control; # indicates statistical significance ($p < 0.01$) of comparison to irradiated control group. P-values were calculated using two-sample t-test. In all experiments, the cells were pre-treated with inhibitors at indicated concentrations or DMSO in control groups (C) 30 minutes prior to IR.

https://doi.org/10.1371/journal.pone.0199349.g001

MOLT-4 cells when the inhibitor was present in cell culture media only transiently, for the first 24 hours of the treatment, and was then washed out (Fig 1F). In contrast to continuous treatment, 2 μM VE-821 did not significantly affect the proliferation of sham-irradiated cells when washed out after 24 hours; however, it still enhanced the antiproliferative effects of IR. Taken together, these data showed that VE-821 strongly affected the proliferation of p53-wt MOLT-4 cells, and in combination with IR, the proliferation was influenced even when the inhibitor was present only transiently.

VE-821 increased the ionizing radiation-induced cell death in MOLT-4 cells and disrupted ionizing radiation-induced G2/M arrest in MOLT-4 cells

We further assessed the impact of VE-821 on the viability of MOLT-4 cells after IR. As shown in Fig 1G 10 μM VE-821 significantly affected the viability of MOLT-4 cells 24 hours after the addition of the treatment and/or irradiation. The effect induced by 10 μM VE-821 was comparable to 1 Gy of IR; almost 40% of PI-positive cells were detected under both treatment conditions. When combined with IR, VE-821 in both concentrations significantly increased the IR-induced cell death. Three days after irradiation, in the VE-821 treated groups the percentage of cells with compromised viability further decreased despite the absence of the inhibitor in the cultivation medium (Fig 1H). Importantly, VE-821 increased the sensitivity of MOLT-4 cells to IR. The strongest effect was observed when cells were treated with 10 μM VE-821. Application of these conditions led to more than 90% decrease in viability of MOLT-4 cells 72 hours after irradiation. In conclusion, application of the inhibitor led to increased cell death when combined with IR and thus radiosensitized MOLT-4 cells.

As one of the proposed mechanisms of radiosensitization using ATR inhibitors is the disruption of the G2/M checkpoint in G1 checkpoint-deficient cells [15], we investigated modulation of the cell cycle by ATR inhibition (Fig 1I). None of the conditions we applied affected the cell cycle in sham-irradiated cells except for 10 μM VE-821, which repeatedly caused a significant increase in the number of cells in G1 ($p < 0.01$). In concordance with our previous results [68], irradiation by a dose of 3 Gy led to significant G2/M arrest in viable MOLT-4 cells 24 hours after irradiation. Pre-incubation with VE-821 led to a significant disruption of the G2/M checkpoint in the viable fraction of cells. The abrogation of the G2/M checkpoint by VE-821 10 μM was also achieved when a lower dose of irradiation was applied (1.5 Gy; data not shown). In summary, these results confirmed that ATR is the principal kinase controlling the G2/M DNA damage checkpoint after irradiation in MOLT-4 cells.

Phosphoproteomic analysis of VE-821-modulated cellular response to ionizing radiation identified and quantified thousands of phosphorylation sites

To describe cellular mechanisms underlying the VE-821-mediated radiosensitization of MOLT-4 cells, we employed high-resolution MS to identify and quantify changes in the proteome and phosphoproteome of irradiated VE-821-treated cells (Fig 2B). In total, we identified 9,285 phosphorylation sites from 3,090 protein groups at a site FDR level of 0.01, amongst which 4,504 were quantified in all three biological replicates (nearly 63% of the data set, Fig 2C). The phosphosite ratios correlated very strongly between the replicates (Pearson correlation coefficient was between 0.8 and 0.9, Fig 3C). Only those sites quantified in all replicates were subjected to a non-parametric version of a global rank test ([48]) to identify sites with significantly up- or down-regulated phosphorylation consistently regulated in all three biological replicates. The sites subjected to GRT, their quantification, and basic annotation are given in S1 Table. In GRT, we identified 623 regulated phosphorylation sites (from 455 phosphoproteins), the majority of which were upregulated (431). As discussed previously [43], the higher number of phosphorylation sites upregulated than downregulated in response to a kinase inhibitor treatment was probably caused by the length of the treatment (one hour), which was chosen rather to identify signalling pathways rewired by ATR inhibition in irradiated cells than phosphorylations directly dependent on ATR kinase activity in response to IR.

Analysis of all the proteome samples prepared using the same treatment and time interval resulted in quantification of the unmodified fraction of the proteome (phosphorylated

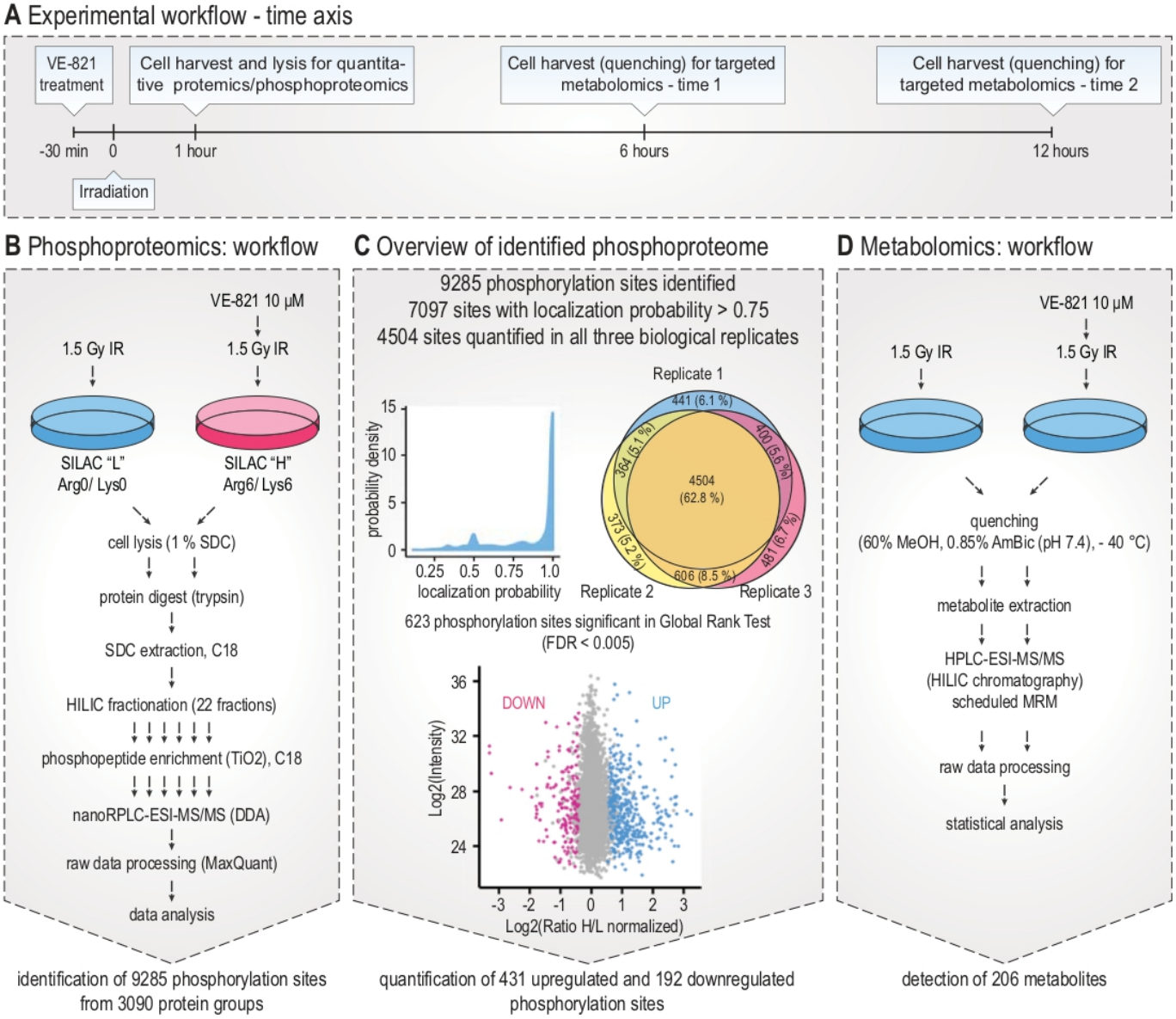

Fig 2. Identification and quantification of the VE-821-regulated phosphoproteome and metabolome in irradiated MOLT-4 cells using tandem mass spectrometry. (A) Overview of time intervals used for both phosphoproteomic and metabolomic analyses of VE-821 perturbed cellular response to ionizing radiation (IR). (B) Overview of experimental design and workflow used for quantitative SILAC-based phosphoproteomics. (C) Summary of the identified and quantified phosphoproteome. (D) Overview of experimental design and workflow used for targeted metabolomics screening.

https://doi.org/10.1371/journal.pone.0199349.g002

peptides were not considered for proteome quantification) and confirmed our expectations that there would be no significant changes of proteome one hour after irradiation combined with VE-821 treatment. As depicted in Fig 3A, the distribution of normalized $\log_2$ SILAC H/L ratios corresponding to quantification of unmodified proteins was very narrow, with most values distributed close to zero. Moreover, Pearson correlation between the replicates was weak (R 0.24–0.387; Fig 3C), which is more likely caused by non-existing trends in an unperturbed system rather than by an irreproducibility of the analysis.

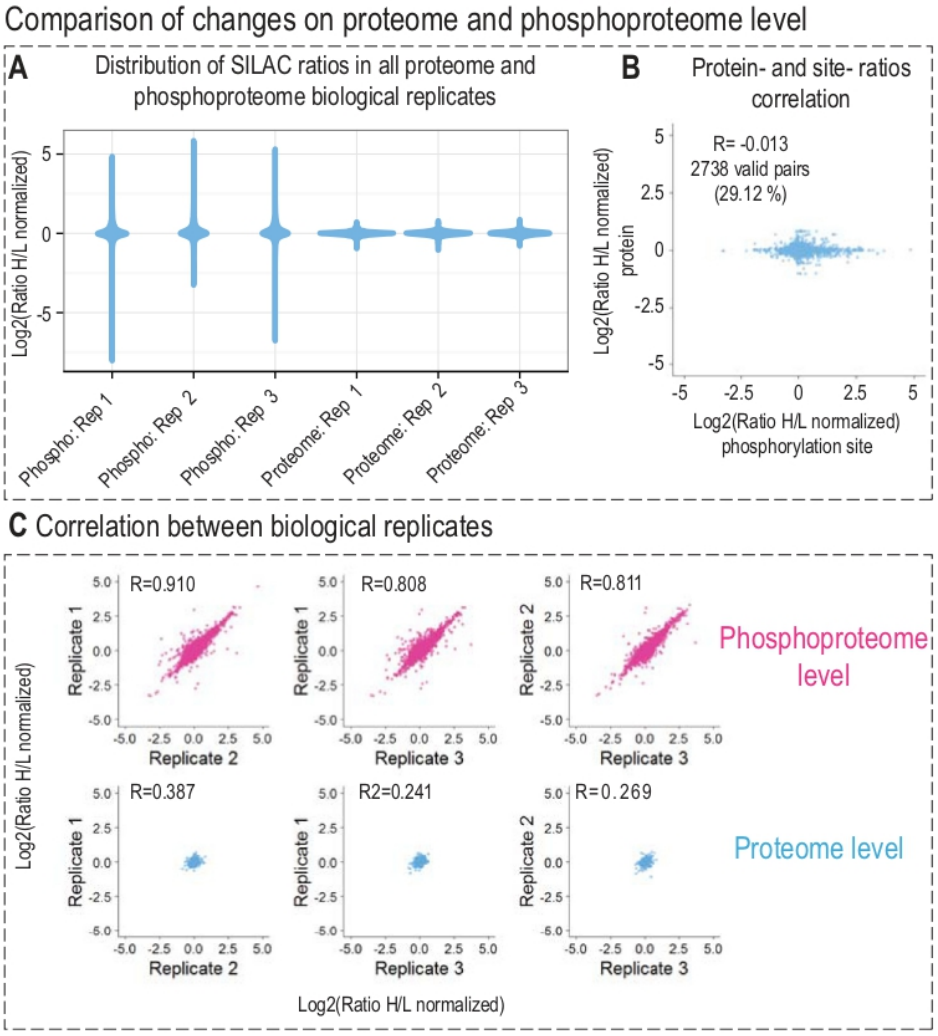

Fig 3. Comparison and correlation of changes on proteome and phosphoproteome level and their quantitative reproducibility. (A) Violin plots depict log_2 transformed normalized SILAC H/L ratios distribution in all proteome and phosphoproteome biological replicates. (B) Pearson correlation between phosphosite and protein ratios. H/L ratios of 2738 phosphorylation sites (29% percent of the identified phosphorylation sites) were plotted against H/L ratios of corresponding proteins and the Pearson correlation value (R) was calculated. (C) Pearson correlation (R) between biological replicates of both proteome and phosphoproteome experiment.

https://doi.org/10.1371/journal.pone.0199349.g003

Pearson correlation between normalized log_2 SILAC H/L ratios of phosphopeptides and log_2 normalized SILAC H/L ratios of corresponding proteins was also calculated (the calculation was based on 2,738 phosphorylation sites which represent almost 30% of the data set), and the low correlation coefficient (*R* was -0.013) further confirmed that the observed changes on the phosphoproteome level were not systematically dependent on changes of the abundance of corresponding proteins (Fig 3B).

Taken together, we showed that VE-821 co-treatment significantly affected the phosphorylation response in cells treated with IR, and that the observed changes were not induced by the changes on the proteome level as the proteome remained unperturbed.

Gene ontology and signalling pathway enrichment analysis of regulated phosphoproteins provided a general description of the VE-821 modulated phosphoproteome

To functionally classify phosphoproteins quantified in our study, we performed a functional annotation and over-representation analysis using the ConsensusPathDB over-representation analysis web tool [49,50]. A list of 455 phosphoproteins containing VE-821-regulated sites was tested against a custom background reference set derived from our data comprising all phosphoproteins with at least one phosphorylation site quantified in all three biological replicates. As shown in Fig 4A, regulated phosphoproteins were over-represented in the nucleus, specifically in chromosomes, the mitotic spindle, and the replication fork, and were involved in chromatin organization, DNA repair and metabolism, the cell cycle, and regulation of transcription factors.

Using the ConsensusPathDB tool, we also mapped regulated phosphoproteins to signalling pathways from three different pathways databases; pathway coverage was calculated for selected pathways (Fig 4B). The list of pathways containing proteins with VE-821-regulated phosphorylation sites, and thus pathways potentially modulated by VE-821 treatment contained pathways involved in DNA repair, replication, telomere synthesis, apoptosis, regulation of mitosis, transcription factors regulation, chromatin regulation via histones modification, and also pathways primarily related to cellular metabolism.

Network analysis revealed the complexity of cellular response and multiple functionally-related clusters affected by VE-821

Using the SubExtractor algorithm [55], we extracted multiple subnetworks of interconnected nodes with the most prominent changes in phosphorylation after VE-821 treatment. The largest subnetwork is depicted in Fig 5. For each group of interconnected nodes, we further

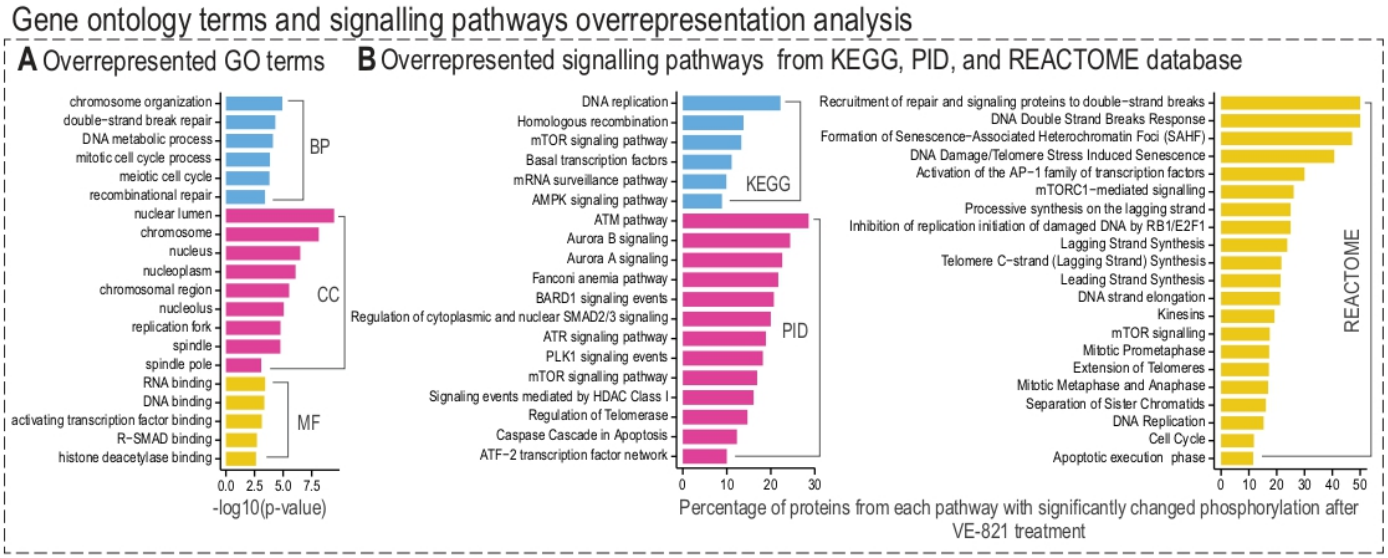

Fig 4. Selected results from gene ontology level 4 terms and signalling pathways overrepresentation analysis. Functional annotation of proteins with phosphorylation sites significantly affected by VE-821 treatment and over-representation analysis were done using ConsensusPathDB overrepresentation-analysis online tool. (A) Overrepresented GO terms (FDR < 0.05, all proteins quantified in our study were used as a statistical background). (B) Regulated phosphoproteins were mapped to signalling pathways from 3 different databases (KEGG, REACTOME, and PID) and pathway-coverage was calculated for overrepresented pathways (FDR < 0.05, all proteins comprised in detected pathways were used as a statistical background).

https://doi.org/10.1371/journal.pone.0199349.g004

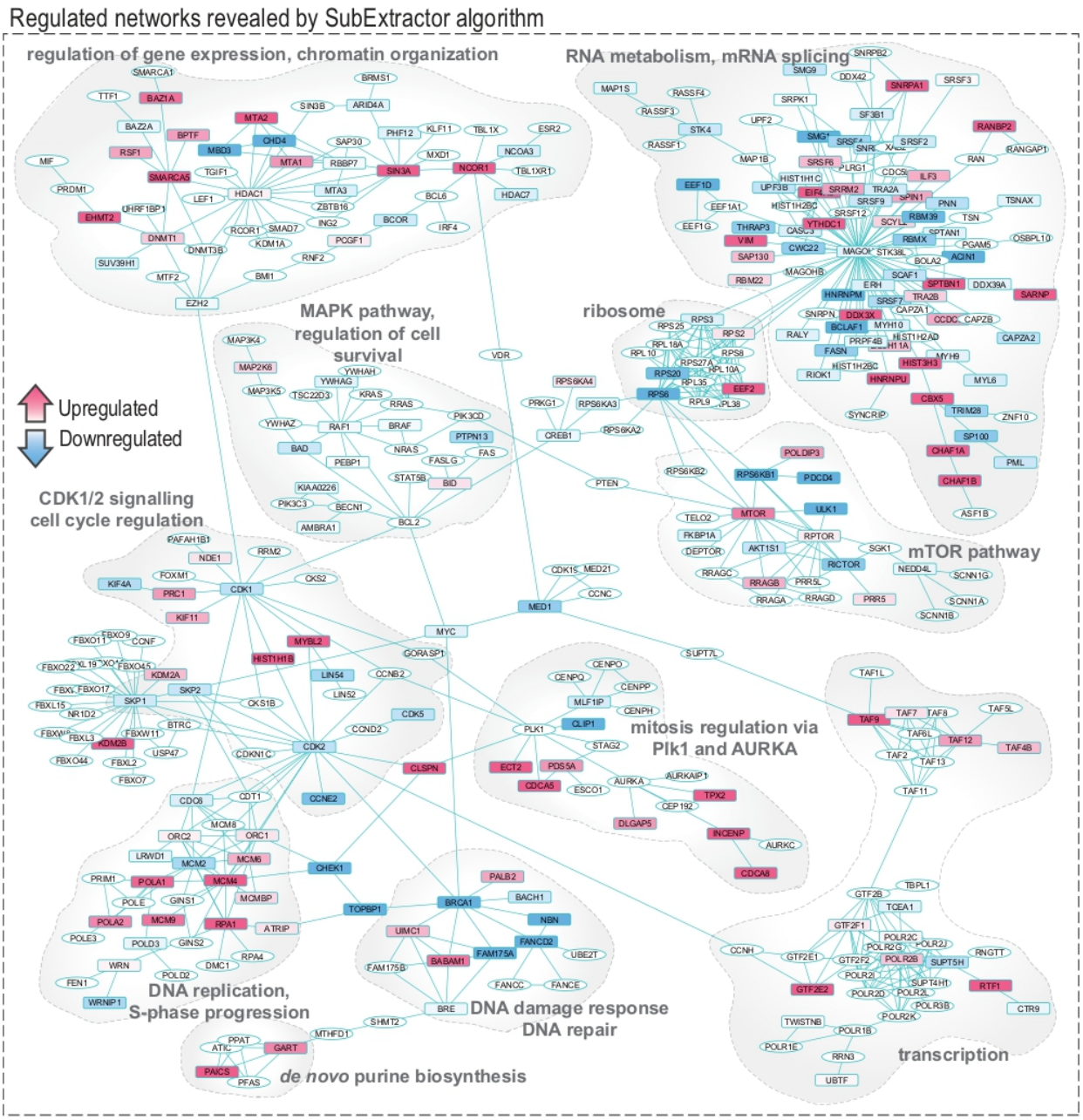

Fig 5. Protein network extracted using SubExtractor algorithm and visualized in Cytoscape. Protein-protein interactions with STRING score above 900 were used as an input for the algorithm and regulated subnetworks were extracted (FDR < 0.005). Proteins in rectangles were identified and quantified in our study; proteins in ellipses were added to the network by the algorithm. Proteins with downregulated phosphorylation are depicted in blue; proteins with upregulated phosphorylations are depicted in pink. The colour intensity corresponds to the degree of regulation (combined z-score).

https://doi.org/10.1371/journal.pone.0199349.g005

performed functional annotation enrichment analysis to better understand its functions. To simplify the interpretation, the clusters were divided into two groups.

The first one can be concisely described as a multi-level stress-induced regulation of gene expression: regulation of RNA biogenesis, its modification and stability, and translation.

Specifically, SubExtractor extracted distinct clusters that contain chromatin-modifying enzymes, transcription initiation and elongation complexes, and proteins from the mRNA splicing machinery. VE-821 treatment also affected phosphorylation of ribosomal proteins, suggesting that it might also alter protein synthesis. Furthemore, the ribosomal cluster is tightly linked to a cluster that mostly contains members of the mTOR pathway, indicating that this pathway might be dysregulated by VE-821 treatment, consequently resulting in affected cell growth and proliferation.

The second group mostly contains clusters corresponding to DDR and stress-induced cell cycle regulation. As shown in Fig 5 we detected a densely interconnected cluster composed of members of the minichromosome maintenance complex (MCMs), origin recognition complex subunits (ORCs), and DNA polymerases; this cluster also includes several known ATR-interacting proteins, and corresponds to the regulation of origin firing and S-phase progression by ATR in response to stress. Further hubs in the extracted network comprised four cell cycle regulating kinases–cyclin dependent kinase 1 (CDK1), cyclin dependent kinase 2 (CDK2), serine/threonine kinase PLK1 (PLK1), and aurora kinase A (AURKA)–and their regulated substrates extracted as their interactors. These kinases refer to the disruption of cell cycle checkpoints associated with IR-induced DNA damage and dysregulation of mitosis and cell division by VE-821 treatment as detected by the DNA content analysis. Interestingly, the algorithm also extracted a small cluster containing enzymes from the *de novo* pyrimidine synthesis metabolic pathway connected to the DNA repair cluster suggesting that metabolism of nucleotides might be also affected by ATR inhibition.

Moreover, we identified multiple protein kinases in the centre of extracted modules indicating their possible dysregulation by the treatment. To investigate kinome dysregulation induced by VE-821 treatment, we performed sequence motif analysis and kinase activity analysis together with statistical evaluation of the possible changes.

Sequence motif and kinase activity analyses confirmed the downregulation of PIKK substrates after VE-821 treatment

To identify global trends in VE-821 induced phosphoproteome changes, we first analysed and visualized sequence motifs using the iceLogo tool [57] and motif-x algorithm [58]. From the sequences surrounding downregulated sites, an SQ motif was extracted using motif-x, and Q at position +1 was significantly overrepresented among downregulated sites in iceLogo analysis, providing a confirmation of the downregulation of PI3K-related kinases ATM, ATR, and DNA-PK (Fig 6A). Additionaly, 1D enrichment analysis of known and predicted kinase motifs repeatedly indicated that the SILAC H/L ratio distribution of the ATM/ATR group substrates shows a significant declining trend (Fig 6B; an overview of all phosphorylation sites with known kinase and kinase predictions is given in S2 Table; an overview of all sites assigned to PIKKs is given in S3 Table). From these ratio shifts, the activity of the ATM/ATR group might be inferred as downregulated. Even though both kinases share the same phosphorylation motif, both prediction algorithms clearly favour ATM over ATR. We argue that this bias is probably introduced by a better annotation of ATM substrates and protein-protein interactions in the databases.

Nevertheless, using antibody against Chk2 phoshorylated at Thr 68, which is a widely-used marker of ATM kinase activation in response to ATM activating stress, we showed that 10 μM VE-821 did not inhibit ATM signalling in our experiments (Fig 1A). Furthermore, we found additional pieces of evidence of unaffected ATM signalling in our phosphoproteomic data: ATM Ser 2996 autophosphorylation site, which has been previously shown to be rapidly induced by IR [69], was not affected by the treatment. Similarly, two IR-induced

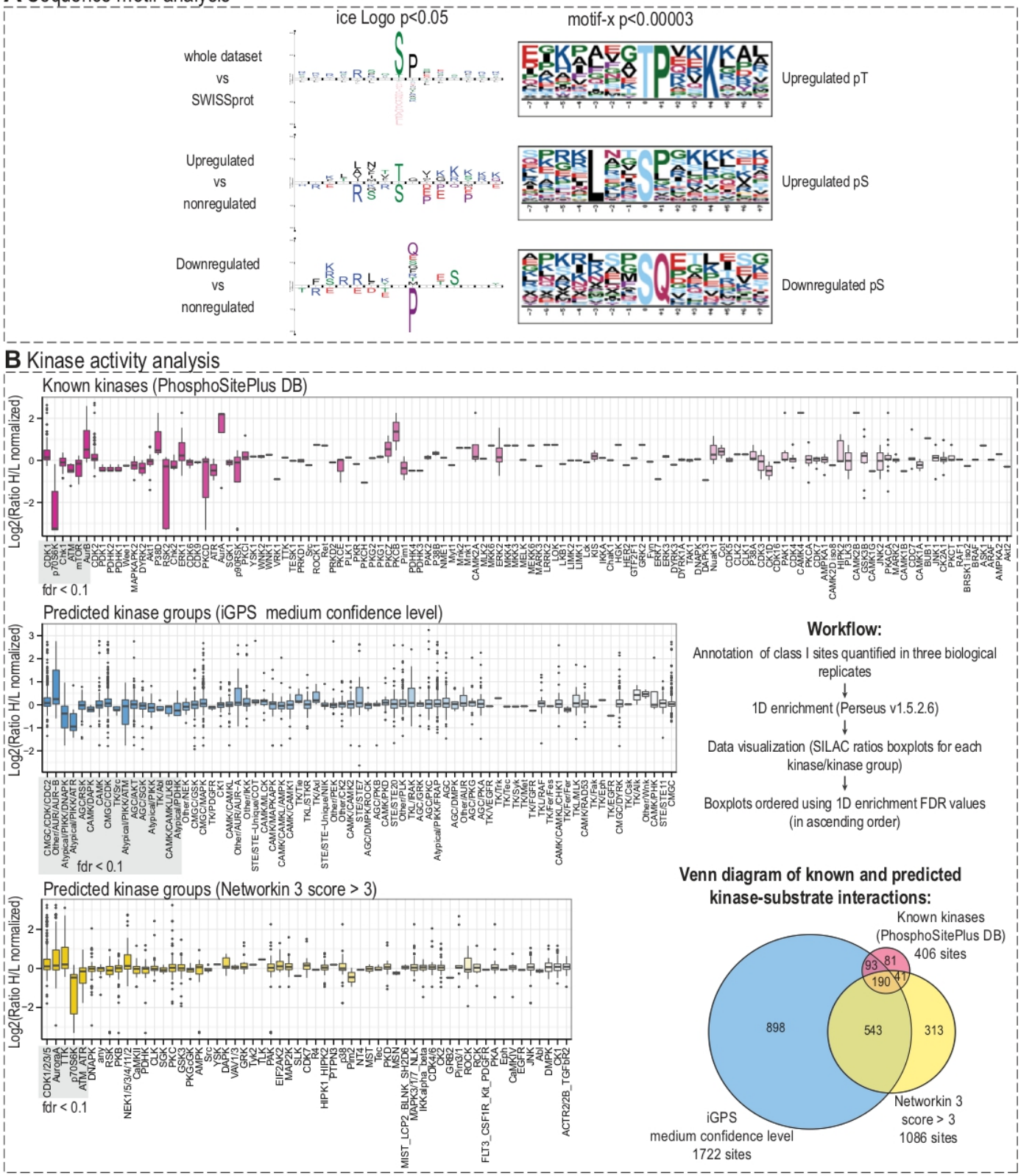
A Sequence motif analysis
ice Logo p<0.05
motif-x p<0.00003
whole dataset vs SWISSprot
Upregulated pT
Upregulated vs nonregulated
Upregulated pS
Downregulated vs nonregulated
Downregulated pS
B Kinase activity analysis
Known kinases (PhosphoSitePlus DB)
Log2(Ratio H/L normalized)
fdr < 0.1
Predicted kinase groups (iGPS medium confidence level)
Predicted kinase groups (Networkin 3 score > 3)
Workflow:
Annotation of class I sites quantified in three biological replicates
1D enrichment (Perseus v1.5.2.6)
Data visualization (SILAC ratios boxplots for each kinase/kinase group)
Boxplots ordered using 1D enrichment FDR values (in ascending order)
Venn diagram of known and predicted kinase-substrate interactions:
Known kinases (PhosphoSitePlus DB) 406 sites
iGPS medium confidence level 1722 sites
Networkin 3 score > 3 1086 sites
898
93
81
190
41
543
313

Fig 6. Sequence motif and kinase activity analyses. (A) Sequence motif analysis was performed using IceLogo and motif-x. Amino acid sequences of differentially up- or down- regulated phosphorylation sites were analysed against a statistical background comprising all class I sites quantified in our study. Depicted motifs were found enriched at indicated significance levels. In IceLogo analysis, amino acids that were more frequently observed in the proximity of a regulated phosphorylation site are indicated over the middle line, whereas the amino acids with lower frequency are indicated below the line; phosphorylated amino acid is located at position 0. (B) Kinase activity analysis. Phosphorylation sites were annotated with their known kinases using PhosphoSitePlus database if available. iGPS v1.0 and Networkin 3 were used to predict kinases for all class I sites, and the predictions were filtered as indicated. Venn diagram shows the overlap between phosphorylation sites annotated by each method and applying desired filtering criteria. Boxplots depict SILAC H/L ratios distribution of phosphorylation sites assigned to each kinase/group. The distribution, median, and/or outlier-shifts to positive values indicate a possible upregulation of kinase activity; trends toward negative ratio values show a possible downregulation of kinase activity. Statistical analysis was performed using 1D enrichment analysis in Perseus (v 1.5.2.6), and the test FDR value for each kinase/group was used to rank the boxplots in ascending order. The higher color intensity corresponds to the lower 1D enrichment FDR value and vice versa.

https://doi.org/10.1371/journal.pone.0199349.g006

autophosphorylation sites of a downstream ATM target Chk2, Ser 260 and Ser 379 [70,71], were also not significantly changed.

On the contrary, known ATR targets located within the Chk1 regulatory domain were observed to be downregulated upon VE-821 treatment: Ser 345 phosphorylation was detected by western blotting (Fig 1A), and Ser 317 phosphorylation was quantified in our phosphoproteomic experiment. An important marker of Chk1 activity, the autophosphorylation site Ser 296, was not detected in our study. Chk1 itself was evaluated as significantly downregulated in the 1D enrichment analysis of the known substrates, providing further evidence of the downregulated ATR/Chk1 pathway. Considering the high selectivity of VE-821 towards ATR kinase (IC50 (ATR): 26 nM, Ki (ATR): 13 nM, Ki (DNA-PK): 2.2 μM, Ki (ATM): 16 μM), we can assume that significant changes within SQ/TQ phosphorylations motifs assigned to the ATM/ATR group can be explained by specifically inhibited ATR kinase activity.

DNA-PK, which is also known to share the glutamine directed phosphorylation motif, was evaluated to be significantly downregulated using the iGPS predictions. However, we did not find any known site of DNA-PK that would be downregulated in our study (the only known DNA-PK phosphorylation site was Ser 430 on Vimentin, which was unchanged). Moreover, 10 μM VE-821 was proven to leave DNA-PK signalling unaffected in a cell-based assay [15], and hence we assume that DNA-PK inhibition is rather unlikely.

In all three experimental replicates, we identified and quantified 21 downregulated SQ/TQ class I phosphorylation sites, eleven of which were known substrates of ATM/ATR kinases or predicted by iGPS or Networkin 3. Most of the downregulated sites were located on proteins with confirmed roles in DDR; however, potential functions of some of them have not yet been elucidated. Importantly, VE-821 treatment altered phosphorylation of MRN and BRCA1-BRCT/Abraxas complexes and several other proteins with a known role in DNA damage response. Examples of the most interesting phosporylation sites and their functions are discussed in detail in the S1 File.

Dysregulation of cyclin-dependent kinases and aurora kinases was responsible for disruption of the G2/M checkpoint and faster progression through mitosis

In the DNA content analysis, we showed that VE-821 disrupted IR-induced G2/M arrest in MOLT-4 cells (Fig 1I). Cells treated with ATR inhibitor were not able to activate the G2/M checkpoint, which in turn led to faster progression into mitosis with unrepaired IR-induced DNA damage. Such progression has been shown to cause mitotic catastrophe and apoptotic cell death in haematological malignant cell lines [36,72,73]. Using phosphoproteomics, we aimed to describe which kinases were dysregulated by ATR inhibition and thus may contribute to the G2/M checkpoint disruption. In the sequence motif analyses (Fig 6A), we observed proline-directed motifs followed by basic amino acids significantly over-represented in the

upregulated dataset, which corresponds well to the known sequence logo of CDK 1 and 2. Futhermore, as depicted in Fig 6B, the kinase activity analysis revealed a possible upregulation of G2/M checkpoint controlling CDK1 kinase, mitotic kinases aurora A and B, and kinases from the NEK family, particularly serine/threonine protein kinase NEK2 (NEK2). An overview of detected substrates of mitotic kinases is given in S3 Table.

The kinase activity analysis confirmed a significant upregulation of cyclin dependent kinases, predominantly CDK1 (CDC2), with a median ratio only slightly deviated to positive values, but numerous outliers strongly upregulated after VE-821 pre-treatment (Fig 6B). Many of these outliers were classified as so-called "regulatory" sites (*i.e.* sites with previously discovered and experimentally validated effects on the modified protein) with either a known function in mitosis, or whose function has not yet been elucidated, but whose corresponding phosphoproteins have been shown to have important roles in the onset of mitosis and mitotic progression. Examples of the most interesting CDK1-phosphorylated sites and their functions are given in the S1 File. Additionally, unscheduled CDK1 activity in G1 phase has been shown to trigger apoptosis in X-irradiated MOLT-4 cells [74]. In our data, VE-821 significantly affected viability of MOLT-4 cells. It is possible that in addition to G2/M checkpoint disruption and induction of post-mitotic cell death, the dysregulation of CDK1 by ATR inhibition contributes to the increased rate of apoptosis in MOLT-4 cells.

Kinases from the Aurora kinase family—Aurora kinases A and B—are master regulators of mitosis progression and onset of cytokinesis, whose activities require tight spatial and temporal regulation, and their dysregulation could cause errors in mitosis, faster progression through the abscission checkpoint, and affect postmitotic genome surveillance. In our analysis, we found that the activities of these two kinases might be upregulated by VE-821 treatment (Fig 6B). Examples of the most interesting phosphorylation sites are given in the S1 File.

Taken together, our data indicate that ATR inhibition induced dysregulation of the main mitotic kinases. The results are in concordance with our previous study on HL-60 leukemic cells [43], in which we observed dysregulation of CDK1, PLK1, and NEK2.

The key regulator of cellular metabolism, Serine/threonine protein kinase mTOR and its downstream effector, p70S6K, were inhibited by an off-target effect of 10 μM VE-821 treatment, possibly contributing to the growth inhibition observed in the proliferation assays

As the previous data analyses already indicated, we found a significant downregulation of the serine/threonine protein kinase mTOR (mTOR) in the kinase activity analysis. The protein kinase mTOR is the principle regulator of cellular metabolism promoting anabolic processes and inhibiting catabolic processes such as autophagy [75]. In total, we found seven known direct mTOR targets downregulated in our study and several other proteins included in the mTOR signalling pathway from the KEGG pathway database (depicted in Fig 7A and summarized in Fig 7B). Detailed description of the functions of the most interesting mTOR related phosphorylation sites and their functions are given in the S1 File. Most of the mTOR-phosphorylated or downstream regulated proteins are involved in transcription and translation regulation and thus contribute to regulation of cell growth and proliferation: Eukaryotic translation initiation factor 4E-binding protein 1 (EIF4EBP1; Ser 65), protein PAT1 homolog 1 (PATL1; Ser 179 and Ser 184) and la-related protein 1 (LARP1; Ser 766 and Ser 774), and repressor of RNA polymerase III transcription MAF1 homolog (MAF1). In addition to proteins involved in translation regulation, we also identified significantly changed phosphorylation of two phosphoproteins linked to autophagy: death-associated protein 1 (DAP1) and serine/threonine-protein kinase

A Significantly changed phosphorylation sites in mTOR signalling pathway (KEGG)

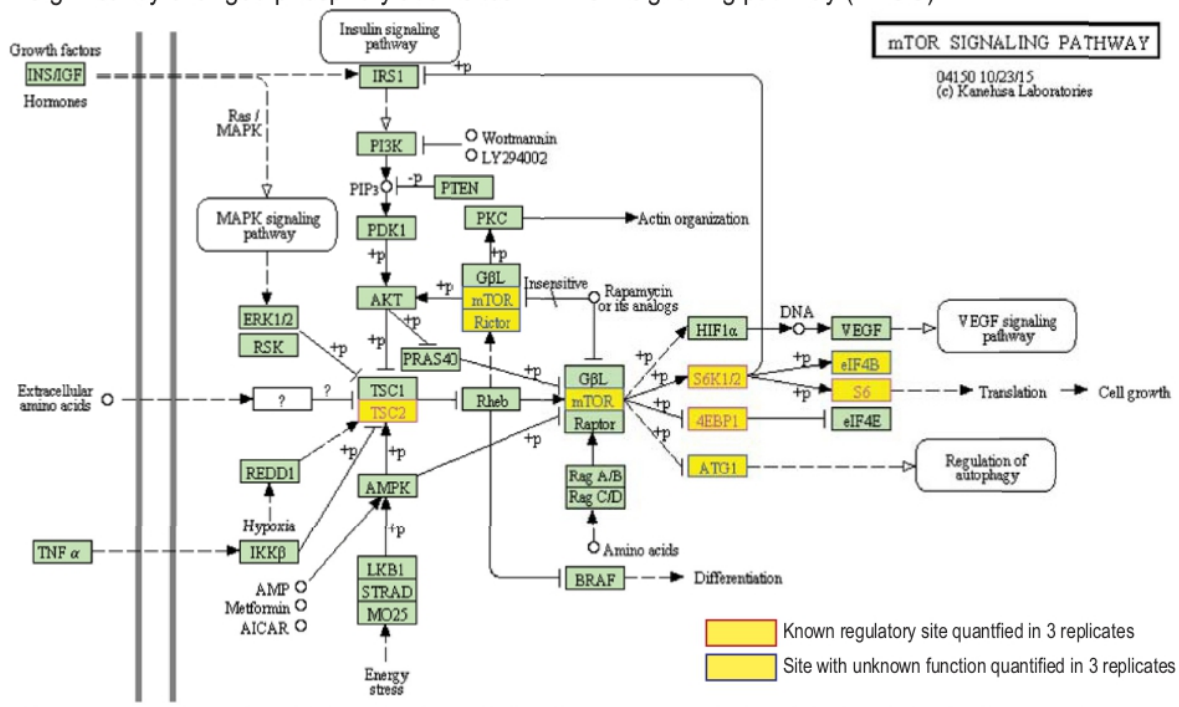

B Summary of phosphorylation sites in mTOR pathway and mTOR substrates detected in our study

AA	Pos.	Gene name	Protein name	regulated	Regulatory site	Known kinase
S	3	DAP	Death-associated protein 1	DOWN	YES	NaN, but mTOR dependent
S	359	EIF4B	Eukaryotic translation initiation factor 4B	DOWN		NaN
S	65	EIF4EBP1; 4EBP1	Eukaryotic translation initiation factor 4E-binding protein 1	DOWN	YES	mTOR
S	65	EIF4EBP1; 4EBP1	Eukaryotic translation initiation factor 4E-binding protein 1	DOWN	YES	DYRK2; ERK1; ERK2; mTOR
S	766	LARP1	La-related protein 1	DOWN		mTOR
S	774	LARP1	La-related protein 1	DOWN		mTOR
S	75	MAF1	Repressor of RNA polymerase III transcription MAF1 homolog	DOWN	YES	mTOR
S	1261	MTOR	Serine/threonine-protein kinase mTOR	UP		NaN
S	179	PATL1	Protein PAT1 homolog 1	DOWN		mTOR
S	184	PATL1	Protein PAT1 homolog 1	DOWN		mTOR
S	1177	RICTOR	Rapamycin-insensitive companion of mTOR	DOWN		NaN
S	236	RPS6; S6	40S ribosomal protein S6	DOWN	YES	p70S6K; p90RSK; PKCD; RSK2
S	240	RPS6; S6	40S ribosomal protein S6	DOWN		p70S6K
S	235	RPS6; S6	40S ribosomal protein S6	DOWN	YES	p70S6K; p90RSK; PKCD; RSK2
S	427	RPS6KB1; S6K	Ribosomal protein S6 kinase beta-1	DOWN	YES	NaN
T	1462	TSC2	Tuberin	UP	YES	Akt1
S	450	ULK1; ATG1	Serine/threonine-protein kinase ULK1	DOWN		NaN

C Effect of irradiation and VE-821 treatment on S6k pT389 phosphorylation (marker of mTOR activity)

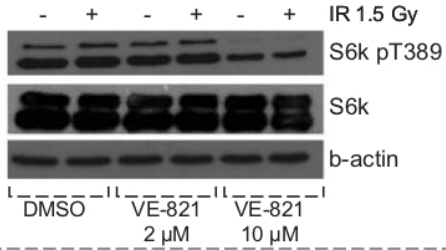

Fig 7. Significant changes in mTOR signalling pathway. (A) Proteins with significantly changed phosphorylation sites were mapped onto KEGG signalling pathways. (B) Summary of all phosphorylation sites comprised in "mTOR signalling pathway" pathway in KEGG database and phosphorylation sites that are known mTOR substrates or known to be mTOR-dependent. (C) Immunoblotting analysis of mTOR activity. Cells were collected 2 hour after IR (1.5 Gy). Activity of mTOR was monitored via the detection of its target pT389 of p70S6K (S6K, RPS6KB1). The expression state of p70S6K was also evaluated. β-actin expression was analysed as a loading control.

https://doi.org/10.1371/journal.pone.0199349.g007

ULK1 (ULK1). These observations might indicate that mTOR inhibition by 10 μM could further affect the phenotype observed after irradion via suppression of autophagy [76].

To further validate the VE-821-mediated mTOR inhibition, we performed a confirmation experiment using an antibody detection of a regulatory ribosomal protein S6 kinase beta-1 (p70s6K) Thr 389 phosphorylation site that is commonly used to examine the activity of mTOR. As shown in Fig 7C, while irradiation by a dose of 1.5 Gy did not affect p70S6K phosphorylation, mTOR-dependent p70S6K phosphorylation was almost diminished after 10 μM VE-821 treatment in both irradiated and sham-irradiated cells. However, 2 μM VE-821 did not have any significant effect on the Thr 389 phosphorylation site.

The inhibition of mTOR by 10 μM VE-821 but not by 2 μM treatment is coherent with the results of our proliferation and DNA analysis experiments, and explains the difference we observed between the 2 μM and 10 μM VE-821 treated groups. While both concentrations of the inhibitor radiosensitized MOLT-4 cells, 10 μM had much stronger inhibitory effect on the number of viable sham-irradiated cells (Fig 1B and 1F). Likewise, while both concentrations caused the disruption of the IR-induced G2/M arrest, it was only the higher concentration which caused a significant accumulation in G1 phase in sham-irradiated cells (Fig 1I). These conclusions are supported by the fact that mTOR inhibition triggers the G1 metabolic checkpoint and inhibits cell growth and proliferation [77]. The mTOR inhibition by 10 μM VE-821 might also explain the high sensitivity of the MOLT-4 cell line to VE-821 treatment. Consistently with MOLT-4 homozygous deletion of *PTEN* [30], it has been shown that *PTEN*-deficient tumours were more likely to be sensitive to mTOR inhibition [78,79].

In addition to the downregulation of mTOR, we also observed a significant downregulation of the p70S6K (or RPS6KB1) in all kinase activity analyses (Fig 6B). P70S6K is an important kinase that acts downstream of mTOR to promote protein synthesis and cellular proliferation [80,81]. In addition to the western blotting detection of changes in Thr 389 phosphorylation (Fig 7C) induced by VE-821 treatment, we also detected another downregulated mTOR-dependent "regulatory" phosphorylation site (Ser 427) in our phosphoproteomic data. From the known p70S6K substrates, we detected three strongly downregulated phosphorylation sites on 40S ribosomal protein S6 (RPS6)–Ser 235, Ser 236, and Ser 240. These phosphorylation sites are phosphorylated by ribosomal kinases to initiate translation [82], and thus the inhibition of their phosphorylation causes inhibition of protein synthesis. Moreover, iGPS and Networkin 3 predicted two more members of the translation machinery to be downregulated substrates of RSKs—eukaryotic translation initiation factor 3 subunit A (EIF3A) Ser 584 and eukaryotic translation initiation factor 4B (EIF4B) Ser 119, providing further evidence for translation inhibition caused by inhibitor treatment.

The downregulation of dihydroorotase phosphorylation, a substrate of p70S6K, showed a possible link to nucleotide synthesis alteration induced by VE-821 treatment

Surprisingly, on the list of known/predicted p70S6K substrates detected in our study, we did not find phosphoproteins involved solely in protein synthesis. Dihydroorotase (CAD) is an

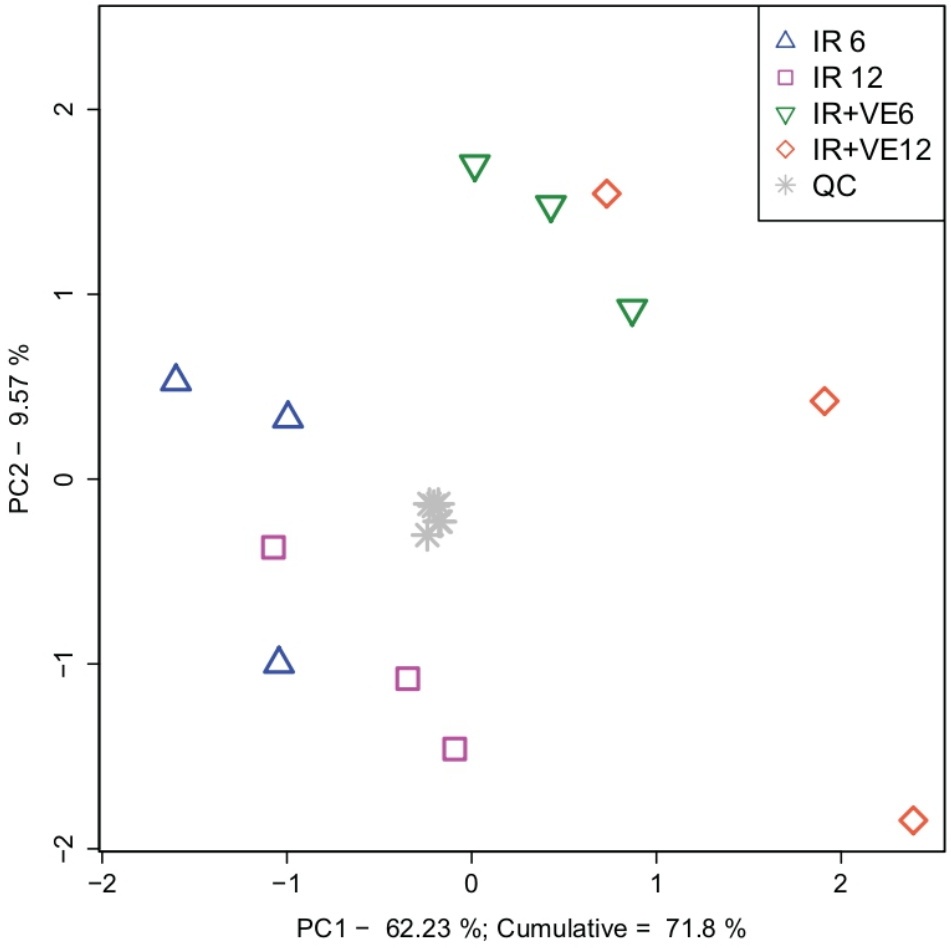

Fig 8. Principal component analysis score plot of VE-821 induced metabolome changes in irradiated MOLT-4 cells. IR–irradiated cells pre-treated with DMSO, IR+VE–irradiated cells pre-treated with 10 μM VE-821, both groups were analysed 6 and 12 hours after irradiation. Grey stars represent quality control samples.

https://doi.org/10.1371/journal.pone.0199349.g008

enzyme required for the first steps of *de novo* pyrimidine synthesis. Phosphorylation on Ser 1859 by p70S6K downstream of mTOR stimulates dihydroorotase activity of CAD to induce pyrimidine synthesis [83]. Ser 1859 was detected to be downregulated in our study, suggesting that VE-821 treatment might also hamper synthesis of nucleotides, which are necessary for both cellular proliferation and DNA repair after DNA damage induction.

Possible VE-821-induced nucleotide synthesis dysregulation was striking enough to encourage us towards further data examination and to search for regulated phosphorylation sites located on enzymes included in nucleotide synthesis pathways. Indeed, in all three replicates, we identified two additional regulated phosphorylation sites on proteins from the *de novo* purine synthesizing pathway: phosphoribosylglycinamide formyltransferase (GART) Tyr 348 and phosphoribosylaminoimidazole carboxylase (PAICS) Ser 27; the latter has been identified as a potential substrate of CDKs in two high-throughput phosphoproteomic screenings [84,85]. However, none of these enzymes has been proven to be regulated by phosphorylation, and thus we can only speculate whether these two phosphorylation events might have some effect on *de novo* purine synthesis or not.

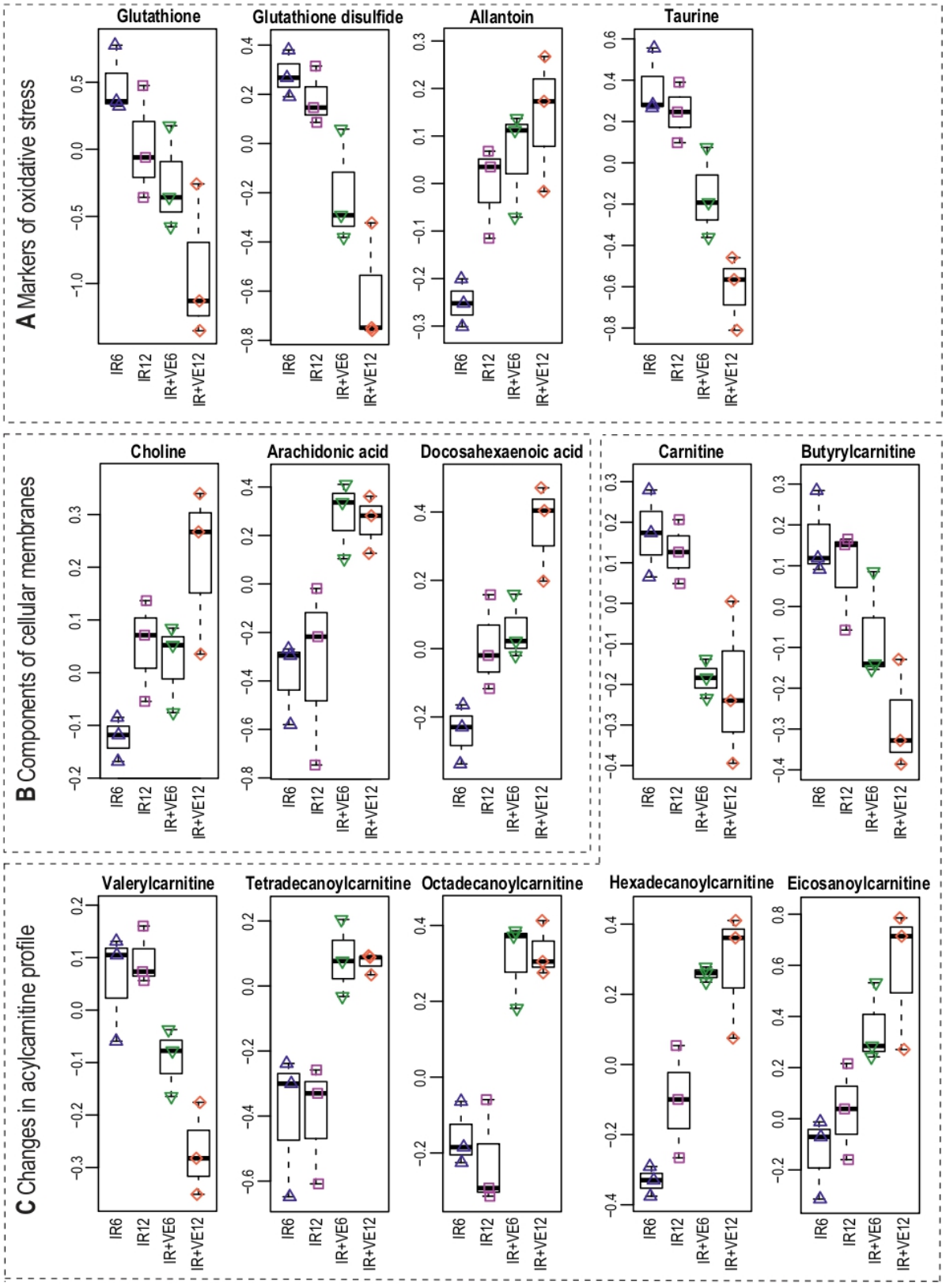
A Markers of oxidative stress
Glutathione
Glutathione disulfide
Allantoin
Taurine
B Components of cellular membranes
Choline
Arachidonic acid
Docosahexaenoic acid
Carnitine
Butyrylcarnitine
C Changes in acylcarnitine profile
Valerylcarnitine
Tetradecanoylcarnitine
Octadecanoylcarnitine
Hexadecanoylcarnitine
Eicosanoylcarnitine
IR6
IR12
IR+VE6
IR+VE12

Fig 9. VE-821 induced changes in cellular response to oxidative stress, degradation of membranes, and acylcarnitine profile. (A) Boxplots of selected markers of oxidative stress, (B) selected components of cellular membranes, and (C) selected changes in acylcarnitine profile are depicted. IR–irradiated cells pre-treated with DMSO, IR+VE–irradiated cells pre-treated with 10 μM VE-821; both groups were analysed 6 and 12 hours after irradiation.

https://doi.org/10.1371/journal.pone.0199349.g009

Targeted metabolomic analysis of VE-821 treated MOLT-4 cells resulted in detection of 206 intermediary metabolites

In the phosphoproteomic analysis of VE-821-treated and irradiated cells, changes in the mTOR activity were detected as a result of an off-target effect of the inhibitor. As mTOR is the principal regulator of cellular metabolism [75], this finding raised an intriguing question–whether the inhibitor treatment modulates cellular metabolism after irradiation. We further examined our data and found several metabolic enzymes containing phosphorylation sites affected by VE-821. In addition to the aforementioned enzymes involved in the metabolism of purine and pyrimidine, we detected changes in enzymes from the metabolism of glucose, namely phosphofructokinase 1 (Ser 775), triosephosphate isomerase (Thr 28), phosphoglycerate mutase 1 (Ser 189), and pyruvate dehydrogenase E1 component subunit alpha (Ser 293 and Ser 300).

The metabolic responses of different cell lines to various doses of IR have been investigated in several studies, for instance [86–88]. Briefly, these studies showed that IR-triggered production of oxygen free radicals by radiolysis of water induced changes in glutathione level, disturbed energy metabolism resulting in a rapid decrease of cellular ATP level, and increased levels of free amino acids, choline and lipids, which are produced by degradation of damaged proteins and membranes. However, to our best knowledge, no study has yet been published investigating the modulation of this response by small molecular kinase inhibitors of any of the PIKK family. Therefore, we performed a metabolomic analysis of irradiated MOLT-4 cells, whose response to IR was modulated by inhibition of ATR (and, as shown above, mTOR) using 10 μM VE-821.

Metabolite profiling performed by a label-free targeted analysis of cellular extracts collected 6 and 12 h after irradiation (Fig 2A) resulted in detection of 206 intermediary metabolites (Fig 2D). As shown in Fig 8, PCA revealed clear separation in metabolic profiles between both treatment groups and controls with explained variance of 72%. Localization of samples in PCA indicated that the inhibitor had a more significant impact on the group clustering than the incubation time.

The detected metabolites were further mapped on KEGG pathways to visualize metabolic pathways affected by the inhibitor 6 and 12 hours after irradiation (S2 File). This analysis showed that the main changes in the metabolome of the VE-821-treated MOLT-4 cell line occurred in a group of metabolites involved in the cellular antioxidant system, glycolysis and the citrate cycle. Differences in levels of nucleosides, nucleotides, deoxynucleotides, free amino acids, and acylcarnitines were also observed.

Treatment with VE-821 potentiated changes in cellular antioxidant defence, degradation of proteins and membranes, and mitochondrial damage induced by IR

When cells are exposed to IR, cellular structures can be damaged by ionization directly by deposition of energy, but also indirectly by water radiolysis and stimulation of nitric oxide synthases and NADPH oxidases [89]. Reduced glutathione (GSH) is an important cellular antioxidant and the reduced/oxidized glutathione ratio (GSH/GSSG) is a sensitive biomarker of oxidative stress [90]. It has been reported previously that IR induced a significant decrease

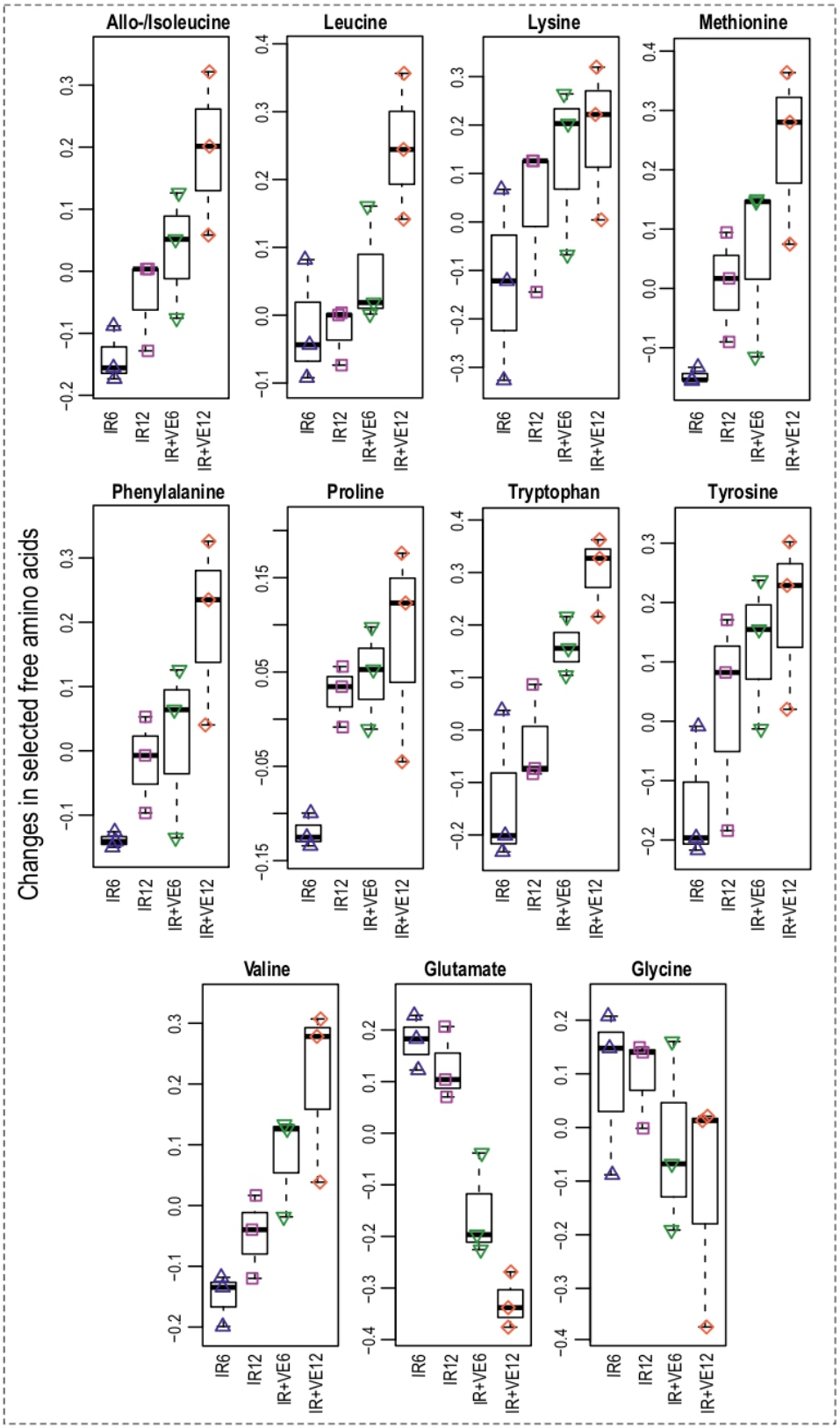
Changes in selected free amino acids
Allo-/Isoleucine
Leucine
Lysine
Methionine
Phenylalanine
Proline
Tryptophan
Tyrosine
Valine
Glutamate
Glycine
IR6
IR12
IR+VE6
IR+VE12

Fig 10. Changes in free amino acids levels in irradiated and VE-821 treated cells. Boxplots of selected amino acids in irradiated cells pre-treated with DMSO (IR) and irradiated cells pre-treated with 10 μM VE-821 (IR+VE); both groups were analysed 6 and 12 hours after irradiation.

https://doi.org/10.1371/journal.pone.0199349.g010

in cellular glutathione level [86,87]. In our study, we observed a decrease in GSH over time and this decrease was amplified by inhibitor treatment (Fig 9A). However, GSSG was also depleted, as well as important precursors of GSH biosynthesis (glutamate and glycine, Fig 10). Therefore, we assume that the overall decrease in the GSH/GSSG pair was caused by increased turnover of GSH and simultaneously missing precursors. Additionally, we observed increased levels of allantoin and decreased levels of taurine (Fig 9A). Allantoin can be formed in the presence of ROS by non-enzymatic reactions, and similarly to GSH, it can be used as a marker of oxidative stress [91]. Taurine is an intermediate in metabolism of methionine and an anti-oxidant, and its decrease might indicate its elevated consumption in VE-821 treated cells as a part of preventive mechanisms counteracting oxidative stress. Taken together, our data provide indirect evidence that the cellular response to oxidative stress induced by IR might have been affected by the pre-incubation with VE-821.

In addition to the changes in the cellular redox system, direct effects on proteins and membranes were also observed. Increased levels of several amino acids (phenylalanine, proline, tryptophan, tyrosine, valine, isoleucine, glutamate, glycine, and methionine) can indicate increased turnover of proteins which were damaged by ROS/RNS exposure (Fig 10). Elevated levels of docosahexaenoic acid, arachidonic acid, and choline may be evidence for increased membrane degradation induced by the inhibitor treatment (Fig 9B). IR induces autophagy by inhibition of mTOR [92] probably via a pathway involving ATM and AMPK [93]. VE-821 10 μM, but not 2 μM inhibited mTOR in both sham-irradiated and irradiated MOLT-4 cells (Fig 7C), and we also detected several significantly changed phosphorylations in autophagy-regulating proteins. Thus, we can hypothesize that the treatment might have induced degradation of damaged structures (presumably via autophagy), resulting in increased accumulation of degradation products in cells.

We further observed prominent changes in the acylcarnitine profile (Fig 9C), which might indicate mitochondrial disturbances induced by VE-821. Increased levels of long-chain acylcarnitines (tetradecanoyl-, palmitoyl-, and stearoylcarnitine) and decreased levels of free carnitine, isovaleryl-/ methylbutyrylcarnitine, and malonyl-/ 3-hydroxybutyrylcarnitine were observed. Acylcarnitine changes have been already observed in two independent studies investigating metabolic effects of IR [88,94]. Moreover, it has been shown that L-carnitine acts as a free-radical scavenger protecting irradiated mice from oxidative damage in response to IR [95]. Our observation of the lipid changes in cellular membranes could be explained by lipid peroxidation induced by increased ROS generation in VE-821 treated cells, which was evidenced above as decreased GSH and altered allantoin and taurine levels. However, it would be necessary to perform a lipidomic analysis to specifically address oxidation of lipids induced by IR and VE-821 [96].

VE-821 potentiated the energy metabolism disruption induced by IR

IR has been shown to disturb energy metabolism, which was demonstrated by a rapid decrease of cellular ATP levels in irradiated cells [86,97] and serum glucose levels in irradiated mice [98]. In our study, we found decreased levels of nucleoside triphosphates (NTPs; ATP, GTP, CTP, and UTP), diphosphates (NDPs; ADP and UDP), and diphosphate derivatives (UDP-hexoses, GDP-hexoses, and UDP-N-acetylglucosamine), and by contrast increased levels of ribonucleosides (adenosine, guanosine, and pseudouridine) and bases (uracil). The overview

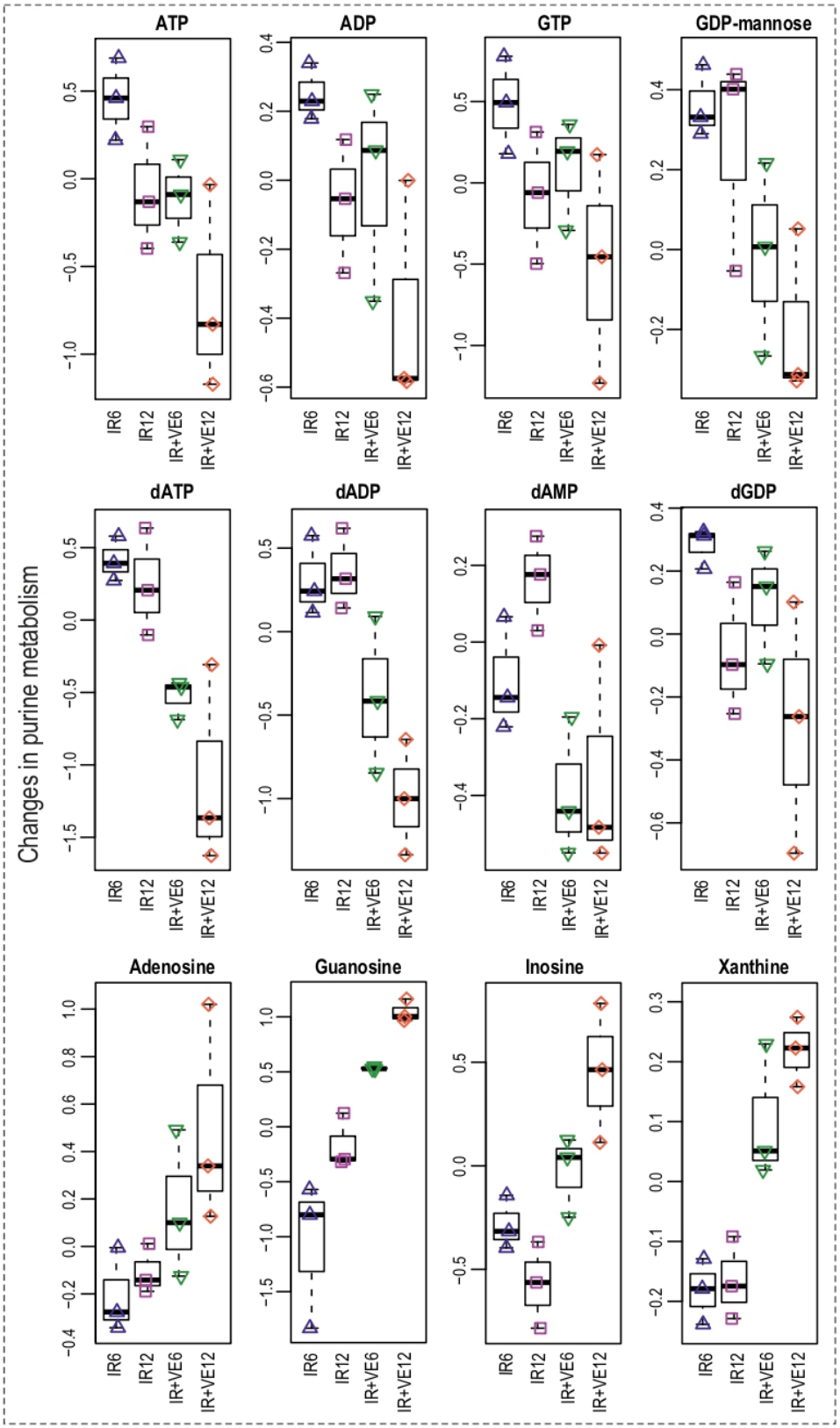
Changes in purine metabolism
ATP
ADP
GTP
GDP-mannose
dATP
dADP
dAMP
dGDP
Adenosine
Guanosine
Inosine
Xanthine
IR6
IR12
IR+VE6
IR+VE12

Fig 11. Changes in purine metabolism induced by VE-821 in irradiated cells. Boxplots of selected nucleoside and deoxynucleoside triphosphates, diphosphates, diphosphate derivatives ribonucleosides, and bases from the metabolism of purine are shown. IR–irradiated cells pre-treated with DMSO, IR+VE–irradiated cells pre-treated with 10 μM VE-821; both groups were analysed 6 and 12 hours after irradiation.

https://doi.org/10.1371/journal.pone.0199349.g011

of changes in purine and pyrimidine metabolism induced by VE-821 is given in Figs 11 and 12.

Decreased levels of high-energy phosphorylated compounds might indicate disruption in energy metabolism induced by exposure to IR. Importantly, VE-821 amplified the energy depletion caused by IR. It is not clear from our data whether the observed time-dependent decrease is due to increased utilization of NTPs needed as "molecular fuel" for cellular signalling, reparation processes, and programmed cell death following DNA damage induction by IR, or to their decreased synthesis following damaged ATP synthesis in mitochondria.

Significant changes were also found in glycolysis (Figs 13 and 14). Decreased intermediates of glycolysis can be interpreted as preferential utilization of glycolysis. This hypothesis could be supported by pronounced time-dependent increase in lactate in irradiated control and VE-821-treated cells. We also detected an activating phosphorylation on phosphofructokinase 1 (PFKL) Ser 775 in two experimental replicates of our phosphoproteomic analysis, which has been previously shown to be responsive to insulin treatment and activating glycolysis [99]. This suggests that the metabolic flux through glycolysis might be increased one hour after irradiation.

We further observed significant modulation of citric acid cycle metabolites (Fig 13). Markedly lower levels of aconitate, malate, and citrate/isocitrate were found in VE-821 treated cells; moreover, citrate/isocitrate showed a time-dependent decrease in irradiated cells without any inhibitor treatment. On the contrary, succinate and fumarate were slightly increased in VE-821 treated cells. We assume that these intermediates could have been replenished by anaplerotic reaction from the amino acids obtained by protein degradation.

VE-821 affected deoxynucleotide pools in irradiated cells

Decreased levels of deoxynucleoside diphosphates (dNDPs; dADP and dTDP) and triphosphates (dNTPs; dATP, dGTP, and dTTP) were found in VE-821 treated irradiated cells. dCTP was also decreased as a result of VE-821 pre-incubation; moreover, time-dependent reduction was observed in irradiated control cells. We also found several purine and pyrimidine bases and ribosides (xanthine, inosine, cytidine, uridine, and thymidine) elevated in VE-821 treated cells. Besides that, nucleoside monophosphates (AMP and GMP) were slightly reduced (Figs 11 and 12).

Deoxyribonucleotides arise either via *de novo* pathways or preferably, by salvage pathways involving reutilization of nucleosides and nucleobases [100]. Thus, in principle, the deoxynucleotide levels might have decreased either by downregulation of their *de novo* synthesis or due to their degradation and downregulation of the salvage pathways. Importantly, dNTPs damaged by IR and oxidised due to increased levels of ROS in irradiated cells are degraded by hydrolysis, largely contributing to dNTP depletion upon irradiation.

As discussed above, in our study, we observed a time-dependent decrease in NDPs and NTPs, i.e. the precursors of dNDPs and dNTPs in *de novo* pathways, which was further amplified by VE-821 inhibitor, supporting the hypothesis that the decrease in dNTPs may have been induced by insufficiency of the precursors for their *de novo* synthesis. Furthermore, we also detected a significantly decreased stimulating phosphorylation on CAD Ser 1859, an important regulator of *de novo* pyrimidine synthesis, and two phosphorylations on two enzymes involved

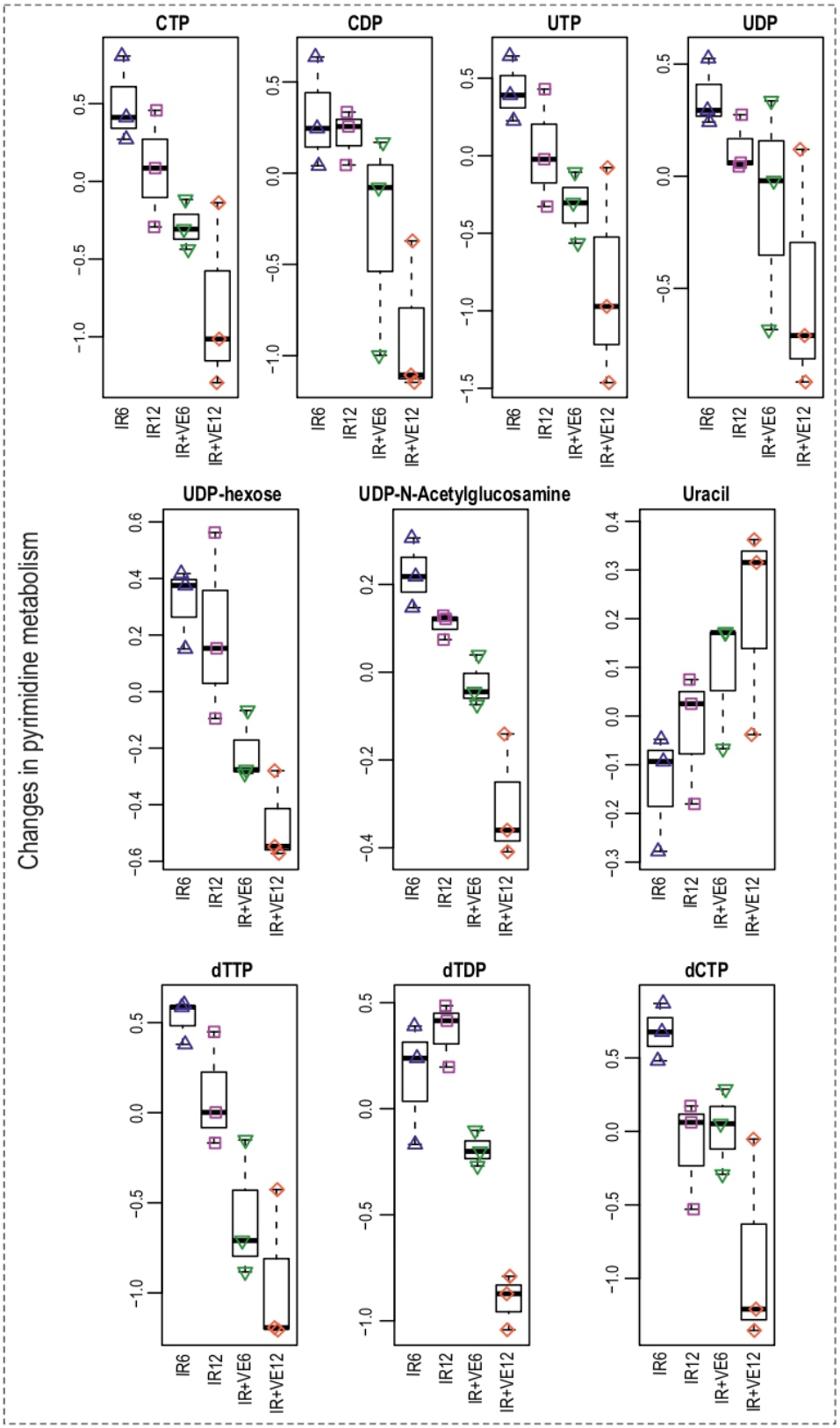
Changes in pyrimidine metabolism
CTP
CDP
UTP
UDP
UDP-hexose
UDP-N-Acetylglucosamine
Uracil
dTTP
dTDP
dCTP
IR6
IR12
IR+VE6
IR+VE12

Fig 12. Changes in metabolism of pyrimidine induced by VE-821 in irradiated MOLT-4 cells. Boxplots of selected nucleoside and deoxynucleoside triphosphates, diphosphates, diphosphate derivatives ribonucleosides, and bases from the metabolism of purine are shown. IR–irradiated cells pre-treated with DMSO, IR+VE–irradiated cells pre-treated with 10 μM VE-821; both groups were analysed 6 and 12 hours after irradiation.

https://doi.org/10.1371/journal.pone.0199349.g012

in *de novo* purine biosynthesis (GART and PAICS) with unknown functions. The salvage pathways could have been affected also by the inhibitor treatment; this idea correlates with a recent study showing that activity of deoxycytidine kinase (dCK) is ATR-dependent after stress induction [101]. dCK catalyses the first and rate limiting step of the deoxyribonucleotide salvage pathway as a consequence of its broad substrate specificity [102,103]. Beyaert *et al.* investigated the dCK activity dependency on ATM and ATR after different stress-inducing stimuli. VE-821 significantly reduced upregulation of dCK induced by various genotoxic agents. Importantly, after irradiation, dCK activity was dependent on ATR only in ATM-deficient cells [101]. However, it is necessary to note that the authors examined short time-intervals after irradiation (two hours), when ATM signalling is predominant. It is possible that after longer incubation with the inhibitor, VE-821 might inhibit dCK even in irradiated cells with a functional ATM pathway. Notably, the basal activity of dCK has been shown to be significantly downregulated by ATR silencing [101].

Taken together, it is obvious that several mechanisms could contribute to dNTP depletion upon IR in VE-821 treated cells. Further validation experiments would be necessary to reveal the exact mechanism.

Conclusion

In recent years, much effort has been focused on discovery and development of tumour specific treatment, which would specifically target only cancer cells and not affect the normal tissues, taking advantage of the tumour specific abnormalities in DDR. In the presented study, we aimed to describe molecular mechanisms underlying radiosensitization of the MOLT-4 cell line (T-ALL) via inhibition of ATR by a potent and specific small molecule inhibitor–VE-821. A brief overview of the most important findings is given in Fig 15.

We employed high-resolution MS to identify and quantify changes in the proteome, phosphoproteome, and metabolome of irradiated VE-821-treated cells. In response to the inhibitor treatment, we revealed changes not only in DDR related pathways and kinases, but also in pathways and kinases involved in maintaining cellular metabolism. Notably, we found downregulation of mTOR, the main regulator of cellular metabolism, which was also confirmed by antibody detection. Although there are multiple signalling pathways interconnecting IR-induced DDR and mTOR regulation that might be potentially affected by ATR inhibition, we assumed that in our case the downregulation was most likely caused by an off-target effect of VE-821 at 10 μM concentration. We further concluded that mTOR inhibition could be one of the factors contributing to the phenotype we observed after treating MOLT-4 cells with 10 μM VE-821, which was different from that observed after treatment with an mTOR non-inhibitory 2 μM concentration.

Targeted metabolomic analysis showed that VE-821 potentiated both IR-induced metabolic disruption and oxidative stress. Our data also indicate that in response to IR, recovery of dNTPs might be affected by VE-821, leading to dNTP deficiency possibly hampering DNA repair.

To our best knowledge, no study has yet been published investigating the modulation of cellular metabolism by a small molecular kinase inhibitor of any of the PIKK family kinases. Nevertheless, even using a highly specific inhibitor might lead to a complex response and similar MS-based phosphoproteomic and metabolomic studies are well-suited to reveal additional

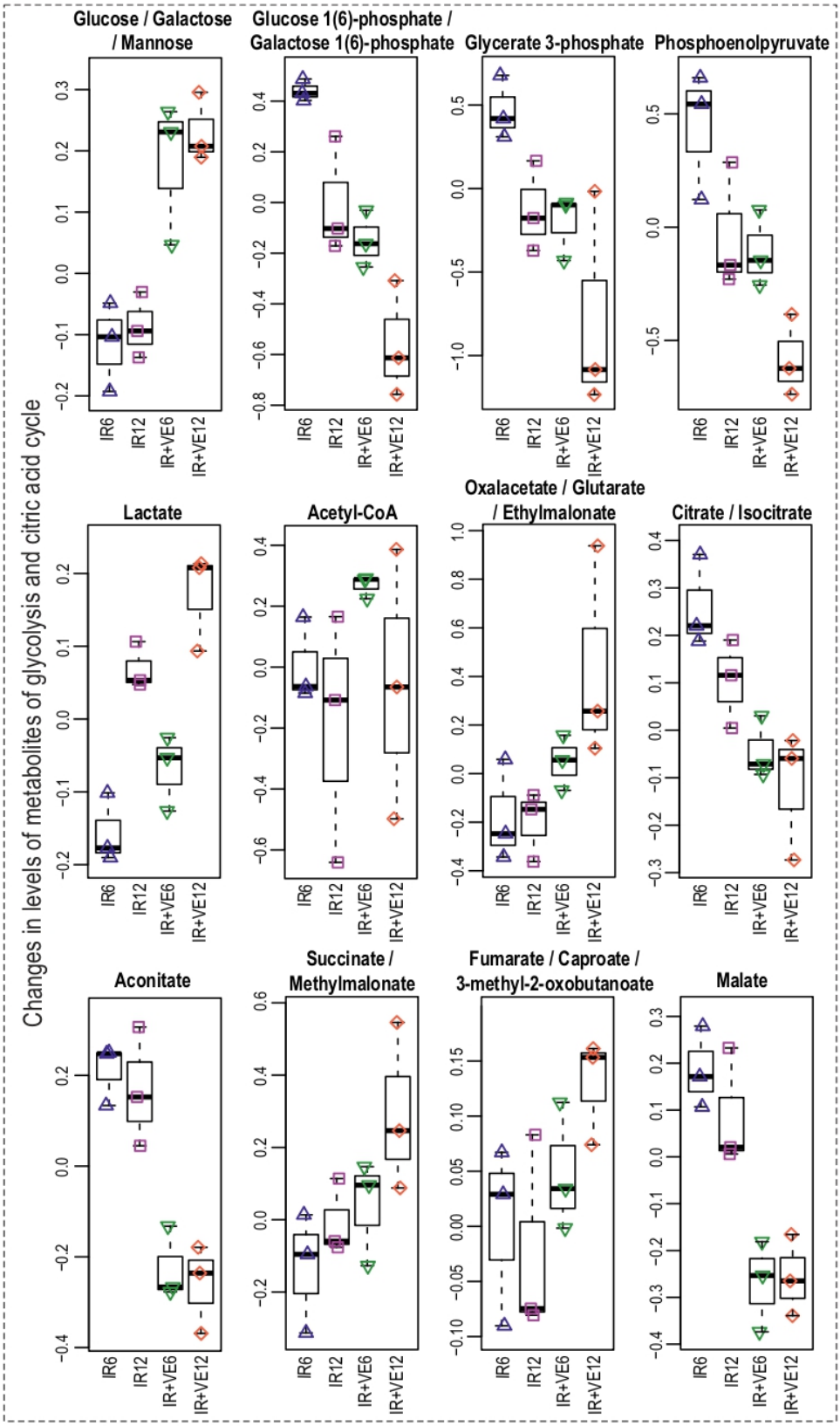
Changes in levels of metabolites of glycolysis and citric acid cycle
Glucose / Galactose / Mannose
Glucose 1(6)-phosphate / Galactose 1(6)-phosphate
Glycerate 3-phosphate
Phosphoenolpyruvate
Lactate
Acetyl-CoA
Oxalacetate / Glutarate / Ethylmalonate
Citrate / Isocitrate
Aconitate
Succinate / Methylmalonate
Fumarate / Caproate / 3-methyl-2-oxobutanoate
Malate
IR6
IR12
IR+VE6
IR+VE12

Fig 13. Boxplots of selected metabolites included in metabolism of glucose and citric acid cycle. IR–irradiated cells pre-treated with DMSO, IR+VE–irradiated cells pre-treated with 10 μM VE-821; both groups were analysed 6 and 12 hours after irradiation.

https://doi.org/10.1371/journal.pone.0199349.g013

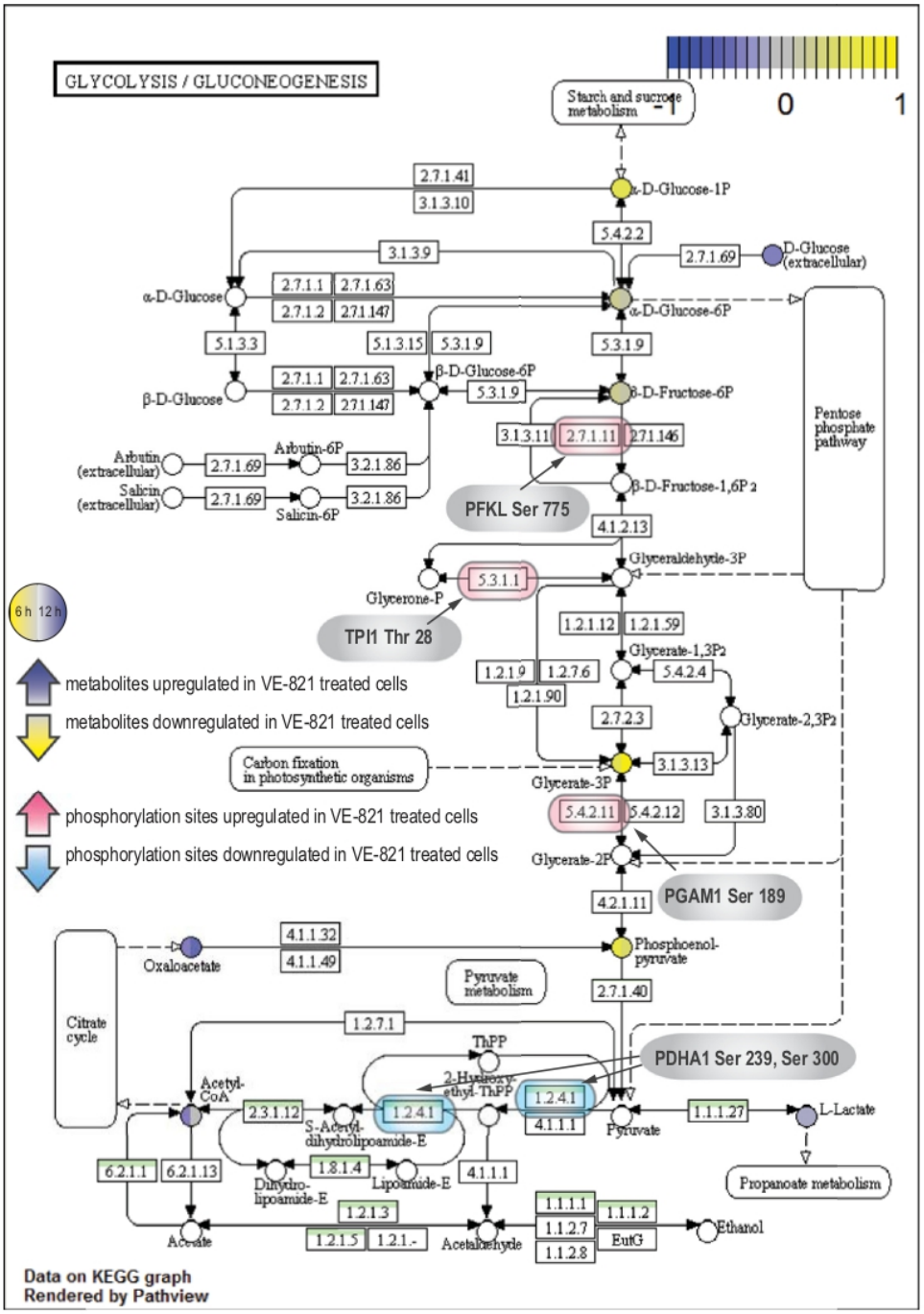

Fig 14. Metabolomic and phosphoproteomic changes detected in metabolism of glucose. Metabolite changes were visualized in KEGG pathway maps. Purple and yellow circles represent metabolites upregulated and downregulated, respectively, in response to VE-821 treatment. Left and right halves of the indicated metabolites show changes 6 and 12 hours after irradiation, respectively. Enzymes containing phosphorylation sites affected by VE-821 treatment are indicated by red and blue rounded rectangles.

https://doi.org/10.1371/journal.pone.0199349.g014

- **VE-821 radiosensitized MOLT-4 cells** (T-ALL).
- Two distinct dose-dependent phenotypes observed. **2 μM VE-821** treatment caused mostly radiosensitization and disruption of the G2/M arrest w/o affecting viability of sham-irradiated cells; **10 μM VE-821** treatment was characterized by marked proliferation inhibition and decreased viability of MOLT-4 cells in both single inhibitor treatment and its combination with IR.
- In phosphoproteomic analysis of VE-821 treated (10 μM) irradiated MOLT-4 cells, 9285 phosphorylation sites from 3090 protein groups were detected. By applying GRT, **623 differentially regulated phosphorylation sites** identified; most of them upregulated (431).
- Gene ontology terms over-representation analysis revealed proteins with regulated phosphorylation sites significantly over-represented in **nucleus**, specifically in **chromosomes**, **mitotic spindle**, and **replication fork**; involved in **chromatin organization**, **DNA repair** and **metabolism**, **cell cycle**, and **regulation of transcription factors**.
- Based on kinase activity inference, we detected a **decreased activity of ATR** (in concordance with immuno-blotting-based detection of ATR activity) providing crucial **validation of our data**.
- The activity of several mitotic kinases was probably modulated by VE-821 treatment (in concordance reported dominant role of ATR/Chk1 pathway in triggering the S- and G2/M phase checkpoints. Besides VE-821-induced **CDKs** upregulation, known/predicted substrates of **aurora A**, **aurora B**, and **NEK** kinases found with upregulated phosphorylation.
- The main regulator of cellular metabolism **mTOR** and its downstream effectors **P70S6K** and **CAD** were shown to be inhibited by VE-821 treatment, which might contribute to the phenotype observed in proliferation and viability and indicate possible VE-821-induced **protein and nucleotide synthesis inhibition**. Possible link to **autophagy modulation** was found.
- mTOR inhibition by 10 μM VE-821 occurred also in sham-irradiated cells, and 2 μM VE-821 did not induce any mTOR inhibition detectable by western-blotting, suggesting **mTOR inhibition most likely induced by an off-target of the inhibitor**. This finding is of the utmost importance as in several studies VE-821 has been used in 10 μM concentration, and possible contribution of mTOR inhibition to the observed phenotype has not been considered.
- In the **first metabolomic profile of cells treated with a PIKKs family kinase inhibitor - 206 intermediary metabolites** were detected (targeted metabolomics analysis). VE-821 potentiated the metabolic disruption induced by IR affecting the levels of **NDPs**, **NTPs**, **intermediates of glycolysis** and **citric acid cycle**, and **lactate**.
- IR induced oxidative stress might be increased upon the addition of VE-821 as demonstrated by changes in **GSH**, **allantoin** and **taurine**. Increased degradation of proteins and cellular membranes were also observed.
- VE-821 induced decrease in **dNDPs** and **dNTPs** levels. The **downregulation of salvage pathways** by ATR inhibition might be the main cause of the decrease of dNTPs necessary for DNA damaged repair.

Fig 15. Summary of the most important findings revealed in the presented study.

https://doi.org/10.1371/journal.pone.0199349.g015

information on off-target effects and provide insights into other, possibly non-reported, regulatory mechanisms.

Supporting information

S1 File. Supplemetary discussion. The most interesting substrates of kinases discussed in this paper are described.
(PDF)

S2 File. KEGG pathway maps visualization. Metabolite changes were visualized in KEGG pathway maps. Purple and yellow circles represent metabolites upregulated and downregulated, respectively, in response to VE-821 treatment. Left and right halves of the metabolites show changes 6 and 12 hours after irradiation, respectively.
(PDF)

S1 Table. Overview of phosphorylation sites identified in all three replicates.
(XLSX)

S2 Table. Overview of known kinase-substrate interactions and kinase prediction results.
(XLSX)

S3 Table. Overview of phosphorylations sites assigned to selected kinases or kinase groups.
(XLSX)

Acknowledgments

This work was supported by Ministry of Defence, Czech Republic (project: Long-term organization development plan 1011), by the Czech Science Foundation Grant 18-12204S. The infrastructural part (Institute of Molecular and Translational Medicine) was supported by NPU I (LO1304). The funders had no role in study design, data collection and analysis, decision to publish, or preparation of the manuscript. The authors are grateful to Ian McColl MD, PhD for assistance with the manuscript.

Author Contributions

Conceptualization: David Friedecký, Aleš Tichý.

Data curation: Barbora Šalovská.

Formal analysis: Barbora Šalovská, Hana Janečková, Radana Karlíková.

Investigation: Barbora Šalovská, Hana Janečková, Ivo Fabrik, Lucie Čecháková, Martin Ondrej.

Methodology: Barbora Šalovská, Hana Janečková, Ivo Fabrik, Marek Link, David Friedecký.

Supervision: David Friedecký, Aleš Tichý.

Validation: Barbora Šalovská, Hana Janečková, Aleš Tichý.

Visualization: Barbora Šalovská, Radana Karlíková.

Writing – original draft: Barbora Šalovská, Hana Janečková.

Writing – review & editing: Ivo Fabrik, Radana Karlíková, David Friedecký, Aleš Tichý.

References

1. O'Connor MJ. Targeting the DNA Damage Response in Cancer. Molecular Cell. 2015; 60: 547–560. https://doi.org/10.1016/j.molcel.2015.10.040 PMID: 26590714
2. Chen T, Stephens PA, Middleton FK, Curtin NJ. Targeting the S and G2 checkpoint to treat cancer. Drug Discovery Today. 2012; 17: 194–202. https://doi.org/10.1016/j.drudis.2011.12.009 PMID: 22192883
3. Kandoth C, McLellan MD, Vandin F, Ye K, Niu B, Lu C, et al. Mutational landscape and significance across 12 major cancer types. Nature. 2013; 502: 333–339. https://doi.org/10.1038/nature12634 PMID: 24132290
4. Toledo LI, Murga M, Fernandez-Capetillo O. Targeting ATR and Chk1 kinases for cancer treatment: a new model for new (and old) drugs. Mol Oncol. 2011; 5: 368–373. https://doi.org/10.1016/j.molonc.2011.07.002 PMID: 21820372
5. Macheret M, Halazonetis TD. DNA Replication Stress as a Hallmark of Cancer. Annual Review of Pathology: Mechanisms of Disease. 2015; 10: 425–448. https://doi.org/10.1146/annurev-pathol-012414-040424 PMID: 25621662
6. Ferrao PT, Bukczynska EP, Johnstone RW, McArthur GA. Efficacy of CHK inhibitors as single agents in MYC-driven lymphoma cells. Oncogene. 2012; 31: 1661–1672. https://doi.org/10.1038/onc.2011.358 PMID: 21841818

7. Gilad O, Nabet BY, Ragland RL, Schoppy DW, Smith KD, Durham AC, et al. Combining ATR suppression with oncogenic Ras synergistically increases genomic instability, causing synthetic lethality or tumorigenesis in a dosage-dependent manner. Cancer Res. 2010; 70: 9693–9702. https://doi.org/10.1158/0008-5472.CAN-10-2286 PMID: 21098704
8. Höglund A, Nilsson LM, Muralidharan SV, Hasvold LA, Merta P, Rudelius M, et al. Therapeutic Implications for the Induced Levels of Chk1 in Myc-Expressing Cancer Cells. Clin Cancer Res. 2011; 17: 7067–7079. https://doi.org/10.1158/1078-0432.CCR-11-1198 PMID: 21933891
9. Murga M, Campaner S, Lopez-Contreras AJ, Toledo LI, Soria R, Montaña MF, et al. Exploiting oncogene-induced replicative stress for the selective killing of Myc-driven tumors. Nat Struct Mol Biol. 2011; 18: 1331–1335. https://doi.org/10.1038/nsmb.2189 PMID: 22120667
10. Schoppy DW, Ragland RL, Gilad O, Shastri N, Peters AA, Murga M, et al. Oncogenic stress sensitizes murine cancers to hypomorphic suppression of ATR. J Clin Invest. 2012; 122: 241–252. https://doi.org/10.1172/JCI58928 PMID: 22133876
11. Toledo LI, Murga M, Zur R, Soria R, Rodriguez A, Martinez S, et al. A cell-based screen identifies ATR inhibitors with synthetic lethal properties for cancer-associated mutations. Nat Struct Mol Biol. 2011; 18: 721–727. https://doi.org/10.1038/nsmb.2076 PMID: 21552262
12. Fokas E, Prevo R, Pollard JR, Reaper PM, Charlton PA, Cornelissen B, et al. Targeting ATR in vivo using the novel inhibitor VE-822 results in selective sensitization of pancreatic tumors to radiation. Cell Death Dis. 2012; 3: e441. https://doi.org/10.1038/cddis.2012.181 PMID: 23222511
13. Fokas E, Prevo R, Hammond EM, Brunner TB, McKenna WG, Muschel RJ. Targeting ATR in DNA damage response and cancer therapeutics. Cancer Treat Rev. 2014; 40: 109–117. https://doi.org/10.1016/j.ctrv.2013.03.002 PMID: 23583268
14. Peasland A, Wang L-Z, Rowling E, Kyle S, Chen T, Hopkins A, et al. Identification and evaluation of a potent novel ATR inhibitor, NU6027, in breast and ovarian cancer cell lines. Br J Cancer. 2011; 105: 372–381. https://doi.org/10.1038/bjc.2011.243 PMID: 21730979
15. Reaper PM, Griffiths MR, Long JM, Charrier J, Maccormick S, Charlton PA, et al. Selective killing of ATM- or p53-deficient cancer cells through inhibition of ATR. Nature Chemical Biology. 2011; 7: 428–30. http://dx.doi.org.ezproxy.is.cuni.cz/10.1038/nchembio.573 https://doi.org/10.1038/nchembio.573 PMID: 21490603
16. Vendetti FP, Lau A, Schamus S, Conrads TP, O'Connor MJ, Bakkenist CJ. The orally active and bioavailable ATR kinase inhibitor AZD6738 potentiates the anti-tumor effects of cisplatin to resolve ATM-deficient non-small cell lung cancer in vivo. Oncotarget. 2015; https://doi.org/10.18632/oncotarget.6247 PMID: 26517239
17. Szkanderová S, Vávrová J, Rézacová M, Vokurková D, Pavlová S, Smardová J, et al. Gamma irradiation results in phosphorylation of p53 at serine-392 in human T-lymphocyte leukaemia cell line MOLT-4. Folia Biol (Praha). 2003; 49: 191–196.
18. Vávrová J, Rezácová M, Vokurková D, Psutka J. Cell cycle alteration, apoptosis and response of leukemic cell lines to gamma radiation with high- and low-dose rate. Physiol Res. 2004; 53: 335–342. PMID: 15209542
19. Szkanderová S, Vávrová J, Hernychová L, Neubauerová V, Lenco J, Stulík J. Proteome alterations in gamma-irradiated human T-lymphocyte leukemia cells. Radiat Res. 2005; 163: 307–315. PMID: 15733044
20. Záskodová D, Rezácová M, Vávrová J, Vokurková D, Tichy A. Effect of valproic acid, a histone deacetylase inhibitor, on cell death and molecular changes caused by low-dose irradiation. Ann N Y Acad Sci. 2006; 1091: 385–398. https://doi.org/10.1196/annals.1378.082 PMID: 17341630
21. Tichý A, Záskodová D, Rezácová M, Vávrová J, Vokurková D, Pejchal J, et al. Gamma-radiation-induced ATM-dependent signalling in human T-lymphocyte leukemic cells, MOLT-4. Acta Biochim Pol. 2007; 54: 281–287. PMID: 17565390
22. Rezácová M, Tichý A, Vávrová J, Vokurková D, Lukásová E. Is defect in phosphorylation of Nbs1 responsible for high radiosensitivity of T-lymphocyte leukemia cells MOLT-4? Leuk Res. 2008; 32: 1259–1267. https://doi.org/10.1016/j.leukres.2007.12.014 PMID: 18262646
23. Tichý A, Záskodová D, Pejchal J, Rezácová M, Osterreicher J, Vávrová J, et al. Gamma irradiation of human leukaemic cells HL-60 and MOLT-4 induces decrease in Mcl-1 and Bid, release of cytochrome c, and activation of caspase-8 and caspase-9. Int J Radiat Biol. 2008; 84: 523–530. https://doi.org/10.1080/09553000802078404 PMID: 18470751
24. Tichý A, Záskodová D, Zoelzer F, Vávrová J, Sinkorová Z, Pejchal J, et al. Gamma-radiation-induced phosphorylation of p53 on serine 15 is dose-dependent in MOLT-4 leukaemia cells. Folia Biol (Praha). 2009; 55: 41–44.
25. Tichý A, Muthná D, Vávrová J, Pejchal J, Šinkorová Z, Zárybnická L, et al. Caffeine-suppressed ATM pathway leads to decreased p53 phosphorylation and increased programmed cell death in gamma-

irradiated leukaemic molt-4 cells. Journal of Applied Biomedicine. 2011; 9: 49–56. https://doi.org/10.2478/v10136-009-0031-7

26. Tichý A, Novotná E, Durisová K, Salovská B, Sedlaríková R, Pejchal J, et al. Radio-sensitization of human leukaemic molt-4 cells by DNA-dependent protein kinase inhibitor, NU7026. Acta Medica (Hradec Kralove). 2012; 55: 66–73. https://doi.org/10.14712/18059694.2015.57 PMID: 23101268
27. Muthna D, Vavrova J, Lukasova E, Tichy A, Knizek J, Kohlerova R, et al. Valproic acid decreases the reparation capacity of irradiated MOLT-4 cells. Mol Biol (Mosk). 2012; 46: 122–128.
28. Tichy A, Durisova K, Salovska B, Pejchal J, Zarybnicka L, Vavrova J, et al. Radio-sensitization of human leukaemic MOLT-4 cells by DNA-dependent protein kinase inhibitor, NU7441. Radiat Environ Biophys. 2013; 53: 83–92. https://doi.org/10.1007/s00411-013-0494-5 PMID: 24100951
29. Shinohara K, Nakano H. Interphase death and reproductive death in X-irradiated MOLT-4 cells. Radiat Res. 1993; 135: 197–205. PMID: 8367590
30. Forbes SA, Beare D, Gunasekaran P, Leung K, Bindal N, Boutselakis H, et al. COSMIC: exploring the world's knowledge of somatic mutations in human cancer. Nucl Acids Res. 2015; 43: D805–D811. https://doi.org/10.1093/nar/gku1075 PMID: 25355519
31. Mendes RD, Canté-Barrett K, Pieters R, Meijerink JPP. The relevance of PTEN-AKT in relation to NOTCH1-directed treatment strategies in T-cell acute lymphoblastic leukemia. Haematologica. 2016; 101: 1010–1017. https://doi.org/10.3324/haematol.2016.146381 PMID: 27582570
32. Bendall SC, Hughes C, Stewart MH, Doble B, Bhatia M, Lajoie GA. Prevention of Amino Acid Conversion in SILAC Experiments with Embryonic Stem Cells. Mol Cell Proteomics. 2008; 7: 1587–1597. https://doi.org/10.1074/mcp.M800113-MCP200 PMID: 18487603
33. Ong S- E, Mann M. Identifying and quantifying sites of protein methylation by heavy methyl SILAC. Curr Protoc Protein Sci. 2006;Chapter 14: Unit 14.9. https://doi.org/10.1002/0471140864.ps1409s46 PMID: 18429299
34. Tichý A, Záškodová D, Pejchal J, ŘezáČová M, Österreicher J, Vávrová J, et al. Gamma irradiation of human leukaemic cells HL-60 and MOLT-4 induces decrease in Mcl-1 and Bid, release of cytochrome c, and activation of caspase-8 and caspase-9. Int J Radiat Biol. 2008; 84: 523–530. https://doi.org/10.1080/09553000802078404 PMID: 18470751
35. Tichý A, Záskodová D, Zoelzer F, Vávrová J, Sinkorová Z, Pejchal J, et al. Gamma-radiation-induced phosphorylation of p53 on serine 15 is dose-dependent in MOLT-4 leukaemia cells. Folia Biol (Praha). 2009; 55: 41–44.
36. Vávrová J, Rezácová M, Vokurková D, Psutka J. Cell cycle alteration, apoptosis and response of leukemic cell lines to gamma radiation with high- and low-dose rate. Physiol Res. 2004; 53: 335–342. PMID: 15209542
37. Ong S, Mann M. A practical recipe for stable isotope labeling by amino acids in cell culture (SILAC). Nature Protocols. 2006; 1: 2650–60. https://doi.org/10.1038/nprot.2006.427 PMID: 17406521
38. Rogers LD, Fang Y, Foster LJ. An integrated global strategy for cell lysis, fractionation, enrichment and mass spectrometric analysis of phosphorylated peptides. Mol BioSyst. 2010; 6: 822–829. https://doi.org/10.1039/b915986j PMID: 20567768
39. Yeung Y- G, Stanley ER. Rapid Detergent Removal From Peptide Samples With Ethyl Acetate For Mass Spectrometry Analysis. Curr Protoc Protein Sci. 2010;CHAPTER: Unit-16.12. https://doi.org/10.1002/0471140864.ps1612s59 PMID: 20155730
40. McNulty DE, Annan RS. Hydrophilic interaction chromatography reduces the complexity of the phosphoproteome and improves global phosphopeptide isolation and detection. Mol Cell Proteomics. 2008; 7: 971–980. https://doi.org/10.1074/mcp.M700543-MCP200 PMID: 18212344
41. Larsen MR, Thingholm TE, Jensen ON, Roepstorff P, Jørgensen TJD. Highly selective enrichment of phosphorylated peptides from peptide mixtures using titanium dioxide microcolumns. Mol Cell Proteomics. 2005; 4: 873–886. https://doi.org/10.1074/mcp.T500007-MCP200 PMID: 15858219
42. Salovska B, Tichy A, Fabrik I, Rezacova M, Vavrova J. Comparison of Resins for Metal Oxide Affinity Chromatography with Mass Spectrometry Detection for the Determination of Phosphopeptides. Analytical Letters. 2013; 46: 1505–1524. https://doi.org/10.1080/00032719.2013.773437
43. Salovská B, Fabrik I, Durišová K, Link M, Vávrová J, Rezáčová M, et al. Radiosensitization of Human Leukemic HL-60 Cells by ATR Kinase Inhibitor (VE-821): Phosphoproteomic Analysis. Int J Mol Sci. 2014; 15: 12007–12026. https://doi.org/10.3390/ijms150712007 PMID: 25003641
44. Fabrik I, Link M, Putzova D, Plzakova L, Lubovska Z, Philimonenko V, et al. The early dendritic cell signaling induced by virulent Francisella tularensis strain occurs in phases and involves the activation of ERKs and p38 in the later stage. Mol Cell Proteomics. 2017; mcp.RA117.000160. https://doi.org/10.1074/mcp.RA117.000160 PMID: 29046388

45. Vizcaíno JA, Csordas A, del-Toro N, Dianes JA, Griss J, Lavidas I, et al. 2016 update of the PRIDE database and its related tools. Nucleic Acids Res. 2016; 44: D447–456. https://doi.org/10.1093/nar/gkv1145 PMID: 26527722

46. Cox J, Mann M. MaxQuant enables high peptide identification rates, individualized p.p.b.-range mass accuracies and proteome-wide protein quantification. Nature Biotechnology. 2008; 26: 1367–1372. https://doi.org/10.1038/nbt.1511 PMID: 19029910

47. Cox J, Neuhauser N, Michalski A, Scheltema RA, Olsen JV, Mann M. Andromeda: a peptide search engine integrated into the MaxQuant environment. J Proteome Res. 2011; 10: 1794–1805. https://doi.org/10.1021/pr101065j PMID: 21254760

48. Zhou Y, Cras-Méneur C, Ohsugi M, Stormo GD, Permutt MA. A global approach to identify differentially expressed genes in cDNA (two-color) microarray experiments. Bioinformatics. 2007; 23: 2073–2079. https://doi.org/10.1093/bioinformatics/btm292 PMID: 17550914

49. Kamburov A, Wierling C, Lehrach H, Herwig R. ConsensusPathDB—a database for integrating human functional interaction networks. Nucl Acids Res. 2009; 37: D623–D628. https://doi.org/10.1093/nar/gkn698 PMID: 18940869

50. Kamburov A, Pentchev K, Galicka H, Wierling C, Lehrach H, Herwig R. ConsensusPathDB: toward a more complete picture of cell biology. Nucl Acids Res. 2011; 39: D712–D717. https://doi.org/10.1093/nar/gkq1156 PMID: 21071422

51. Kanehisa M, Sato Y, Kawashima M, Furumichi M, Tanabe M. KEGG as a reference resource for gene and protein annotation. Nucleic Acids Res. 2016; 44: D457–462. https://doi.org/10.1093/nar/gkv1070 PMID: 26476454

52. Kanehisa M, Goto S. KEGG: kyoto encyclopedia of genes and genomes. Nucleic Acids Res. 2000; 28: 27–30. PMID: 10592173

53. Croft D. Building models using Reactome pathways as templates. Methods Mol Biol. 2013; 1021: 273–283. https://doi.org/10.1007/978-1-62703-450-0_14 PMID: 23715990

54. Schaefer CF, Anthony K, Krupa S, Buchoff J, Day M, Hannay T, et al. PID: the Pathway Interaction Database. Nucleic Acids Res. 2009; 37: D674–679. https://doi.org/10.1093/nar/gkn653 PMID: 18832364

55. Klammer M, Godl K, Tebbe A, Schaab C. Identifying differentially regulated subnetworks from phosphoproteomic data. BMC Bioinformatics. 2010; 11: 351. https://doi.org/10.1186/1471-2105-11-351 PMID: 20584295

56. Shannon P, Markiel A, Ozier O, Baliga NS, Wang JT, Ramage D, et al. Cytoscape: A Software Environment for Integrated Models of Biomolecular Interaction Networks. Genome Res. 2003; 13: 2498–2504. https://doi.org/10.1101/gr.1239303 PMID: 14597658

57. Colaert N, Helsens K, Martens L, Vandekerckhove J, Gevaert K. Improved visualization of protein consensus sequences by iceLogo. Nat Methods. 2009; 6: 786–787. https://doi.org/10.1038/nmeth1109-786 PMID: 19876014

58. Chou MF, Schwartz D. Biological sequence motif discovery using motif-x. Curr Protoc Bioinformatics. 2011;Chapter 13: Unit 13.15–24. https://doi.org/10.1002/0471250953.bi1315s35 PMID: 21901740

59. Olsen JV, Blagoev B, Gnad F, Macek B, Kumar C, Mortensen P, et al. Global, In Vivo, and Site-Specific Phosphorylation Dynamics in Signaling Networks. Cell. 2006; 127: 635–648. https://doi.org/10.1016/j.cell.2006.09.026 PMID: 17081983

60. Hornbeck PV, Kornhauser JM, Tkachev S, Zhang B, Skrzypek E, Murray B, et al. PhosphoSitePlus: a comprehensive resource for investigating the structure and function of experimentally determined post-translational modifications in man and mouse. Nucleic Acids Res. 2012; 40: D261–D270. https://doi.org/10.1093/nar/gkr1122 PMID: 22135298

61. Horn H, Schoof EM, Kim J, Robin X, Miller ML, Diella F, et al. KinomeXplorer: an integrated platform for kinome biology studies. Nat Meth. 2014; 11: 603–604. https://doi.org/10.1038/nmeth.2968 PMID: 24874572

62. Song C, Ye M, Liu Z, Cheng H, Jiang X, Han G, et al. Systematic analysis of protein phosphorylation networks from phosphoproteomic data. Mol Cell Proteomics. 2012; mcp.M111.012625. https://doi.org/10.1074/mcp.M111.012625 PMID: 22798277

63. Franceschini A, Szklarczyk D, Frankild S, Kuhn M, Simonovic M, Roth A, et al. STRING v9.1: protein-protein interaction networks, with increased coverage and integration. Nucleic Acids Res. 2013; 41: D808–815. https://doi.org/10.1093/nar/gks1094 PMID: 23203871

64. Cox J, Mann M. 1D and 2D annotation enrichment: a statistical method integrating quantitative proteomics with complementary high-throughput data. BMC Bioinformatics. 2012; 13 Suppl 16: S12. https://doi.org/10.1186/1471-2105-13-S16-S12 PMID: 23176165

65. Sellick CA, Hansen R, Stephens GM, Goodacre R, Dickson AJ. Metabolite extraction from suspension-cultured mammalian cells for global metabolite profiling. Nat Protocols. 2011; 6: 1241–1249. https://doi.org/10.1038/nprot.2011.366 PMID: 21799492

66. Yuan M, Breitkopf SB, Yang X, Asara JM. A positive/negative ion–switching, targeted mass spectrometry–based metabolomics platform for bodily fluids, cells, and fresh and fixed tissue. Nature protocols. 7: 872. https://doi.org/10.1038/nprot.2012.024 PMID: 22498707

67. Karlíková R, Mičová K, Najdekr L, Gardlo A, Adam T, Majerová P, et al. Metabolic status of CSF distinguishes rats with tauopathy from controls. Alzheimers Res Ther. 2017; 9. https://doi.org/10.1186/s13195-017-0303-5 PMID: 28934963

68. Tichý A, Novotná E, Durisová K, Salovská B, Sedlaríková R, Pejchal J, et al. Radio-sensitization of human leukaemic molt-4 cells by DNA-dependent protein kinase inhibitor, NU7026. Acta Medica (Hradec Kralove). 2012; 55: 66–73.

69. Kozlov SV, Graham ME, Jakob B, Tobias F, Kijas AW, Tanuji M, et al. Autophosphorylation and ATM activation: additional sites add to the complexity. J Biol Chem. 2011; 286: 9107–9119. https://doi.org/10.1074/jbc.M110.204065 PMID: 21149446

70. Gabant G, Lorphelin A, Nozerand N, Marchetti C, Bellanger L, Dedieu A, et al. Autophosphorylated Residues Involved in the Regulation of Human Chk2 In Vitro. Journal of Molecular Biology. 2008; 380: 489–503. https://doi.org/10.1016/j.jmb.2008.04.053 PMID: 18538787

71. Guo X, Ward MD, Tiedebohl JB, Oden YM, Nyalwidhe JO, Semmes OJ. Interdependent Phosphorylation within the Kinase Domain T-loop Regulates CHK2 Activity. J Biol Chem. 2010; 285: 33348–33357. https://doi.org/10.1074/jbc.M110.149609 PMID: 20713355

72. Mareková M, Vávrová J, Vokurková D. Monitoring of premitotic and postmitotic apoptosis in gamma-irradiated HL-60 cells by the mitochondrial membrane protein-specific monoclonal antibody APO2.7. Gen Physiol Biophys. 2003; 22: 191–200. PMID: 14661731

73. Vávrová J, Zárybnická L, Lukášová E, Řezáčová M, Novotná E, Sinkorová Z, et al. Inhibition of ATR kinase with the selective inhibitor VE-821 results in radiosensitization of cells of promyelocytic leukaemia (HL-60). Radiat Environ Biophys. 2013; 52: 471–479. https://doi.org/10.1007/s00411-013-0486-5 PMID: 23934411

74. Wu J, Feng Y, Xie D, Li X, Xiao W, Tao D, et al. Unscheduled CDK1 activity in G1 phase of the cell cycle triggers apoptosis in X-irradiated lymphocytic leukemia cells. Cell Mol Life Sci. 2006; 63: 2538–2545. https://doi.org/10.1007/s00018-006-6138-z PMID: 17013563

75. Shimobayashi M, Hall MN. Making new contacts: the mTOR network in metabolism and signalling crosstalk. Nat Rev Mol Cell Biol. 2014; 15: 155–162. https://doi.org/10.1038/nrm3757 PMID: 24556838

76. Ondrej M, Cechakova L, Durisova K, Pejchal J, Tichy A. To live or let die: Unclear task of autophagy in the radiosensitization battle. Radiotherapy and Oncology. 2016; https://doi.org/10.1016/j.radonc.2016.02.028 PMID: 26993419

77. Fingar DC, Blenis J. Target of rapamycin (TOR): an integrator of nutrient and growth factor signals and coordinator of cell growth and cell cycle progression. Oncogene. 2004; 23: 3151–3171. https://doi.org/10.1038/sj.onc.1207542 PMID: 15094765

78. Dillon LM, Miller TW. Therapeutic targeting of cancers with loss of PTEN function. Current drug targets. 2014; 15: 65. PMID: 24387334

79. Meric-Bernstam F, Akcakanat A, Chen H, Do K-A, Sangai T, Adkins F, et al. PIK3CA/PTEN Mutations and Akt Activation As Markers of Sensitivity to Allosteric mTOR Inhibitors. Clin Cancer Res. 2012; 18: 1777–1789. https://doi.org/10.1158/1078-0432.CCR-11-2123 PMID: 22422409

80. Fingar DC, Richardson CJ, Tee AR, Cheatham L, Tsou C, Blenis J. mTOR Controls Cell Cycle Progression through Its Cell Growth Effectors S6K1 and 4E-BP1/Eukaryotic Translation Initiation Factor 4E. Molecular and Cellular Biology. 2004; 24: 200. https://doi.org/10.1128/MCB.24.1.200-216.2004 PMID: 14673156

81. Holz MK, Ballif BA, Gygi SP, Blenis J. mTOR and S6K1 Mediate Assembly of the Translation Preinitiation Complex through Dynamic Protein Interchange and Ordered Phosphorylation Events. Cell. 2005; 123: 569–580. https://doi.org/10.1016/j.cell.2005.10.024 PMID: 16286006

82. Roux PP, Shahbazian D, Vu H, Holz MK, Cohen MS, Taunton J, et al. RAS/ERK Signaling Promotes Site-specific Ribosomal Protein S6 Phosphorylation via RSK and Stimulates Cap-dependent Translation. J Biol Chem. 2007; 282: 14056–14064. https://doi.org/10.1074/jbc.M700906200 PMID: 17360704

83. Ben-Sahra I, Howell JJ, Asara JM, Manning BD. Stimulation of de Novo Pyrimidine Synthesis by Growth Signaling Through mTOR and S6K1. Science. 2013; 339: 1323–1328. https://doi.org/10.1126/science.1228792 PMID: 23429703

84. Blethrow JD, Glavy JS, Morgan DO, Shokat KM. Covalent capture of kinase-specific phosphopeptides reveals Cdk1-cyclin B substrates. Proc Natl Acad Sci U S A. 2008; 105: 1442–1447. https://doi.org/10.1073/pnas.0708966105 PMID: 18234856

85. Chi Y, Welcker M, Hizli AA, Posakony JJ, Aebersold R, Clurman BE. Identification of CDK2 substrates in human cell lysates. Genome Biol. 2008; 9: R149. https://doi.org/10.1186/gb-2008-9-10-r149 PMID: 18847512

86. Kwon Y-K, Ha IJ, Bae H-W, Jang WG, Yun HJ, Kim SR, et al. Dose-Dependent Metabolic Alterations in Human Cells Exposed to Gamma Irradiation. PLoS One. 2014; 9. https://doi.org/10.1371/journal.pone.0113573 PMID: 25419661

87. Patterson AD, Li H, Eichler GS, Krausz KW, Weinstein JN, Fornace AJ, et al. UPLC-ESI-TOFMS-Based Metabolomics and Gene Expression Dynamics Inspector Self-Organizing Metabolomic Maps as Tools for Understanding the Cellular Response to Ionizing Radiation. Anal Chem. 2008; 80: 665–674. https://doi.org/10.1021/ac701807v PMID: 18173289

88. Tsuyama N, Mizuno H, Katafuchi A, Abe Y, Kurosu Y, Yoshida M, et al. Identification of low-dose responsive metabolites in X-irradiated human B lymphoblastoid cells and fibroblasts. J Radiat Res. 2015; 56: 46–58. https://doi.org/10.1093/jrr/rru078 PMID: 25227127

89. Azzam EI, Jay-Gerin J-P, Pain D. Ionizing radiation-induced metabolic oxidative stress and prolonged cell injury. Cancer Lett. 2012; 327: 48–60. https://doi.org/10.1016/j.canlet.2011.12.012 PMID: 22182453

90. Lee R, Britz-McKibbin P. Differential rates of glutathione oxidation for assessment of cellular redox status and antioxidant capacity by capillary electrophoresis-mass spectrometry: an elusive biomarker of oxidative stress. Anal Chem. 2009; 81: 7047–7056. https://doi.org/10.1021/ac901174g PMID: 19610656

91. Yardim-Akaydin S, Sepici A, Özkan Y, Torun M, Şimşek B, Sepici V. Oxidation of Uric Acid in Rheumatoid Arthritis: Is Allantoin a Marker of Oxidative Stress? Free Radical Research. 2004; 38: 623–628. https://doi.org/10.1080/10715760410001694044 PMID: 15346653

92. Paglin S, Lee N-Y, Nakar C, Fitzgerald M, Plotkin J, Deuel B, et al. Rapamycin-Sensitive Pathway Regulates Mitochondrial Membrane Potential, Autophagy, and Survival in Irradiated MCF-7 Cells. Cancer Res. 2005; 65: 11061–11070. https://doi.org/10.1158/0008-5472.CAN-05-1083 PMID: 16322256

93. Park JM, Tougeron D, Huang S, Okamoto K, Sinicrope FA. Beclin 1 and UVRAG confer protection from radiation-induced DNA damage and maintain centrosome stability in colorectal cancer cells. PLoS ONE. 2014; 9: e100819. https://doi.org/10.1371/journal.pone.0100819 PMID: 24956373

94. Cheema AK, Pathak R, Zandkarimi F, Kaur P, Alkhalil L, Singh R, et al. Liver Metabolomics Reveals Increased Oxidative Stress and Fibrogenic Potential in Gfrp Transgenic Mice in Response to Ionizing Radiation. J Proteome Res. 2014; 13: 3065–3074. https://doi.org/10.1021/pr500278t PMID: 24824572

95. Dokmeci D, Akpolat M, Aydogdu N, Uzal C, Doganay L, Turan FN. The Protective Effect of L-carnitine on Ionizing Radiation-induced Free Oxygen Radicals. Scandinavian Journal of Laboratory Animal Sciences. 2006; 33: 75–83.

96. Najdekr L, Gardlo A, Mádrová L, Friedecký D, Janečková H, Correa ES, et al. Oxidized phosphatidylcholines suggest oxidative stress in patients with medium-chain acyl-CoA dehydrogenase deficiency. Talanta. 2015; 139: 62–66. https://doi.org/10.1016/j.talanta.2015.02.041 PMID: 25882409

97. Goodwin PM, Lewis PJ, Davies MI, Skidmore CJ, Shall S. The effect of gamma radiation and neocarzinostatin on NAD and ATP levels in mouse leukaemia cells. Biochim Biophys Acta. 1978; 543: 576–582. PMID: 214144

98. Khan AR, Rana P, Devi MM, Chaturvedi S, Javed S, Tripathi RP, et al. Nuclear magnetic resonance spectroscopy-based metabonomic investigation of biochemical effects in serum of γ-irradiated mice. Int J Radiat Biol. 2011; 87: 91–97. https://doi.org/10.3109/09553002.2010.518211 PMID: 21087167

99. Yugi K, Kubota H, Toyoshima Y, Noguchi R, Kawata K, Komori Y, et al. Reconstruction of Insulin Signal Flow from Phosphoproteome and Metabolome Data. Cell Reports. 2014; 8: 1171–1183. https://doi.org/10.1016/j.celrep.2014.07.021 PMID: 25131207

100. Mathews CK. Deoxyribonucleotide metabolism, mutagenesis and cancer. Nat Rev Cancer. 2015; 15: 528–539. https://doi.org/10.1038/nrc3981 PMID: 26299592

101. Beyaert M, Starczewska E, Van Den Neste E, Bontemps F. A crucial role for ATR in the regulation of deoxycytidine kinase activity. Biochem Pharmacol. 2016; 100: 40–50. https://doi.org/10.1016/j.bcp.2015.11.022 PMID: 26620371

102. Arnér ES, Eriksson S. Mammalian deoxyribonucleoside kinases. Pharmacol Ther. 1995; 67: 155–186. PMID: 7494863

103. Staub M, Eriksson S. The Role of Deoxycytidine Kinase in DNA Synthesis and Nucleoside Analog Activation. In: Peters GJ, editor. Deoxynucleoside Analogs In Cancer Therapy. Humana Press; 2006. pp. 29–52. https://doi.org/10.1007/978-1-59745-148-2_2

Publication no. 5

Fractionation of enriched phosphopeptides using pH/acetonitrile-gradient-reversed-phase microcolumn separation in combination with LC–MS/MS analysis.

Ondrej M, Rehulka P, Rehulkova H, Kupcik R, Tichy A

International Journal of Molecular Sciences. 2020;21(11):3971

IF(2019) = 4.183; Q2

Author contribution (70%)—main author; the author participated in the drafting of the manuscript, its revision, and editing as well as submitting. The author took the lead in most of the experimental steps, such as cell cultivation and treatment, enrichment for phosphopeptides, purification and fractionation, and data analysis.

The main idea of this study was to develop a method for simple fractionation of phosphopeptides after their enrichment to enhance the quantification of identified phosphopeptides while simplifying the whole fractionation process. The authors presented an effective microgradient chromatographic technique that used an optimized pH/acetonitrile-gradient-RP elution mobile phase to separate the phosphopeptide sample into fractions. Using this technique, the authors obtained optimally distributed phosphopeptide fractions with just moderate input material requirements and more than 3-fold enhanced protein identification compared to a conventional approach.

International Journal of
Molecular Sciences

MDPI

Article

Fractionation of Enriched Phosphopeptides Using pH/Acetonitrile-Gradient-Reversed-Phase Microcolumn Separation in Combination with LC–MS/MS Analysis

Martin Ondrej [1], Pavel Rehulka [2], Helena Rehulkova [1], Rudolf Kupcik [3] and Ales Tichy [1,*]

1 Department of Radiobiology, Faculty of Military Health Sciences, University of Defense in Brno, 500 01 Hradec Kralove, Czech Republic; martin.ondrej@unob.cz (M.O.); helena.rehulkova@unob.cz (H.R.)
2 Department of Molecular Biology and Pathology, Faculty of Military Health Sciences, University of Defense in Brno, 500 01 Hradec Kralove, Czech Republic; pavel.rehulka@unob.cz
3 Department of Biological and Biochemical Sciences, Faculty of Chemical Technology, University of Pardubice, 532 10 Pardubice, Czech Republic; rudolf.kupcik@upce.cz
* Correspondence: ales.tichy@unob.cz; Tel.: +420-973-253-216

Received: 15 April 2020; Accepted: 28 May 2020; Published: 1 June 2020

Abstract: Mass spectrometry (MS) is a powerful and sensitive method often used for the identification of phosphoproteins. However, in phosphoproteomics, there is an identified need to compensate for the low abundance, insufficient ionization, and suppression effects of non-phosphorylated peptides. These may hamper the subsequent liquid chromatography–mass spectrometry/mass spectrometry (LC–MS/MS) analysis, resulting in incomplete phosphoproteome characterization, even when using high-resolution instruments. To overcome these drawbacks, we present here an effective microgradient chromatographic technique that yields specific fractions of enriched phosphopeptides compatible with LC–MS/MS analysis. The purpose of our study was to increase the number of identified phosphopeptides, and thus, the coverage of the sample phosphoproteome using the reproducible and straightforward fractionation method. This protocol includes a phosphopeptide enrichment step followed by the optimized microgradient fractionation of enriched phosphopeptides and final LC–MS/MS analysis of the obtained fractions. The simple fractionation system consists of a gas-tight microsyringe delivering the optimized gradient mobile phase to reversed-phase microcolumn. Our data indicate that combining the phosphopeptide enrichment with the microgradient separation is a promising technique for in-depth phosphoproteomic analysis due to moderate input material requirements and more than 3-fold enhanced protein identification.

Keywords: phosphopeptides; fractionation; acetonitrile; gradient; enrichment; mass spectrometry; titanium dioxide

1. Introduction

Reversible protein phosphorylation, one of the crucial post-translational modifications, alters the structural conformation of proteins, affecting their role in cell signaling networks. Overall, phosphorylation controls the protein functions and their subcellular localization and targeting, as well as signal transduction and protein degradation [1,2]. Although phosphorylation is the most frequent post-translational modification of proteins, the number of phosphoproteins to the whole proteome is still relatively low [3].

Phosphoproteomics is a branch of proteomics that identifies, characterizes, and quantifies proteins possessing phosphate groups in their structure. It often uses liquid chromatography–mass

spectrometry/mass spectrometry (LC–MS/MS) as a sensitive and specific detection method that is robust both for identification and quantification of phosphoproteins, including localization of present phosphorylation in their primary structure [4,5]. The main advantage of the MS-based phosphoproteomics is the ability to analyze a large number of proteins at once. The use of a high-resolution LC–MS/MS method for this purpose has been particularly advantageous in this regard. However, due to the relatively low stoichiometry of phosphoproteins in the whole proteome, specific methods leading to the enrichment for phosphopeptides in the bottom-up phosphoproteomics are necessary for a successful analysis.

Several studies describing various approaches of phosphoproteins or phosphopeptides enrichment have been published so far [6–8]. These approaches include immunoprecipitation, immobilized metal affinity chromatography (IMAC), metal oxide affinity chromatography (MOAC) using titanium dioxide (TiO_2) or zirconium dioxide (ZrO_2), sequential elution from IMAC (SIMAC), and more [7].

Enrichment for phosphopeptides using MOAC based on TiO_2 is probably the most widely regarded approach because of the outstanding enrichment performance and the simple manipulation of the TiO_2 resins [9]. In 2004, Pinkse et al. introduced a promising and now prevalent strategy for the selective phosphopeptide enrichment with the microspherical TiO_2 particles (Titansphere®) prior to LC–MS/MS analysis [10]. They loaded a peptide sample onto a column filled with TiO_2 microspheres in 0.25 M acetic acid (pH 2.9). After that, they washed away unbound, non-phosphorylated peptides, and subsequently eluted the phosphopeptides from the column using an alkaline buffer (pH 9) [10].

Although other successful phosphopeptide enrichment procedures provide an improved phosphopeptide identification [11], simple detection of phosphopeptides is not sufficient for an in-depth phosphoproteomic analysis. In this regard, appropriate improvements in the relative quantification of phosphopeptides come to the forefront. There are many studies that review possible approaches in the relative quantification of peptides in phospho/proteomic analysis [12–14]. The common enhancing strategy of all label-based quantification methods is phospho/peptide fractionation prior to LC–MS/MS analysis. In general, fractionation significantly increases the proteome coverage due to the higher number of peptides identified and quantified by LC–MS/MS. In fact, there are several fractionation methods used in phospho/proteomics [15–17]. One of the most employed is high-pH-reversed-phase (high-pH-RP) fractionation. High-pH-RP fractionation is preferred due to its robustness and high resolution of quantified peptides [18]. However, in the conventional setting of the high-pH-RP fractionation, many phosphopeptides do not efficiently bind to the RP under the high pH conditions; they remain in the flow-through fraction, and attention has to be paid not to lose them during the analysis.

In our study, we modified the high-pH-RP fractionation setup for simple microgradient separation apparatus based on C18 microcolumns used in our laboratory. For this purpose, we have adopted the microgradient elution system previously used in capillary electrochromatography [19], RP separation of peptides [20], glycopeptides [21–23], permethylated glycans [24] and in on-line connection with nano-electrospray ionization-mass spectrometry (nanoESI-MS) for analysis of peptide mixtures [25]. We optimized this microgradient elution system for the fractionation of phosphopeptides. For the phosphopeptide enrichment, we used the 5 µm TiO_2 microspheres (Titansphere®), although other enrichment strategies for phosphopeptides could also be applied here. Figure 1 depicts a diagram of our workflow. Compared to the conventional high-pH-RP fractionation, where peptides are usually eluted with the acetonitrile (ACN)-gradient mobile phase under high pH, we used a gradient of both pH and ACN in the mobile phase during the phosphopeptide elution from RP microcolumn. Thus, the goal of our study was to optimize the conditions for simple microgradient separation to increase the number of identified phosphopeptides when compared to a purified sample only. Applying our optimized protocol, we obtained significantly enhanced coverage of identified phosphopeptides (approximately 3-fold increase) compared to the non-fractionated sample. Besides, our in-house fractionation technique is fully repeatable, easy to use, and low-cost in comparison with other fractionation methods requiring expensive instrumentation.

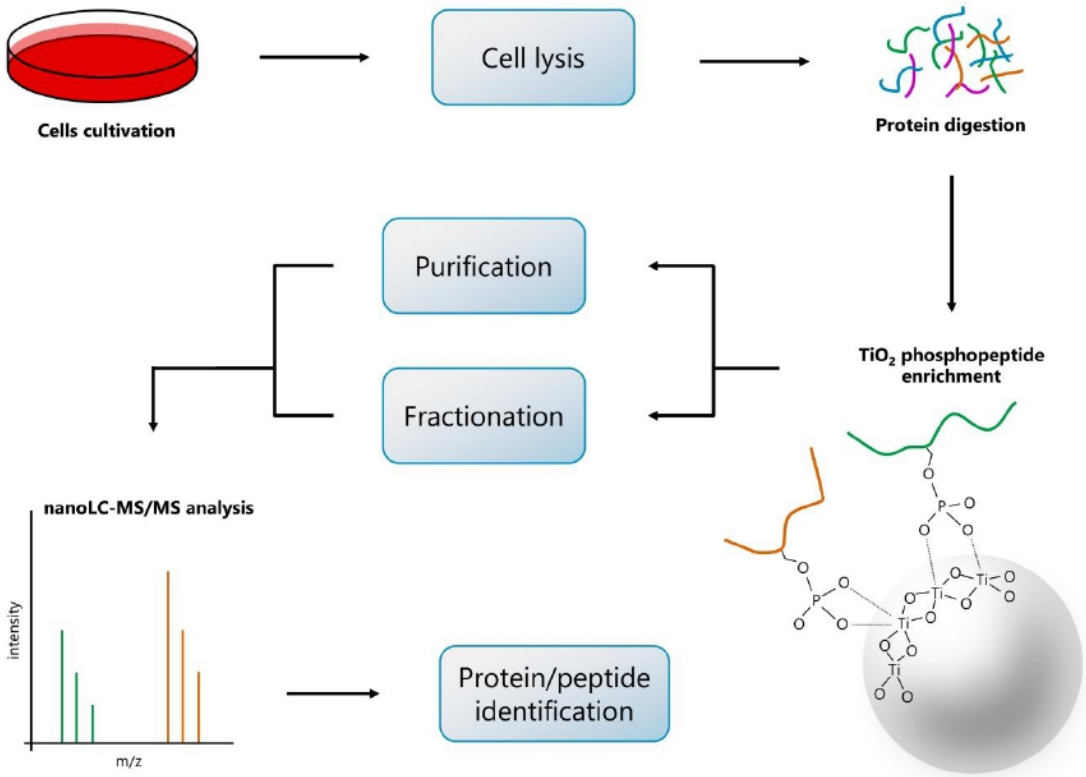

Figure 1. The workflow of sample processing. All samples were processed in the same way except for the step following after the TiO_2 enrichment, where two types of samples were prepared: 1. TiO_2-enriched phosphopeptides further purified on C18 reversed-phase (RP) microcolumn (single fraction); 2. TiO_2-enriched phosphopeptides further fractionated on C18 RP microcolumn using manually formed pH/acetonitrile microgradient (17 fractions).

2. Results

2.1. Conventional High-pH-RP Fractionation Was Not Suitable for Phosphopeptides

Phosphopeptide fractionation in quantitative phosphoproteomics provides better coverage of identified and quantified phosphopeptides. In this respect, we have developed a simple in-house technique enabling easy fractionation of enriched phosphopeptides. This technique is based on a microcolumn filled with RP C18 microparticles tightly attached to the gas-tight microsyringe. For comprehension and a full description of our in-house made microcolumn apparatus, see the description in Figure S1.

The high-pH-RP fractionation is a standard fractionation method for peptides in proteomics [26,27]. Considering that our original idea was to apply the microcolumn apparatus to fractionate TiO_2-enriched phosphopeptides according to the high-pH-RP fractionation protocol, similarly to how it is commonly performed for standard complex peptide mixtures, we used the conventional high-pH-RP mobile phase with the gradient concentration of ACN ranging from 2% to 40% to elute the phosphopeptides in 17 fractions. For the complete composition of the conventional high-pH-RP mobile phase, see Table 1.

HPLC analysis with UV detection of all 17 fractions showed that many peptides eluted in the first fraction (flow-through). LC–MS/MS analysis identified 1580 phosphopeptides and 363 non-phosphorylated peptides in the first fraction, whereas only 85 phosphopeptides from this fraction could also be detected in all of the following fractions (Figure S2). In this case, we concluded that using the high-pH-RP fractionation protocol for enriched phosphopeptides is not suitable due to the basic pH character of the mobile phase leading to elution of a significant portion of phosphopeptides within one fraction (Figure 2).

Table 1. Comparison of the composition of the conventional high-pH-RP and our optimized pH/acetonitrile (ACN)-gradient-RP elution mobile phases.

		1	2	3	4	5	6
Conventional elution mobile phase	ACN	400	320	240	160	80	20
	200 mM $HCOONH_4$	100	100	100	100	100	100
	H_2O	500	580	660	740	820	880
	ACN concentration	*40%*	*32%*	*24%*	*16%*	*8%*	*2%*
	Measured pH	*10.0*	*10.0*	*10.0*	*10.0*	*10.0*	*10.0*
Optimized elution mobile phase	1% acetic acid	100	100	100	100	100	100
	80% ACN/ 200 mM NH_4OH	300	250	200	150	100	50
	H_2O	600	650	700	750	800	850
	ACN concentration	*24%*	*20%*	*16%*	*12%*	*8%*	*4%*
	Measured pH	*6.57*	*5.64*	*5.19*	*4.80*	*4.42*	*3.92*

Conventional high-pH-RP elution mobile phase involved gradient of ACN (2–40%). Optimized pH/ACN-gradient-RP elution mobile phase involved a gradient of both pH (3.92–6.57) and ACN (4–24%). The volume of each component of mobile phases is given in microliters.

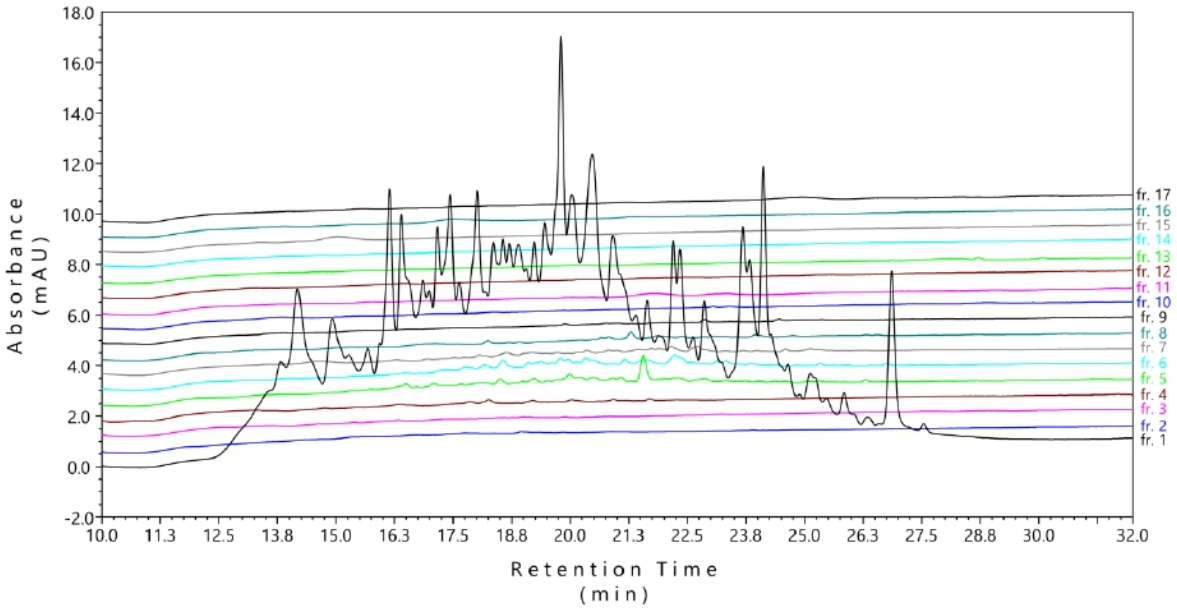

Figure 2. LC–UV chromatograms of the fractionated TiO_2-enriched phosphopeptide sample obtained from trypsin-digested H1299 cell lysate. The fractionation was performed using the conventional reversed-phase microgradient separation with the acetonitrile (ACN) gradient under basic pH conditions. The first fraction was the flow-through of the TiO_2-enriched phosphopeptides dissolved in loading buffer of 2% ACN/20 mM ammonium formate (pH 10), and fractions 2–17 were eluted from the microcolumn using the manually formed ACN gradient containing 20 mM ammonium formate buffered at pH 10 (see Table 1 for a detailed composition of the mobile phase used for phosphopeptide fractionation in conventional elution scheme).

2.2. pH/ACN-Gradient-RP Procedure Provided Improved Phosphopeptide Fractionation

Considering that the high pH causes elution of a significant portion of phosphopeptides into one fraction, we made subtle modifications to our former protocol and used the pH/ACN-gradient-RP fractionation. The conventional high-pH-RP fractionation utilizes fixed pH conditions with the gradient of ACN that is usually applicable for peptide fractionation. On the contrary, our pH/ACN-gradient-RP fractionation technique employed a simultaneous gradient of both pH (3.9–6.6) and ACN (4–24%). We specifically optimized it for the fractionation of phosphopeptides obtained from TiO_2 enrichment.

Table 1 compares the composition of the conventional high-pH-RP and our pH/ACN-gradient-RP elution mobile phases.

As previously, at first, we analyzed the purified sample and all 17 fractions by HPLC. The purified phosphopeptide sample provided a typical LC–UV chromatogram (Figure 3A). Chromatograms of the fractions from the fractionated sample indicated successful fractionation of the TiO_2-enriched phosphopeptides (Figure 3B). We observed that fractions 6 to 16 were evenly distributed and contained approximately the same absorbance peaks referring to a roughly similar amount of peptide material included in each fraction. Fraction 17 yielded a high-intensity chromatogram, indicating the elution of the rest of the peptide material towards the end of the chromatographic fraction (Figure 3B). For the detailed comparison of the absorbance peaks of individual fractions among replicates, see chromatograms in Figure S3.

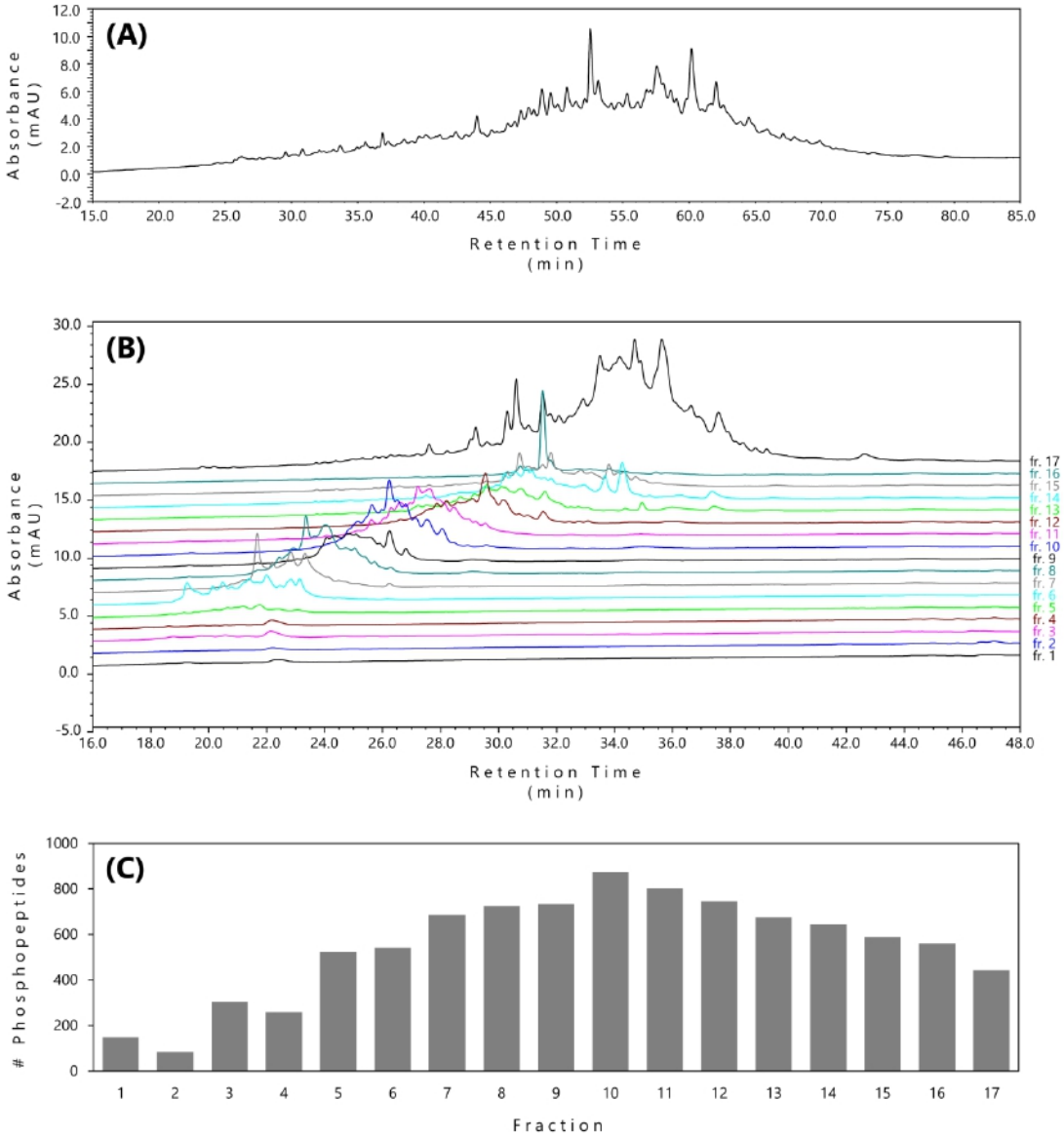

Figure 3. Comparison of the LC–UV chromatograms of purified (**A**) or fractionated (**B**) TiO_2-enriched phosphopeptide sample obtained from trypsin-digested H1299 cell lysate. The fractionation scheme of the microgradient elution was optimized for a more uniform distribution of peptides throughout the elution fractions (see Table 1 for the detailed composition of the mobile phases used for phosphopeptide fractionation in the optimized elution scheme). Phosphopeptides identified using LC–MS/MS in each fraction were visualized as a histogram (**C**).

Regarding the fractionated sample, fraction 17 appeared to contain a considerably higher amount of peptide material than the rest of the fractions, questioning the elution of the last fraction in a larger volume. However, the overall number of phosphopeptides eluted in each replicate followed the normal distribution within each fraction with a decreasing tendency at the end of the fractionation (Figure 3C).

2.3. LC–MS/MS Analysis Confirmed a Significant Improvement in Phosphopeptide Fractionation

We performed the LC–MS/MS analysis with the proteomic identification: (i) to compare the exact numbers of phosphopeptides identified after purification and fractionation and (ii) to verify the applicability of phosphopeptide fractionation for phosphoproteomics. We analyzed both samples in three biological replicates.

For the purified sample, we identified 4554, 4130, and 3873 peptides (including non-phosphorylated ones) in replicate one, two, and three, respectively, with the coefficient of variation (CV) of 8.22%. For the fractionated sample, we identified 10,128, 12,647, and 10,653 peptides in replicate one, two, and three, respectively, with the CV of 11.93% (Figure 4A–C). These values correspond to 2.22-fold, 3.06-fold, and 2.75-fold increase in peptide identification in the first, second, and third replicate, respectively. Regarding the common peptides shared in both purified and fractionated samples, we identified 3405, 3375, and 3069 peptides in replicate one, two, and three, respectively (Figure 4A–C).

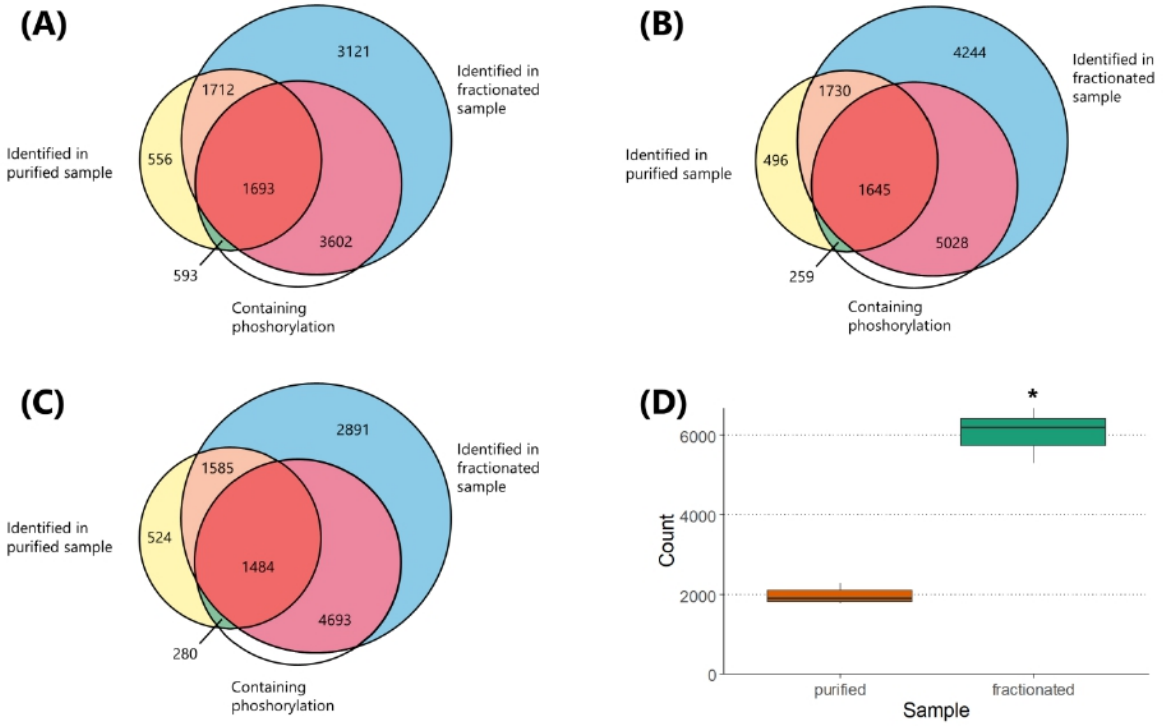

Figure 4. Overview of the peptides identified by the LC–MS/MS analysis. Data from experiments performed within three biological replicates from the H1299 cell line are shown. Venn diagrams of all peptides identified in the first (**A**), second (**B**), and third (**C**) replicate of the purified and fractionated sample with the included number of phosphorylated and non-phosphorylated peptides, respectively. Statistical comparison between phosphopeptides identified in the purified sample and the fractionated sample is visualized as a boxplot of all three replicates (**D**). * Significant difference compared to purified sample (p-value ≤ 0.005).

In parallel, for the purified sample, we identified 2286, 1904, and 1764 phosphopeptides in replicate one, two, and three, respectively, with the CV of 13.61%. For the fractionated sample, we identified 5295, 6673, and 6177 phosphopeptides in replicate one, two, and three, respectively, with the CV of 11.54%. These values correspond to 2.32-fold, 3.50-fold, and 3.50-fold increase in phosphopeptide identification

in the first, second, and third replicate, respectively. Regarding the common phosphopeptides shared in both purified and fractionated samples, we identified 1693, 1645, and 1484 peptides in replicate one, two, and three, respectively (Figure 4A–C). In summary, LC–MS/MS analysis confirmed the significant increase in the peptide (more than 2.5-fold) and phosphopeptide identification (more than 3-fold) in the fractionated sample compared to the purified one (Figure 4D). For summary statistics, see Table S1.

3. Discussion

Phosphoprotein enrichment methods are essential for state-of-the-art phosphoproteomic analysis. MOAC is a powerful enrichment method allowing selective ion exchange between the phosphate group and a metal oxide matrix [28]. Although other enrichment approaches in an optimized setup were successfully introduced for phosphoproteomic research [11], TiO_2-based MOAC is probably the most widespread enrichment method. This is mainly due to the robustness of the protocol, selectivity of TiO_2 for phosphopeptides, and also due to the commercial availability of various TiO_2 materials such as TiO_2 microparticles (Titansphere, GL Sciences, and Sachtopore-NP, Sachtleben Chemie GmbH), pre-packed TiO_2 tips (Pierce™ Spin Tips, Thermo Scientific and Glygen NuTips, Glygen Corp.), TiO_2 columns for on-line applications (TiO_2 Nano-Trap Columns, Thermo Scientific), and more.

For more in-depth analysis in phospho/proteomics in general, it is inevitable and also a good practice to fractionate the complex peptide mixtures as it improves peptide identification and also quantification [15,29]. However, in the case of phosphoproteomics, there is a dilemma of whether it is better to fractionate first and consequently enrich each fraction for phosphopeptides or to enrich the whole sample for phosphopeptides and fractionate the enriched sample afterward. In general, both approaches are applicable. In the first case, a more selective enrichment may be achieved, while the latter one may be less elaborate, yet still adequately efficient.

Strong cation exchange (SCX) is a traditional first-dimensional separation method. It was widely used as a pre-enrichment fractionation method, although it often suffers from the low resolution of separations [30]. In this regard, hydrophilic interaction chromatography (HILIC) and electrostatic repulsion hydrophilic interaction chromatography (ERLIC) have been developed. Nowadays, they are both commonly applied for pre-fractionation prior to phosphopeptide enrichment [31,32]. Hydrophilic strong anion exchange (hSAX) has also been used successfully for the fractionation of peptide mixtures and phosphopeptides [11,33]. High-pH-RP fractionation is an alternative method providing several practical advantages—robustness, proper separation resolution, and compatibility with further ESI–LC–MS analysis. It typically operates with mobile phases buffered around pH 10 with the gradient of an organic solvent such as ACN. Currently, offline high-pH-RP fractionation has been routinely applied prior to phosphopeptide enrichment by IMAC [34,35] or MOAC using the TiO_2 approach [27].

In our study, we developed a protocol for a simple microgradient separation of phosphopeptides based on C18 microcolumns. This protocol followed the principles of the conventional high-pH-RP peptide fractionation, but it was significantly modified for efficient fractionation of enriched phosphopeptides. It currently enables enrichment for phosphopeptides before their fractionation, which substantially simplifies the entire workflow and extends the degree of phosphoproteome analysis straightforwardly.

The starting setup of phosphopeptide fractionation with our microgradient separation apparatus was based on the commonly used proteomic protocol for high-pH-RP fractionation of complex peptide mixtures [18] and phosphoproteomic analyses [27,36]. We loaded the sample dissolved in a mobile phase buffered to pH 10 to the microcolumn. The flow-through then represented the first fraction, and further fractions eluted from the gradient. Although the fractionated phosphopeptides were successfully detected also in fractions 2 to 10, many of them eluted in the first fraction because a substantial part of phosphopeptides does not retain effectively on the RP under basic pH conditions (Figure 2). The fraction 1 (flow-through) contained about 25% of all identified phosphopeptides (Figure S2), and thus, these phosphopeptides have to be carefully processed as well to avoid undesirable losses.

This finding is in agreement with our previous experiences with SPE phosphopeptide purification, where we observed a similar lack of retention for some phosphopeptides in solutions with higher pH and generally expected lower retention of acidic compounds under basic pH conditions [37]. Moreover, it is obvious that the application of ACN at a concentration of up to 40% in the mobile phase is not necessary for the fractionation of phosphopeptides since we observed the last LC–UV signal already in fraction 10. These experiments led us to a series of modifications and optimizations of the conventional fractionation protocol that involved (i) changes in solvent composition for phosphopeptide sample loading, (ii) introduction of pH gradient into phosphopeptide elution, (iii) narrowing the range of ACN concentration in the elution gradient, and (iv) setting up the suitable elution volumes for particular fractions.

The initial high-pH-RP fractionation involved loading of the sample to a stationary RP in a buffer of pH 10. However, only partially effective capture of phosphopeptides on RP caused by high pH led us to the loading of the phosphopeptide sample immediately after its elution from TiO_2 acidified to pH 2. In this case, the phosphopeptide sample was efficiently loaded onto the microcolumn with the simultaneous simplification of the sample preparation step. Moreover, this modification also minimizes the hydrolysis of phosphopeptides under alkaline conditions [38,39]. To optimize the phosphopeptides elution, we adjusted the pH of the mobile phase to a gradient with pH ranging from 3.9 to 6.6. In parallel with the pH adjustment, the ACN gradient increased from 4% to 24%. Such optimization led to more evenly distributed phosphopeptide fractions. Although the last fraction collected a greater part of the elution volume (6 µL of 24 µL) and the LC–UV analysis showed a significant portion of peptides, the number of identified phosphopeptides was similar to the previous fractions (Figure 3C).

Although the microgradient elution system could be automated for obtaining an excellent chromatographic reproducibility [40], the straightforward sample processing and the simplicity of the introduction of the presented manual microgradient elution system in the laboratory are important advantages of such an approach. The direct comparison of corresponding fractions for all three sample preparations in this work is shown in the Figure S3, where the UV chromatograms for each fraction are presented. It is evident that the phosphopeptides are not significantly shifted in their elution across the fractions for different sample fractionations. For this reason, we assume that our protocol is sufficiently reproducible for phosphopeptide fractionation in phosphoproteome studies.

Some may argue that compared to the purified sample, the LC–MS/MS analysis run time of the fractions rises inadequately while the fold change increase of the identified phosphopeptides does not correspond to the prolonged instrument analysis time. In that case, it may be worth considering applying a suitable pooling scheme for particular fractions to decrease the time for the LC–MS/MS analysis. However, a certain decrease in the number of identified phosphopeptides may be expected then, and a balanced trade-off for a particular study has to be selected. Hence, it is therefore up to the eventual end-user to decide whether to pool individual fractions to shorten the analysis time or not.

Taken together, using our in-house microgradient separation apparatus with the properly optimized elution schema, we obtained an optimal distribution of TiO_2-enriched phosphopeptides over several fractions with a more profound phosphoproteome coverage.

4. Materials and Methods

4.1. Cell Cultures and Cultivation

We obtained non-small cell lung carcinoma cells (H1299) from the American Type Culture Collections (Manassas, VA, USA). We cultured the cells at 37 °C in a humidified incubator under controlled 5% CO_2 atmosphere and maintained them in RPMI medium 1640 (Gibco, Paisley, UK) supplemented with a 10% fetal bovine serum, 150 Ul·mL^{-1} penicillin and 50 mg·mL^{-1} streptomycin (all from Sigma-Aldrich, St. Louis, MO, USA). The maintenance culture was divided twice per week by dilution to a concentration of 2×10^5 cells/10 mL.

4.2. Cell Treatment and Recovery of Proteins

We irradiated the cells, placed in a flask using a ^{60}Co gamma-ray source with a dose rate of 1.04 Gy·min^{-1}, to stimulate phosphorylation within the cell culture. After irradiation, we transferred the cells back into an incubator and cultivated further for one hour.

After irradiation, we lysed H1299 cells using lysis buffer with a composition of 50 mM ammonium bicarbonate, 1% sodium deoxycholate, and phosphatase inhibitor cocktails 2 and 3 (Sigma-Aldrich, St. Louis, MO, USA) by heating them to 100 °C for 5 min followed by cooling on ice and addition of 1.5 mM $MgCl_2$ and 2.5 U·mL^{-1} Benzonase® Nuclease (Sigma-Aldrich, St. Louis, MO, USA) to degrade all forms of DNA and RNA. We precipitated the obtained proteins using the chloroform/methanol precipitation [41], desalted them using C18 solid-phase extraction cartridges (3M™ Empore™, St. Paul, MN, USA), reduced by dithiothreitol, alkylated by iodoacetamide (both Sigma-Aldrich, St. Louis, MO, USA), and digested with trypsin (Sequencing Grade Modified Trypsin, Promega Corporation, Madison, WI, USA) overnight at 37 °C.

4.3. Enrichment for Phosphopeptides

After digestion, we extracted redundant sodium deoxycholate by ethyl acetate [42] and enriched phosphopeptides using titanium dioxide chromatography [43]. We performed the enrichment for phosphopeptides using Mobicol spin columns (MoBiTec GmbH, Goettingen, Germany).

At first, we supplemented samples with trifluoroacetic acid (TFA; 2% *v*/*v*) and glutamic acid (100 mM). Then, we added titanium dioxide microspheres (Titansphere® 5 µm particles, GL Sciences, Torrance, CA, USA) suspended in loading buffer (LB; 65% ACN, 2% TFA, 100 mM glutamic acid) to the samples (peptide:TiO_2 ratio, 1:10) and incubated under continuous mixing for 30 min at room temperature. Afterward, we washed the microspheres with 200 µL of LB, 200 µL of washing buffer 1 (WB1; 65% ACN with 0.5% TFA), 200 µL of washing buffer 2 (WB2; 65% ACN with 0.1% TFA), and again with 100 µL of WB2. Then, we eluted phosphopeptides by 150 µL of elution buffer (EB; NH_4OH, pH 11.5).

In order to fractionate enriched phosphopeptides using the conventional high-pH-RP method, we desiccated the eluted sample in an Eppendorf™ Concentrator Plus (Eppendorf, Hamburg, Germany) and dissolved in 2% ACN/20 mM ammonium formate (pH 10). Subsequently, we loaded such a prepared sample directly to the microcolumn.

In the case of the samples enriched for phosphopeptides that were going to be purified and fractionated using our pH/ACN-gradient-RP fractionation, respectively, we acidified the phosphopeptides with 10% TFA to pH 2, divided them into two groups, and continued with purification and fractionation, respectively.

4.4. Purification of Phosphopeptides

In the beginning, we prepared our capillary microcolumn and the purification/fractionation apparatus. The microcolumn was composed of the fluorinated ethylene propylene tubing (1/16" × 0.25 mm ID; Valco Instruments Co. Inc. and VICI AG+) and stationary phase particles (Kinetex EVO C18 2.6 µm core-shell particles, Phenomenex Inc., Torrance, CA, USA) suspended in ACN. The purification/fractionation apparatus was composed of a laboratory stand and the 25 µL SGE Gas Tight Syringe (Trajan Scientific and Medical, Melbourne, Victoria, Australia). For a more in-depth description of our microcolumn apparatus, see Figure S1.

The purification itself consisted of 5 steps: 1. wetting, 2. equilibrating, 3. sample loading, 4. washing, and 5. elution. We performed wetting by 25 µL of 80% ACN/0.1% TFA and equilibrating by 25 µL of 2% ACN/0.1% TFA. We loaded the acidified sample onto the column and discarded the flow-through solution. Then, we washed the loaded sample by 25 µL of 2% ACN/0.1% TFA and eluted the purified phosphopeptides by 25 µL of 40% ACN/0.1% TFA. The purified phosphopeptides were immediately desiccated in an Eppendorf™ Concentrator Plus (Eppendorf, Hamburg, Germany).

4.5. Fractionation of Phosphopeptides

Similarly to phosphopeptide purification, we also performed fractionation in 5 steps: 1. wetting, 2. equilibrating, 3. sample loading, 4. washing, and 5. elution. The first two steps were consistent with the purification.

In the case of the conventional high-pH-RP strategy, we loaded the sample dissolved in 2% ACN/20 mM ammonium formate (pH 10) directly to the microcolumn and collected the flow-through fraction. Afterward, we washed the sample by 25 µL of 2% ACN/20 mM ammonium formate (pH 10). Before elution, we prepared six solutions of the conventional mobile phase according to Table 1 (conventional elution mobile phases). We aspirated four microliters of each solution into the microsyringe in order from one to six. We then collected the eluates in tubes in the following volumes: 1st fraction—flow-through, 2nd–17th fraction—1.5 µL. The obtained fractions of eluted phosphopeptides were immediately desiccated in an Eppendorf™ Concentrator Plus (Eppendorf, Hamburg, Germany).

In the case of the pH/ACN-gradient-RP strategy, we prepared six solutions of the optimized mobile phase according to Table 1 (optimized elution mobile phases). We aspirated four microliters of each solution into the microsyringe in order from one to six. We then collected the eluates in tubes in the following volumes: 1st fraction—3 µL, 2nd–16th fraction—1 µL, and 17th fraction—6 µL. The obtained fractions of eluted phosphopeptides were immediately desiccated in an Eppendorf™ Concentrator Plus (Eppendorf, Hamburg, Germany).

4.6. Liquid Chromatography and Mass Spectrometry Analysis

At first, we dissolved both C18-purified and fractionated peptide samples in 20 µL of 2% ACN/0.1% TFA. In the case of LC–UV analysis, we analyzed 1 µL of each sample using the UltiMate 3000 HPLC system (Dionex, USA). This system coupled with UV detection included µ-Precolumn (300 µm × 5 mm, C18PepMap 5 µm 100 Å particles; Dionex, USA) connected to the analytical NanoEase column (100 µm × 150 mm, Atlantis C18 3 µm 100 Å particles; Waters, USA). We separated the peptides using the bilinear gradient of 5–45% ACN/0.1% TFA over 81 min under a flow rate of 360 nL·min^{-1} and UV detection set to 215 nm. In the end, we collected data and visualized the respective chromatograms using the Chromeleon software (v. 6.80, Dionex, Sunnyvale, CA, USA).

In the case of LC–MS/MS, we separated peptides using the UltiMate 3000 RSLC-nano HPLC system (Dionex, USA) with a trap column (75 µm × 20 mm) packed with 3 µm Acclaim PepMap100 C18 particles and a separation column (75 µm × 150 mm) packed with 2 µm Acclaim PepMap RSLC C18 particles. We performed the separation with the dual linear gradient using 3–44% ACN in 0.1% formic acid over 89 min for the non-fractionated sample and over 63 min for the obtained fractions under the flow rate of 300 nL·min^{-1}. We monitored the separation using the UV detection system at 214 nm. The separation was directly coupled to MS analysis with the QExactive system (Thermo Fisher Scientific, Waltham, MA, USA) in the positive mode with full MS scan (350–1750 *m/z*) at 70,000 FWHM, maximum filling time 100 ms, and AGC target 1E6. We selected the top 12 or top 10 precursors in MS/MS at 17,500 FWHM for purified and fractionated samples, respectively, with maximum filling time 100 ms and AGC target 1E5.

4.7. Phosphoproteomic Data Processing

We used Proteome Discoverer software (Thermo Fisher Scientific, Waltham, MA, USA, v. 2.4.0.305) to identify the MS/MS spectra. The raw files from the QExactive mass spectrometer were processed within the processing workflow containing spectrum selector, non-fragment filter, top N peaks filter, precursor detector, SequestHT search engine, target decoy PSM validator, and IMP-ptmRS nodes. The parameters for SequestHT database searching were: protein database—UniProt human reference proteome UP000005640 (19 December 2019); enzyme—trypsin; maximum missed cleavage sites—2; min. peptide length—7; precursor mass tolerance—20 ppm; fragment mass tolerance—0.02 Da;

weight of b- and y-ions—1; static modifications—Carbamidomethyl/+57.021 (C); dynamic modifications—Oxidation/+15.995 Da (M), Phospho/+79.966 (S,T,Y); dynamic modifications (protein terminus)—Acetyl/+42.011 Da (N-terminus), Met-loss/−131.040 Da (M), Met-loss+Acetyl/−89.030 Da (M); dynamic modifications (peptide terminus)—Gln→pyro-Glu/-17.027 Da (Q). We further processed the search results obtained in the msf file via the consensus workflow containing PSM Grouper, Peptide Validator, Protein and Peptide Filter, Protein Scorer, Protein FDR Validator, Protein Grouping, and Protein in Peptide Annotation nodes. We set the minimum number of peptide sequences with high confidence (strict target FDR 0.01) to 1 because the enriched samples may often contain only a single peptide per protein. For Venn diagrams reports, we used the Proteome Discoverer graphic tools. We deposited the MS proteomic data to the ProteomeXchange Consortium via the PRIDE partner repository with the dataset identifier PXD018663.

4.8. Statistical Analysis

We performed a statistical comparison between the number of only purified and fractionated phosphopeptides using an independent two-sample t-test with unequal variances and critical *p*-values equal to 0.005. Microsoft Excel was used for statistical calculations as fold changes and coefficients of variations. Boxplot diagram was prepared using R version 3.6.1 [44].

5. Conclusions

In summary, our optimized procedure resulted in a dramatic increase in phosphopeptide identification. We identified a more than 3-times-higher number of phosphopeptides in the fractionated sample compared to the solely purified one.

Of course, our study has certain limitations such as the manual handling of the separation, the limited upper pressure applied during chromatography separation (given by the resistance of the microsyringe), and the prolonged LC–MS/MS analysis time.

On the other hand, we proved that our microcolumn fractionation is a fully reproducible method. Moreover, the most beneficial aspect of our in-house microgradient fractionation apparatus is in the fast and easy setup. Above that, the method is truly inexpensive. Using the C18 microgradient column for fractionation also simultaneously purifies the sample prior to LC–MS/MS analysis.

According to these conclusions, we believe that using pH/ACN-gradient-RP microcolumn fractionation of enriched phosphopeptides could be a suitable strategy to significantly increase the number of identified phosphopeptides when combined with the sensitive LC–MS/MS analysis usually relying on high-resolution instruments such as the quadrupole-Orbitrap hybrid we used in our study. This work contributes to the optimization of enrichment protocols required for in-depth phosphoproteomic studies.

Supplementary Materials: The following are available on-line at http://www.mdpi.com/1422-0067/21/11/3971/s1. Figure S1: Description of our in-house apparatus, Figure S2: Distribution of phosphopeptides into the fractions by high-pH-RP fractionation, Figure S3: Nano LC–UV chromatograms of individual fractions originating from the pH/acetonitrile-gradient-reversed-phase fractionation of the TiO_2-enriched phosphopeptide sample in three replicates. The corresponding fractions compared across all three replicates show good reproducibility of the fractionation method. Table S1: Summary statistics of phosphopeptides identified in each replicate of purified and fractionated sample.

Author Contributions: Conceptualization, M.O., P.R., and A.T.; formal analysis, M.O., P.R., H.R., and R.K.; funding acquisition, A.T.; investigation, M.O. and P.R.; methodology, M.O., and P.R.; supervision, P.R. and A.T.; visualization, M.O. and P.R.; writing – original draft, M.O., P.R., and A.T.; writing – review and editing, M.O., P.R., H.R., R.K., and A.T. All authors have read and agreed to the published version of the manuscript.

Funding: This work was supported by the Ministry of Defense of the Czech Republic through the long-term organization development plan Medical Aspects of Weapons of Mass Destruction of the Faculty of Military Health Sciences, University of Defense in Brno (DZRO-ZHN-2017) and by a grant from Ministry of Health of the Czech Republic No: NV19-02-00297.

Acknowledgments: The authors are grateful to Ian McColl, MD, Ph.D. for assistance with the manuscript.

Conflicts of Interest: The authors declare that they have no conflicts of interest.

References

1. Cohen, P. The origins of protein phosphorylation. *Nat. Cell Biol.* **2002**, *4*, E127–E130. [CrossRef]
2. Ardito, F.; Giuliani, M.; Perrone, D.; Troiano, G.; Lo Muzio, L. The crucial role of protein phosphorylation in cell signaling and its use as targeted therapy (Review). *Int. J. Mol. Med.* **2017**, *40*, 271–280. [CrossRef] [PubMed]
3. Vlastaridis, P.; Kyriakidou, P.; Chaliotis, A.; Van de Peer, Y.; Oliver, S.G.; Amoutzias, G.D. Estimating the total number of phosphoproteins and phosphorylation sites in eukaryotic proteomes. *Gigascience* **2017**, *6*, 1–11. [CrossRef] [PubMed]
4. Chan, C.Y.X.; Gritsenko, M.A.; Smith, R.D.; Qian, W.-J. The current state of the art of quantitative phosphoproteomics and its applications to diabetes research. *Expert Rev. Proteom.* **2016**, *13*, 421–433. [CrossRef] [PubMed]
5. Mayya, V.; Han, D.K. Phosphoproteomics by Mass Spectrometry: insights, implications, applications, and limitations. *Expert Rev. Proteom.* **2009**, *6*, 605–618. [CrossRef]
6. Tichy, A.; Salovska, B.; Rehulka, P.; Klimentova, J.; Vavrova, J.; Stulik, J.; Hernychova, L. Phosphoproteomics: searching for a needle in a haystack. *J. Proteom.* **2011**, *74*, 2786–2797. [CrossRef]
7. Fíla, J.; Honys, D. Enrichment techniques employed in phosphoproteomics. *Amino Acids* **2012**, *43*, 1025–1047. [CrossRef]
8. Dunn, J.D.; Reid, G.E.; Bruening, M.L. Techniques for phosphopeptide enrichment prior to analysis by mass spectrometry. *Mass Spectrom. Rev.* **2010**, *29*, 29–54. [CrossRef]
9. Thingholm, T.E.; Larsen, M.R. The use of titanium dioxide for selective enrichment of phosphorylated peptides. *Methods Mol. Biol.* **2016**, *1355*, 135–146. [CrossRef]
10. Pinkse, M.W.H.; Uitto, P.M.; Hilhorst, M.J.; Ooms, B.; Heck, A.J.R. Selective isolation at the femtomole level of phosphopeptides from proteolytic digests using 2D-NanoLC-ESI-MS/MS and titanium oxide precolumns. *Anal. Chem.* **2004**, *76*, 3935–3943. [CrossRef]
11. Ruprecht, B.; Koch, H.; Medard, G.; Mundt, M.; Kuster, B.; Lemeer, S. Comprehensive and reproducible phosphopeptide enrichment using iron immobilized metal ion affinity chromatography (Fe-IMAC) columns. *Mol. Cell. Proteom.* **2015**, *14*, 205–215. [CrossRef] [PubMed]
12. Fenselau, C. A review of quantitative methods for proteomic studies. *J. Chromatogr. B Analyt. Technol. Biomed. Life Sci.* **2007**, *855*, 14–20. [CrossRef] [PubMed]
13. Nita-Lazar, A.; Saito-Benz, H.; White, F.M. Quantitative phosphoproteomics by mass spectrometry: past, present, and future. *Proteomics* **2008**, *8*, 4433–4443. [CrossRef] [PubMed]
14. Deracinois, B.; Flahaut, C.; Duban-Deweer, S.; Karamanos, Y. Comparative and quantitative global proteomics approaches: an overview. *Proteomes* **2013**, *1*, 180–218. [CrossRef]
15. Manadas, B.; Mendes, V.M.; English, J.; Dunn, M.J. Peptide fractionation in proteomics approaches. *Expert Rev. Proteom.* **2010**, *7*, 655–663. [CrossRef]
16. Ly, L.; Wasinger, V.C. Protein and peptide fractionation, enrichment and depletion: tools for the complex proteome. *Proteomics* **2011**, *11*, 513–534. [CrossRef]
17. Cao, Z.; Tang, H.-Y.; Wang, H.; Liu, Q.; Speicher, D.W. Systematic comparison of fractionation methods for in-depth analysis of plasma proteomes. *J. Proteome Res.* **2012**, *11*, 3090–3100. [CrossRef]
18. Gilar, M.; Olivova, P.; Daly, A.E.; Gebler, J.C. Two-dimensional separation of peptides using RP-RP-HPLC system with different pH in first and second separation dimensions. *J. Sep. Sci.* **2005**, *28*, 1694–1703. [CrossRef]
19. Que, A.H.; Kahle, V.; Novotny, M.V. A microgradient elution system for capillary electrochromatography. *J. Microcolumn Sep.* **2000**, *12*, 1–5. [CrossRef]
20. Moravcová, D.; Kahle, V.; Rehulková, H.; Chmelík, J.; Rehulka, P. Short monolithic columns for purification and fractionation of peptide samples for matrix-assisted laser desorption/ionization time-of-flight/time-of-flight mass spectrometry analysis in proteomics. *J. Chromatogr. A* **2009**, *1216*, 3629–3636. [CrossRef]

21. Franc, V.; Řehulka, P.; Medda, R.; Padiglia, A.; Floris, G.; Šebela, M. Analysis of the glycosylation pattern of plant copper amine oxidases by MALDI-TOF/TOF MS coupled to a manual chromatographic separation of glycans and glycopeptides. *Electrophoresis* **2013**, *34*, 2357–2367. [CrossRef] [PubMed]
22. Franc, V.; Řehulka, P.; Raus, M.; Stulík, J.; Novak, J.; Renfrow, M.B.; Šebela, M. Elucidating heterogeneity of IgA1 hinge-region O-glycosylation by use of MALDI-TOF/TOF mass spectrometry: role of cysteine alkylation during sample processing. *J. Proteom.* **2013**, *92*, 299–312. [CrossRef] [PubMed]
23. Franc, V.; Sebela, M.; Rehulka, P.; Končitíková, R.; Lenobel, R.; Madzak, C.; Kopečný, D. Analysis of N-glycosylation in maize cytokinin oxidase/dehydrogenase 1 using a manual microgradient chromatographic separation coupled offline to MALDI-TOF/TOF mass spectrometry. *J. Proteom.* **2012**, *75*, 4027–4037. [CrossRef] [PubMed]
24. Rehulka, P.; Zahradnikova, M.; Rehulkova, H.; Dvorakova, P.; Nenutil, R.; Valik, D.; Vojtesek, B.; Hernychova, L.; Novotny, M.V. Microgradient separation technique for purification and fractionation of permethylated N-glycans before mass spectrometric analyses. *J. Sep. Sci.* **2018**, *41*, 1973–1982. [CrossRef] [PubMed]
25. Lenobel, R.; Rehulkova, H.; Sebela, M.; Franc, V.; Kahle, V.; Moravcova, D.; Rehulka, P. Analysis of peptide mixtures for proteomics research using LC–ESI-MS with a simple microgradient device. *LC GC N. Am.* **2015**, *33*, 420–428.
26. Yang, F.; Shen, Y.; Camp, D.G.; Smith, R.D. High-pH reversed-phase chromatography with fraction concatenation for 2D proteomic analysis. *Expert Rev. Proteom.* **2012**, *9*, 129–134. [CrossRef]
27. Batth, T.S.; Francavilla, C.; Olsen, J.V. Off-line high-pH reversed-phase fractionation for in-depth phosphoproteomics. *J. Proteome Res.* **2014**, *13*, 6176–6186. [CrossRef]
28. Matsuda, H.; Nakamura, H.; Nakajima, T. New ceramic titania: selective adsorbent for organic phosphates. *Anal. Sci.* **1990**, *6*, 911–912. [CrossRef]
29. Wang, H.; Chang-Wong, T.; Tang, H.-Y.; Speicher, D.W. Comparison of extensive protein fractionation and repetitive LC-MS/MS analyses on depth of analysis for complex proteomes. *J. Proteome Res.* **2010**, *9*, 1032–1040. [CrossRef]
30. Yeh, T.-T.; Ho, M.-Y.; Chen, W.-Y.; Hsu, Y.-C.; Ku, W.-C.; Tseng, H.-W.; Chen, S.-T.; Chen, S.-F. Comparison of different fractionation strategies for in-depth phosphoproteomics by liquid chromatography tandem mass spectrometry. *Anal. Bioanal. Chem.* **2019**, *411*, 3417–3424. [CrossRef]
31. McNulty, D.E.; Annan, R.S. Hydrophilic interaction chromatography reduces the complexity of the phosphoproteome and improves global phosphopeptide isolation and detection. *Mol. Cell. Proteom.* **2008**, *7*, 971–980. [CrossRef] [PubMed]
32. Chien, K.-Y.; Liu, H.-C.; Goshe, M.B. Development and application of a phosphoproteomic method using electrostatic repulsion-hydrophilic interaction chromatography (ERLIC), IMAC, and LC-MS/MS analysis to study Marek's Disease Virus infection. *J. Proteome Res.* **2011**, *10*, 4041–4053. [CrossRef] [PubMed]
33. Ritorto, M.S.; Cook, K.; Tyagi, K.; Pedrioli, P.G.A.; Trost, M. Hydrophilic strong anion exchange (hSAX) chromatography for highly orthogonal peptide separation of complex proteomes. *J. Proteome Res.* **2013**, *12*, 2449–2457. [CrossRef] [PubMed]
34. Mertins, P.; Yang, F.; Liu, T.; Mani, D.R.; Petyuk, V.A.; Gillette, M.A.; Clauser, K.R.; Qiao, J.W.; Gritsenko, M.A.; Moore, R.J.; et al. Ischemia in tumors induces early and sustained phosphorylation changes in stress kinase pathways but does not affect global protein levels. *Mol. Cell. Proteom.* **2014**, *13*, 1690–1704. [CrossRef] [PubMed]
35. Mertins, P.; Qiao, J.W.; Patel, J.; Udeshi, N.D.; Clauser, K.R.; Mani, D.R.; Burgess, M.W.; Gillette, M.A.; Jaffe, J.D.; Carr, S.A. Integrated proteomic analysis of post-translational modifications by serial enrichment. *Nat. Methods* **2013**, *10*, 634–637. [CrossRef]
36. Batth, T.S.; Olsen, J.V. Offline high pH reversed-phase peptide fractionation for deep phosphoproteome coverage. *Methods Mol. Biol.* **2016**, *1355*, 179–192. [CrossRef]
37. Snyder, L.R.; Kirkland, J.J.; Dolan, J.W. Ionic samples: Reversed-phase, ion-pair, and ion-exchange chromatography. In *Introduction to Modern Liquid Chromatography*; John Wiley & Sons, Ltd.: Hoboken, NJ, USA, 2010; pp. 303–360. ISBN 978-0-470-50818-3.
38. Kemp, B.E. Relative alkali stability of some peptide o-phosphoserine and o-phosphothreonine esters. *FEBS Lett.* **1980**, *110*, 308–312. [CrossRef]
39. Sickmann, A.; Meyer, H.E. Phosphoamino acid analysis. *Proteomics* **2001**, *1*, 200–206. [CrossRef]

40. Kahle, V.; Vázlerová, M.; Welsch, T. Automated microgradient system for capillary electrochromatography. *J. Chromatogr. A* **2003**, *990*, 3–9. [CrossRef]
41. Potel, C.M.; Lin, M.-H.; Heck, A.J.R.; Lemeer, S. Defeating major contaminants in Fe^{3+}- immobilized metal ion affinity chromatography (IMAC) phosphopeptide enrichment. *Mol. Cell. Proteom.* **2018**, *17*, 1028–1034. [CrossRef]
42. Yeung, Y.-G.; Stanley, E.R. Rapid detergent removal from peptide samples with ethyl acetate for mass spectrometry analysis. *Curr. Protoc. Protein Sci.* **2010**, *59*. [CrossRef]
43. Larsen, M.R.; Thingholm, T.E.; Jensen, O.N.; Roepstorff, P.; Jørgensen, T.J.D. Highly selective enrichment of phosphorylated peptides from peptide mixtures using titanium dioxide microcolumns. *Mol. Cell. Proteom.* **2005**, *4*, 873–886. [CrossRef] [PubMed]
44. R Development Core Team. *R: A Language and Environment for Statistical Computing*; R Foundation for Statistical Computing: Vienna, Austria, 2009. Available online: https://www.R-project.org/ (accessed on 25 May 2020).

© 2020 by the authors. Licensee MDPI, Basel, Switzerland. This article is an open access article distributed under the terms and conditions of the Creative Commons Attribution (CC BY) license (http://creativecommons.org/licenses/by/4.0/).

Publication no. 6

Guidelines for the use and interpretation of assays for monitoring autophagy (4th edition).

Klionsky D, …, **Ondrej M**, et al.

Autophagy. 2020 (in press)

IF(2018) = 11.059; Q1

Author contribution (<1%)— co-author; editing the manuscript

This article represents a set of recommendations for identifying autophagy and interpretation of assays for monitoring autophagy. Nowadays, it is the most comprehensive guideline for autophagy detection and interpretation. This is its 4th edition.

Publication no. 7

DNA repair inhibitors as radiosensitizers in human lung cells.

Durisova K, Cechakova L, Jost P, Sinkorova Z, Kmochova A, Pejchal J, **Ondrej M**, Vavrova J, Tichy A

Journal of Applied Biomedicine. 2018;16:66-74

IF(2018) = 1.573; Q3

Author contribution (2%)— co-author; writing and editing the manuscript

This experimental work investigates the effect of DNA repair inhibitors on the radiosensitization of NHLF and H1299 cells. Inhibition of DNA-PK and ATM in combination with IR caused the most severe DNA damage and G2 block in both NHLF and H1299 cells. On the contrary, inhibition with ATR resulted in no effect on NHLF proliferation compared to H1299.